Time series of atmospheric halogenated trace gases from Arctic and Antarctic firn air

Christopher James Hogan

February 2013

A thesis submitted for the degree of Doctor of Philosophy at the University of East Anglia, Norwich, UK.

Acknowledgements

I wish to express my appreciation to a number of people whose enormous generosity and patience have contributed so much to the completion of this thesis. I am eternally grateful to all of you. First and most importantly I would like to express sincere thanks to Professor Bill Sturges for his continuous help, advice and supervision throughout my PhD studies. I would also like to thank the other members of the supervisory panel Dr Claire Reeves and Dr Robert Mulvaney for their guidance and ability to shine a new light on any problem.

Special thanks are extended to Dr Johannes Laube who generously helped with the setting up and running of the lab as well as supporting me with valuable recommendations. In addition I thank Dr David Oram (for the Cape Grim data), Mike Newland (for the halons time series), Dr Graham Mills (for the calibration system), Dr Dave Worton (for the $CHCl_3$ data), Dr Francis Mani (for the CH_3Cl data) and all members past and present of the Trace Gas Laboratory at UEA for their time, work and advice given throughout the duration of this project as well as providing their data to be used in this study.

I express great thanks to Dr Patricia Martinerie for her assistance and time in helping to produce the atmospheric time series from the air firn measurements. I thank Dr John Daniel for the use of the time series of EESC from the chlorine and bromine ODSs. I thank the staff at the Cape Grim station and at CSIRO GASLAB Aspendale for collecting and maintaining the Cape Grim air archive and preparing the UEA flask and sub-samples. I also acknowledge CSIRO and the Bureau of Meteorology for funding these activities. I thank all members of the NEEM firn sampling project for collecting and preparing the UEA samples. I would like to pay special thanks to Dr Christo Buizert, Dr Vasilii Petrenko and Dr Emmanuel Witrant and everyone involved in developing and tuning the firn models used in this project. I also thank the Centre of Ice and Climate at the Niels Bohr Institute and US NSF, Office of Polar Programs for their management and organisation of the NEEM project. My gratitude and thanks go to the individual funding agencies and institutions that have supported the NEEM project in Belgium (FNRS-CFB and FWO), Canada (GSC), China (CAS), Denmark (FIST), France (IPEV, CNRS/INSU, CEA and ANR), Germany (AWI), Iceland (RannIs), Japan (NIPR), Korea (KOPRI), The Netherlands (NWO/ALW), Sweden (VR), Switzerland (SNF), UK (NERC) and the USA (US NSF, Office of Polar Programs). I would like to express special thanks to the UK Natural Environment Research Council for funding this research project.

Finally, I would like to thank my Mum, Dad, Erika and James as well as the rest of my family and friends for their constant love and emotional support during my PhD.

Publications arising from this thesis

Jones, C., Andrews, S., Carpenter, L., **Hogan, C.**, Hopkins, F., Laube, J., Robinson, A., Spain, T., Archer, S., and Harris, N. (2011), Results from the first national UK inter-laboratory calibration for very short-lived halocarbons, *Atmos. Meas. Tech.*, *4*(1), 865–874

Buizert, C., Martinerie, P., Petrenko, V. V., Severinghaus, J. P., Trudinger, C. M., E.Witrant, Rosen, J. L., Orsi, A., Rubino, M., Etheridge, D. M., Steele, L. P., **Hogan, C.**, Laube, J. C., Sturges, W. T., Levchenko, V. A., Smith, A. M., Levin, I., Conway, T. J., Dlugokencky, E. J., Lang, P. M., Kawamura, K., Jenk, T. M., Sowers, T., Schwander, J., and Blunier, T. (2011), Gas transport in firn: multiple-tracer characterisation and model intercomparison for NEEM, Northern Greenland, *Atmos. Chem. Phys., 12, 4259–4277*, 15975-16021

Witrant, E., Martinerie, P., **Hogan, C**., Laube, J., Kawamura, K., Capron, E., Montzka, S., Dlugokencky, E., Etheridge, D., and Blunier, T. (2011), A new multi-gas constrained model of trace gas non-homogeneous transport in firn: evaluation and behavior at eleven polar sites, *Atmopsheric Chemistry and Physics (11) 23029-23080*

Laube, J., **Hogan, C**., Newland, M., Mani, F., Fraser, P., Brenninkmeijer, C., Martinerie, P., Oram, D., Röckmann, T., and Schwander, J. (2012), Distributions, long term trends and emissions of four perfluorocarbons in remote parts of the atmosphere and firn air, *Atmos. Chem. Phys.,*, *12*, 4081–4090

Sturges, W., Oram, D., Laube, J., Reeves, C., Newland, M., **Hogan, C**., Martinerie, P., Witrant, E., Brenninkmeijer, C., and Schuck, T. (2012), Emissions halted of the potent greenhouse gas SF_5CF_3, *Atmos. Chem. Phys.*, *12, 3653-3658*

Abstract

The main aim of this study was to investigate the atmospheric histories of several important halogenated trace gases since the middle of the last century. These compounds affect the atmosphere by either destroying stratospheric ozone (chlorocarbons and bromocarbons) or by significantly affecting the Earths radiative budget (fluorinated greenhouse gases). I report measurements of these compounds in air extracted from firn air samples from the North Greenland Eemian Ice Drilling (NEEM) project as well as other Arctic and Antarctic firn air sampling projects. Using a firn diffusion model and a number of dating techniques, I was able to reconstruct both northern and southern hemispheric atmospheric time series. The compounds observed in this study consisted of the chlorocarbons CH_3Cl, $CHCl_3$, CH_2Cl_2, CCl_2CCl_2, CH_2ClCH_2Cl, C_2H_5Cl and $CHClCCl_2$; the bromocarbons, CH_3Br, $CHBr_3$, CH_2Br_2, CH_2BrCH_2Br, C_2H_5Br, CH_2BrCl, $CHBrCl_2$, $CHBr_2Cl$ and $CF_3CHBrCl$; and the fluorinated greenhouse gases SF_6, SF_5CF_3, n-C_4F_{10}, n-C_5F_{12}, n-C_6F_{14}, n-C_7F_{16} and CH_2F_2. The chlorocarbon atmospheric time series indicate that their mixing ratios generally increased between 1950 and the 1980s, and after peaking they have decreased significantly. However, since 2000 the rate of this decline has deceased and some chlorocarbons (CH_2Cl_2 and CH_2ClCH_2Cl) have shown signs of increasing mixing ratios. The bromocarbon atmospheric time series indicate that their mixing ratios generally increased between the 1930s and the 1970s, and after peaking they have decreased significantly and are currently back to around their natural pre-industrial background mixing ratios. The fluorinated greenhouse gas atmospheric time series show them to have first appeared in detectable amounts in the atmosphere after 1950. Since their introduction into the atmosphere all of these compounds have shown significant growth and, apart from SF_5CF_3, all are showing continuing growth. Emissions estimates have been derived for all compounds. The Equivalent Effective Stratospheric Chlorine (EESC) has also been estimated for the ozone depleting substances, and equivalent CO_2 emissions estimates for the greenhouse gases.

Table of Contents

Chapter 1: Scientific Background

1.1 The role of trace gases in the atmosphere

1.2 Trace gases and climate

1.3 The effect of halogenated compounds on stratospheric ozone

1.4 Atmospheric pathways of trace gases into the stratosphere

1.5 Firn structure and processes

1.6 Scientific rationale and research questions addressed in the current study

1.1 The role of trace gases in the atmosphere

In recent years there has been an increased interest in the atmosphere especially with regard to perturbations within the climate system, from the media and the general public as well as the scientific community. This interest has largely been focussed on the effects that climate change and stratospheric ozone depletion are having and will continue to have on the atmosphere.

The atmosphere is defined as the layers of gases surrounding the planet that are retained by Earth's gravity. These layers are in excess of several kilometres thick and are characterised by variations in pressure and temperature with altitude. The temperature-altitude profile leads to the layering of the atmosphere, as a result of transitions from negative to positive temperature gradient with altitude. These layers which start at the Earth's surface are known as the troposphere, stratosphere, mesosphere and thermosphere.

The troposphere is the lowest region of the atmosphere and contains ~80 % of atmospheric mass. It extends from the Earth's surface to the tropopause, with its height varying with latitude and season; being the highest at the tropics during summer and lowest at the poles during winter. However the tropopause height typically remains between 10 and 18 km. The troposphere is characterised by turbulent mixing as a result of the negative lapse rate, resulting in convective instability. The lowest part of the troposphere is known as the planetary boundary layer, this layer contains inversion regions that hinder the vertical mixing into the free troposphere above. Above the troposphere is the stratosphere, which is characterised by limited vertical mixing due to a positive lapse rate, restricting vertical motions. This positive lapse rate is a result of local heating due to relatively high mixing ratio of ozone (O_3) in this region. This layer of relatively high mixing ratio in the stratosphere is generally referred to as the ozone layer.

The atmosphere is composed mostly of molecular nitrogen (N_2) (~ 78 % by volume) and molecular oxygen (O_2) (~ 21 % by volume). The remaining 1 % of the atmosphere is made up of a number of gases, known as trace gases because they are present in such small mixing ratios. The most abundant of the trace gases is the noble gas argon (~ 1 % by volume). However, noble gases, which also include neon, helium, krypton and xenon, are all very inert and do not generally engage in any chemical reactions within the atmosphere.

The most important of the trace gases in the atmosphere are the greenhouse gases (GHGs) (section 1.2 for more details) and ozone depleting substances (ODS) (section 1.3 for more details). The greenhouse gases include carbon dioxide (CO_2), methane (CH_4), nitrous oxide

(N_2O), water vapour (H_2O), ozone as well as a range of halocarbon gases. These gases are involved in the Earth's natural greenhouse effect which keeps the Earth warmer than it would be without these gases present in the atmosphere. Apart from water vapour, the most abundant greenhouse gas (by volume) is CO_2, with CO_2 currently estimated as ~ 390 parts per million (ppm) (Updated from *Forster et al.*, 2007). However, in recent years anthropogenic emissions of greenhouse gases, have enhanced this greenhouse effect which may have led to a warming of the climate system (*Forster et al.*, 2007). In the troposphere ozone behaves like a greenhouse gas, whereas in the stratosphere it forms the ozone layer, which filters out incoming ultraviolet radiation from the Sun and helps to protect life from its harmful effects. However, several groups of compounds destroy ozone in the atmosphere, thus increase the incoming ultraviolet radiation that reaches the surface. These compounds are known as ozone-depleting substances. In this study I will define an ozone-depleting substance ODS as any compound that destroys ozone and not just substances controlled under the Montreal Protocol as defined in *Montzka et al.* (2010). These ODSs include the chlorofluorocarbons (CFCs), the halons, the hydrochlorofluorocarbons (HCFCs), the chlorocarbons and the bromocarbons.

In this study, I have concentrated my research on trace gases containing at least one halogen atom (Table 1.1); these gases are known as halogenated compounds. The halogens are a series of non-metal elements from Group 17 of the periodic table, comprising of: fluorine, (F); chlorine, (Cl); bromine, (Br); iodine, (I); and astatine, (At). However, in this study I have only researched halogenated compounds containing fluorine, chlorine and bromine. These halogen-compounds play an important role in the chemistry of both the troposphere and the stratosphere. Chlorinated and brominated compounds are very important in the ozone chemistry of the atmosphere, which is discussed in more detail in section 1.3. Fluorinated compounds are more important in the energy budget of the atmosphere, which is discussed in more details in section 1.2. However, it should be noted that some halogenated compounds are both ODSs and GHGs, notably the CFCs.

One of the key factors, which determine how much effect a trace gas has on the atmosphere, is the length of time that gas can remain in the atmosphere. This time is known as the total atmospheric lifetime (τ) or turnover time, and is defined as the time required to remove or chemically transform a trace gas by 1-1/e (~ 63 %) of its global atmospheric burden. The length of the atmospheric lifetime of a trace gas is also used to define a number of groups of compounds. The groups of trace gases in this study include the very long-lived substances (lifetime greater than ~100 years up to thousands of years), long-lived substances (lifetime

greater than a few years but less than ~100 years), the short-lived substances (lifetimes of greater than 6 months but less than a few years) and the very short-lived substances (VSLS). VSLS are defined as trace gases whose local lifetimes are comparable to, or shorter than, the tropospheric transport timescales and that have non-uniform tropospheric abundances (*Montzka et al.*, 2010). In this study the lifetimes of VSLS are generally defined as being present in the atmosphere for less than 6 months.

Table 1.1: key information on the trace gases measured in the current study

Trace gas	**Formula**	**Atmospheric lifetime (τ)[#]**	**Major sources: natural (N) / anthropogenic (A)**	**important in the atmosphere: ODS / GHG**
Chlorocarbons				
methyl chloride	CH_3Cl	1.0 y	N	ODS
chloroform	$CHCl_3$	149 d	N / A	ODS
dichloromethane	CH_2Cl_2	144 d	N / A	ODS
tetrachloroethene	CCl_2CCl_2	90 d	A	ODS
1,2-dichloroethane	CH_2ClCH_2Cl	65 d	A	ODS
chloroethane	C_2H_5Cl	39 d	A	ODS
trichloroethene	$CHClCCl_2$	4.9 d	A	ODS
methyl chloroform	CH_3CCl_3	5.0 y	A	ODS
Bromocarbons				
methyl bromide	CH_3Br	0.8 y	N / A	ODS
bromoform	$CHBr_3$	76 d	N / A	ODS
dibromomethane	CH_2Br_2	123 d	N	ODS
1,2-dibromoethane	CH_2BrCH_2Br	70 d	N / A	ODS
bromoethane	C_2H_5Br	41 d	N / A	ODS
bromochloromethane	CH_2BrCl	137 d	N / A	ODS
bromodichloromethane	$CHBrCl_2$	121 d	N / A	ODS
dibromochloromethane	$CHBr_2Cl$	94 d	N / A	ODS
halothane	$CF_3CHBrCl$	1.0 y	A	ODS
Halon-1202	CBr_2F_2	2.9 y	A	ODS
Halon-1211	$CBrClF_2$	16 y	A	ODS
Halon-2402	$CBrF_2CBrF_2$	20 y	A	ODS
Halon-1301	$CBrF_3$	65 y	A	ODS
Fluorinated greenhouse gases				
sulphur hexafluoride	SF_6	650–950 y	A	GHG
trifluoromethyl sulphur pentafluoride	SF_5CF_3	3200 y	A	GHG
n-decafluorobutane	n-C_4F_{10}	2600 y	A	GHG
n-dodecafluoropentane	n-C_5F_{12}	4100 y	A	GHG
n- tetradecafluorohexane	n-C_6F_{14}	3200	A	GHG
n-hexadecafluoroheptane	n-C_7F_{16}	-	A	GHG
HFC-32	CH_2F_2	5.5 y	A	GHG

- *Montzka et al.* (2010) ,y – years, d – days, ODS – Ozone depleting substances, GHG - Greenhouse gas

1.2 Trace gases and climate

The climate system is a complex, interactive system consisting of the atmosphere, land surface, snow and ice, oceans and other bodies of water, and living organisms (*IPCC*, 2007). Climate is usually described in terms of the mean and variation in temperature, precipitation and wind over a period of time, ranging from months to millions of years (the classical period is 30 years) (*IPCC*, 2007). The climate system evolves under the influence of its own internal dynamics, as well as due to changes in external factors that affect climate (known as 'forcings'). These external forcings include natural phenomena such as volcanic eruptions and solar variations, as well as human-induced changes in atmospheric composition. The climate system is driven by radiation from the sun (Figure 1.1).

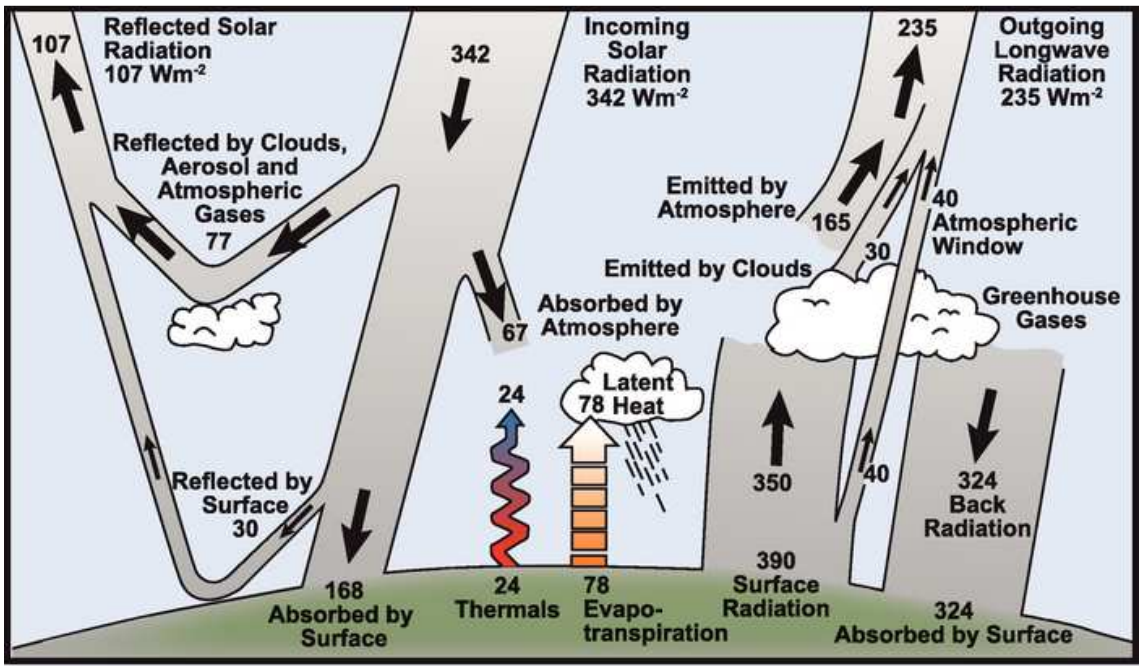

Figure 1.1: Estimate of the Earth's annual and global mean energy balance. Over the long term, the amount of incoming solar radiation absorbed by the Earth and atmosphere is balanced by the Earth and atmosphere releasing the same amount of outgoing longwave radiation (*Kiehl and Trenberth*, 1997).

There are a number of ways that the energy budget of the Earth can be changed. Changes in the radiation output of the Sun or the Earth's orbit affect the incoming solar radiation and thus the radiation balance. The Earth's albedo changes, when there are changes in cloud cover, amounts of atmospheric particles or vegetation cover. Lastly, changes in the mixing ratio of greenhouse gases in the atmosphere alters the amount of longwave radiation emitted from Earth which reaches the top of the atmosphere. This last effect is commonly known as the 'greenhouse effect'. Climate, in turn, responds directly as well as indirectly, to such changes, through a variety of feedback mechanisms

In this study, I have been investigating the change in greenhouse gas mixing ratio in the atmosphere and the effect on global climate. A greenhouse gas (GHG) is defined as a gas in the atmosphere that absorbs and emits radiation within the thermal infrared spectrum (λ - 5.6 μm to 1.0 cm) (*Forster et al.*, 2007). However, the most abundant gases in the atmosphere (N_2 and O_2) absorb or emit almost no radiation within the thermal infrared range. Therefore, the greenhouse effect is mainly governed by trace gases within the atmosphere. This greenhouse effect from individual compounds is often quantified using their radiative forcing (RF). *Ramaswamy et al.* (2001) define RF as the change in net irradiance (W m^{-2}, with + taken as towards the surface) at the tropopause after allowing for stratospheric temperatures to readjust to radiative equilibrium, but with surface and tropospheric temperatures and state held fixed at the unperturbed values.

Currently, the combined RF from anthropogenic emissions is estimated to be + 1.6 W m^{-2}, which means that it is '*extremely likely*' that humans have exerted a substantial warming influence on climate, since 1750 (*Forster et al.*, 2007). *Forster et al.* (2007) have also shown that it is '*exceptionally unlikely*' that the combined natural RF (changes in solar irradiance plus volcanic aerosol) have had a warming influence comparable to that of the combined anthropogenic RF between 1950 and 2005.

However, is not straightforward to assess the potential change in climate resulting from an individual compound due to its RF. This is because to evaluate the overall climate response associated with a forcing agent, the temporal evolution and the spatial and vertical structure of the compound need to be taken into account. In addition, RF does not take into account the different atmospheric lifetimes of the forcing agents. One way to try and estimate these effects is by calculating Global Warming Potentials (GWPs). GWPs compare the integrated RF over a specified period (normally 20, 100 or 500 years) from a unit mass pulse emission relative to CO_2 (*Forster et al.*, 2007). Therefore, a high GWP correlates to a compound with large absorption within the thermal infrared spectrum and a long atmospheric lifetime

In the current study, I have been researching into a group of compounds known as the fluorinated greenhouse gases (Table 1.1). These gases absorb strongly in the thermal infrared spectrum with SF_5CF_3 having the largest RF of any compound measured in the atmosphere (*Sturges et al.*, 2000). These compounds also have very long atmospheric lifetimes (*Velders et al.*, 2005) resulting in large GWPs, with SF_6 having the largest GWPs of any compound measured in the atmosphere (*Forster et al.*, 2007). As a result because of their long

atmospheric lifetime, these gases are making an essentially permanent contribution to the energy budget of the atmosphere.

The importance of the effects of the fluorinated greenhouse gases on the atmospheric energy budget are so great, that a number of organizations have been set up to mitigate against their effects on global climate change. Climate change mitigation is designed to decrease the intensity of radiative forcing in order to reduce the effects of potential global warming. The Intergovernmental Panel on Climate Change (IPCC) was established to provide a clear scientific view on the current state of knowledge in climate change and its potential environmental and socio-economic impacts. The IPCC was set up by the United Nations Environment Programme (UNEP) and the World Meteorological Organization (WMO) in 1988 to review and assess the most recent scientific, technical and socio-economic information, relevant to the understanding of climate change. Although the work by the IPCC is relevant to policy, the work produced is policy-neutral and is never policy-prescriptive.

Policy on climate change is undertaken by the United Nations Framework Convention on Climate Change (UNFCCC). Since 1992, 194 countries have joined the UNFCCC, to cooperatively consider what they could do to limit average global temperature increases and resulting climate change, and to cope with any inevitable impacts.

In 1997, the UNFCCC adopted the Kyoto Protocol which legally binds developed countries to emission reduction targets. These targets amount to an average of five per cent against 1990 levels over the five-year period 2008-2012 (*deBoer*, 2007). The Protocol's first commitment period started in 2008 and ends in 2012, a second commitment period from 2013, with an undetermined length, has also been set by the UNFCCC. As of September 2011, 191 states have signed and ratified the protocol. The major distinction between the protocol and the convention is that while the convention encouraged industrialised countries to stabilize GHG emissions, the protocol commits them to do so.

1.3 The effect of halogenated compounds on stratospheric ozone

Ozone (O_3) is a naturally occurring gas in the atmosphere. Approximately 90 % of atmospheric ozone is found in the stratosphere, with the region of the stratosphere with the highest ozone mixing ratio known as the "ozone layer" (*Montzka et al.*, 2010). This layer extends over the entire globe with some variation in its altitude and thickness. The remaining ozone (~ 10 %), is generally found in the troposphere. Stratospheric ozone is important as it absorbs ultraviolet-B (UV-B) and ultraviolet-C (UV-C) radiation. This is essential, because in humans extended periods of exposure to UV-B radiation results in an increased risk of skin cancer, cataracts and a suppressed immune system (*Kricker et al.*, 1994). However, tropospheric ozone is also harmful to humans, plants and other living organisms because ozone reacts strongly to destroy or alter many biological molecules.

The major mechanism for the production of ozone in the stratosphere is the photolysis of molecular oxygen (O_2) by UV radiation ($\lambda < 242$ nm) to form oxygen atoms (O). These oxygen atoms then react with molecular oxygen to form ozone. In the troposphere, ozone is produced when nitrogen oxides (NOx), carbon monoxide (CO) and volatile organic compounds (VOCs) react with O_2 in the presence of UV radiation.

The abundance of ozone in the stratosphere is controlled by a combination of production rates, destruction rates, and transport of both ozone and other chemicals into and out of the region of interest. The abundance of ozone varies across a range of time scales: daily variations in the ozone column are driven by meteorological variability, seasonal variations are driven by changes in stratospheric temperature and winds and multiannual variations are driven by changes in solar radiation, by variations in the abundance of ozone reactive gases, and by interannual variability in stratospheric winds (*Montzka et al.*, 2010). Total ozone values are often reported in Dobson units (DU), with one Dobson unit defined as a layer of gas that would be 10 mm thick under standard temperature and pressure (*Montzka et al.*, 2010). Typical ozone values vary between 200 and 500 DU over the globe (*Montzka et al.*, 2010).

The destruction of ozone occurs via the reaction of oxygen atoms with ozone, as well as through cyclic chemical reactions involving either odd-hydrogen radicals (HOx: OH and HO_2), nitrogen oxide radicals (NOx: mostly NO and NO_2), and halogen radicals. Therefore, any increase in the abundance of these radicals can result in an enhancement in the destruction term, leading to a decline in stratospheric ozone. In this study I have researched the effect of halogenated compounds containing chlorine and bromine atoms on the atmosphere, as a result of their ability to destroy ozone.

These halogenated radicals get into the stratosphere through the transport pathways discussed in section 1.4. Once in the stratosphere halogen containing compounds can be divided into either halogenated source gases or reactive halogen gases. The halogenated source gases (e.g. CFCs, Halons, chlorocarbons and bromocarbons) are emitted at Earth's surface and have been unchanged in their transport into the stratosphere. Once in the stratosphere, the halogen source gases are converted at different rates to form the reactive halogen gases, mainly through photolysis. This conversion occurs in the stratosphere because of the greater intensity of ultraviolet radiation compared to the troposphere.

The most abundant of these reactive halogen gases are typically hydrogen chloride (HCl) and chlorine nitrate ($ClONO_2$). While these two compounds do not react directly with ozone, they can be converted easily into more reactive compounds. The most reactive forms are chlorine monoxide (ClO), bromine monoxide (BrO), and chlorine and bromine atoms (Cl and Br). Available reactive bromine is generally in the form of BrO, whereas only a small fraction of available reactive chlorine is in the form of ClO. However reactions on polar stratospheric clouds in the winter result in $ClONO_2$ and HCl nearly being completely converted into ClO. These gases are then able to destroy ozone through three principal reaction cycles that are shown in Table 1.2.

Table 1.2: Ozone destruction cycles

Cycle	**1**	**2**	**3**
Reactions	$ClO + O \rightarrow Cl + O_2$ $Cl + O_3 \rightarrow ClO + O_2$	$ClO + ClO \rightarrow (ClO)_2$ $(ClO)_2 + h\vartheta \rightarrow ClOO + Cl$ $ClOO \rightarrow Cl + O_2$ $2\ Cl + 2\ O_3 \rightarrow 2\ ClO + 2\ O_2$	$ClO + BrO \rightarrow Cl + Br + O_2$ or $ClO + BrO \rightarrow BrCl + O_2$ $BrCl + h\vartheta \rightarrow Cl + Br$ ---------- $Cl + O_3 \rightarrow ClO + O_2$ $Br + O_3 \rightarrow BrO + O_2$
Net reaction	$O + O_3 \rightarrow 2\ O_2$	$2\ O_3 \rightarrow 3\ O_2$	$2\ O_3 \rightarrow 3\ O_2$

Table 1.2 shows that in each cycle, the halogen acts as a catalyst because BrO, ClO and Cl react and are then reformed. In this way, one halogen atom participates in many cycles, destroying many ozone molecules. This has been highlighted by *Montzka et al.* (2010) who calculated that for typical stratospheric conditions at middle or low latitudes, a single chlorine atom can destroy up to tens of thousands of ozone molecules during its time within the stratosphere.

Cycle 1 is the most important destruction process in the tropical stratosphere at middle latitudes, where ultraviolet radiation is at its most intense. Solar ultraviolet radiation is needed to produce atomic oxygen (O) from ozone and molecular oxygen. Cycles 2 and 3 are the more dominant reaction mechanisms in the polar stratosphere, due to the abundance of ClO and the relatively low abundance of atomic oxygen. However, during the polar night and other periods of darkness, ozone is not destroyed by these reaction mechanisms as ultraviolet is required to complete each cycle and to form and maintain BrO and ClO.

As well as reactive halogened compounds, global ozone abundances are controlled by many reactions. These include reactions with hydrogen and nitrogen gases, that also act as catalysts in ozone-destruction cycles. The sources gases for these reactive hydrogen and nitrogen gases are methane (CH_4) and nitrous oxide (N_2O), respectively. Both of these compounds do also have natural as well as anthropogenic sources. The importance of reactive hydrogen and nitrogen gases relative to reactive halogen gases is expected to increase in the future, because the atmospheric abundances of reactive halogen gases are decreasing as a result of the Montreal Protocol, while CH_4 and N_2O abundances are projected to increase substantially due to human activities (*Montzka et al.*, 2010)

The importance of these effects on the ozone layer are so great that a number of organizations have been set up to mitigate against the release of ODS. The World Meteorological Organization (WMO) / United Nations Environment Programme (UNEP) as well as the National Aeronautics and Space Administration (NASA) established the Scientific Assessments of Ozone Depletion to provide a clear scientific view on the current state of knowledge in ozone deletion and its potential environmental impacts. However, policy decisions on ozone depletion are undertaken through the Montreal Protocol on Substances that Deplete the Ozone Layer. The Montreal Protocol was designed to reduce the production and consumption of ozone depleting substances in order to reduce their abundance in the atmosphere, and thereby protect the ozone Layer (*González et al.*, 2006). The original Montreal Protocol was agreed on 16 September 1987 and entered into force on 1 January 1989, currently 197 states are signed up to the protocol. The Montreal Protocol also allows for an acceleration in the reductions requirements of compounds already covered by the protocol when new scientific information becomes available. The Protocol has also been amended to enable the control of new chemicals and the creation of a financial mechanism to enable developing countries to comply. Since its initial adoption, the Montreal Protocol has been adjusted five times. The latest of these amendments was the 'Beijing Amendment' in 1999, which entered into force in February 2002, for the 178 parties which have ratified the amendment.

1.4 Atmospheric pathways of trace gases into the stratosphere

There are two distinct pathways that lead to the arrival of total inorganic chlorine (Cl_y) and inorganic bromine (Br_y) into the stratosphere, namely source gas injection (SGI) and product gas injection (PGI) (e.g. *Ko and Poulet*, 2003). SGI refers to the transport of a source gas (SG, e.g. CH_3Cl, CH_3Br) into the stratosphere in the same form as they are emitted at the surface, where they can be degraded and provided an *in-situ* source of Cl_y or Br_y. Whereas, PGI is when a SG degrades in the troposphere to either an organic intermediate (e.g. CBr_2O) or an inorganic product (e.g. HCl, BrO), which can then be transported into the stratosphere. The efficiency of these transport pathways depends upon the competition between fast vertical transport and chemical destruction, or removal via washout before reaching the stratosphere (*Hossaini et al.*, 2010). The probability of washout decreases with increasing height within the troposphere and becomes relatively small in the tropical tropopause layer (TTL). The TTL is defined as the level of the atmosphere between the level of maximum convection outflow (~ 12 km or a potential temperature of 345 K) and the cold point tropopause (~ 17 km or a potential temperature of 380 K) (*Gettelman and Forster*, 2002). This is similar to the "sub-stratosphere" region as defined by *Thuburn and Craig* (2002). The potential temperature of an air parcel is define as the temperature that the air parcel would acquire if adiabatically brought to a standard reference pressure (1000 hPa).

The halogenated compounds are considered to have reached the "tropical stratosphere" when they are above the cold point tropopause (CPT), which is climatologically located at 380 K (~17 km altitude) (*Montzka et al.*, 2010). This makes the TTL the source region for both the stratospheric overworld and the extra-tropical lowermost stratosphere. Figure 1.2 shows a detailed schematic of the principal dynamical pathways of compounds in the tropics into the stratosphere (based on *Montzka et al.*, 2010 and *Fueglistaler et al.*, 2009).

Figure 1.2: Schematic diagram showing the principal dynamical pathways of compounds in the tropics into the stratosphere (based on *Montzka et al.*, 2010 and *Fueglistaler et al.*, 2009). The position of the tropopause as defined by *Montzka et al.*, 2010 and *Clerbaux and Cunnold et al.*, 2006) is designated by the bold black line. TTL - tropical tropopause layer, OC - overshooting convection, RDT - Radiatively driven transport Ci – Cirrus cloud, CPT – cold point tropopause, MCO – maximum convective outflow, MT - meridional transport, Z_0 - clear-sky zero radiative heating, LMS – lowermost stratosphere.

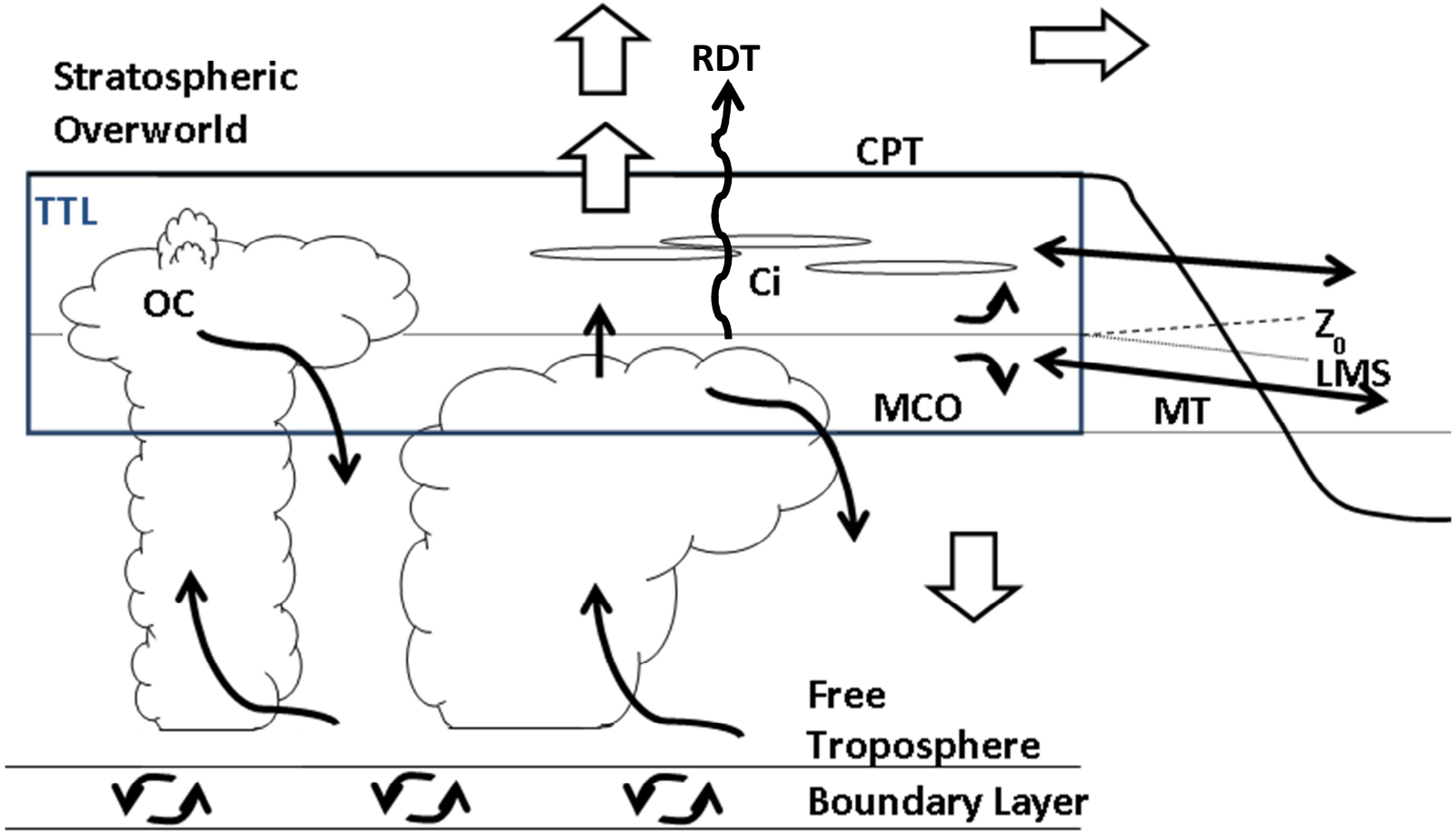

Figure 1.2 shows that vertical transport in the lower tropical troposphere above the boundary layer is dominated by ascent in convective clouds. The outflow from these clouds are either in a lower layer from about 2 to 5 km (800-550 hPa), or an upper layer from about 10 to 15 km (300-150 hPa) (*Fueglistaler et al.*, 2009). During this ascent in the strong moist convective updrafts, soluble chemical species are also scavenged by precipitation (*Barth et al.*, 2001, *Crutzen and Lawrence*, 2000 and *Mari et al.*, 2000). Furthermore the descent of compounds in this region is associated with evaporative cooling in the lower layer, and radiative cooling in the upper layer (*Folkins and Martin*, 2005).

Unless emitted directly into the active cell of tropical deep convection, it is unlikely that shorter lived VSLS (lifetime from a few hours to days) will reach the TTL, whereas longer lived VSLS (lifetimes from weeks to months) can reach the TTL via a range of transport pathways (as described in Figure 1.2).

This transport pathway of VSLS has been validated by *Aschmann et al.* (2009) using a three-dimensional chemical transport model. *Aschmann et al.* (2009) also show that the tropical Western Pacific transports a significant amount of VSLS into the TTL. As well as varying with region TTL transport has been shown to vary with season by *Aschmann et al.* (2009) and *Gettelman et al.* (2009). Higher VSLS mixing ratio in the TTL are modelled in NH winter compared against the rest of the year. This is a result of a combination of higher convective cloud tops reaching the TTL and higher vertical velocities within the TTL (*Gettelman et al.*, 2009). Deep convection associated with the Indian summer monsoon could lead to more efficient transport of surface emissions into the TTL in certain regions during the NH summer (*Randel et al.*, 2010, *James et al.*, 2008 and *Donner et al.*, 2007). The estimated timescale for this atmospheric pathway is a week compared with the average timescale of three weeks in NH winter (*Stohl et al.*, 2002). Space-borne observations of trace compounds by *Ricaud et al.* (2007) have shown that tropical overshooting convection can directly inject surface air into the upper TTL and stratosphere. However, due to the rarity in events and location (*Liu and Zipser*, 2005), the amount of trace gases that reaches the stratosphere via overshooting convection is expected to be small on a global basis (*Homan et al.*, 2010 and *Fueglistaler et al.*, 2009). As well as overshooting convection, *Hossaini et al.* (2010) have suggested that large-scale transport and mixing of planetary boundary layer air into the TTL could also be an important transport pathway for longer-lived VSLS (e.g., CH_2Br_2).

Once in the TTL the net exchange into the stratospheric overworld across the cold point tropopause is regarded as being dominated by large-scale ascent associated with the Brewer-Dobson circulation (*Fueglistaler et al.*, 2009, *Gettelman et al.*, 2009 and *Holton et al.*, 1995). The strength of this ascent is controlled by large-scale dynamical processes (*Holton et al.*, 1995) and this transport allows air to move into regions of the stratosphere where ozone is depleted. However, the general transport in the upper TTL is large-scale horizontal motion, with only slow vertical motion (25 to 45 days for compounds to be transported through the upper TTL (*Ploeger et al.*, 2010 and *Krüger et al.*, 2009)). Nonetheless, there are infrequent, localized and rapid (hours) vertical ascent pathways associated with overshooting convection (*Montzka et al.*, 2010 and *Fueglistaler et al.*, 2009).

Another important pathway into the stratosphere is through the slow, vertical motion driven by radiative heating in TTL cirrus clouds, above the level of clear-sky zero radiative heating (*Jensen et al.*, 2011). Again, this transport of compounds through the TTL varies with location and seasonality (*Aschmann et al.*, 2009, *Gettelman et al.*, 2009 and *Krüger et al.*, 2009). The annual mass transport peaks over the tropical Western Pacific during the NH winter and over the Indian monsoon regions during the NH summer (*Montzka et al.*, 2010 and *Fueglistaler et al.*, 2005). Currently, observational evidence for direct transport of trace gases from the surface to the TTL and then into the stratosphere are scarce. Therefore, the relative effect of boundary layer mixing, convection, and overshooting convection and the influence of washout on the amount of a trace compound that actually reach the stratosphere are still a matter of some debate (*Montzka et al.*, 2010).

1.5 Firn structure and processes

In the current study I will research into how the GHGs and ODSs have changed in abundance over time. This was achieved by observing air extracted from firn in the polar regions. Firn is defined as the metamorphic transition phase between snow and ice, and is present as a porous layer overlying an ice sheet. The primary distinction between firn and ice is that firn has interconnected air-filled pores (open porosity) between the ice crystals, while ice has closed air bubbles (closed porosity), between which air cannot move. The firn-ice transition occurs at the bottom of the firn column where the porosity falls to zero. Above this depth the air in the firn column can still interact with the atmosphere through the open pores. Therefore, the composition of the firn air is modified by variations in the atmosphere, diffusion, convection/advection, gravitation and thermal gradient within the firn column. This interstitial air from within the firn can then be extracted and analysed. The firn column is typically 50-

110m in depth (*Schwander and Stauffer*, 1984). The firn column is categorized into three layers (*Sowers et al.*, 1992) and is primarily based on the porosity of the firn structure and the diffusion of gases within the column. The three layers are the convective zone, diffusive zone and the lock-in zone. Figure 1.3 shows these layers as well as the physical processes that effect the movement of gases in the firn column.

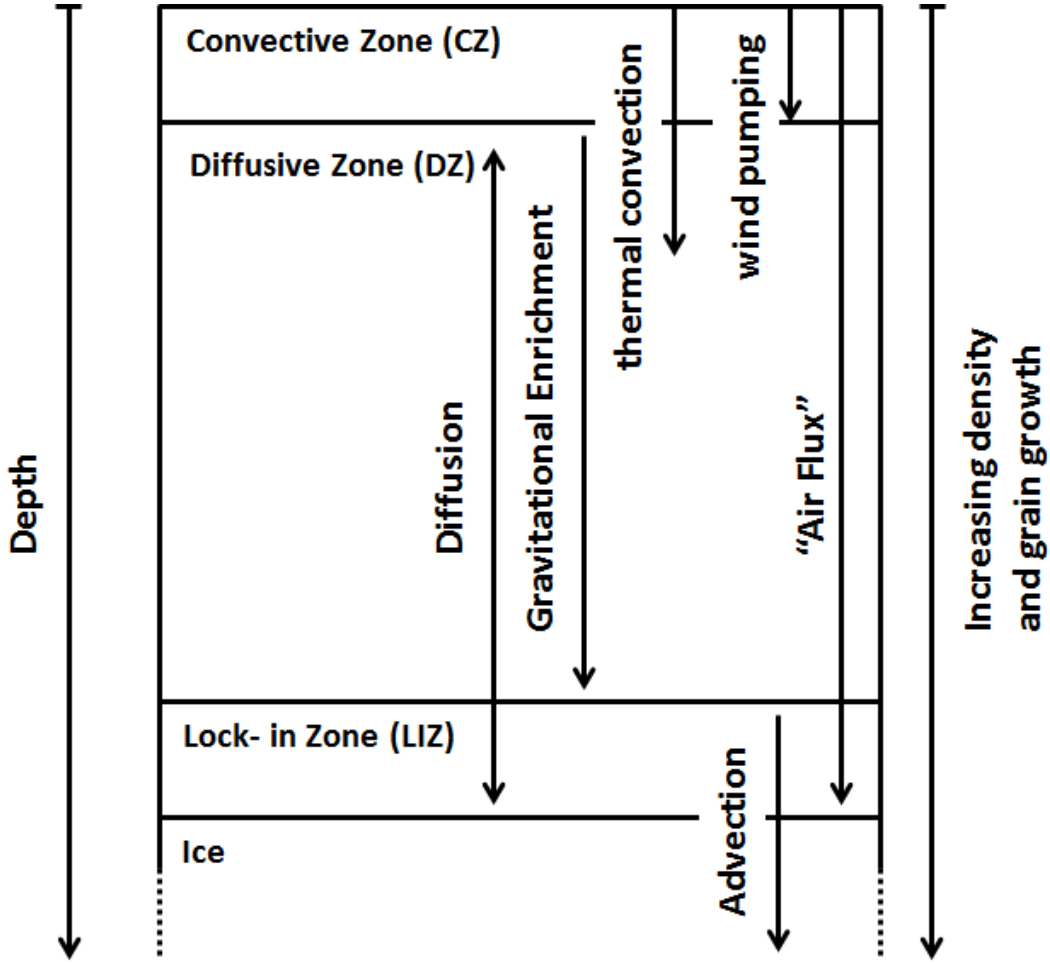

Figure 1.3: Cross section of firn column to illustrate the changing structure with depth and the physical processes that effect the movement of gases (Adapted from *Bales and Wolff*, 1995 and *Sowers et al.*, 1992)

The convective zone (CZ) is typically confined to the first few meters of the firn column (e.g. 4.5 m at the NEEM site (*Buizert et al.*, 2011)) This depth does vary between different locations as a result of local meteorological conditions. The CZ is characterised by a low density (typically ≤ 200 kg m^{-3} (*Bales and Wolff*, 1995)), with the uppermost layer representing the most recent precipitation. The firn in this layer is very porous, resulting in the firn air being well mixed with the overlying atmosphere and thus has a similar chemical composition. Air movement in this region results from thermal convection and wind pumping (*Kaspers*, 2004). Thermal convection is the movement of air in the snow or firn due to a temperature gradient. This

convection is restricted to the top of the firn column (20 - 30 m (*Huber et al.*, 2006 and *Landais et al.*, 2006)) where there is a strong temperature gradient and is more prominent in highly porous layers with large gradients (*Sowers et al.*, 1992). This does mean that there is some thermal convection in the diffusive zone. Wind pumping results in movement of air in the firn column in response to atmospheric pressure variations (*Sowers et al.*, 1992). Wind pumping also effects the thickness of the convective zone, with a deeper region occurring with larger pressure variations. These variations are a result of changes in barometric pressure, turbulent winds at the surface of the ice sheet, or pressure gradients induced by winds travelling over surface undulations (*Sowers et al.*, 1992).

The airflow associated with wind pumping deceases with depth, due to the decrease in porosity and permeability, until it becomes negligible compared to that from molecular diffusion. Therefore, shallower CZ are characteristic of a high density firn layer with high tortuosity (*Sowers et al.*, 1992). *Kawamura et al.* (2006) suggested that there is a relationship between low accumulation rate and deep convection zones. Also, *Colbeck* (1989) suggested that deeper sections are produced by high wind speeds over topographic features producing long wavelengths. The extent of the CZ can be inferred from measurements of $\delta^{15}N$, which should increase linearly with depth within the firn column as a result of gravitational separation. Measurements of $\delta^{15}N$ remain consistent with depth within the CZ (*Buizert et al.*, 2011). Measurements of very rapidly growing atmospheric compounds (e.g., HCFC-22, HFC-141b, 142b) can also be used to infer the depth of the zone (*O'Doherty et al.*, 2004).

The zone below the CZ is called the diffusive zone or DZ, because transport is dominated by diffusion (*Sowers et al.*, 1992). The zone is characterised by increasing density with depth due to the augmenting weight of the overlying firn (*Bales and Wolff*, 1995). Density in this zone is typically between ~200 and 800 kg m^{-3} (*Bales and Wolff*, 1995). In the diffusive zone, porosity decreases within the firn, and transport of gases becomes unaffected by surface turbulence and pressure variations. The movement of air in this region is primarily due to diffusion and movement of gases due to gravity (*Sowers et al.*, 1992). The diffusion within the firn is governed by Fick's laws of diffusion and is composed of both molecular and eddy diffusion. Molecular diffusion is a microscopic process originating in the thermal motion of the molecules, whereas eddy diffusion refers to mass transfer caused by macroscopic flow patterns in the open porosity of the firn (*Buizert et al.*, 2011 and *Rommelaere et al.*, 1997). This diffusion of compounds in the firn column decreases with depth as the diffusive path becomes increasingly tortuous as a result of the densification process (*Schwander et al.*, 1988). The chemical composition in the overlying atmosphere which is in equilibrium will also deviate in

the firn column due to gravitational enrichment. Gravitational enrichment results in heavier molecules and isotopes becoming progressively enriched with depth (*Sowers et al.*, 1989 and *Craig et al.*, 1988). This means that in the DZ, movement is controlled by diffusion and gravitational settling, which are dependent on the effective diffusivity of the firn as well as the mass and molecular diffusivity of an individual species.

The lock-in depth is defined as the depth at which gravitational enrichment stops, (63 m at the NEEM site (*Buizert et al.*, 2011)). Below this depth is the lock-in zone or LIZ. In this region, transport is dominated by advection within the firn matrix. This is also the region where the majority of bubble closure/occlusion occurs (*Sander et al.*, 2003 and *Rommelaere et al.*, 1997). The diffusivity in this zone is so low that gas transport ceases and the composition of air composition is no longer modified until it reaches the 'close-off' and is occluded into ice bubbles. However, recent research by *Buizert et al.* (2011) found strong evidence that diffusivity does not vanish completely in the firn lock-in zone. *Landais et al.* (2006) and *Schwander et al.* (1997) show that LIZ is generally around 10 m at most sites. However, the depth varies from site-to-site depending on the site temperature and accumulation rates, with a larger LIZ typical at high accumulation sites (*Sowers et al.*, 1992).

At the bottom of the LIZ is the close off zone / firn-ice transition zone where complete pore close off occurs isolating the air from the overlying atmosphere. This is then preserved for thousands of years in the ice. The close off zone is characterised by the critical density interval between 800 kg m^{-3} and 830 kg m^{-3} (*Schwander et al.*, 1997). Usually, sites with higher accumulation rates and colder temperatures will have deeper close off zones and thus, a longer firn column (*Sowers et al.*, 1992). The trapping of air at the bottom of the firn column, has to be balanced by an air flux divergence. This results in a downward "air flux" in the whole firn column, with the vertical velocity of this flux depending on the trapping of air into ice bubbles and on the open porosity of the column (*Rommelaere et al.*, 1997). As a result of these physical processes, the air that is diffusing through the firn experiences a certain degree of smoothing such that at any particular depth, the age of the air is not specific to any particular year but is representative of a spread of ages (*Schwander et al.*, 1993). The spread of ages increases with depth and depends on the individual firn column.

Firn air provides a continuous record of atmospheric composition which is ideal for reconstructing atmospheric time series from the present up to a century back in time (*Battle et al.*, 1996 and *Schwander et al.*, 1989). The porous structure of the firn enables large volumes of air to be extracted and sampled for a wide range of trace gas analyses.

1.6 Scientific rationale and research questions addressed in the current study

Since the publication by *Schwander et al.* (1989), many studies have used firn air to reconstruct the atmospheric time series of trace gases. This has increased the scientific knowledge of these compounds by bridging the age gap between direct atmospheric observations and any ice core records (*Etheridge et al.*, 1998). Several of these studies include *Butler et al.* (1999) who obtained records for CFCs and chlorocarbons from firn air at the South Pole (Antarctica), Siple Dome and Tunu (Greenland). *Sturges et al.* (2001a and 2001b) presented reconstructed atmospheric time series for several organobromine gases ($CHBr_3$, CH_2Br_2, $CHBrCl_2$, $CHBr_2Cl$ and CH_2BrCl) and carbonyl sulfide (COS) in firn air sampled at Dronning Maud Land, and the Dome C site. Mixing ratios of CO_2, CFCs and chloroform have been reported by *Trudinger et al.* (2004, 2002 and 1997). *Sturges et al.* (2012 and 2000) presented atmospheric records of SF_6 and SF_5CF_3 from northern (including the NEEM site) and southern hemispheric firn air. *Aydin et al.* (2004) presented time series of CH_3Cl from Antarctic firn air. *Worton et al.* (2007) presented the long term atmospheric time series of CF_4 and C_2F_6 in Berkner Island and NGRIP firn air, whilst *Laube et al.* (2012 and 2008) reported the time series of n-C_4F_{10}, n-C_5F_{12}, n-C_6F_{14}, n-C_7F_{16} and HFC-227ea from the NEEM site. There are currently no published northern and southern hemispheric time series from firn air of most of the chlorocarbon and bromocarbons. The majority of the published atmospheric time series for the fluorinated greenhouse gases have used the air firn measures produced in the current study.

In this study, the reconstructed atmospheric time series of the chlorocarbons, bromocarbons and the fluorinated greenhouse gases from northern and southern hemispheric firn air are discussed in Chapter 3, 4 and 5. Comprehensive literature reviews of the individual compounds are also presented in the individual Chapters. Some of the key research questions that form the scientific basis of the current study include:

- Can firn air measurements combined with a multi-site firn model be used to reconstruct both northern and southern hemispheric atmospheric time series of traces gases?

- What effects have chlorocarbons and bromocarbons had on the atmosphere in the 20th and early 21st centuries?

- What effects have the fluorinated long-lived greenhouse gases had on the atmosphere in the 20th and early 21st centuries?

- How have the emissions rates of these compounds varied in the 20th and early 21st centuries?

- What has been the relative importance of naturally emitted trace gases to the atmosphere compared with purely anthropogenic emitted trace gases in the 20th and early 21st centuries?

Chapter 2: Methodology

2.1 Introduction

2.2 Firn air extraction (NEEM Site)

2.3 Trace gas measurements

2.4 Calibration

2.5 Atmospheric modelling

2.5.1 Firn modelling

2.5.2 Atmospheric time series produced using the LGGE method

2.5.3 Atmospheric time series produced using iterative dating methods

2.5.4 Emissions estimates

2.5.5 2-Box atmospheric model

2.1 Introduction

In Chapter 1 it was highlighted that measurements of trace gases are needed to obtain a full understanding of the chemical composition of the atmosphere. The development of high precision measurements from firn air samples at the University of East Anglia (UEA) was an essential prerequisite for this study.

Details of the firn air extraction methodology and details of the North Greenland Eemian Ice Drilling (NEEM) firn site are presented in Section 2.2. The methodology for halocarbon measurements from NEEM firn air samples is presented in Section 2.3, with the firn air / atmospheric modelling used in this study presented in Section 2.4.

2.2 Firn air extraction (NEEM Site)

Firn air can be used as an archive of old air and when extracted and analysed for its gas composition, the firn record can potentially produce a time series dating back to the early twentieth century. The advantages of using firn air to reconstruct atmospheric time series, are that relatively large volumes of samples (compared to ice core sampling) are collected. Therefore a number of repetitive measurements can be made on the same sample which helps to improve the analytical precision. Also the firn air samples represent a spectrum of different ages which can be analysed in a short span of time, whereas real-time observations measured over a long period have a problem with potential drifts in instrumental analysis or reference scales. Nevertheless the atmospheric time series from firn air are subjected to several uncertainties pertaining to the structure of the firn and the physical processes that modifies the trace gas concentrations.

In this study firn air samples collected from the NEEM firn site, were measured for a number of trace gases. These observations along with measurements from previous firn air measurements from other northern hemispheric firn sites, North Grip (NGRIP) and Devon Island (DI), as well as from southern hemispheric firn sites, Dronning Maud Land (DML) and Dome Concordia (DC), were used to reconstruct the atmospheric time series of these compounds. The general properties of these firn air sites can be found in Table 2.1.

Further details of the NGRIP site can be found in *Worton et al.* (2006) and *Reeves et al.* (2005). Information on the Devon Island, Dome C and DML sites is contained in *Sturges et al.* (2001a), with the sampling procedures at these sites presented in *Sturges et al.* (2001a) and *Schwander et al.* (1993).

Table 2.1: General properties of firn air drill sites.

	Northern Hemisphere			Southern Hemisphere	
Firn Sites	NEEM	NGRIP	DI	DC	DML
Drill date	July. 2008	July. 2001	April. 1998	Jan. 1999	Jan. 1998
Location	77° 27’ N 51° 3’ W	75° 10’ N 42° 30’ W	75° 20’N 82° 08’W	75° 10’ S 123° 35’ E	77° S 10° W

NEEM is an international ice core and firn air research project aimed at retrieving an ice core and firn air samples from North-West Greenland. The project logistics was managed by the Centre for Ice and Climate, Denmark, and the air support is carried out by US ski equipped Hercules managed through the US Office of Polar Programs, National Science Foundation**.** The co-ordinates of the NEEM sites are 77.445°N, 51.066°W, 2484 m.a.s.l with the main camp infrastructure being constructed during the 2008 season (Figure 2.1) (*Schwander et al.*, 2008).

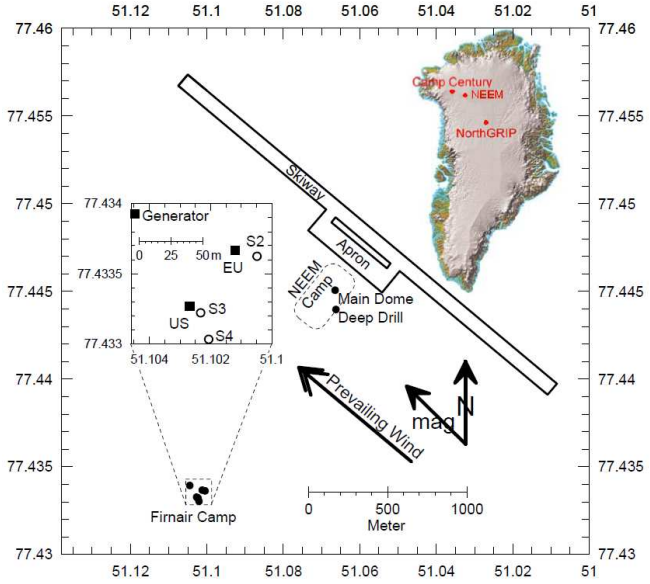

Figure 2.1: Location of NEEM and firn-air sampling sites (Image courtesy of Jakob Schwander)

An automatic weather station was located 7 km away from the main NEEM camp. This weather station indicated that the prevailing wind direction at the site was from 130 degrees, with an average atmospheric pressure of ~745 hPa. The climatic data of the site indicates that the annual mean temperature was -28 °C (from downhole measurements) and an ice accumulation rate of 224 mm yr^{-1} (*Schwander et al.*, 2008).

The firn air sampling was located at 77.43 °N, 51.10 °W, which was 1.5 km SW (220°) from the main camp on the edge of the NEEM clean air sector (Figure 2.1). This location was selected so

that the sampling would avoid contamination from the main camp (e.g. generator and vehicles). This was achieved by going up wind of the prevailing wind. The sampling also had to be at least 1 km away from the skiway, however it still needed to be a reasonable distance to the main camp in order to limit the time needed for movement of equipment and personnel. The sampling also need to take place outside of the designated clean sector, with was designated as a 90 degree sector between SE and SW. The generator for the firn sampling was placed 80 m downwind inorder to minimize air contamination. Vehicles were parked near the generator and within the last 80 m all equipment was transported by manhauling.

The main sampling was done from 2 downholes (EU: S2 and US: S3) separated by 63.5 meters (Figure 2.1). In this study only measurements from the EU : S2 will be reported. The downholes were drilled with a diameter of 103.6 mm using a Danish electromechanical shallow drill. This drill produces an ice core of 78 mm diameter. In order to have an undisturbed surface for the first sampling levels, the first 10 m were drilled with a hand auger which produced the same diameter hole and core. The EU hole was drilled in 17 days between the 14th and 30th of July 2008, with a maximum depth of 86 m (Table 2.2) (*Schwander et al.*, 2008).

Two separate firn air sampling systems were used for the EU and US firn air extractions. Both sites were powered by one 50Hz generator, which was changed on the 25th of July due to a slight problem with the voltage regulator. The sampling procedure for trace gases was similar to that used during previous projects (*Sturges et al.* 2001b and *Schwander et al.* 1993) in that the hole was drilled to a certain depth level. The exact depth was determined using a measuring tape. Immediately afterwards, the bladder was lowered and inflated and the gas pumps were started. The CO_2 mixing ratio was monitored by a MAIHAK CO_2 analyzer to check the quality of the air pumped from the firn. Filling of the 3 l SilcoCans was started after the CO_2 mixing ratio reached a constant level. The sample flasks were then generally stored outside of the shelter in the original boxes. The Bern bladder assembly used for the extraction of firn air is shown in Figure 2.2. The outside diameter of the bladder was 95 mm, leaving a 4.3 mm clearance with the hole wall (*Schwander et al.*, 2008).

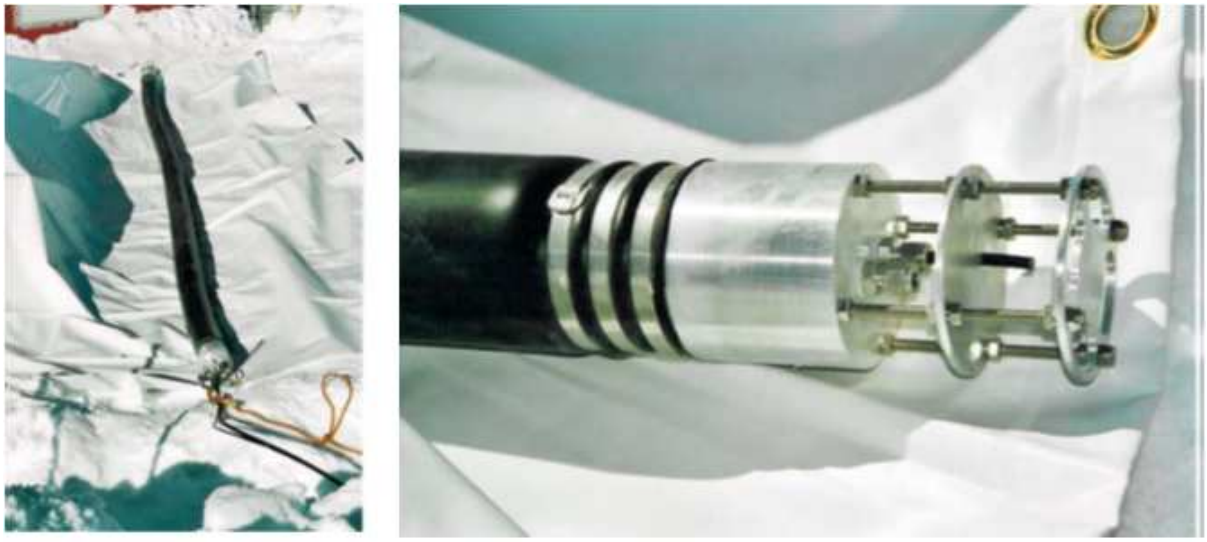

Figure 2.2: Bern Bladder: Left: 4-meter butyl bladder. Right: Lower end-cap. The air from above the central disk (Bender baffle) is in general vented to the atmosphere (reduce potential contamination from bladder). SYNFLEX-1300 tube ends were plugged with small amount of glass wool to prevent ice dust to enter. (Image courtesy of Jakob Schwander)

The tubing and bladder were leak-tested, with slight changes in pressure during these tests being taken as artefact of the pressure gauges and not a leak in the system. This conclusion was supported by a breathing air test on the fittings while analysing for CO_2 which showed no signs of leaks. The bladder reached the diameter of the hole with an overpressure of 0.1 to 0.2 bar. The exact pressure was dependent upon the temperature and relaxation time. Tests then showed that the bladder formed an air tight seal at pressures above 0.2 bar. During sampling the bladder was pressurised to an overpressure of 0.35 bar, apart from at the lowest level, when an overpressure of 0.4 bar was used (*Schwander et al.*, 2008). The hole was drilled about 18 m from the (University of Bern) firn gas pumping equipment (Figure 2.3). The length of tubing used was ~120 m, resulting in a maximum sample depth of 100 m.

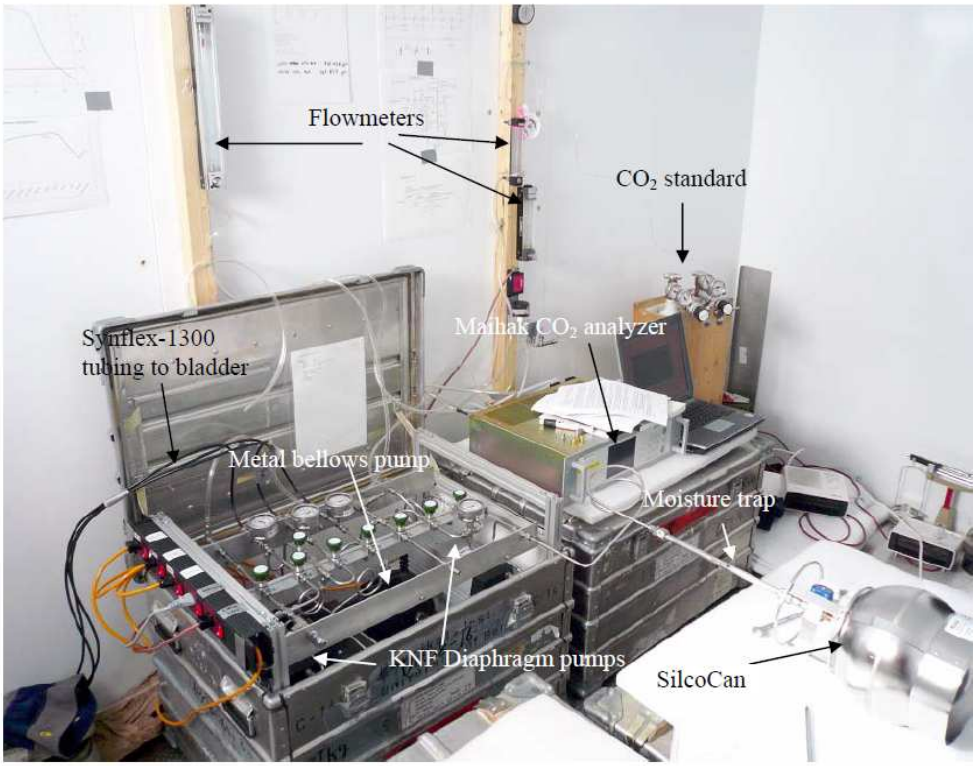

Figure 2.3: (University of Bern) Firn gas pumping equipment. The moisture trap was not used for the UEA samples (Image courtesy of Jakob Schwander).

The samples were filled according to the instructions of the participating laboratories. The sampling method used for the samples collected for this study were similar to those used by other laboratories. However the $Mg(ClO_4)_2$ water trap was not used for the UEA samples (Figure 2.3). This was to make sure that no traces gases were scrubbed from the sample. The samples were filled into 3 l SilcoCans that had been evacuated and baked out at 100 ^{0}C for 24 hours, and then filled with 2 bar Oxygen Free Nitrogen (OFN), before being sent to Greenland. After the SilcoCans were attached to the firn gas pumping equipment, they were evacuated, then twice filled to 1 bar over ambient before being evacuated again. Finally the SilcoCans were filled to 2.8 bar (40 psi) at a constant flow rate of ~ 5 l min^{-1}.

A total of 34 firn air samples were taken for this study between the 15th and the 29th of July 2008 (Table 2.2). Also 10 atmospheric samples were taken on three different days (16th, 17th and 29th of July 2008) during the sampling period. No serious problems were recorded during the sampling produce. However, the CO_2 concentrations at 75.9 m and 77.75 m (*Schwander et al.*, 2008), were slightly higher than expected. This was most likely due to the interconnecting layers within the firn porous structures. As the number of interconnections decrease with depth, the probability of interconnections to higher strata is larger than to deeper strata. Therefore the average sampling depth is most likely to be closer to the surface than the actual depth of the sample inlet.

Table 2.2: Sampling depths and collection date of the UEA samples

Sample No.	Depth (m)	Collection Date
1	Surface	16/07/2008
2	Surface	16/07/2008
3	Surface	17/07/2008
4	Surface	17/07/2008
5	Surface	17/07/2008
6	Surface	29/07/2008
7	Surface	29/07/2008
8	Surface	29/07/2008
9	Surface	29/07/2008
10	Surface	29/07/2008
11	2.50	15/07/2008
12	4.90	16/07/2008
13	4.90	16/07/2008
14	7.55	16/07/2008
15	10.10	17/07/2008
16	14.80	17/07/2008
17	19.75	18/07/2008
18	19.75	18/07/2008
19	27.54	18/07/2008
20	34.72	20/07/2008
21	42.42	21/07/2008
22	42.42	21/07/2008
23	50.00	21/07/2008
24	54.90	21/07/2008
25	57.40	22/07/2008
26	57.40	22/07/2008
27	59.90	22/07/2008
28	61.95	23/07/2008
29	61.95	23/07/2008
30	63.85	23/07/2008
31	65.75	23/07/2008
32	65.75	23/07/2008
33	68.05	24/07/2008
34	68.05	24/07/2008
35	70.05	24/07/2008
36	70.05	24/07/2008
37	72.00	25/07/2008
38	72.00	25/07/2008
39	74.08	25/07/2008
40	74.08	25/07/2008
41	75.90	27/07/2008
42	75.90	27/07/2008
43	77.75	27/07/2008
44	77.75	27/07/2008

2.3 Trace gas measurements

Trace gases (CH_3Cl, $CHCl_3$, CH_2Cl_2, CCl_2CCl_2, CH_2ClCH_2Cl, C_2H_5Cl, $CHClCCl_2$, CH_3Br, $CHBr_3$, CH_2Br_2, CH_2BrCH_2Br, C_2H_5Br, CH_2BrCl, $CHBr_2Cl$, $CHBrCl_2$, $CF_3CHBrCl$, SF_6, SF_5CF_3, n-C_4F_{10}, n-C_5F_{12}, n-C_6F_{14} and n-C_7F_{16}, HFC-32) were measured in firn air samples from NEEM firn site. The methodology for the analysis of trace amounts of atmospheric halocarbons is well established at UEA. A brief description is included below and further details can be found in *Laube et al.* (2012), *Oram et al.* (2011) and *Laube et al.* (2010).

The trace gas measurements in this study were performed on a Waters® Micromass® AutoSpec PremierTM Mass Spectrometer (MS). This instrument uses electron ionization (EI) and has double-focusing electric sectors and a magnetic sector in an EBE configuration which provides measurements that have high sensitivity, high resolution and low background noise. The first electric sector has de-magnifying optics that give high resolution and sensitivity whereas the second electric sector improves abundance sensitivity by filtering unwanted metastable ions and reducing background noise. The mass spectrometer was coupled with an Agilent 6890 gas chromatograph, which was used to separate the analytes.

An in depth analysis of Gas Chromatography (GC) and the principles of Gas Chromatography-Mass Spectrometry (GC-MS) is beyond the scope of this study. A brief description of the techniques I used in this study are included below and further details can be found in *Heard* (2006) and *Skoog* (2004)

In gas chromatography, a mobile phase, known as the carrier gas, transports components of a gas mixture to be separated through or over a stationary phase (column), separating them according to differences in the rates of migration. In this study I used an Agilent 6890 gas chromatograph with an Agilent GS- GasPro column (length 30 m, ID 0.32mm). The GC was run in "constant flow" mode of 2.0 ml min^{-1}. In "constant flow" mode, inlet pressure increases automatically to maintain constant outlet flow rate as the oven temperature increases during the run. Constant flow mode reduces run time and ensures that flow-sensitive detectors see a constant column effluent flow. The carrier gas used in this study was research grade helium. Table 2.3 below shows the temperature programme for the GC.

Table 2.3: Temperature Programme for the GC

Stage	Start Time (mins)	End Time (mins)	Initial Temp (˚C)	Final Temp (˚C)	Rate (˚C/min)
1	0.00	2.00	- 10	- 10	0
2	2.00	23.00	- 10	200	10
3	23.00	26.00	200	200	0

After the samples have been separated by the GC, they are introduced in to the ion source of the MS. In the ion source, the analytes eluting from the GC undergo electron ionisation, which produces molecular ions and ion fragments. The initial step of electron ionisation is that the molecule (e.g. SF_6) gains a high energy electron and produces the $SF_6^{+\bullet}$ molecular ion:

$SF_6 + e^- \rightarrow SF_6^{+\bullet} + 2e^-$ (Equation 1)

Then due to sufficient excess energy the charged $SF_6^{+\bullet}$ ions may undergo further fragmentation into lower mass ions by losing one or more fluorine atoms. For example, the loss of one F atom will produce a SF_5^+ ion:

$SF_6^{+\bullet} \rightarrow SF_5^+ + F^\bullet$ (Equation 2)

This would give a peak with mass 127 in the mass spectrum in addition to the molecular ion peak at mass 146. Similarly, peaks at masses 108 and 89 may also be present, due to SF_4^+ and SF_3^+ ions respectively. These ions are then focused and accelerated towards the magnetic sector by a series of electrostatic slits and then on to a photomultiplier tube for detection. The MS was run in the Selective Ion recording (SIR) mode, in which the mass analyser is set to pass only ions of a particular mass to charge ratio (m/z) at a set time. Table 2.4 shows the SIR programme used in this study.

As well as EI, this study also used chemical ionisation in combination with gas chromatography to measure the Halons from the firn air samples. In chemical ionisation, ions are produced through the collision of the molecule to be analysed with primary ions present in the source. In the EI method, the ions tend to acquire a large amount of excess energy, which leads to additional fragmentation. However, in CI technique, the ions acquire less energy which leads to less fragmentation and therefore is known as a "softer" ionization technique (*Heard*, 2006). In CI, both positive ions and negative ions can be produced. In this study only negative ionisation was used. The reactant gas ions are created by leaking a reactant gas into an ion

source where they interact with an electron beam to produce primary ions. In this study methane was used as the reagent. The reagent ions then react with the sample molecules of interest to produce ions. The advantages of this method, is that only a few negative ions are produced, which results in a low signal background and thus a clear peak shape. This helps with the identification of peaks and the precision of the measurements. Also the mass spectrum produced is easily decipherable, especially for complex sample mixtures (e.g. ambient air). This means that trace gases of interest in the sample can be detected preferentially over the more abundant species (e.g. N_2 and O_2). The disadvantage of this method, is that there is poor specificity between the analytes. This is a result of the CI producing the same ions and thus the mass to charge ratio for all chlorine or bromine substances (e.g. ^{79}Br and ^{81}Br for bromine substances). Therefore analytes can only be identified by their retention time.

Table 2.4: Experimental SIR programme used in the GC-MS analysis of compounds in this study

Function #	Start Time (min)	End Time (min)	Compound	Retention Time (min)	Quantification m/z	Qualification m/z	Channel Time (ms)	Monitored Ion
1	4.00	7.00	SF_6	4.75	126.96410		80.0	SF_5^+
			$C_{16}F_{34}$	Lock Mass	113.13300		40.0	$C_8H_{17}^+$
2	7.00	8.70	CH_2F_2	7.90	51.00460		60.0	CHF_2^+
						52.01250	60.0	$CH_2F_2^+$
			$C_{16}F_{34}$	Lock Mass	57.07040		40.0	$C_4H_9^+$
3	8.70	11.50	SF_5CF_3	9.80	88.96730		60.0	SF_3^+
			CFC - 12	10.20	86.96270		40.0	$CF_2{}^{37}Cl^+$
						100.96410	60.0	$CF^{35}Cl_2^+$
			$C_{16}F_{34}$	Lock Mass	99.11740		40.0	$C_7H_{15}^+$
4	11.50	12.40	CH_3Cl	11.90	49.99230		5.0	$CH_3{}^{35}Cl^+$
						51.98940	40.0	$CH_3{}^{37}Cl^+$
			$C_{16}F_{34}$	Lock Mass	57.07040		20.0	$C_4H_9^+$
5	12.40	14.15	CH_3Br	13.80	93.94180		60.0	$CH_3{}^{79}Br^+$
						95.93980	60.0	$CH_3{}^{81}Br^+$
			$C_{16}F_{34}$	Lock Mass	99.11740		40.0	$C_7H_{15}^+$
6	14.15	15.50	CFC-11	14.60	101.93610		10.0	$CF^{35}Cl_2^+$
						102.93320	10.0	$CF^{35}Cl^{37}Cl^+$
			$C_{16}F_{34}$	Lock Mass	99.11740		20.0	$C_7H_{15}^+$
7	15.50	17.00	C_2H_5Cl	16.00	64.00800		20.0	$C_2H_5{}^{35}Cl^+$
			CH_2Cl_2	16.30	83.95340		20.0	$CH_2{}^{35}Cl_2^+$
						85.95040	20.0	$CH_2{}^{35}Cl^{37}Cl^+$

Function #	Start Time (min)	End Time (min)	Compound	Retention Time (min)	Quantification m/z	Qualification m/z	Channel Time (ms)	Monitored Ion
			$C_{16}F_{34}$	Lock Mass	85.10170		20.0	$C_6H_{13}^+$
8	17.00	17.60	CFC-113	17.35	100.93610		10.0	$C^{35}Cl_2F^+$
			C_2H_5Br	17.54	107.95750		60.0	$C_2H_5{}^{79}Br^+$
						109.95540	60.0	$C_2H_5{}^{81}Br^+$
			$C_{16}F_{34}$	Lock Mass	99.11740		20.0	$C_7H_{15}^+$
9	17.60	18.70	CH_2BrCl	17.90	129.90080		100.0	$CH_2{}^{81}Br^{35}Cl^+$
			$CHCl_3$	18.00	82.94550		20.0	$CH^{35}Cl_2^+$
						84.94260	20.0	$CH^{35}Cl^{37}Cl^+$
			$C_{16}F_{34}$	Lock Mass	99.11740		40.0	$C_7H_{15}^+$
10	18.70	19.25	$CF_3CHBrCl$	19.10	156.9514		80.0	$CFC^{79}Br^{35}Cl^+$
			CHClCCl2	19.35	129.91440		40.0	$CH^{35}ClC^{35}Cl_2^+$
						133.90850	40.0	$CH^{35}ClC^{37}Cl_2^+$
			$C_{16}F_{34}$	Lock Mass	141.16430		60.0	$C_{10}H_{21}^+$
11	19.25	20.10	CH_2Br_2	20.00	92.93400		20.0	$CH_2{}^{79}Br^+$
						94.93190	20.0	$CH_2{}^{81}Br^+$
			$CHBrCl_2$	20.07	82.94550		20.0	$CH^{35}Cl_2^+$
						84.94260	20.0	$CH^{35}Cl^{37}Cl^+$
			CH_3CCl_3	20.11	96.96120		20.0	$CH_3C^{35}Cl_3^+$
			$C_{16}F_{34}$	Lock Mass	85.10170		20.0	$C_6H_{13}^+$
12	20.10	21.00	CCl_2CCl_2	21.00	93.93770		40.0	$C_2{}^{35}Cl_2^+$
						95.93480	40.0	$C_2{}^{35}Cl^{37}Cl^+$
			CH_2ClCH_2Cl	21.00	61.99230		60.0	$CH_2{}^{35}ClCH^+$
						63.98940	60.0	$CH_2{}^{37}ClCH^+$
			$C_{16}F_{34}$	Lock Mass	71.08610		30.0	$C_5H_{11}^+$

Function #	Start Time (min)	End Time (min)	Compound	Retention Time (min)	Quantification m/z	Qualification m/z	Channel Time (ms)	Monitored Ion
13	21.00	22.50	$CHClBr_2$	21.80	128.89300		100.0	$CH^{35}Cl^{81}Br^+$
						126.86500	80.0	$CH^{35}Cl^{79}Br^+$
			$C_{16}F_{34}$	Lock Mass	127.14860		60.0	$C_9H_{19}^+$
14	22.5	26.00	$CHBr_3$	23.60	172.84250		100.0	$CH^{79}Br^{81}Br^+$
						170.84450	20.0	$CH^{79}Br_2^+$
			CH_2BrCH_2Br	23.60	106.94760		160.0	$CH_2{}^{79}BrCH_2^+$
						108.94760	20.0	$CH_2{}^{81}BrCH_2^+$
			$C_{16}F_{34}$	Lock Mass	141.16430		60.0	$C_{10}H_{21}^+$

The mass spectrometer was tuned and mass calibrated every day before any measurements were made. This was achieved by introducing hexadecane ($C_{16}F_{34}$) as a reference gas into the source, before tuning the electron energy and emission current to maximise ionisation efficiency. The ion repeller and the focusing lenses were also adjusted to optimise the peak shape and intensity. After this tuning was competed it was saved in the tuning file, before the mass calibration procedure were carried out for the SIR programme. In the mass calibration process, the accelerating voltage is scanned over the selected mass range and the major peaks matched with the tuning file. This ensures that the peak positions and the masses are correctly identified with each function in the SIR programme being calibrated separately. A lock mass is used to provide corrective measures to account for small changes in the peak position that can be caused by slight fluctuations in the magnetic field during SIR measurements. As a result a mass corresponding to a hexadecane ion is included in each SIR function as a lock mass (Table 2.4). The computer software makes sure that the centroid of the lock mass peak is monitored. Therefore if the lock mass peak position changes then the mass calibration is automatically corrected accordingly for all the masses monitored in that function.

Before the samples were injected into the GC-MS they were pre-concentrated to increase the sensitivity of the measurements. The main process of the pre-concentration, is to separate the measured compounds from the bulk of the air sample (primarily N_2 and O_2) by cryogenic trapping. In this study the cryogenic trapping consisted of a 1/8" stainless steel tubing packed with Hayesep D, 80/100 mesh (HD trap) and immersed in a ethanol and dry ice (-72 ˚C) mixture. After pre-concentration, the compounds on the HD trap were thermally desorbed using boiling water (100 ^{0}C) and injected into the analytical column of the GC.

There was a possibility that samples were not consistently being fully flushed off the HD trap and onto the column especially if there were large concentrations introduced. To establish the capacity of the HD trap, several measurements of different volumes of a sample were compared to different volumes of the standard gas were carried out. Figure 2.4 shows that CH_3Br peak area is linearly correlated with the volume of sample injected up to 250 ml of sample volume, indicating that CH_3Br is being fully flushed off the HD trap. However $CHBr_3$ peak area is not linearly correlated with the volume of sample injected, indicating that $CHBr_3$ was not being fully flushed off the trap and into the column of the GC-MS.

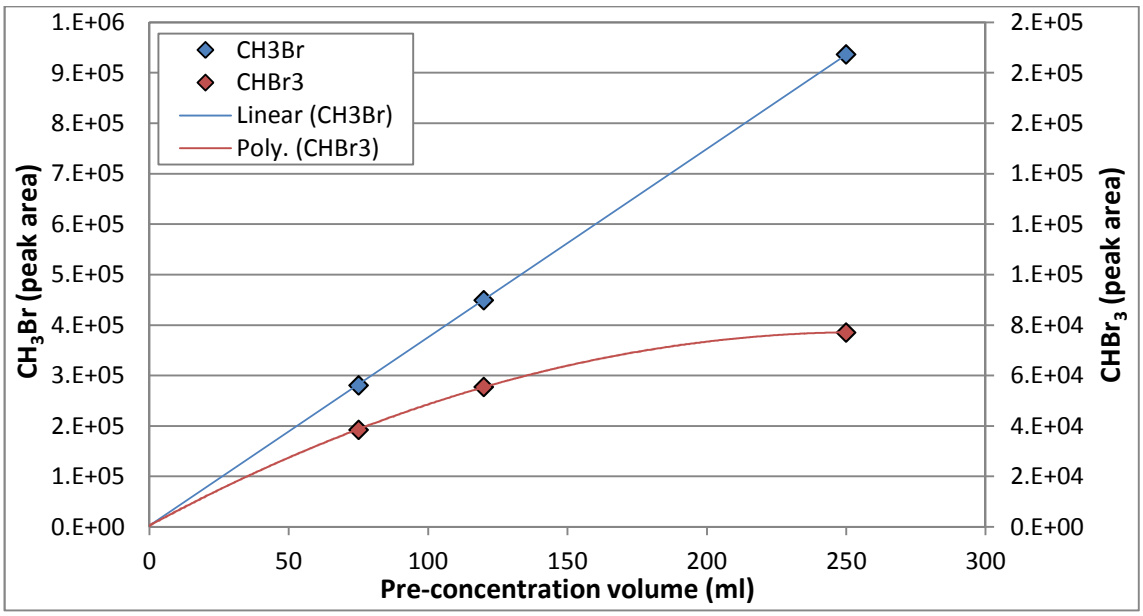

Figure 2.4: Sampling linearity test for CH_3Br (blue point) and $CHBr_3$ (red points) trapping.

A schematic of the manual inlet system used for GC-MS analysis during this work is shown in Figure 2.5. The inlet system consists of Nupro valves used to isolate the inlet line from the vacuum, glass tubing packed with magnesium perchlorate (MPC) to remove any water vapour from the samples, the HD trap for sample pre-concentration and a manually operated Valco 6 port Valve (*Homan et al.*, 2010) for injecting samples into the GC. The flow rate of sample through the pre-concentration trap was controlled by a needle valve. A consistent flow rate is important in order to achieve efficient trapping and to avoid sample breakthrough. A reference canister was located downstream of the trap and had a volume of 6 L. The pressure was measured downstream by a baratron. The reference canister prevented any back diffusion of lab air into the inlet system and also made it possible to measure the sample volume. Therefore once the desired sample volume was collected then the HD trap was isolated from the sample flow. Then the Valco valve was switched into the sample injection position and the ethanol and dry ice dewar was swapped with a dewar containing boiling water to desorb the analytes off the HD trap. After sample injection, the entire line including the reference canister was evacuated.

Figure 2.5: Schematic diagram of the inlet and pre-concentration set-up for the GC-MS

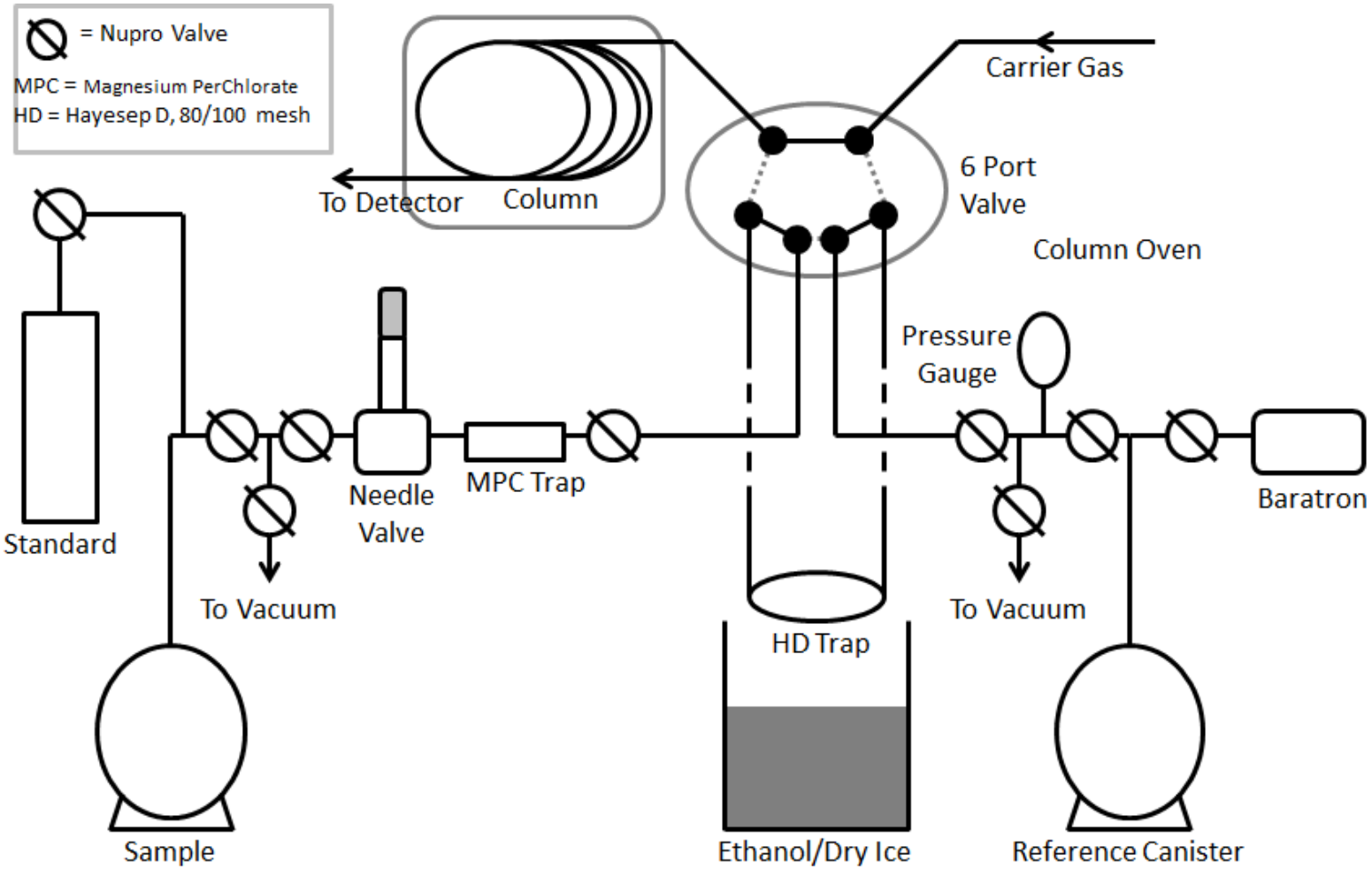

At the beginning of each measurement day, the reference standard (AAL-071170) held at UEA was analysed to allow for the instrument to settle down. Once the instrument response was stable, a He blank was run to show if there were any contaminants in the pre-concentration system or the GC-MS. After the He blank then a reference air standard was run, followed by 2 duplicate runs of the same sample and then another reference air standard run. This pattern of 2 duplicate runs of the same sample followed by a reference air standard run was then repeated up to end of the measurement day.

Peak areas were used to quantify each compound of interest in a sample. These peak areas were then calculated as a relative ratio to the average area of the working standard, and then multiplied by the concentration of that compound in the working standard (Table 2.3). During a measurement day the instrument response factor may change (known as instrumental drift), resulting in the working standard recording slight variations in area response values. Therefore data for every sample was corrected for this instrumental drift. The drift correction was applied by fitting a time dependent straight line between the peak areas of the reference standards measurement before and after the sample measurements. The sample peak areas were then normalised to this line by interpolating a correction factor. The precision of replicate measurements was further improved by correcting the peak areas for the differences between pre-concentration volumes.

The analysis of trace gases in firn air, archive air and in background air is well established at UEA (e.g. *Worton et al.*, 2006, *Reeves et al.*, 2005 and *Sturges et al.*, 2001). Peak identification was made based on retention time and the ions being monitored in each SIR function (Table 2.4). Below are the typical chromatograms of a SF_6 peak, CH_2Cl_2 peak and $CF_3CHBrCl$ peak (Figure 2.6).

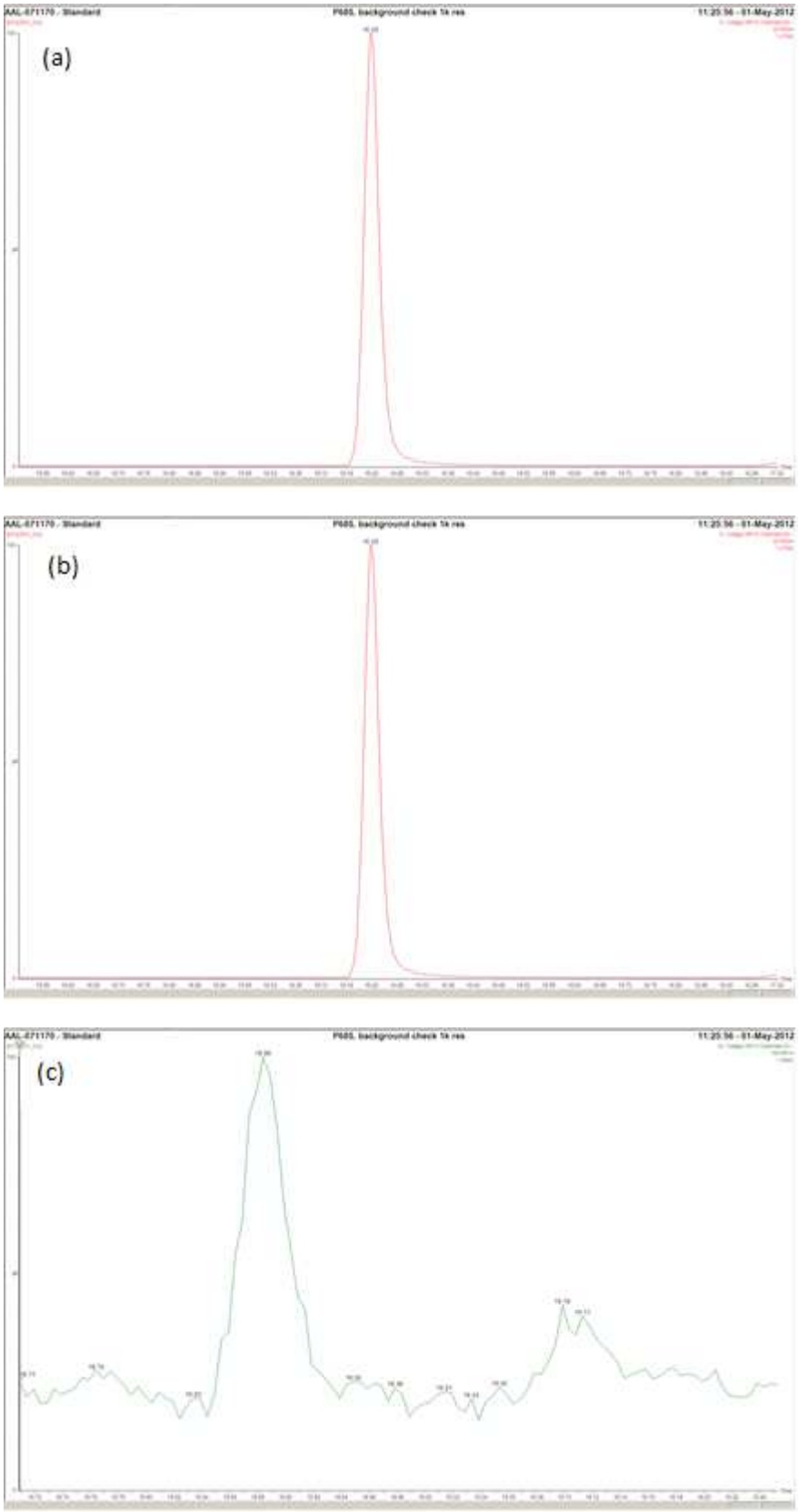

Figure 2.6: A typical chromatogram of (a) SF_6 peak (m/z = 126.96410, ppt = 5.89), (b) CH_2Cl_2 peak (m/z = 83.95340, ppt = 31.08) and (c) $CF_3CHBrCl$ peak (m/z = 156.9514, ppt = 0.007), monitored on in 250 ml of AAL-071170 standard.

The analytical precision of the sample measurements was calculated as the square root of the sum of the squares of one standard deviation (1 σ) of the replicate analyses at each sampling depth (either 2 or 4 measurements see Table 2.2 for details), 1 σ of the reproducibility of the standard on the measurement day and the 1 σ of the reproducibility of the He blank taken throughout the measurement process. The replicate analysis defines the 2 duplicate runs of the same sample that were taken next to each other during that days sampling process for every sample measured. The reproducibility of the standard is the taken as one standard deviation of all the standards measured throughout the day. The reproducibility of the He blank is taken a 1 σ of every He Blank measurement taken throughout the whole of the measurement procedure (10 in total).

The limit of detection is the lowest concentration that can be determined by an analytical method. In this study the detection limit was defined as the analyte concentration that has a signal three times the standard deviation of the blank/background signal. It should be noted that the detection limit varies, depending on the compound being analysed, the choice of monitored ion, the background noise, the ionising conditions and the volume of air sample analysed. Table 2.5 shows the typical value of the detection limit for each individual compound measured in this study, as well as the typical analytical uncertainties.

Table 2.5: The detection limits of the individual compounds based on 250 ml of standard air analysed and typical analytical uncertainties.

Compound	Detection limit (ppt)	Typical analytical uncertainties
CFC-11	0.061	0.5 %
CFC-12	0.094	0.6 %
CFC-113	0.015	1.3 %
CH_3Cl	3.377	0.5 %
$CHCl_3$	0.027	2.6 %
CH_2Cl_2	0.093	0.9 %
CCl_2CCl_2	0.026	1.3 %
CH_3CCl_3	0.026	1.0 %
CH_3Br	0.008	0.8 %
CH_2Br_2	0.013	1.8 %
CH_2BrCH_2Br	0.061	5.2 %
C_2H_5Br	0.010	6.1 %
CH_2BrCl	0.0004	4.7 %
$CHBrCl_2$	0.011	3.9 %
$CHClBr_2$	0.010	2.0 %
$CF_3CHBrCl$	0.0001	5.4 %
SF_6	0.002	0.6 %
SF_5CF_3	0.001	1.7 %

2.4 Calibration

All measurements were referenced to one working standard (AAL-071170) contained in a pressurised Aculife-treated aluminium cylinder. This standard was purchased from the National Oceanic and Atmospheric Administration (NOAA) and consists of a real air sample collected at Niwot Ridge, Colorado (40 ^{0}N) in 2006. In addition, the NOAA standard was pre-calibrated at NOAA-CMDL (Climate Monitoring and Diagnostic laboratory) for a number of compounds enabling us to report our values on the NOAA calibration scale. There have been a number of updates to the NOAA calibration scales since 2006. Therefore two other working standards purchased from NOAA were analysed against the AAL-071170 standard in April 2011, as well as other working standards used in the measurements of the other firn site samples. This was then used to update all compounds to the lasted calibration scale. This was also done to take into effect any drift in concentration with the standards, to make sure that all measurements where on the same calibration scale. The mixing ratios of various halocarbons in AAL-071170 used for calibration are shown in Table 2.6.

Table 2.6: Concentration of compounds in AAL-071170 reference standard

Compound	Scale	Scale year	AAL-071170 mixing ratio (ppt)	Scale uncertainty (ppt)
CFC-11	NOAA	1993	250.23	2.99
CFC-12	NOAA	2008	543.15	2.66
CFC-113	NOAA	2002	80.21	1.42
CH_3Cl	NOAA	2003	580.90	7.49
$CHCl_3$	NOAA	2003	8.68	0.33
CH_2Cl_2	NOAA	2003	31.08	0.96
CCl_2CCl_2	NOAA		2.61	0.16
CH_3CCl_3	NOAA	2003	16.43	0.49
CH_3Br	NOAA	2003	8.28	0.18
$CHBr_3$	NOAA	2003	4.35	0.65
CH_2Br_2	NOAA	2004	2.66	0.14
CH_2BrCH_2Br	UEA		0.03	0.003
C_2H_5Br	UEA		0.12	0.01
CH_2BrCl	UEA		2.69	0.25
$CHBrCl_2$	UEA		0.176	0.002
$CHClBr_2$	UEA		0.083	0.003
$CF_3CHBrCl$	UEA		0.007	0.0002
SF_6	NOAA	2006	5.89	0.10
SF_5CF_3	UEA		0.152	0.005

A schematic of the dilution system used to calibrate trace gases during this study, are shown in Figure 2.7. At the start of the calibration procedure the 2 ml sample loop (Figure 2.7a) was filled with the pure compound at low pressures (50 to 300 mbar). The sample loop was

connected to a six-port two-position Valco valve which was used to isolate the loop after filling. To stop loss of the compound due to condensation inside the dilution system, all parts except for the pressure sensors and the two 100-litre drums were heated to 80°C. The whole system (apart from the 2 ml sample loop) was then filled with Oxygen Free Nitrogen (OFN) to ~2 bars before being evacuated to about 1 mbar. This flushing was repeated 10 times to remove the residual compound from the system. The system was then again filled with OFN and the valve leading to an aluminium drum (filled with OFN at atmospheric pressure) was opened. When a constant flow (~300 ml min^{-1}) had been established into the drum, the sample loop with the pure gas was switched and the compound was flushed into the drum for about 4 minutes. The drum was then closed and a fan inside the drum turned on for 30 minutes to create a uniform gas mixture. This procedure was then repeated to add an internal reference compound (usually CFC-12) into the mixture. This reference compound had a known concentration within the working standard. After another 30 minutes of mixing, the drum was reconnected to a second similar system (Figure 2.7b). The second dilution step was carried out following a similar method to the first. At the start of the dilution step the 10 ml sample loop (Figure 2.7b) was filled with an aliquot of air out of the first dilution drum. The whole system (apart from the 10 ml sample loop) was flushing with OFN 10 times to remove the residual compound from the system. The aliquot of air from the first dilution drum was then flushed into the second aluminium drum for 4 minutes. Then after 30 minutes of mixing, an aliquot of air from the second dilution drum was measured on the GC-MS against the reference standard, to determine the concentrations of the target gas and reference compound in the standard.

Figure 2.7a: Schematic diagram of the first dilution system used to calibrate trace gases at UEA

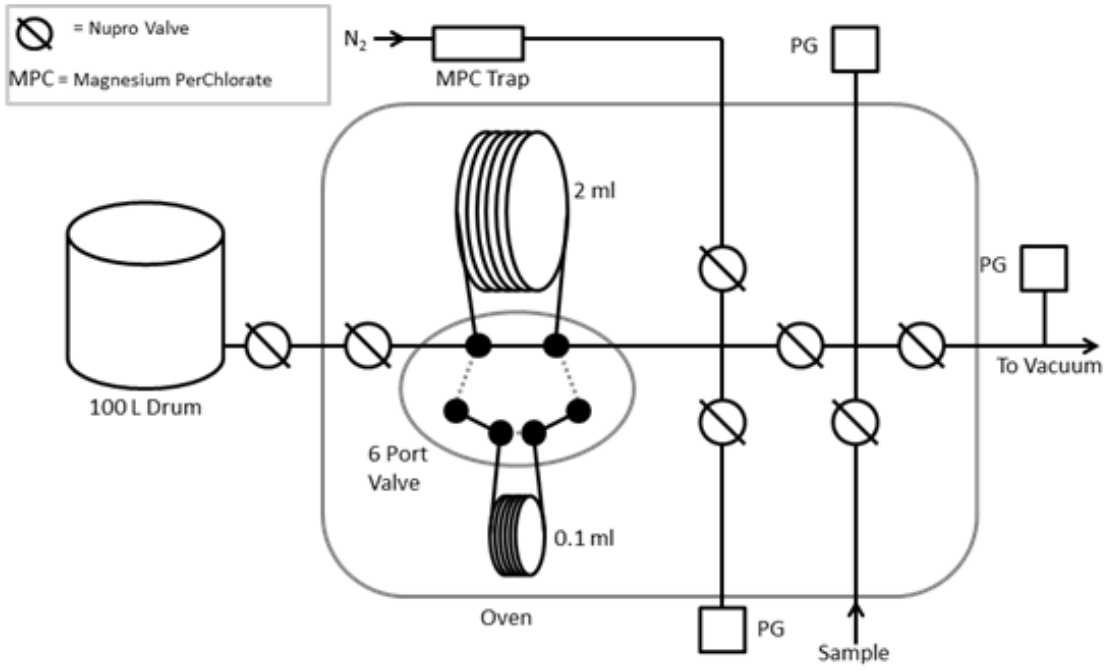

Figure 2.7b: Schematic diagram of the second dilution system used to calibrate trace gases at UEA

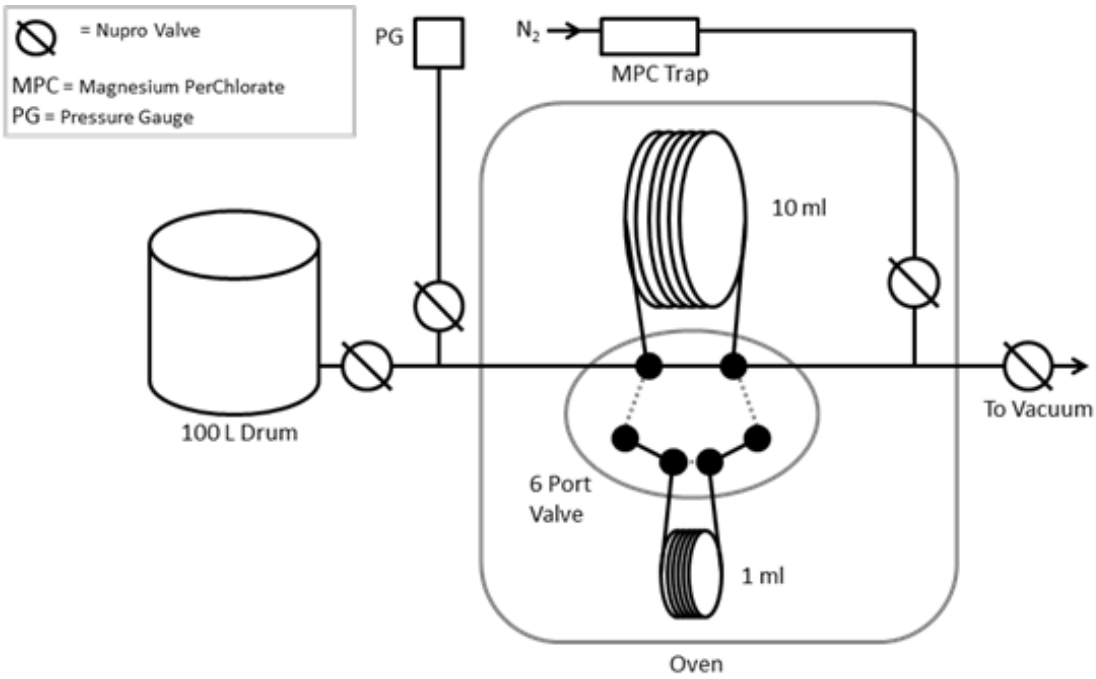

2.5 Atmospheric modelling

2.5.1 Firn modelling

A firn diffusion model is essential for interpreting the firn air trace measurements. The model is generally used as a dating tool to interpret the trace gas measurements with depth. The firn diffusion model used in this study was developed by the Centre National de la Recherché Scientifique - Laboratoire de Glaciologie et Géophysique de l'Environnement (CNRS-LGGE) in Grenoble France and a detailed description of this model is given in *Rommelaere et al.* (1997). This is a numerical model that simulates the movement of a gas through the firn column in firn pores that are still connected with the surface (open porosity) (*Rommelaere et al.*, 1997). The model incorporates factors that influence transport rate such as molecular mass and molecular diffusivity of the gas, gravitational fractionating, as well as the effect of the firn structure. This model incorporates the same physical processes as in the previous models developed by *Trudinger et al.* (1997) and *Schwander et al.* (1993) but it also models the effect of air trapping in ice bubbles at the bottom of the firn column, on the movement of the air within the firn (*Rommelaere et al.*, 1997).

The firn density profiles for the model were assumed to be in steady state, and that the sites have been climatically stable over the study period. Also each individual firn site was characterised through a tuning procedure to several site-specific and gas-related parameters. This tuning procedure was undertaken using the methods reported in *Buizert et al.* (2011) and *Witrant et al.* (2011).

It is important to characterise diffusion through the firn as this is the dominant mechanism by which variations in atmospheric composition are transferred into the firn (*Schwander et al.*, 1993). Diffusion is used as a generic term for processes that are well described by Fick's law. The diffusivity profile in the firn reconstruction is composed of two parts, molecular diffusion and macroscopic flow. The molecular diffusion is a microscopic process originating in the thermal motion of the molecules constituting the firn air (*Buizert et al.*, 2011). However, the eddy diffusion refers to the mass transfer caused by macroscopic flow patterns in the open porosity (*Buizert et al.*, 2011). The model used in the current study, was tuned by adjusting the effective diffusivity at each depth in order to optimise the agreement between the modelled and measured concentration of a selection of reference gases with a known atmospheric time series (*Buizert et al.*, 2011). In this study the model was tuned using an ensemble of ten reference tracers, to constrain the diffusivity reconstruction. These are shown in Table 2.7. The effective diffusivity is defined as an increasing function of open porosity or rather as a

decreasing function of depth and therefore does not take into account the effect of refrozen melt layers or other heterogeneities in the firn (*Martinerie et al.*, 2009).

Table 2.7: Ten reference tracers used to constrain the diffusivity reconstruction

Tracer	Measured By.
CO_2	NOAA, CSIRO, IUP
CH_4	NOAA, CSIRO
SF_6	NOAA, CSIRO, UEA*
CFC-11	UEA*
CFC-12	UEA*
CFC-113	UEA*
HFC-134a	UEA
CH_3CCl_3	UEA*
$\Delta^{14}CO_2$	ANSTO
$\delta^{15}N_2$	SIO

*I personally measured

A "best- estimate" of the atmospheric time series was reconstructed for each of the tracers used from direct atmospheric measurements from the NOAA and AGAGE sampling networks or archived air (e.g. *Geller et al.*, 1997). In addition, emission-based estimates from a 2-D atmospheric transport model that includes latitudinal source and sink distributions were used so in *Martinerie et al.* (2009). Together these were, used to achieve complete time coverage for SF_6 and the halocarbons from before the onset of direct atmospheric measurements. Also firn air and ice core measurements were used from the high accumulation Law Dome site, Antarctica (*Etheridge et al.*, 1998) and tree-ring measurements were used for the isotope atmospheric history of Carbon-14 (^{14}C) (*Reimer et al.*, 1997). The "best- estimate" of the atmospheric history of CFC-12 and CH_3CCl_3 produced by *Buizert et al.* (2011) with the corresponding depth profile measured at the NEEM site are shown in Figure 2.8.

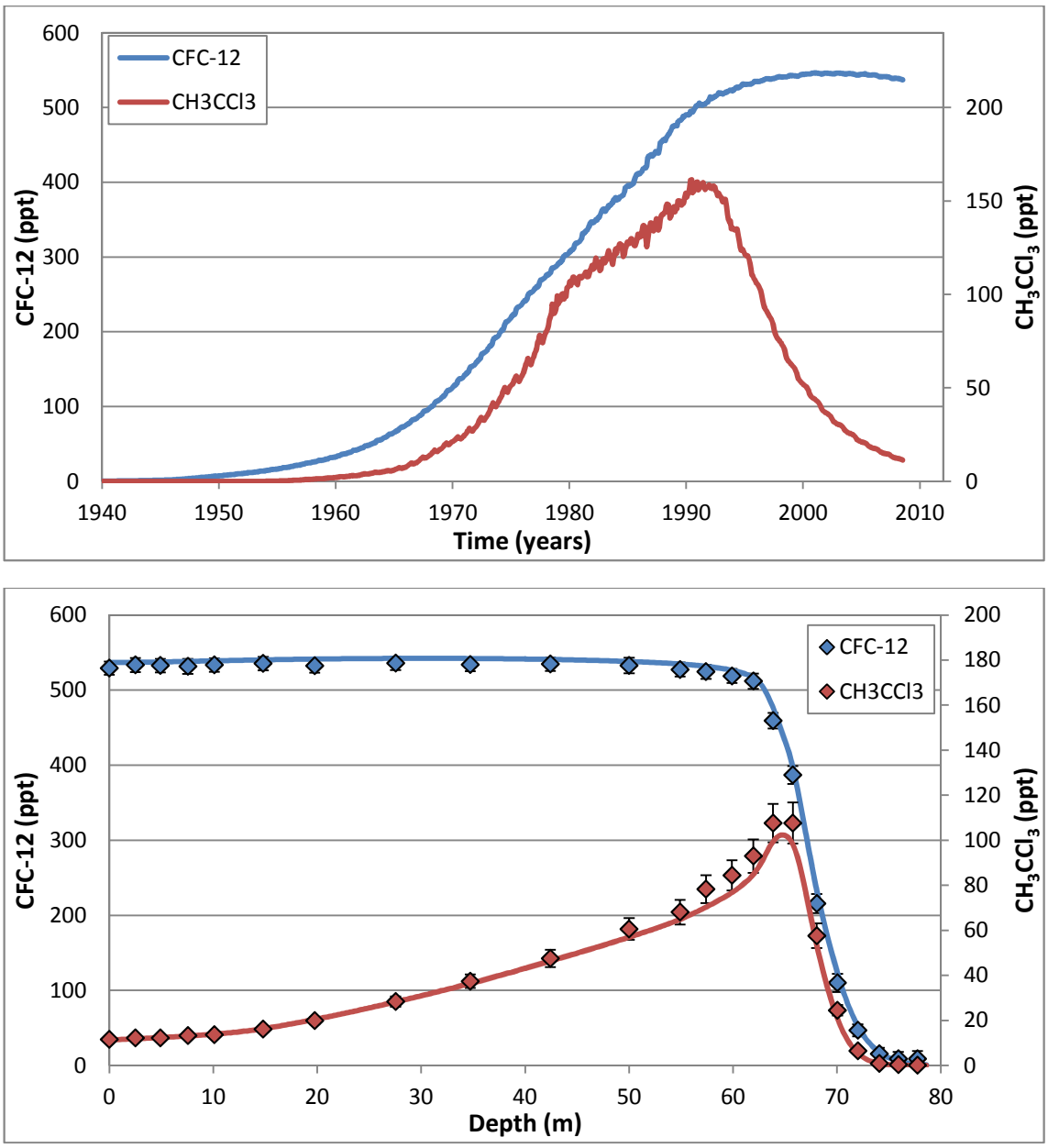

Figure 2.8: Top panel, "best-estimate" of the northern hemispheric atmospheric history of CFC-12 (blue line) and CH_3CCl_3 (red line) produced by *Buizert et al.* (2011). Bottom panel, depth profiles of CFC-12 (blue points) and CH_3CCl_3 (red points) concentration with depth at the NEEM firn site, compared with model simulations based on the "best-estimate" of the northern hemispheric atmospheric history indicated in the top panel. The error bars represent the 1 σ of the measurements.

Each of these tracers constrains the firn profile differently because of its unique atmospheric history and its free air diffusivity. This method also determines the uncertainties in both the measured data and the reference gas atmospheric time series so that weightings can be assigned to each of the tracers for the model tuning, as well as defining a root mean square criterion that can then be minimised in the tuning process. This multiple-tracer characterisation method of tuning is therefore an improvement over the commonly used single-tracer tuning method (*Buizert et al.* 2011).

After the effective diffusivity profile was obtained, the concentration depth profile of any gas could be modelled using a reference diffusion coefficient of CO_2. The different trace gases have different molecular masses (M_{gas}) and diffusion coefficients in air (D_{gas}), which results in different diffusion speed within the firn. Therefore, the reference diffusion coefficient of CO_2 can be applied to any another gas by scaling with D_{gas}/D_{CO2}. However, this does mean that any bias in the effective diffusivity is implicated in the data interpretation of all the gases. The diffusion coefficients for trace gases modelled in this study were estimated using a semi-empirical formula developed in terms of critical temperature (in K) and molar volumes (in cm^3 mol^{-1}) (*Chen and Othmer*, 1962). The values of M_{gas} and D_{gas}/D_{CO2} used in this study can be found in Table 2.8.

Table 2.8: Values of M_{gas} and D_{gas}/D_{CO2} used in this study

Compound	M_{gas} (g/mol)	D_{gas}/D_{CO2}
CFC-11	137.37	0.575
CFC-12	120.90	0.618
CFC-113	187.38	0.495
CH_3CCl_3	133.40	0.537
CH_3Cl	50.49	0.789
$CHCl_3$	119.38	0.595
CH_2Cl_2	84.93	0.709
CCl_2CCl_2	165.83	0.496
CH_2ClCH_2Cl	98.96	0.600
C_2H_5Cl	64.51	0.743
$CHClCCl_2$	131.39	0.504
CH_2Br_2	173.84	0.522
CH_2BrCH_2Br	98.96	0.540
C_2H_5Br	65.71	0.191
CH_2BrCl	129.38	0.559
$CHBrCl_2$	163.83	0.499
$CHClBr_2$	208.28	0.474
$CF_3CHBrCl$	197.38	0.465
SF_6	146.06	0.621
SF_5CF_3	196.06	0.467
C_4F_{10}	238.03	0.421
C_5F_{12}	288.03	0.367
C_6F_{14}	338.04	0.316
C_7F_{16}	388.04	0.297

2.5.2 Atmospheric time series produced using the LGGE method

The firn modelling methodologies used for the LGGE method have been briefly described earlier (see Section 2.5.1), with more information being given in *Buizert et al.* (2011) and *Witrant et al.* (2011). Further information on the scenario reconstruction method is given in *Martinerie et al.* (2009) and *Rommelaere et al.* (1997).

The main problem with producing atmospheric time series from firn air measurements is that mathematically the solution is under-determined, resulting in several possible solutions (*Rommelaere et al.*, 1997). The LGGE method obtains a solution that is between the simplest solution (which is a straight line that almost invariably does not match the firn data), and the most complex solution (which, although it nearly matches all the firn data, produces an oscillating and unrealistic scenario).

The model aims at finding a unique solution, which is intended to be the simplest/smoothest acceptable solution. This is addressed by adding a regularization term. The LGGE method always attempts to find a smooth solution, this is because diffusion within the firn column smoothes the atmospheric time series of a compound. Also, the errors in the firn air extraction and measurements and errors in the LGGE, means that it is unrealistic that an unsmoothed solution can be accurately produced. The method defines an acceptable solution as being directly related to the uncertainty of the firn data. This is because the uncertainties on the firn data help to define what is considered as an effect of an atmospheric signal and what is considered as noise within the firn data. Therefore the regularization term is formulated with an adjustable scalar, which is adjusted so that the output error of the method ($RMSD_{model-data}$) matches the uncertainty of the data (*Rommelaere et al.*, 1997). This means that the LGGE method is sensitive to relative errors (shifting one point with respect to another in the depth profile) but not to absolute errors (which shift the whole firn dataset with respect to an absolute scale). In multi-site modelling the method is sensitive to calibration shifts between datasets. Therefore in this study all compounds from the different firn sites were placed on the same calibration scale and were checked for calibration between measurements.

The regularization term imposes a smoothness on the scenario which prevents short-term mixing ratio variations (such as seasonal variations) to be modelled (*Wang et al.*, 2012). Thus, the effect of seasonality has to be dealt with by excluding the upper firn data that is influenced by seasonality from the inverted dataset. In this study, the evaluation of the effect of seasonality on the firn profile was assessed using atmospheric data as an input to the direct firn model.

Trace gas concentrations in firn air can only provide information about past atmospheric trends for a limited period of time, because the air gets trapped into closed bubbles in the deepest firn. The significant length of a reconstructed scenario from firn air measurements has been estimated in previous studies, based on the proportion of air of a given age present in the open versus closed porosity of the firn (*Bernard et al.*, 2006 and *Sowers et al.*, 2005). In this study, I define the significant length of the time series as the mean age at the depth for which the open/closed porosity ratio is 0.5 (76 m depth for NEEM). Following the Green's function approach, the age distributions of air with in the firn column can be established by studying the response of the model to a pulse in trace gas concentration (*Martinerie et al.*, 2009, *Trudinger et al.*, 1997 and *Schwander et al.*, 1993). It allows for the calculation of the probability of having a trace gas of a given age at a given firn depth. An example of this is given in Figure 2.9 which shows the Green's function of CCl_2CCl_2 at the NEEM site.

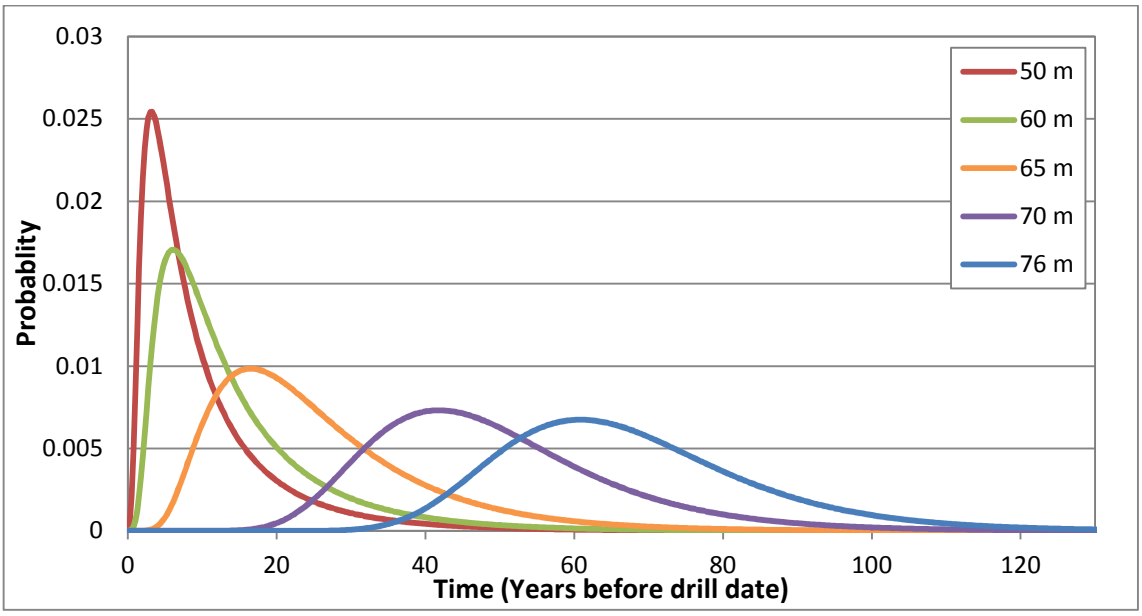

Figure 2.9: Green function for CCl_2CCl_2 in firn air at the NEEM site at a number of different depths.

Figure 2.9 shows that at 76 m the mean age of CCl_2CCl_2 is 60 years before the drill date. This results means that the time series produced in this study for CCl_2CCl_2 will be shown back to 1950. Once the length of time series was determined for each compound the LGGE method was used in single site mode to produce time series from the individual firn profiles. This was done to make sure that the individual firn sites were indicating similar atmospheric time series. These single sites runs for CCl_2CCl_2 are shown in Figure 2.10.

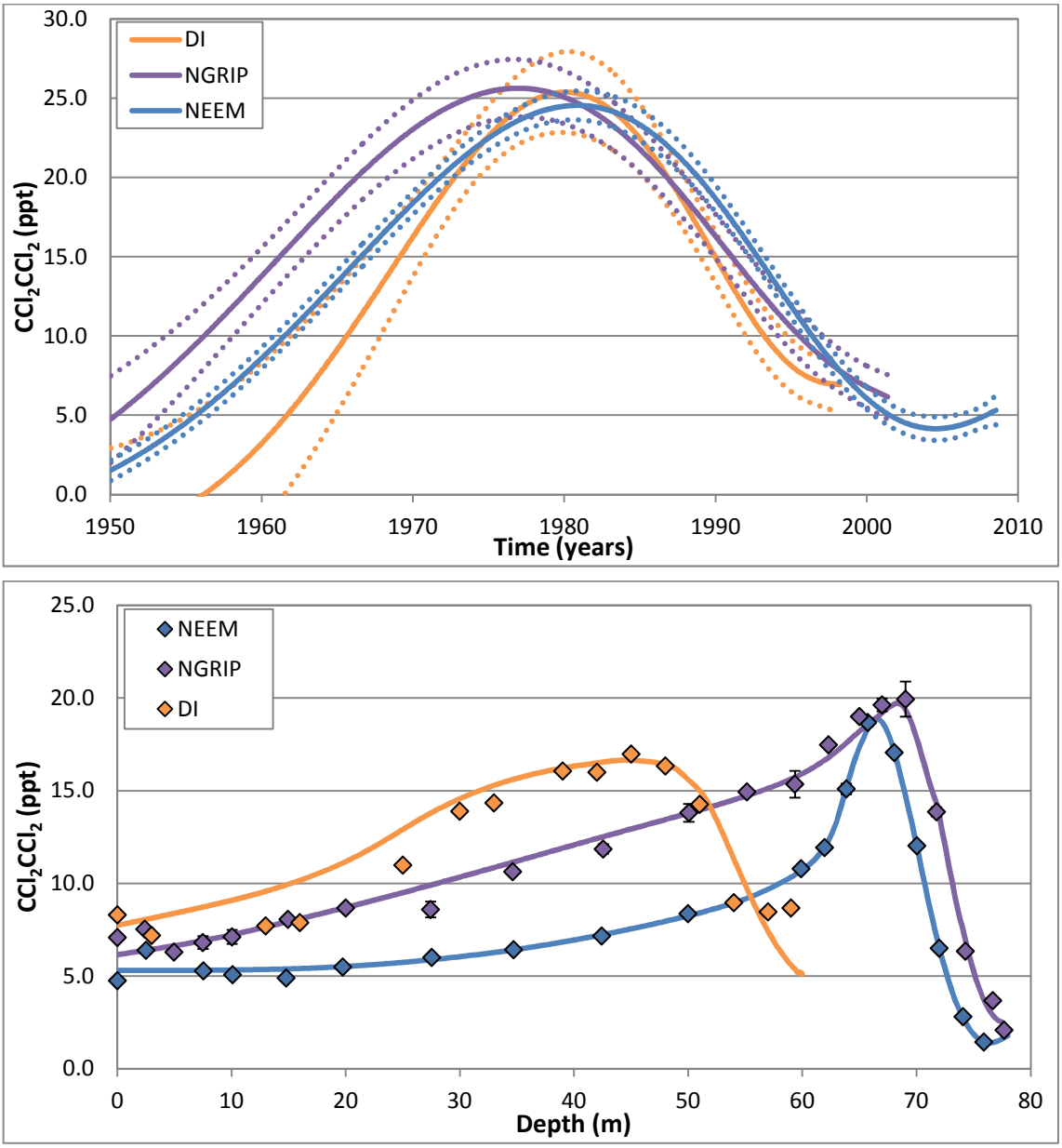

Figure 2.10: Top panel, atmospheric time series produced by a single site inversion modelling of the NEEM, (blue lines), NGRIP (purple lines) and DI (orange line) firn air measurements using the LGGE method. The dashed lines represent the uncertainty envelope of the time series. The dash lines are taken as RMS (root mean square) of the RMSD (Root-mean-square-deviation), of the difference between the firn concentrations and the modelled firn profile and the smoothing factor of the model. The smoothing factor is taken as RMSD of the difference between one box and another within the model (i.e. the less stability there is in the model the greater the uncertainties in the different atmospheric time series). Bottom panel, depth profiles of northern hemispheric CCl_2CCl_2 concentration with depth at the; NEEM (blue points), NGRIP (purple points) and DI (orange points) firn sites, compared with model simulations based on the corresponding atmospheric time series in the top panel.

Figure 2.10 shows that that there is reasonable agreement between the individual firn sites; therefore all three sites can be used in the multi-site model. Figure 2.10 also shows that the greater the scatter in the depth profile at a given firn site (e.g. DI firn site), the larger the uncertainty in the derived atmospheric time series (dashed lines, top panel Figure 2.10). Therefore the uncertainty of the time series depends on the accuracy of the firn air

measurements. Therefore when the time series are derived using the multi-site model it was run in two modes. Firstly it was run with equal weighting between the sites and secondly it was run with weighting given to the sites with the smaller uncertainties in their single sites runs (dotted lines Figure 2.10). The multi-site runs for CCl_2CCl_2 are shown in Figure 2.11.

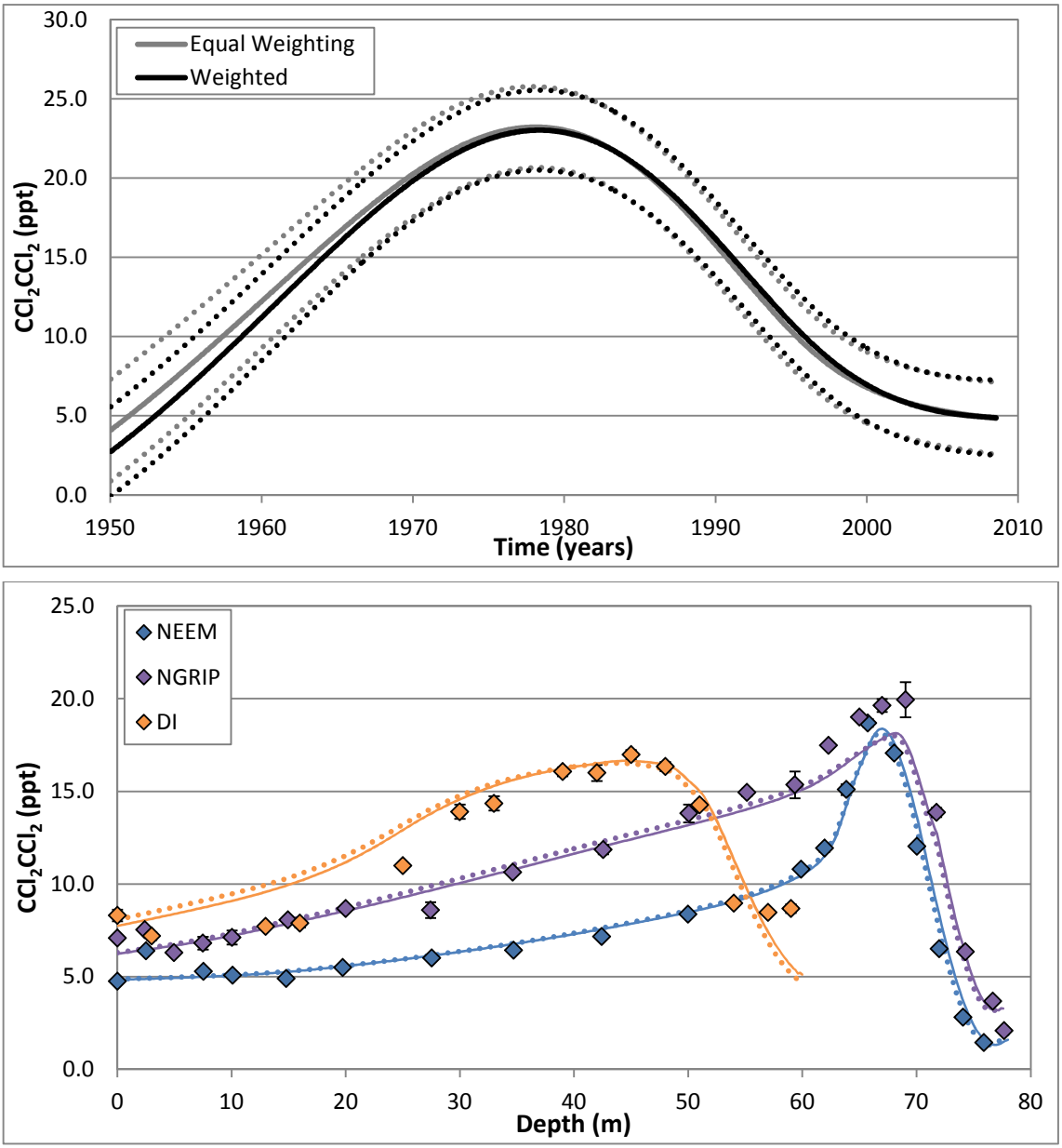

Figure 2.11: Top panel, atmospheric time series derived by a weighted and equal weighted multi-site inversion modelling of the NEEM, NGRIP and DI firn air measurements using the LGGE method. As the firn sites have different drill dates the LGGE method produces an atmospheric time series using all of the firn sites up to the drill date, after this the atmospheric time series is derived using the remaining sites. The dashed lines represent the uncertainties envelope of the time series (as described Figure 2.10). Bottom panel, depth profiles of northern hemispheric CCl_2CCl_2 concentration with depth at the NEEM, NGRIP and DI firn sites compared with model simulations based on the weighted (solid line) and equal weighted (dotted line) atmospheric time series indicated in the top panel.

Figure 2.11 shows that there is good agreement between the weighted and equal weighted multi sites runs. In this case, the weighted site was taken as the atmospheric time series of

CCl_2CCl_2 as it has smaller uncertainties (dotted lines top panel Figure 2.11). To validate this atmospheric time series the multi-site model was run again with the regularization term increasing / decreasing by factors of 100 (Figure 2.12).

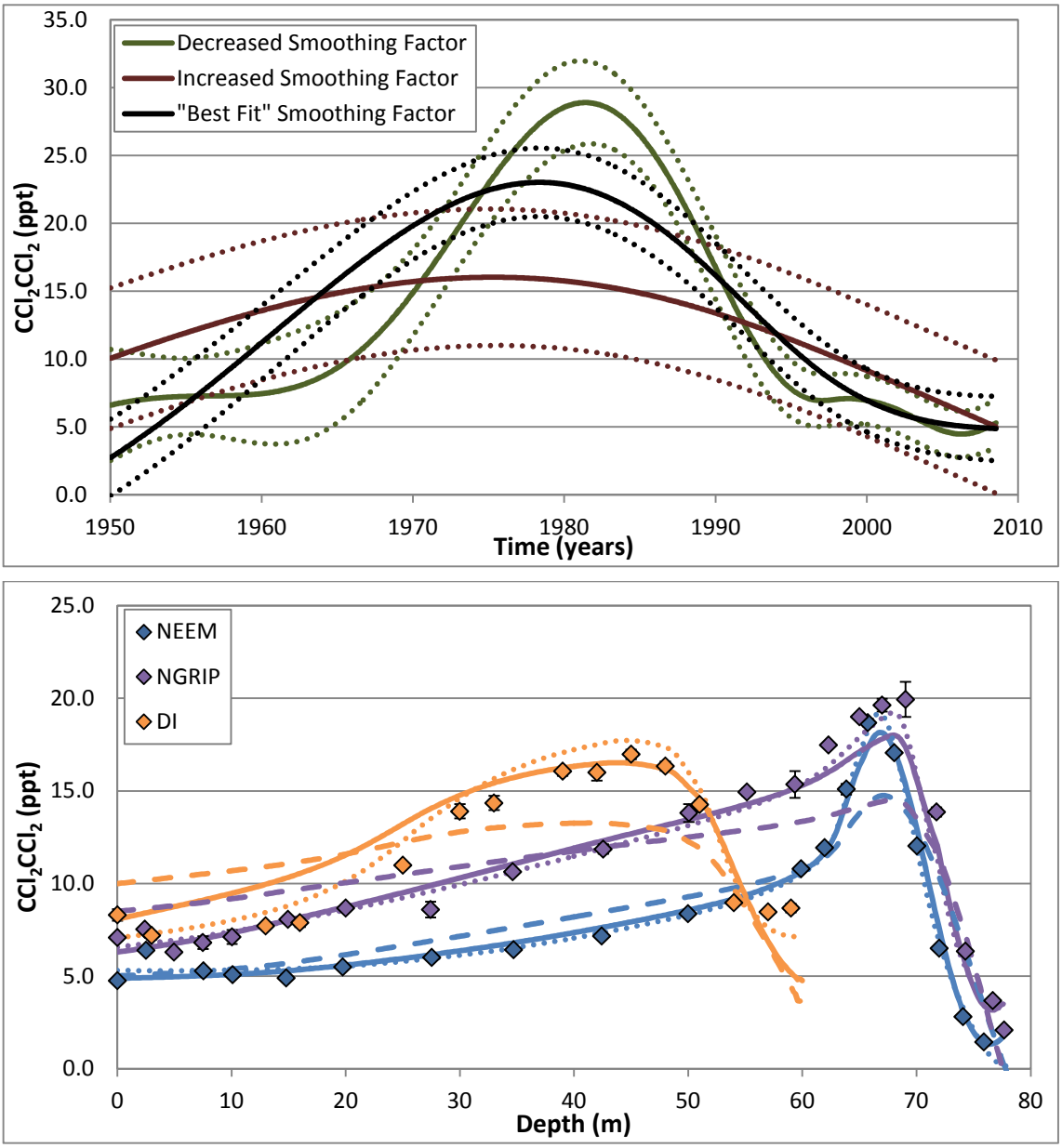

Figure 2.12: Top panel, atmospheric time series derived by an optimal, increased and decreased smoothing factors, multi-site inversion modelling of the NEEM, NGRIP and DI firn air measurements using the LGGE method. As the firn sites have different drill dates the LGGE method derives an atmospheric time series using all of the firn sites up to the drill date of a firn site, after this the atmospheric time series is derived using the remaining sites. The dashed lines represent the uncertainties envelope of the time series (as described Figure 2.10). Bottom panel, depth profiles of northern hemispheric CCl_2CCl_2 concentration with depth at the; NEEM, NGRIP and DI firn sites compared with model simulations based on the optimal (solid lines), increased smoothing factor (dotted lines) and the decreased smoothing factor (dashed lines) atmospheric time series indicated in the top panel.

Figure 2.12 indicates that the optimal solution is well centred between the increased smoothing factor and the decreased smoothing factor, suggesting that the regularization term

is at the optimum value. This helps to validate the time series. It should also be noted that even though the imposed variations of the regularization term were relatively large, their impacts on the fit of the firn data and $RMSD_{model-data}$ was relatively small.

The time series derived by the LGGE method is able to model the depth profile of concentration within the firn column. However, the time series is unable to model the variations in the concentration in the shallowest part of the firn columns, which forms as a result of the seasonal cycle in atmospheric mixing ratios. These variations in the shallowest part of the firn columns have been described in more detail in *Kaspers et al.* (2004) and *Sturges et al.* (2001a). To model these variations, as well as assessing the seasonal cycle in atmospheric mixing ratios, the input into the direct firn model was the time series derived using the LGGE method that was modulated by a sinusoidal seasonal cycle with a winter maximum and summer minimum. This modulation to the time series only applied to dates between 1990 and present, because annual variations are rapidly smoothed out with depth in the firn (*Schwander et al.*, 1993) and an oscillating time series causes spurious effects in the model output closest to firn close-off (*Sturges et al.*, 2001a). An example of these sinusoidal seasonal cycles and the effect they have on the firn depth profiles are shown in Figure 2.13.

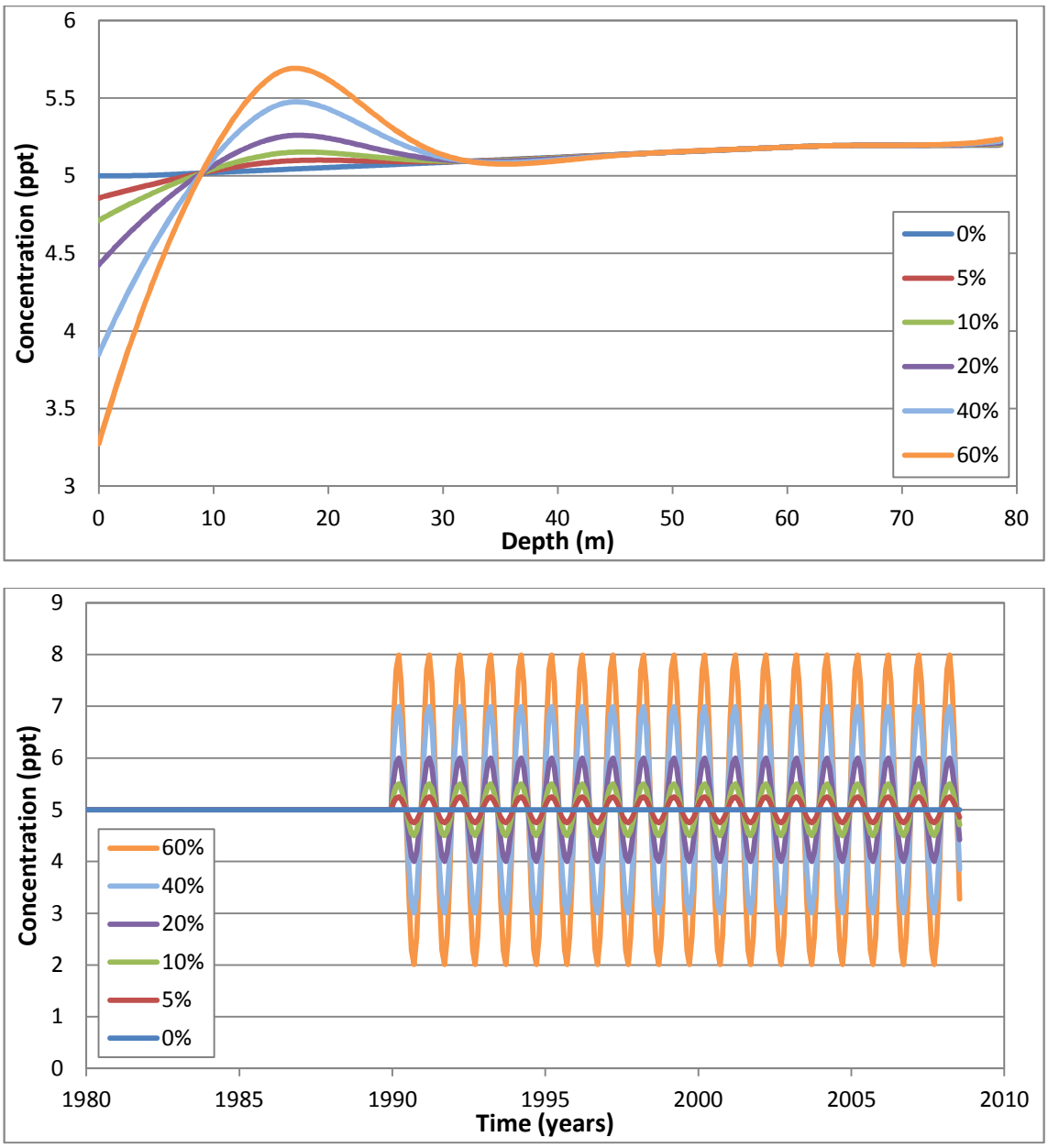

Figure 2.13: Top panel, modelled depth profiles of concentration, based on the time series indicated in the bottom panel, using a D_{gas}/D_{CO2} of 0.5. Bottom panel, Atmospheric time series held at a constant 5 ppt between 1900 and 2008.5 (1980 to 2008.5 shown) with sinusoidal seasonal cycles added to the time series between 1990 and 2008.5. The sinusoidal seasonal cycles are indicated as, 0% (dark blue line), 5% (red line), 10% (green line), 20% (purple line), 40% (light blue line) and 60% (orange line).

Figure 2.13 indicates that the effect of a seasonal cycle for a compound that has a D_{gas}/D_{CO2} of 0.5 on the concentration depth profile occurs down to a depth of 30 m. Figure 2.13 also indicates that a 60 % seasonal cycle produces a 14 % variation in the firn depth profile.

This same procedure described in this section was used to derive the time series of the majority of compounds reported in the current study. However, for convenience, only the optimal solution is shown hereafter.

2.5.3 Atmospheric time series produced using iterative dating methods

For species that had not been modelled by the full multi-site procedure described above, I used an iterative modelling approach to convert the measured concentrations with firn depth profiles of SF_6, SF_5CF_3, n-C_4F_{10}, n-C_5F_{12}, n-C_6F_{14}, n-C_7F_{16} and HFC-32 into atmospheric time series. This method was developed by *Trudinger* (2002) and was used with the firn model described earlier. This method has few assumptions about the atmospheric time series, other than that compounds were increasing monotonically from negligible abundances to the known present day atmospheric mixing ratios. This technique has proven to work well in previous studies for several species of anthropogenic origin such as halocarbons, CFC's (*Sturrock et al.*, 2002) and PFCs (*Worton et al.*, 2007) as well as that of *Laube et al.* (2012) which included the time series of n-C_4 to n-C_7 produced in this study. However this method is not able to derive atmospheric time series for compound that have mixing ratios that have increased and then decreased in the atmosphere. This results in a number of periods of time having the same atmospheric mixing ratio. Therefore the iterative technique yields non-unique 'pseudo' dates and thus can not derive a new time series.

The iterative dating methods requires an initial time series, that was generated by producing a linear fit from the concentration at the bottom of the firn column to the surface mixing ratio at the firn site (black line in top panel Figure 2.14), which was then used to generate a modelled concentration – depth profile (black line in bottom panel Figure 2.14). This output was then compared with the input time series, so that "pseudo" dates could be assigned to each sampling depth based on the modelled concentration at that depth and the corresponding date from the input atmospheric scenario. This mixing ratio - age profile was then used to generate another atmospheric time series by fitting a polynomial trend line (blue line in Figure 2.14). This new time series could then be, used as a new input scenario for the firn modelled. This procedure was then repeated until the age estimate was refined, this usually occurred after two runs when the atmospheric time series converge towards a similar atmospheric time series and an optimal fit is obtained between the modelled and measured depth profile.

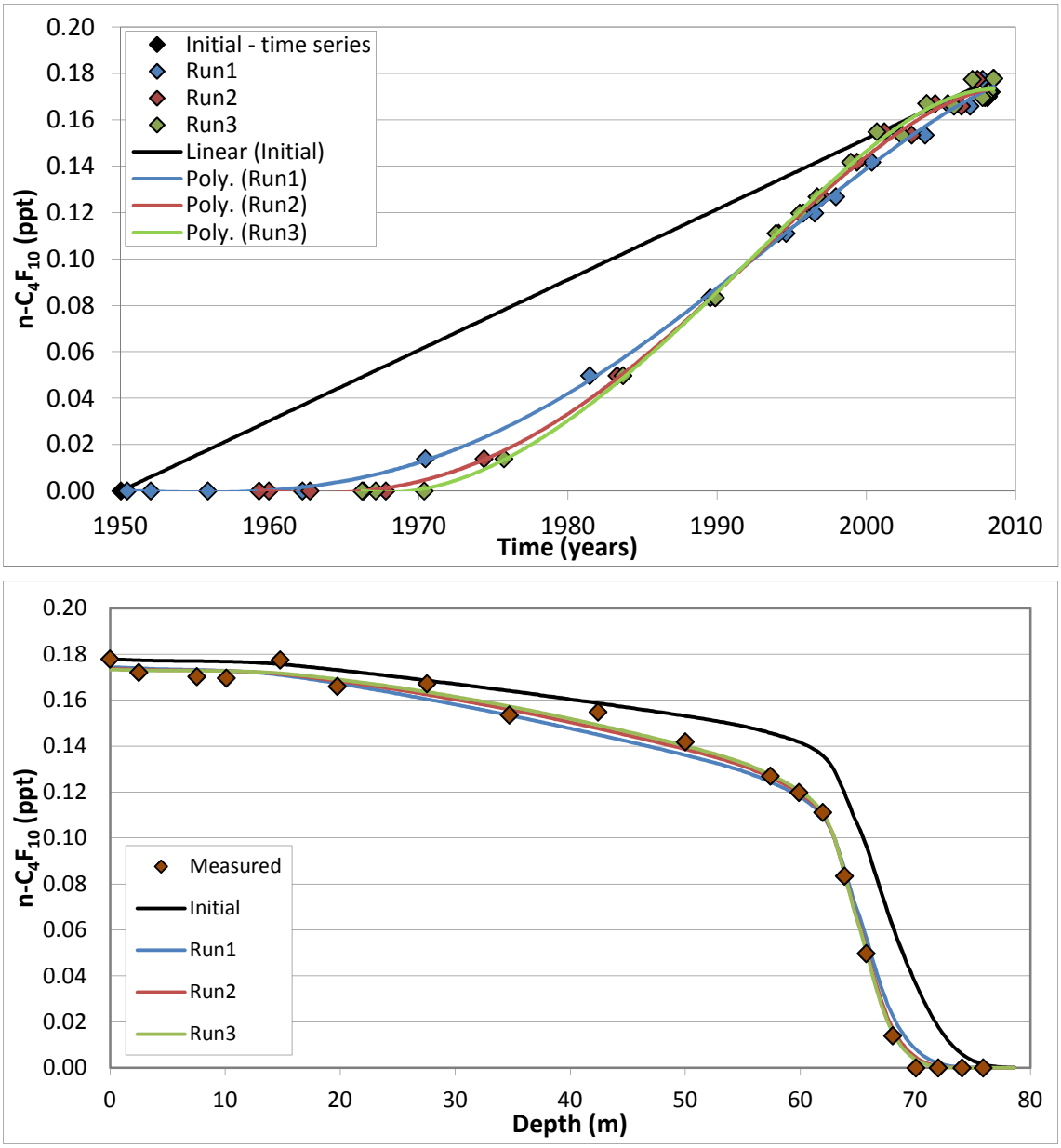

Figure 2.14: Top panel: The generated atmospheric time series used in the firn diffusion model to reconstruct the atmospheric time series of n-C_4F_{10}, "initial guess" (black line), Run1 (blue line), Run2 (red line) and Run3 (green line). The concentration- age profile for Run 2 and Run 3 (green line) converged to similar atmospheric time series and an optimal fit is obtained between the modelled and measured depth profile so the iterative dating deemed to be optimal. Bottom: depth profiles of n-C_4F_{10} firn air measurements (points), compared with model simulations based on the atmospheric time series, initial (black line), Run1 (blue line), Run2 (red line) and Run3 (green line), indicated in the top panel.

Figure 2.14 indicates that the iterative dating process used in this study was able to produce a consistent time series for the atmospheric trace gas. It should be noted that these atmospheric time series from firn air measurements have been smoothed relative to the original record due to firn processes and mixing (*Trudinger*, 2002). Any short scale variations in the time series such as inter-annual variations are not recorded, with medium scale variations being damped. The time series are smoothed because they have polynomials fitted to them (up to 6^{th} order)

which can not follow every small variation in the data, but this seems appropriate because of the known smoothing from diffusive transport in the firn.

In the current study I have are also used a new iterative modelling approach to convert the measured concentrations with firn depth profiles of non-monotonic trends (e.g. CH_2BrCl, $CHBrCl_2$ and $CHBr_2Cl$) into atmospheric time series. This method uses the same iterative method (*Trudinger*, 2002) and also the same firn model both of which have been described earlier (Section 2.5.1 and 2.5.3). This method is an extension of the iterative method developed by *Trudinger* (2002) and I devised it for this current study. The method was developed to account for species with atmospheric time series that reverse, for which the iterative technique yields non-unique 'pseudo' dates. I dealt with this problem by splitting the time series into two and apply the 'pseudo' dating method separately to the ascending and descending parts of the time series.

This new method makes assumptions that the atmospheric time series of a trace gas has increased monotonically before peaking in the atmosphere and then declining to current atmospheric mixing ratios. I then assumed that any measurements in firn air samples that are increasing in concentration towards the surface (purple points in Figure 2.15) occurred before the peak in atmospheric mixing ratio and are assigned dates accordingly. Any measurements in firn air samples that decrease in concentration towards the surface (brown points in Figure 2.15) are assumed to have occurred after the peak in atmospheric mixing ratio and are also assigned dates accordingly. An initial time series was generated by producing a polynomial fit from the concentration at the bottom of the firn column in 1950 to the surface mixing ratio with a peak in 1980 (black line in top panel Figure 2.15). 1980 was used as the initial peak date as it is around the mid-point between 1950 and 2008. Tests were under taken with different initial peak data and there was very good general agreement between all optimal time series derived. The "initial guess" was used to generate a model concentration – depth (black line in bottom panel Figure 2.15). This output was then compared with the input time series, so that dates could be assigned to each sampling depth, based on the modelled concentration at depth and the corresponding date from the input atmospheric scenario, using the assumptions stated earlier. The mixing ratio - age profile obtained from this run was then used to generate another atmospheric time series by fitting a polynomial trend line (blue line in Figure 2.15). This new time series was then used as the input scenario for the firn air model. This procedure was then repeated until the age estimate was refined, this usually occurred after two runs when the atmospheric scenario generated tended to converge towards a similar atmospheric time series.

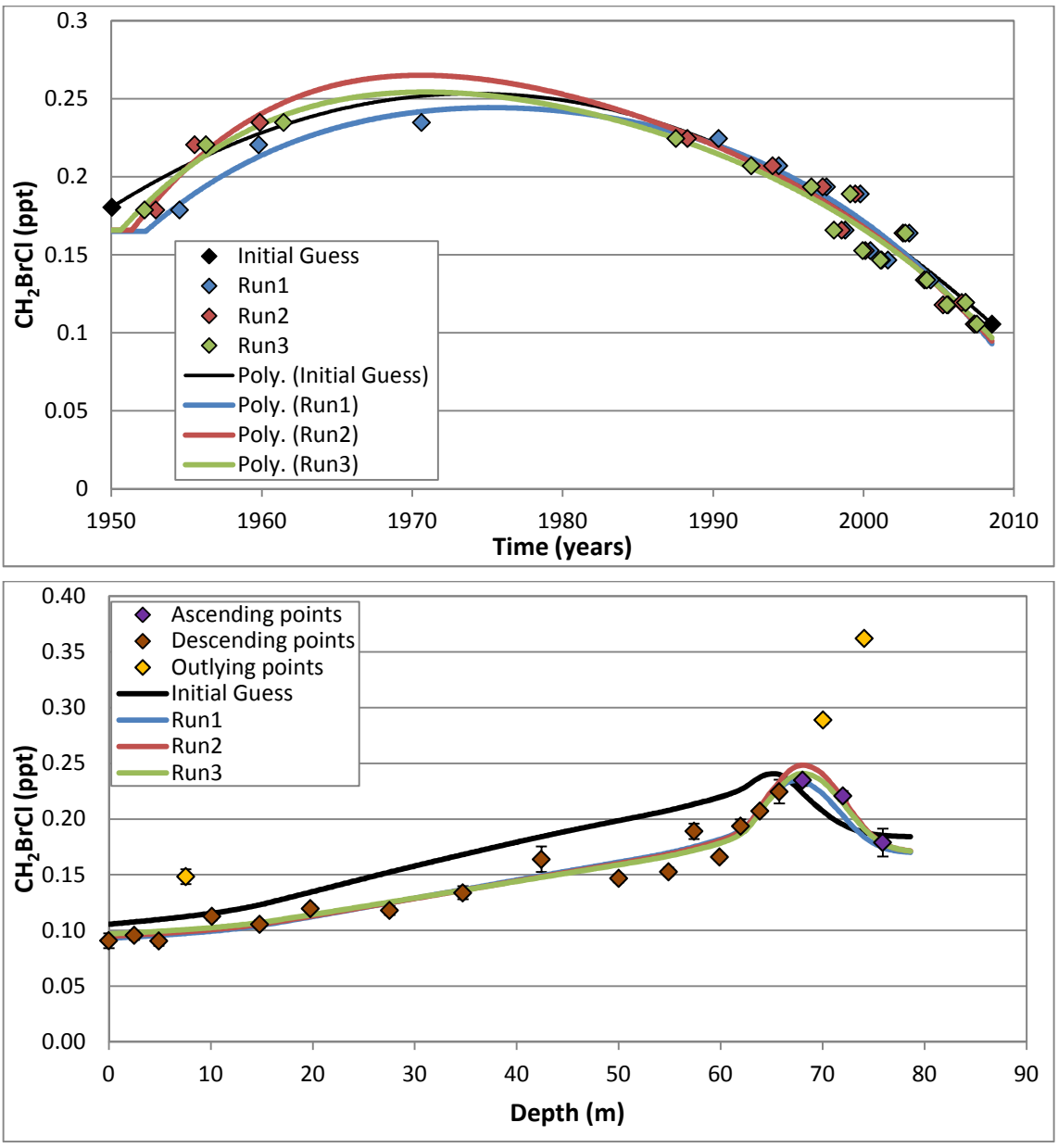

Figure 2.15: Top panel: The generated atmospheric time series used in the firn diffusion model to reconstruct the atmospheric history of CH_2BrCl, "initial guess" (black line), Run1 (blue line), Run2 (red line) and Run3 (green line). The concentration- age profile for Run 2 and Run 3 (green line) converged to similar atmospheric time series and an optimal fit is obtained between the modelled and measured depth profile so the iterative dating deemed to be optimal. Bottom panel: depth profiles of CH_2BrCl firn air measurements, ascending data (purple points), descending data (brown points) and outlying data not used in the dating process (yellow points) compared with model simulations based on the atmospheric time series, initial (black line), Run1 (blue line), Run2 (red line) and Run3 (green line), indicated in the top panel.

Figure 2.15 indicates that the iterative dating process used in this study was able to produce time series for atmospheric trace gases. Again, it should be noted that these atmospheric time series from firn air measurements have been smoothed relative to the original record due to firn processes and mixing (*Trudinger*, 2002), as well as the assumptions stated earlier. To validate that this new iterative modelling approach can produce time series for compounds

that have increased, peaked and then deceased in the atmosphere, it was compared with a time series of a compound that has also been dated using the LGGE model (Figure 2.16).

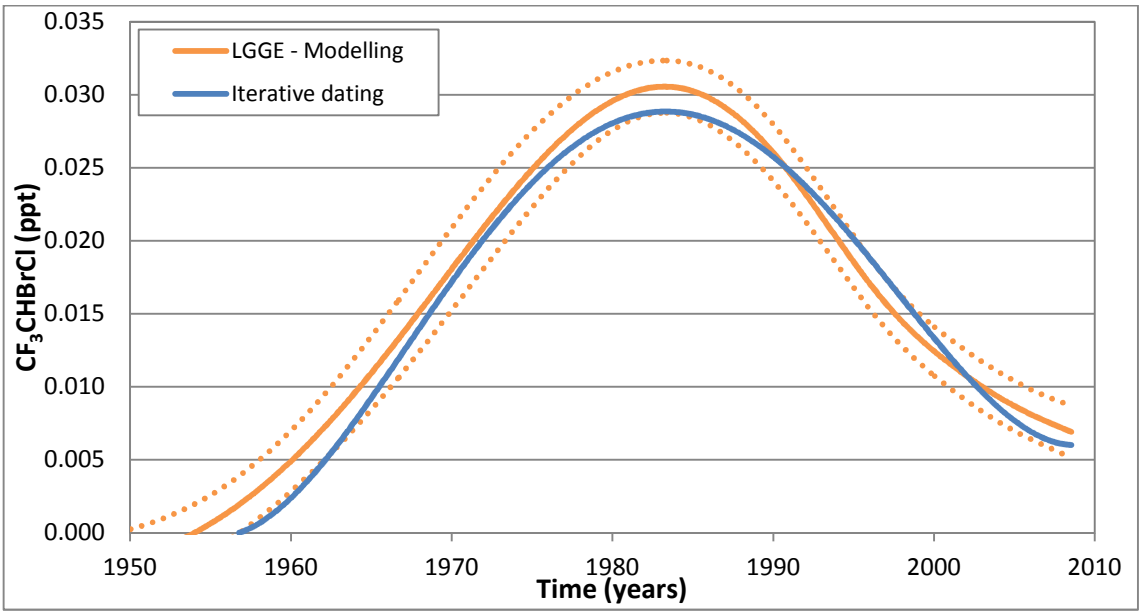

Figure 2.16: atmospheric time series of $CF_3CHBrCl$ produced by a multi-site inversion modelling of the NEEM, NGRIP and DI firn air measurements (orange line) using the LGGE method, and the iterative method developed in this study. The dashed lines represent the uncertainties envelope (as described Figure 2.10) of the LGGE method.

Figure 2.16 indicates that the atmospheric time series produced using the iterative dating process is in good general agreement with time series produced using the LGGE method. This helps to validate this method of dating firn air measurements.

2.5.4 Emissions estimates

Annual emissions estimates of gases were produced in this study using the atmospheric time series and a 1 - box model (Figure 2.17) based on the method used by *Maiss and Brenninkmeijer* (1998) and *Maiss and Levin* (1994). This model uses Equation 3 to estimate emission rates.

$$E_{(i)} = \left[C_{(i)t} - \left(C_{(i)0} \times e^{(-\Delta t/\tau)}\right)\right] \times M_{(a)} \times m_{(i)}$$ - Equation 3

In which $E_{(i)}$ – emission rate of compound i, $C_{(i)t}$ – average atmospheric mixing ratio at time t, $C_{(i)0}$ – initial atmospheric mixing ratio, Δt – change in time (taken as 1 year), τ – atmospheric lifetime in years, $M_{(a)}$ - total number of moles in the atmosphere (taken as 1.771×10^{20} (*Maiss and Brenninkmeijer*, 1998)), $m_{(i)}$ – molecular mass.

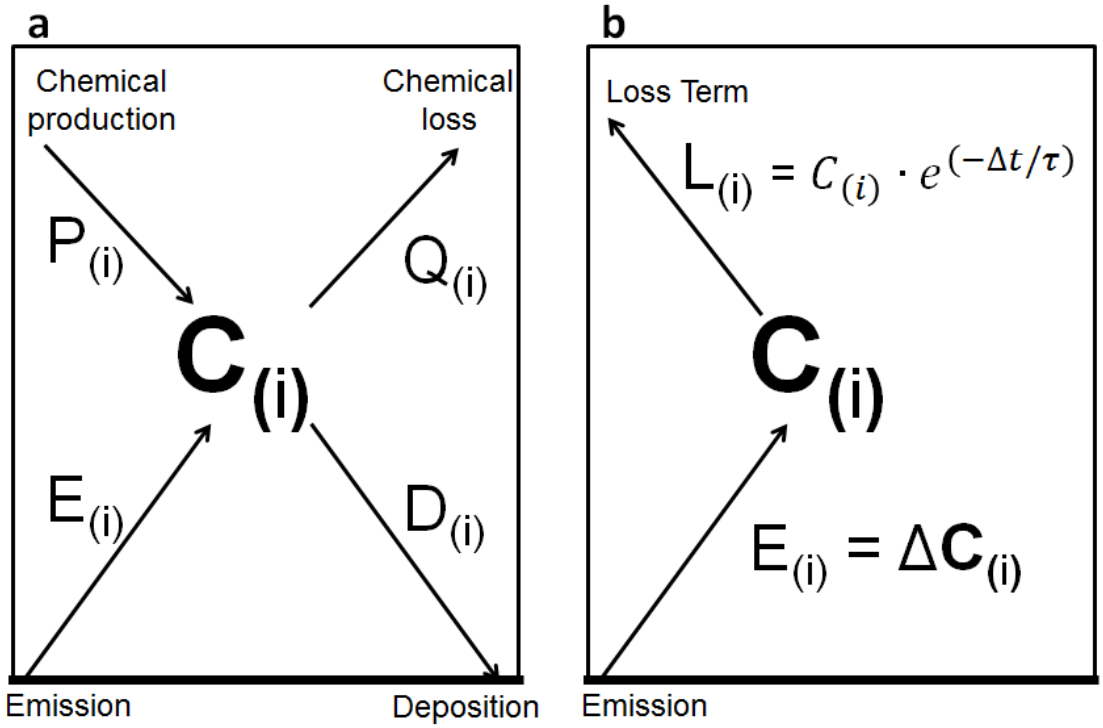

Figure 2.17: a) schematic diagram of one-box model for the atmospheric mixing ratio (C) of species i based on *Jacob* (1999). In which $E_{(i)}$ – emissions, $P_{(i)}$ – chemical production, $Q_{(i)}$ – chemical loss and $D_{(i)}$ – deposition. b) schematic diagram of one-box model used in this study to calculate emissions estimate, assuming that the difference between annually averaged atmospheric mixing ratio is wholly due to emission rates $E_{(i)}$. Note, all the loss terms from Figure 2.17 a) have been combined to a single loss term $L_{(i)}$ which is proportional to the atmospheric lifetime (τ) of species i.

A schematic diagram of the one-box model for the atmospheric mixing ratio of species i, is shown in Figure 2.17 a). This model calculates the atmospheric mixing ratio of a compound given the production and loss rates of the compound. Sources of the compound in the atmosphere include contributions from emissions and chemical production, whereas sinks of the compound include contributions from chemical losses and deposition. The one-box model does not resolve the spatial distribution of the mixing ratio of the compound inside the box. The method of estimating emissions rates used in this study does make a number of assumptions. Firstly, that the compounds have a constant atmospheric lifetime (i.e. a homogeneous OH field). Secondly that the total mass of the atmosphere is 5.1×10^{18} kg. Thirdly, that there is instantaneous mixing in the atmosphere and finally that the difference between annually averaged atmospheric mixing ratios is wholly due to emissions rates and that there is an annually averaged OH loss. The resulting one-box model produced by these assumptions is shown in Figure 2.17 b). The emission estimates calculated by the model shown in Figure 2.17 b) produces emissions rates in mixing ratio per year to obtain mass per year estimations, this emission estimate was then multiplied by the molarity of the atmosphere and the molecular mass of the compound.

2.5.5 2-Box atmospheric model

A 2-Box atmospheric model was also used in the current study. The aim of this model is to produce a southern hemispheric (SH) time series from a northern hemispheric (NH) time series. The SH time series are then compared with SH scenarios already derived using Antarctic firn. If the modelled trends from the 2 – Box model and the firn model correlate, it is taken as evidence that the firn profiles and the firn modelling in the two hemispheres are consistent and that the assumed atmospheric lifetime of the gas is correct. The firn modelling method developed at LGGE derives atmospheric time series for the northern and southern hemisphere independently. The model assumes that there is no relationship between the two scenarios; therefore, the 2-box model can be used to validate this approach. The 2-box model uses Equation 4:

$$C_{s(t+\Delta t)} = C_{s(t)} \cdot e^{-\Delta t/\tau} + \left[\frac{\Delta t}{k}\left(C_{n(t)} - C_{s(t)}\right)\right] \cdot e^{-\Delta t/\tau}$$ - Equation 4

In which, C_s – southern hemispheric mixing ratio, C_n – northern hemispheric mixing ratio, k interhemispheric exchange time which is taken as 1.34 years, Δt – change in time (model time step taken as 1 month), τ – atmospheric lifetime in years.

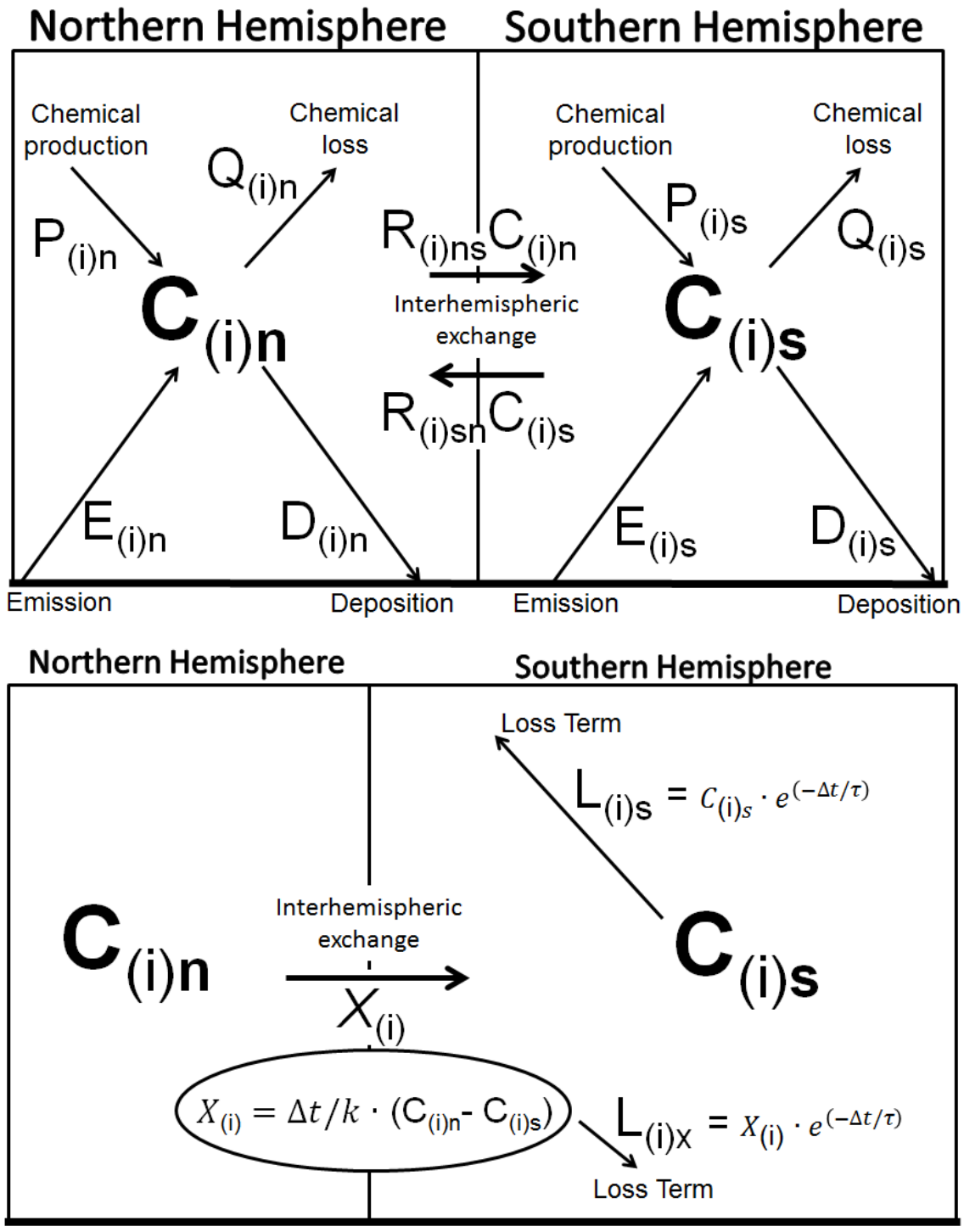

Figure 2.18: Top panel, schematic diagram of two-box model for the atmospheric mixing ratio (C) of species i based on *Jacob* (1999) for the northern hemisphere (n) and the southern hemisphere (s). In which $E_{(i)}$ – emissions, $P_{(i)}$ – chemical production, $Q_{(i)}$ – chemical loss and $D_{(i)}$ – deposition. Interhemispheric exchange rate (R) between northern to southern hemisphere (ns) and southern to northern hemisphere (*Thompson*, 2004). Bottom panel, schematic diagram of two-box model used in this study to produce a southern hemispheric time series from a northern hemispheric time series. This model assumes that that all anthropogenic emissions are from northern hemispheric sources and that the interhemispheric exchange rate is equal to change in time divided by the interhemispheric exchange time. There is also two loss terms, one due to the sink of the compound already in the southern hemisphere ($L_{(i)s}$) and one due to the sink as the compound moves from the northern hemisphere into the southern hemisphere ($L_{(i)X}$). The loss terms are proportional to the atmospheric lifetime (τ) of species i.

A schematic diagram of two-box model for the atmospheric mixing ratio of species i, is shown in Figure 2.18 (top panel). The method of producing a southern hemispheric (SH) time series from a northern hemispheric (NH) time series used in this study does make a number of assumptions. This model assumes that all anthropogenic emissions are from northern hemispheric sources and that air at the north pole will take 1.34 years to travel to the south pole (*Jacob*, 1999). Therefore, this model was only used for compounds with predominantly anthropogenic sources. The model also assumes that there are only two loss terms, one due to the sink of the compound already in the southern hemisphere and one due to the sink as the compound moves from the northern hemisphere into the southern hemisphere. These loss terms are also proportional to the atmospheric lifetime of the compound. The resulting two-box model produced by these assumptions is shown in Figure 2.18 (bottom panel)

To validate this model, it was run with northern and southern hemispheric time series of CH_3CCl_3 produced by *Buizert et al.*, (2011) and *Witrant et al.*, (2011) (Figure 2.19).

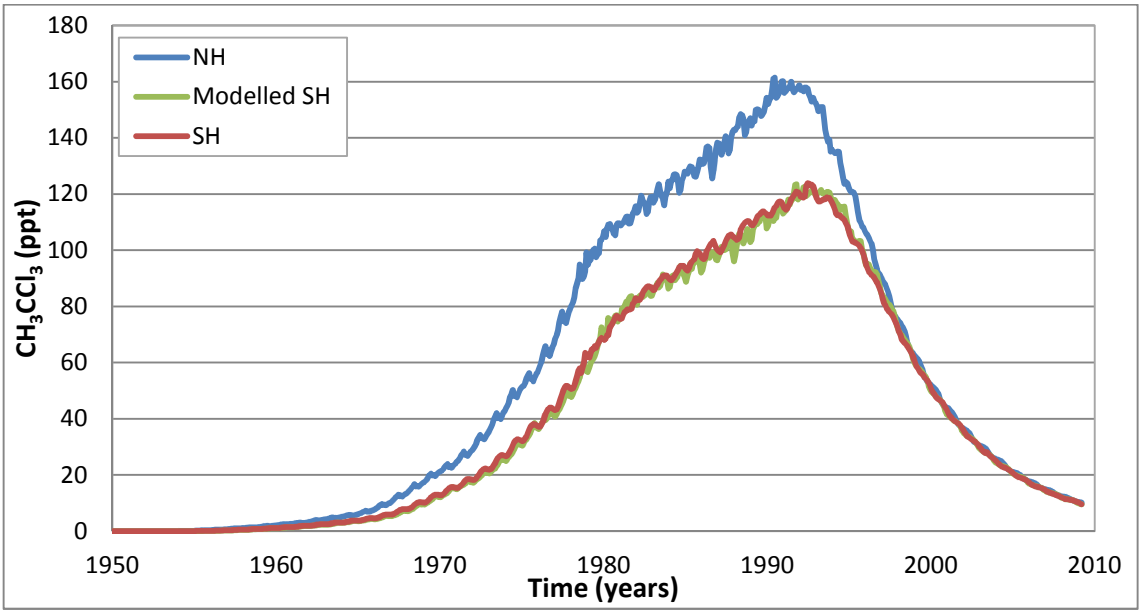

Figure 2.19: Northern (blue line) and Southern (red line) hemispheric atmospheric time series of CH_3CCl_3 produced by *Buizert et al.*, (2011) and *Witrant et al.*, (2011) compared with the modelled Southern hemispheric time series produced using the 2-box model (green line).

Figure 2.19 indicates that the southern hemispheric time series produced using the 2-box model agrees well with the southern hemispheric time series produced by *Buizert et al.*, (2011) and *Witrant et al.*, (2011). This model will be used to validate the time series derived in Chapters 3 and 4.

Chapter 3: Analysis of chlorocarbons from firn extracted from both Arctic and Antarctic firn sites

3.1 Introduction

In this study, firn air samples collected from the North Greenland Eemian Ice Drilling (NEEM), were measured for a number of chlorinated compounds by gas chromatography–mass spectrometry. These observations along with firn air measurements taken previously from other northern hemispheric firn sites, (North Grip (NGRIP) and Devon Island (DI)), and southern hemispheric firn sites, (Dronning Maud Land (DML) and Dome Concordia (DC)), were used to reconstruct the atmospheric time series of the methyl chloride and very short lived chlorinated substances. These histories were derived with the help of a 1-dimensional firn diffusion model and iterative dating techniques. In this chapter, these atmospheric time series for the chlorinated compounds are discussed.

The chlorinated compounds measured are all part of the group of chemicals known as the chlorocarbons. They include, the short-lived chlorine substances (lifetimes of greater than 6 months but less than a few years, e.g. CH_3Cl) and the very short-lived (VSL) chlorine substances (lifetimes of less than 6 months, e.g. $CHCl_3$ and CH_2Cl_2)**.** These compounds originate from both natural and/or anthropogenic sources and are important for the chlorine chemistry of the atmosphere (*Montzka et al.*, 2010). It is generally accepted that reactive chlorine compounds could play a significant role in controlling the composition of the global atmosphere. In recent decades, stratospheric ozone depletion has largely been driven by increases in the atmospheric concentrations of a number of anthropogenic halogen compounds. These anthropogenic compounds are now regulated by the Montreal Protocol and a number of them now shown signs of decline in their atmospheric abundances (*González et al.*, 2006). However there are still a number of short-lived industrial chlorinated chemicals (e.g. CH_2Cl_2 and CCl_2CCl_2) that are not presently controlled under the Montreal Protocol, due to the lack of information on the effect these compounds have on the atmosphere. Naturally emitted species are important for stratospheric ozone chemistry and are likely to become proportionately more important in the future as anthropogenic emissions of halogen compounds decreases.

Chlorinated compounds are important in the atmosphere because of their effect on the stratospheric ozone budget. Chlorinated compounds are subject to photolysis in the stratosphere, forming halogened radicals, which can then act as catalysts in the destruction of ozone. Total tropospheric chlorine from long-lived chemicals was ~3.4 ppb in 2008 with an atmospheric trend of -14 ppt yr^{-1} during 2007–2008 (*Montzka et al.*, 2010). This decrease in tropospheric chlorine has slowed in recent years (-21 ppt yr^{-1} during 2003–2004). This decrease is slower than the decline of -23 ppt yr^{-1} in 2008 projected in the A1 (most likely, or baseline)

scenario of the WMO: Scientific Assessment of Ozone Depletion: 2006 Assessment (*Clerbaux and Cunnold et al.*, 2006).

The principal objective of the study reported in this chapter is to reconstruct atmospheric time series of the chlorocarbons. This will include the first full reconstruction of the atmospheric histories of the VSL chlorocarbons; CCl_2CCl_2, CH_2ClCH_2Cl, C_2H_5Cl and $CHClCCl_2$. These reconstructed time series will then be compared with ambient in situ atmospheric observations or measurements from air archives.

This study provides insights into the growth rates of the chlorinated compounds, the pre-industrial mixing ratios of the compounds with natural emissions, and the date of first significant atmospheric abundance of the compounds that are fully anthropogenic in origin. Also, emissions estimated from the growth rates were calculated, as well as assessing the effect these ozone depleting substances have on the stratospheric ozone budget by estimating their equivalent effective stratospheric chlorine.

This chapter consists of a detailed discussion of each individual chlorocarbon species. Each subsection has its own background information, results and discussion on atmospheric time series from the firn data and estimating emissions from the reconstructed time series. At the end of the chapter, the equivalent effective stratospheric chlorine of individual compounds is calculated.

3.2 Methyl Chloride

Methyl chloride (CH_3Cl) is presently the most abundant chlorine containing organic compound in the atmosphere and contributes 16 % to the total chlorine budget from long-lived gases in the troposphere (*Montzka et al.*, 2010). The global mixing ratio of CH_3Cl was 545 ppt in 2008 (*Montzka et al.*, 2010). A better understanding of the global budget of methyl chloride and its atmospheric history can help inform about the large amount of atmospheric Cl that is not controlled under the Montreal Protocol.

3.2.1 Background information on CH_3Cl

Methyl chloride has both natural and anthropogenic sources, with *Xiao et al.* (2010) estimating the total global emissions for 2000–2004 to be 4.10 ± 0.47 Tg yr^{-1}. Both modelled results and observations indicate that about 55 % or 2.3 ± 0.3 Tg yr^{-1} of these emissions come from tropical terrestrial sources (*Montzka et al.*, 2010). Measurements from South American and Asian rainforests have reinforced the importance of tropical terrestrial CH_3Cl sources (*Gebhardt et al.*, 2008, *Yokouchi et al.*, 2007 and *Saito and Yokouchi*, 2006). Emissions from

terrestrial sources in the tropics have been found to vary with global temperature changes (*Xiao et al.*, 2010). As well as being emitted from living plants, *Blei et al.* (2010) have found emissions from leaf litter. The large source of CH_3Cl in the tropics generates a latitudinal gradient and consequently, the mixing ratio of CH_3Cl is reduced at high latitudes (e.g. at the poles) (*Khalil and Rasmussen*, 1999). *Khalil and Rasmussen* (1999) showed a strong correlation between CH_3Cl mixing ratios and latitude, regardless of hemisphere.

Other major atmospheric sources of methyl chloride include biomass burning, oceans and anthropogenic activities (*Montzka et al.*, 2010) (Table 3.1). Production has been recorded in the open ocean by *Moore* (2008), as well as supersaturations of CH_3Cl reported in coastal waters off of the United States by *Hu et al.* (2010) and China by *Lu et al.* (2010). Emission rates from the total global oceans are estimated to be 0.43 ± 0.1 Tg yr^{-1} *Xiao et al.* (2010).

Table 3.1: Estimated source and sink strengths for atmospheric methyl chloride from observations and three-dimensional model studies based on *Montzka et al.* (2010)

Source	**Reference**	**Strength (Gg yr^{-1})**
Tropical Terrestrial	*Xiao et al.* (2010)	2300 ± 300
Biomass burning	*Andreae and Merlet* (2001)	325 - 1125
Oceans	*Xiao et al.* (2010)	430 ± 100
Salt marshes	*Clerbaux and Cunnold et al.* (2006)	65 - 440
Fungi	*Clerbaux and Cunnold et al.* (2006)	43 - 470
Wetlands	*Varner et al.* (1999)	48
Rice paddies	*Lee-Taylor and Redeker* (2005)	2.4 - 4.9
Fossil fuel burning	*Clerbaux and Cunnold et al.* (2006)	5 - 205
Waste incineration	*Clerbaux and Cunnold et al.* (2006)	15 - 75
Industrial processes	*Clerbaux and Cunnold et al.* (2006)	10
Subtotal		2844 - 5508
Sink		
OH reaction	*Lee-Taylor and Redeker* (2005)	3800 - 4100
Loss to stratosphere	*Clerbaux and Cunnold et al.* (2006)	100 - 300
Cl reaction	*Clerbaux and Cunnold et al.* (2006)	180 - 550
Soil	*Clerbaux and Cunnold et al.* (2006)	100 - 1600
Loss to cold waters (polar oceans)	*Moore* (2000)	93 - 145
Subtotal		4273 - 6695

The major sinks of tropospheric CH_3Cl include oxidation by hydroxyl radicals, loss to the stratosphere, reaction with chlorine radicals, loss to polar ocean waters, and uptake by soils (Table 3.1). The Arctic tundra appears to be a net sink for CH_3Cl, with uptake rates increasing

under drier conditions (*Teh et al.*, 2008 and *Rhew and Abel*, 2007). Measurements from a sub-Arctic wetland show a small net source for CH_3Cl (*Hardacre et al.*, 2009).

Measurements from *National Oceanic and Atmospheric Administration,* Earth System Research Laboratory (NOAA/ESRL) since 1995 and *Advanced Global Atmospheric Gases Experiment* (AGAGE) since 1998 are consistent with an observed global average mixing ratio of 545 – 547 ppt in 2008 (*Montzka et al.*, 2010). A latitudinal gradient results in a higher mixing ratio in the tropics compared with polar regions.

The global mixing ratio of methyl chloride has increased by small amounts during years 2004 to 2008 (2 to 3 ppt yr^{-1}, or 0.4 to 0.5 % yr^{-1}) (*Montzka et al.*, 2010), though these changes follow a large decrease of −2.6 % yr^{-1} reported for the years 1998 to 2001 by *Simmonds et al.* (2004). Changes observed from 2007 to 2008 are small, though variations in increases (AGAGE) or decreases (NOAA) in the global mixing ratio are reported by different measurements networks. The cause of these differences is not fully understood, but the differences are likely to be insignificant relative to measurement errors, or may reflect regional variations in rates of change of CH_3Cl.

Ambient air measurements of methyl chloride extend back only to 1980 (*Khalil and Rasmussen*, 1999b). However, the atmospheric history of CH_3Cl has been determined through the analysis of firn air and air bubbles in ice cores. Measurement of CH_3Cl has been undertaken from several sources, including: firn air from Dronning Maud land, Antarctica, (describing the variability from 1975 – 2000 (*Kaspers et al.*, 2004b)), firn air from Law Dome in Antarctica (dating back to before 1940 (*Trudinger et al.*, 2004)), firn air from the South Pole and an ice core from Siple Dome in Antarctica (showing the variability during the past 300 years (*Aydin et al.*, 2004)). *Butler et al.* (1999) also investigated CH_3Cl levels in firn air collected from South Pole, Siple Dome in Antarctica and from the northern hemisphere at Tunu in Greenland. A comparison of the atmospheric time series for CH_3Cl over the 20^{th} century atmospheric time series derived from firn air studies, along with the general properties of these study sites can be found in Table 3.2.

Table 3.2: General properties of previous firn air studies

Site	South Pole, Antarctica	Siple Dome, Antarctica	Tunu, Greenland	South Pole, Antarctica	Dronning Maud Land, Antarctica	Law Dome, Antarctica
Reference	*Butler et al.*, (1999)	*Butler et al.*, (1999)	*Butler et al.*, (1999)	*Aydin et al.* (2004)	*Kaspers et al.* (2004b)	*Trudinger et al.* (2004)
Location	90° S	81° 40′ S, 148° 49′ W	78° 01′ N, 33° 59′ E	89° 98′ S, 118° 73′ W	75° 00′ S, 15° 00′ E	66°S, 112°E
Elevation (m)	2841	~600	~2400	~2800	3453	~1300
Sampling date	Jan. 1995	Dec. 1996	Apr. 1996	2001	2001	Jan. 2001

A comparison between the atmospheric time series of CH_3Cl derived by *Trudinger et al.* (2004) and *Aydin et al.* (2004) for sties in Antarctica are shown in Figure 3.1. *Aydin et al.* (2004) ‘‘firn air’’ reconstruction (red line, Figure 3.1) shows mixing ratios that are consistently lower in the early part of the 20th century than the *Trudinger et al.* (2004) time series (blue line, Figure 3.1), with the increase in mixing ratios occurring later (in 1965) and more sharply in the *Aydin et al.* (2004) ‘‘firn air’’ time series. The *Aydin et al.* (2004) “sinusoidal” time series (green line, Figure 3.1) again has mixing ratios that are consistently lower in the early part of the 20th century than the *Trudinger et al.* (2004) time series. However, there is reasonably good agreement between the two reconstructions after 1960. The *Kaspers et al.* (2004b) (purple line, Figure 3.1) reconstruction shows little agreement with any study, however there is a lot of uncertainty with this reconstruction. The differences between the atmospheric reconstructions appear to be too significant to result, from differences in the smoothing characteristics of the sites.

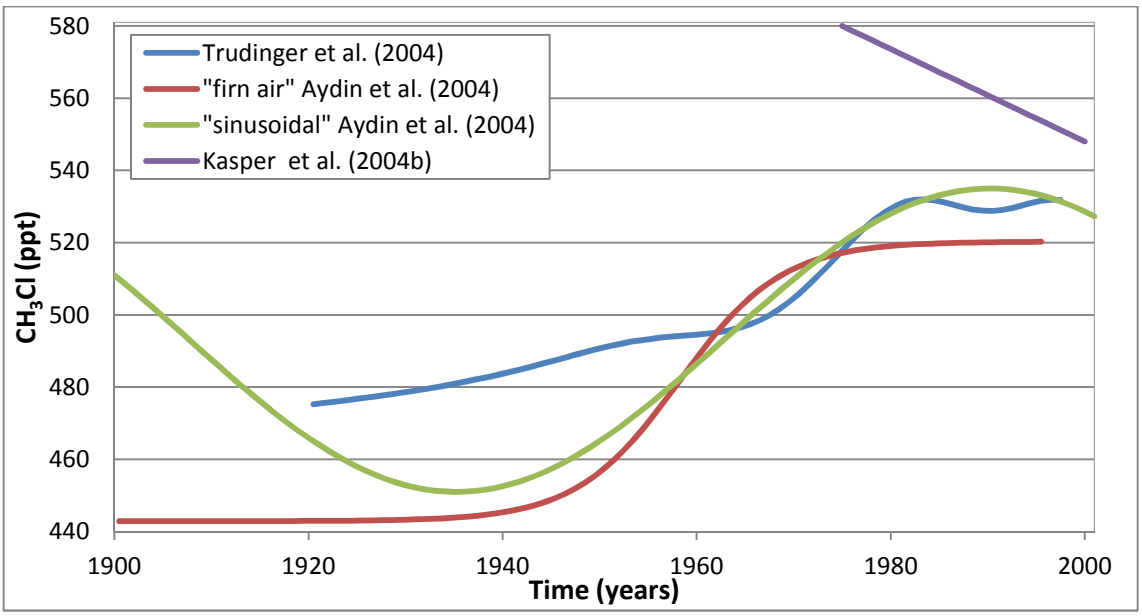

Figure 3.1: Comparison of methyl chloride 20th century southern hemispheric atmospheric concentration obtained from firn air and ice cores data. From; *Trudinger et al.* (2004) blue line, "firn air" history *Aydin et al.* (2004) red line, ''sinusoidal'' history *Aydin et al.* (2004) green line and *Kaspers et al.* (2004b) purple line.

Kaspers et al. (2004b) sampled firn air collected at Dronning Maud Land (DML), during the Norwegian Antarctic Research Expedition (NARE) 2000/ 2001 (*Winther*, 2002). Thirteen samples were collected in total, with samples extracted every 8 m until pore close-off. One drawback associate with this method is that with a vertical resolution of only 8 m, and a standard error of around ± 50 ppt, most of the samples have an uncertainty of ~ 20 % making it difficult to obtain an accurate atmospheric history. This is especially true for the bottom part of the firn column where the diffusion process is slowed due to the closing of pores. In this region of the firn column there is a higher resolution of the atmospheric history of CH_3Cl. Therefore, the greater the number of samples taken in a region, the more precise any atmospheric history inferred from firn air measurements will be. With a vertical resolution of 8 m, *Kaspers et al.* (2004b) has only 2 data points in the last 20 m of the firn column, limiting the accuracy of result obtained.

From the methyl chloride analysis, *Kaspers et al.* (2004b) deduced a background surface concentration of 548 ± 32 ppt in 2000, with a decreasing trend over the previous 25 years towards a present day mixing ratio of 1.2 ± 0.6 ppt per year (Figure 3.1). This result is in reasonable agreement with the reported decreasing trend of *Khalil and Rasmussen* (1999). However the atmospheric time series *Kaspers et al.* (2004b) shows no evidence of the increasing trend from the beginning of the twentieth century to the 1970s that has been reported in other previous firn air studies (e.g. *Trudinger et al.*, 2004). The range of

measurements in the study by *Kaspers et al.* (2004b) varied between 532 and 627 ppt which is in good agreement with the mixing ratio measured at South Pole between 1984 and 1994 which varied between 477 and 596 ppt (*Khalil and Rasmussen*, 1999). However *Butler et al.* (1999) derived a somewhat lower mixing ratio range of 480–521 ppt for the same region and time period (1975– 1999).

Butler et al. (1999) sampled air collected from firn at the South Pole and Siple Dome in Antarctica and at Tunu in Greenland. To date, this is the only study which includes a methyl chloride firn air record from the northern hemisphere. Concentrations of CH_3Cl were found to be significant in the deepest samples. The concentrations of CH_3Cl in samples collected between 20 m and 45 m depth have found to be similar to the mean annual concentrations at Cape Grim, Tasmania, (*Butler et al.*, 1998). There was a difference of 5 - 10 % between bottom and mid-hole samples which suggests that the atmospheric mixing ratio of CH_3Cl has increased by about 5 - 10 % during the past century. This relates to an increase of around 40 ppt in the atmospheric mixing ratio of CH_3Cl over the past century (*Butler et al.*, 1999). This inferred temporal change in CH_3Cl is small relative to its variability in the firn air (*Butler et al.*, 1999).

Aydin et al. (2004) collected firn air samples during three different Antarctic field expeditions: to South Pole in 1995 (SPO-95), to South Pole in 2001 (SPO-01), and to Siple Dome in 1996 (SDM-96). Measurements of methyl chloride in the SPO-95 and SDM-96 firn samples were used in *Butler et al.* (1999). However they were updated in *Aydin et al.* (2004) to account for the revised calibration scales from the 1996 to the 2003 NOAA calibration scale. A 1-D forward model of a firn air column was used to simulate how a specified atmospheric history of CH_3Cl is incorporated into the air in firn or ice (*Schwander et al.*, 1989). The resulting atmospheric history is referred to as the ‘‘firn air’’ history (*Aydin et al.*, 2004). In the ‘‘firn air’’ history, the atmospheric abundance of CH_3Cl increases from about 470 ppt in the 1940’s to nearly 530 ppt in the early 1990’s (Figure 3.1). The steepest change is observed between 1955 and 1985 when CH_3Cl increases by about 50 ppt in 30 years. If it is assumed that any change that occurred during the 20^{th} century is a result of human activities, then the firn record implies that roughly 10% of the CH_3Cl currently in the atmosphere is anthropogenic in origin. This is in agreement with the conclusion of *Butler et al.* (1999).

As well as firn air samples, *Aydin et al.* (2004) collected ice core samples from the Siple Dome C core, drilled in December 1995, West Antarctica (81.65^0S, 148.81^0W) as part of the West Antarctic Ice Sheet Program (WAISCORES). Ice core samples were taken ranged in depth from 57 m to 83 m and had a mean CH_3Cl mixing ratio of 499 ± 28 ppt and range of 462 to 571 ppt

(*Aydin et al.*, 2004). The data from these ice cores have a distinct oscillatory behaviour with two cycles. The resulting atmospheric history is referred to as the ''sinusoidal'' history, two full oscillations occur between 1720 and 1940 C.E., across a period of 110 years and an amplitude of 42 ppt. It is currently unclear what could be driving this cycle (*Aydin et al.*, 2004), but it does appear to predate significant industrial activity. Therefore, this apparently natural variation may reflect climate-driven changes in the CH_3Cl budget.

The ''sinusoidal'' history was extended through the 20th century to examine the implications of such cyclic behaviour on the interpretation of firn air data (*Aydin et al.*, 2004). For the period between 1940 and 1990, the ''sinusoidal'' atmospheric history is similar to the ''firn air only'' history (Figure 3.1). The ability of the ''sinusoidal'' history to simulate the firn air data demonstrates that the evolution of atmospheric CH_3Cl over Antarctica during the 20th century is consistent with preindustrial variability, without invoking anthropogenic contributions to its atmospheric budget.

In *Trudinger et al.* (2004) atmospheric levels of methyl chloride were reconstructed to pre-1940 through the study of firn air collected from Law Dome, East Antarctica. The site used for methyl chloride analysis was the DSSW20K location, 20 km west of the deep DSS drill site near the summit of the dome. Firn air samples were collected in the austral summer of 1997–98 from 8 depths, including 6 specifically select for halocarbon measurements, (*Trudinger et al.*, 2004). One problem with this collection method is that with only 6 samples, any outlying samples will not become evident, and could result in an uncertainty in the reported atmospheric time series. Again, this is especially true for the bottom part of the firn column where the diffusion process is slowed due to the closing of the pores. Firn air data from *Trudinger et al.* (2004) shows methyl chloride mixing ratio increasing from about 1930 to 1980, with steeper growth occurring after about the mid-1960s. The shallowest firn measurements suggest relatively steady levels after 1980 until at least the mid-1990s (Figure 3.1).

3.2.2 Results and discussion of CH_3Cl

In the current study, I will report firn air measurement of CH_3Cl from a number of northern and southern hemispheric firn air records, as well as southern hemispheric observations from the Cape Grim baseline air pollution station. These measurements have then been used to derive the atmospheric time series of CH_3Cl mixing ratios. The time series of atmospheric CH_3Cl mixing ratios were derived using the direct firn modelling method developed at Laboratoire de Glaciologie et Géophysique de l'Environnement (LGGE) Grenoble. These new atmospheric time series are then compared with previous atmospheric time series estimated by *Aydin et al.* (2004), *Kaspers et al.* (2004b), *Trudinger et al.* (2004) and *Butler et al.* (1999). The time series obtained and the output from the inverse model for the northern and southern hemisphere site are shown alongside the measured concentration of CH_3Cl with depth at northern hemispheric firn sites (NEEM and NGRIP) and southern hemispheric (DC and DML) firn sites in Figures 3.2 and Figures 3.3, respectively.

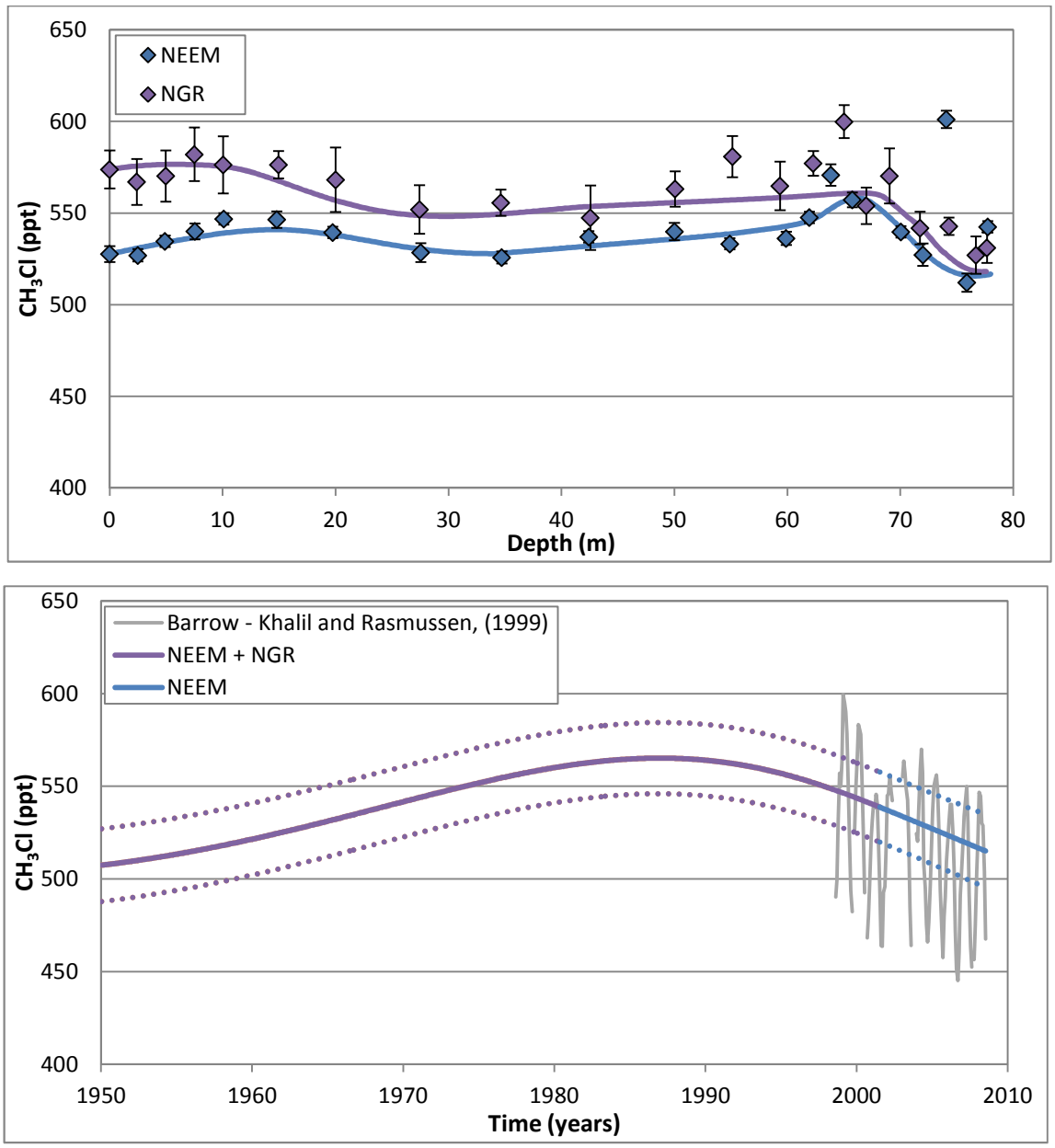

Figure 3.2: Top panel, depth profiles of northern hemispheric CH_3Cl concentration with depth at the, NEEM firn site (blue points) and the NGRIP firn site (purple points) compared with model simulations based on the atmospheric time series indicated in the bottom panel with a seasonal cycle of 13 % added to the time series. The error bars represent the 1 σ of the measurements (see methods chapter for more details). Bottom panel, Atmospheric time series derived by a multi-site inversion modelling of the NEEM and the NGRIP firn air measurements (solid line) using the LGGE method. As the firn sites have different drill dates the LGGE method derives an atmospheric time series using all of the firn sites up to the drill date of a firn site, after this the atmospheric times series is derived using the remaining sites. The time series derived by NEEM and NGRIP – purple line and NEEM only – blue line. The dashed lines represent the uncertainties envelope of the time series (as described Figure 2.10). Observations of atmospheric CH_3Cl from the Barrow observation station updated from *Khalil and Rasmussen* (1999) (grey line).

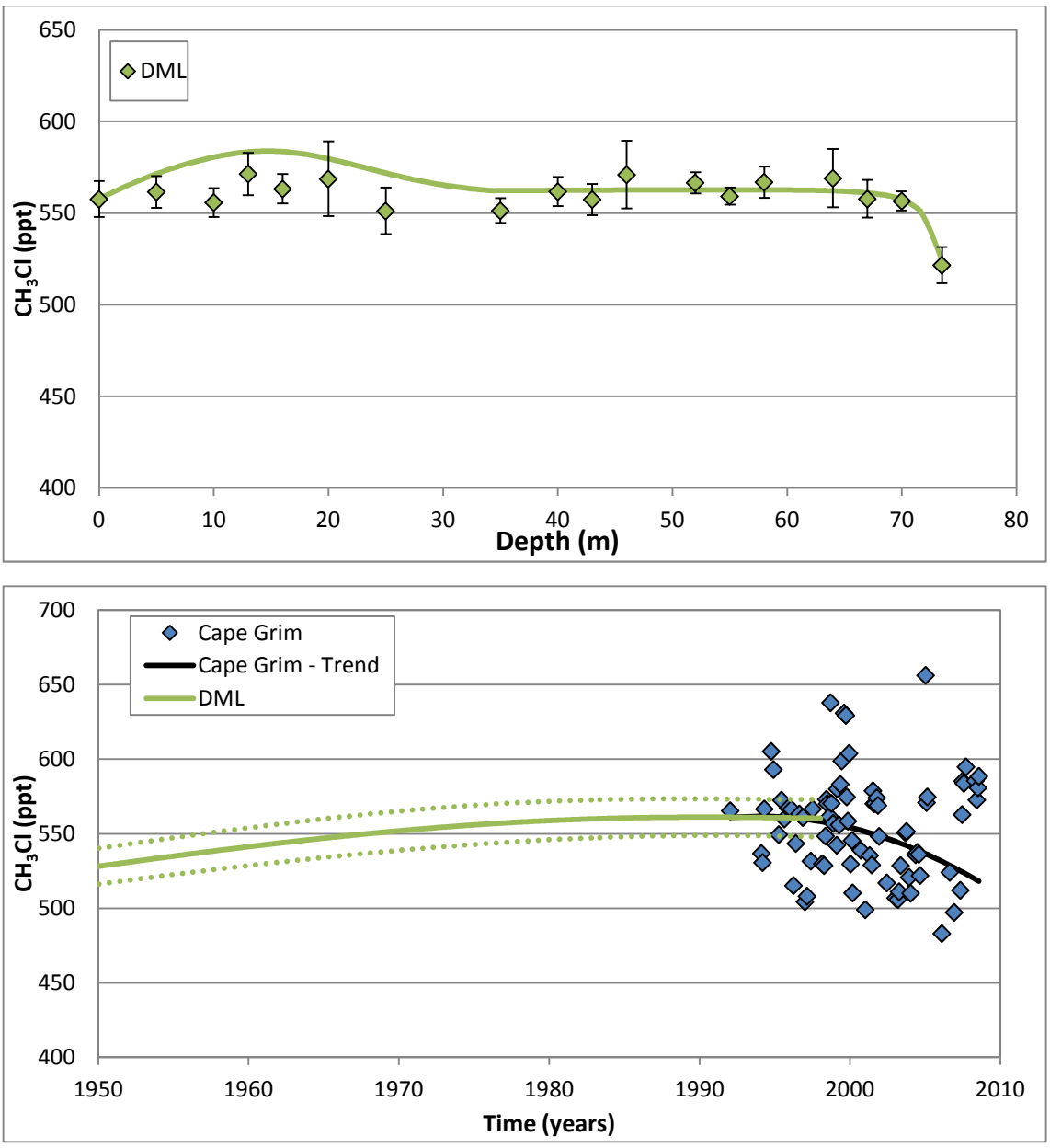

Figure 3.3: Top panel, depth profiles of southern hemispheric CH_3Cl concentration with depth at the DML firn site (green points), compared with model simulations based on the atmospheric time series indicated in the bottom panel with a seasonal cycle of 13 % added to the time series. The error bars represent the 1 σ of the measurements. Bottom panel, Atmospheric time series derived by a single site inversion modelling of the DML firn air measurements (solid line) using the LGGE method. The time series derived by the DML - green line. The dashed lines represent the uncertainties envelope of the time series (as described Figure 2.10). Also the mixing ratios of CH_3Cl as a function of time as measured in air samples collected in the southern hemisphere (blue points, from Cape Grim, Tasmania, 41°S, 145° E). The black line is a sigmoid expression fitted through the Cape Grim time series in order to derive growth rates and emissions.

Ambient air measurements (shown as depth = 0 m) were collected at the NEEM site in July 2008 during the firn air drilling. These ambient air measurements have an average mixing ratio of 527.6 ± 4.3 ppt, and are the most recent northern hemispheric measurements of CH_3Cl in this study. Ambient air measurements were collected at the DML site in December 1997

during the firn air drilling. These ambient air measurements have an average mixing ratio of 557.6 ± 9.8 ppt and are the most recent southern hemispheric in the current study.

Firn data most likely reflects the long term time series in CH_3Cl atmospheric mixing ratio. However, anomalous data points occur in the NEEM firn air measurements at 77.75 m and 74.08 m. These data points do not fit the basic trend of the firn profile. The point at 77.75 m is the deepest data point, and a higher than expected concentration is probably due to contamination with modern day air. This, contamination occurs due to the permeability of the firn diminishing towards zero at the close off depth, such that pumping causes a partial vacuum below the sealing bladder and in the inlet lines. Therefore the pressure gradients to the atmospheric air increases, which makes leaks more likely. This entrainment of modern day air can also be seen in other gases especially CFC-11 and CFC-115, where there is also an increase in concentration at 77.75 m. As both of these CFCs are purely anthropogenic, this increase is unlikely to be a result of any changes in atmospheric concentration, suggesting that the sample is likely to be contaminated. To check that these anomalous points are independent of analytical techniques a duplicate set of measurements were made on the gas chromatograph coupled with a flame ionization detector (GC-FID) system at the Max Planck Institute for Chemistry. Again the data showed elevated concentrations at 74.08 m and 77.75 m, indicating that the anomalous data points are a result of elevated sample concentrations and not as a result of analytical techniques.

With a total atmospheric lifetime of 1 year (*Montzka et al.*, 2010) CH_3Cl should have a short enough lifetime for there to be a seasonal cycle in its atmospheric mixing ratio, compared with other trace gases with similar lifetimes. The seasonal cycle of CH_3Cl has been determined by *Khalil and Rasmussen* (1999) using time series from several atmospheric observation stations. The data was analysed using a moving average filter to subtract cycles of periods longer than 12 months; this includes any long-term trends in the atmospheric mixing ratio. The amplitude of the seasonal cycle was taken to be the difference between average concentrations between the periods February-April and August-October (*Khalil and Rasmussen*, 1999b). *Khalil and Rasmussen* (1999a) observed a seasonal cycle with an amplitude of 15 % of the mean mixing ratio. The effect of a large ice sheet on the seasonal cycle of CH_3Cl has been assessed by *Kaspers et al.* (2004a), in which they demonstrated that the amplitude of the seasonal cycle for CH_3Cl could be significantly increased in firn air compared with nearby observation stations, although the phase is in line. The derived seasonal amplitudes could be as much as 1.6 times larger in the firn air. The cause of this possible increase is unclear, but could be the result of the enhanced oxidation conditions over a large ice sheet in summer (*Swanson et al.*, 2002).

There may also be different sources and transport mechanisms which influence the seasonality of CH_3Cl, especially with it having a relatively short atmospheric lifetime. This seasonal cycle can be seen in variations in CH_3Cl concentration in the shallowest part of the firn column, as described in *Kaspers et al.* (2004) and *Sturges et al.* (2001). This is also supported by the detrended Cape Grim observations which are shown in Figure 3.4.

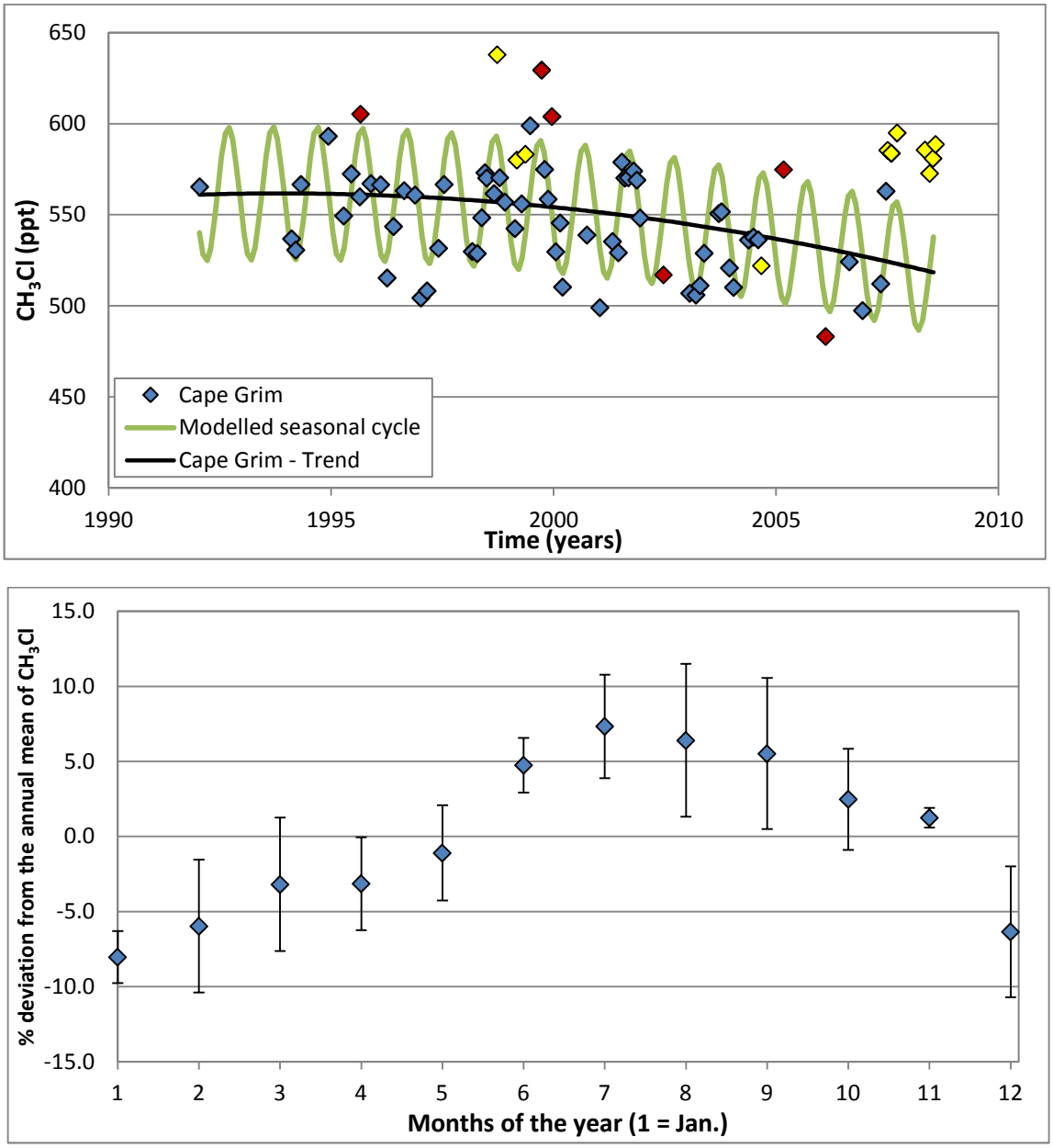

Figure 3.4: Top panel, Atmospheric mixing ratios of CH_3Cl as a function of time from observations of archived samples taken at Cape Grim (blue points), a polynomial expression fitted through the Cape Grim time series in order to detrend the data (black line), a modelled seasonal cycle based on the seasonal cycle observed in the bottom panel (green line). Data points more than 3 standard deviations away from the mean were taken as outliers and removed from the seasonal cycle calculation (yellow points). Six data points at 1995.62, 1999.71, 2000.04, 2002.21, 2005.37 and 2006.12 (red points) were found to be outliers for a number of different compounds thus were taken as unreliable samples and have been removed from all calculations of seasonal cycle from the Cape Grim data. Bottom panel, percentage deviation from the annual mean CH_3Cl mixing ratios based on the Cape Grim observations

(top panel), taken as the mean of the observations made in a particular calendar month (between 3 - 8 data points). The error bars represent the 1 σ of the measurements.

The seasonal patterns of the Cape Grim observations were determined by using a polynomial expression fitted through the data to subtract cycles of periods longer than 12 months, which includes long-term trends. A polynomial expression was used, but I did not use a 12 month moving average filter as used by *Khalil and Rasmussen* (1999) because the Cape Grim data were not measured for every month, and a moving average would not remove cycles of periods shorter than 12 months. The resulting time series after subtracting the long term trend was averaged for each of the 12 months over the years when measurements were taken. Data points more than 3 standard deviations away from the mean were taken as outliers and removed from the seasonal cycle calculation (yellow points, Figure 3.4). Six data points at 1995.62, 1999.71, 2000.04, 2002.21, 2005.37 and 2006.12 (red points, Figure 3.4) were found to be outliers for a number of different compounds thus were taken as unreliable samples and have been removed from all calculations of seasonal cycle from the Cape Grim data. The result is 12 indices which represent an estimate of the CH_3Cl seasonal cycle (Figure 3.4).

Figure 3.4 shows that there is a seasonal cycle in the atmospheric mixing ratio of CH_3Cl. The amplitude of the seasonal cycle is taken as the difference between the average of the winter (June, July and August) and summer months (Decembers, January and February). Therefore the detrended Cape Grim observation indicates a seasonal cycle with an absolute amplitude of 13 % of the annual mean mixing ratio in the southern hemisphere. This would represent a southern hemispheric seasonal cycle with an amplitude of 76.6 ppt in 2008, and the seasonal cycle agrees with that observed seasonal cycle of 80 ppt by *Khalil and Rasmussen* (1999).

Figures 3.2 and 3.3 indicate that the 1950 mixing ratio of CH_3Cl was 507 ppt in the northern hemisphere and 528 ppt in the southern hemisphere. This is evidence that CH_3Cl has sources that existed before the middle of the last century likely both natural and anthropogenic in origin. This is consistent with the findings of *Aydin et al.* (2004) discussed in 3.2.1 who observed significant CH_3Cl in ice core samples, indicating significant natural emissions. After the 1950s, the time series show a sustained growth in both hemispheres until the mid to late 1980s. The average growth rate during this period was 1.6 ppt yr^{-1} or 0.3 % yr^{-1} in the northern hemisphere and 0.8 ppt yr^{-1} or 0.9 % yr^{-1} in the southern hemisphere. The peak in the northern hemisphere atmospheric mixing ratio occurred at 565 ppt in ~1987, which is an 11 % increase from the 1950 mixing ratio. The peak in the southern hemisphere atmospheric mixing ratio occurred at 561 ppt in ~1989 which is a 7 % increase from the 1950 mixing ratio. After the peak in atmospheric mixing ratios in both hemispheres, there is a decease until mid-2008

where the mixing ratio was 515 ppt in the northern hemisphere, and 560 ppt in early 1998 in the southern hemisphere. January 1998 is the drill date of the DML firn air, and therefore this is the end of the southern hemispheric time series that can be derived from firn air in this study. Southern hemispheric measurements of $CHCl_3$ mixing ratios have been made from 1992 onwards at the Cape Grim baseline air pollution station. Figure 3.3 shows that these observations are in general agreement with the firn derived southern hemispheric time series, nevertheless there may be a number of outlying points. Growth rates were inferred for the Cape Grim observations by fitting a three parameter sigmoid expression to the data set (the black line in Figure 3.3). The northern hemispheric time series of atmospheric CH_3Cl mixing ratio agrees with the time series in atmospheric CH_3Cl observed at the Barrow observation station since 1998 (Figure 3.2) (Updated from *Khalil and Rasmussen*, 1999b). Although there is an offset between the absolute mixing ratios, this difference is likely due to a calibration scale offset between the two studies. A comparison of calibration scales by *Cox et al.* (2003) showed a 4 ± 1 %, offset in the NOAA measurements compared with AGAGE. Figures 3.2 and 3.3 indicate that the seasonal cycle with an amplitude of 13 % is able to model variations in the CH_3Cl concentration in the shallowest part of the firn columns (*Kaspers et al.*, 2004) and *Sturges et al.*, 2001). This means that in the current study there is no evidence of an increased seasonal amplitude on a large ice sheet as suggested by *Kaspers et al.* (2004a).

An averaged 'global' atmospheric time series of CH_3Cl was estimated between 1950 and 2008.5 (the drill date of the NEEM site) by averaging northern and southern hemispheric time series (Figure 3.5). The southern hemispheric time series was derived using both the firn derived time series and the Cape Grim time series. These two time series were averaged for the years that are covered by both. This averaged atmospheric time series cannot be taken as the true global average, as CH_3Cl has a strong latitudinal gradient (*Khalil and Rasmussen*, 1999). Therefore this average atmospheric time series does not take into account the high mixing ratios observed in the tropical regions (*Khalil and Rasmussen*, 1999). Consequently, the 'global' averaged time series I have produced also cannot be taken as the true global average as only polar regions observations have been taken.

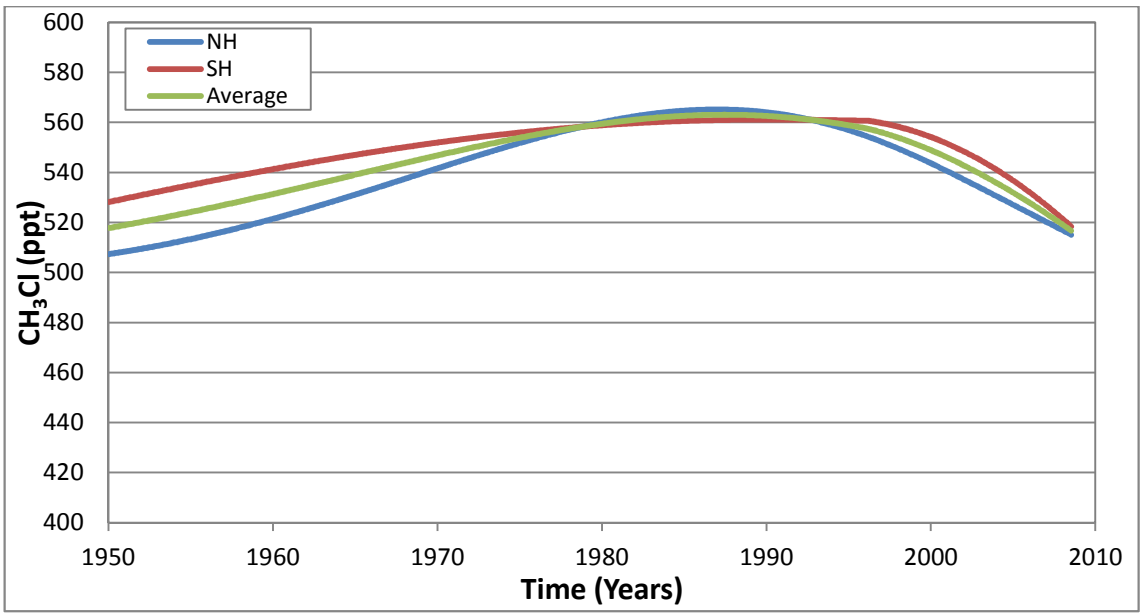

Figure 3.5: Northern hemispheric atmospheric time series of CH_3Cl derived from Arctic firn air (blue line). Southern hemispheric atmospheric time series of CH_3Cl derived from Antarctic firn and Cape Grim observation (red line). The average atmospheric time series of CH_3Cl was estimated by averaging the northern and southern hemispheric time series (green line).

Figure 3.5 indicates that the mixing ratio of CH_3Cl increased from 518 ppt in 1950 to a maximum of 563 ppt in ~1987. In mid-2008 the 'global' mixing ratio was 517 ppt and the growth rate was -4 ppt yr^{-1} in 2007. These 'global' observations are in general smaller than the annual mean mixing ratio in 2008 observed by the AGAGE and NOAA networks (545.0 - 547.0 ppt (*Montzka et al.*, 2010)). This difference is most likely due to the fact that in this study, only polar and mid to low latitude observations have been taken, with no measurements being made in the tropics, which has a higher mixing ratio (*Montzka et al.*, 2010).

Figure 3.5 shows that there is a correlation both in trend and absolute mixing ratio between the different time series. This result indicates that there is a similarity between the overall time series and absolute mixing ratio for northern and southern hemispheric atmospheric CH_3Cl. It is unexpected for a compound that only has a total atmospheric lifetime of 1 year (*Montzka et al.*, 2010), to have such hemispheric symmetry. This probably results from CH_3Cl having such strong in the tropics, spanning the equator and dispersing the compound into both hemispheres equally. This permits that atmospheric time series of CH_3Cl from the southern hemisphere can be used to assess the NEEM data. To validate the southern hemispheric time series, it was used to model the EDML firn air measurements (Figure 3.6). The EDML firn air samples were taken at Dronning Maud Land in Antarctica (75^0 S, 0^0 E) in January 2006. Due to the multi-site model not being tuned for the EDML firn air samples at the time of this study,

these measurements were not able to be used to derive an atmospheric time series from the multi-site inversion modelling.

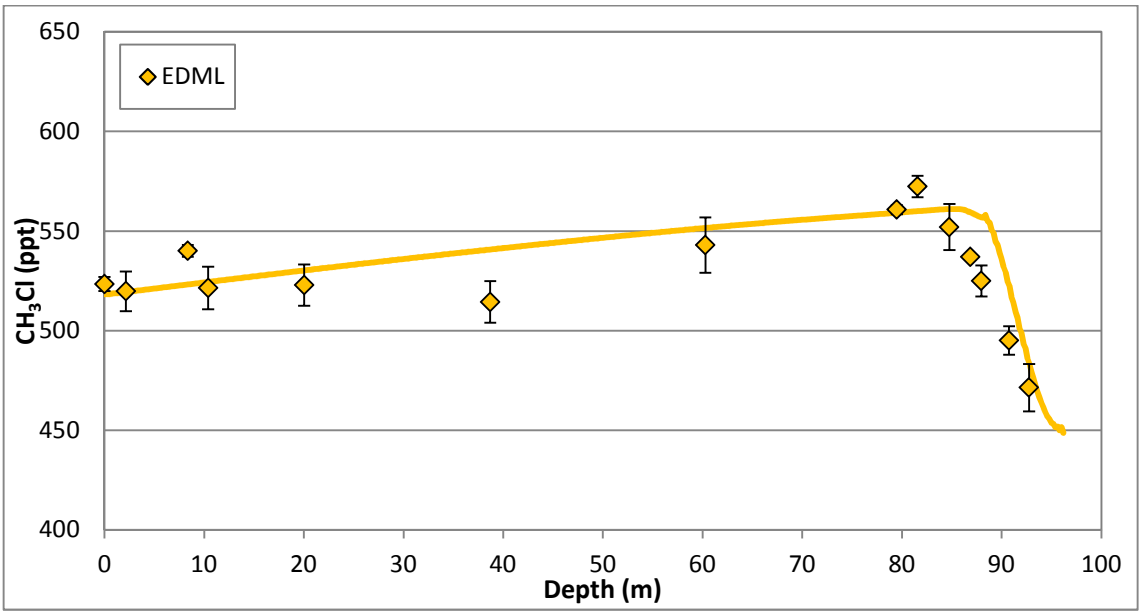

Figure 3.6: Depth profiles of southern hemispheric CH_3Cl concentration at the EDML firn site (yellow points) compared with model simulations based on the atmospheric time series indicated in Figure 3.5. The error bars represent the 1 σ of the measurements.

Figure 3.6 shows that the southern hemispheric time series does agree with the firn air measurements from the EDML firn air site, validating the southern hemispheric time series. However the EDML does show that the concentration of CH_3Cl at 92.75 m was 471 ppt, which is the lowest concentration measured in the firn in this study. Therefore a multi-site model run with this firn profile in may extend the southern hemisphere time series to an earlier date. Therefore I would recommend that this multi-site derived time series be derived when the model is able to assess EDML firn profiles. As well as validating this time series, it was used as a comparison with other firn air and ice core derived time series. These comparisons can be seen in Figure 3.7.

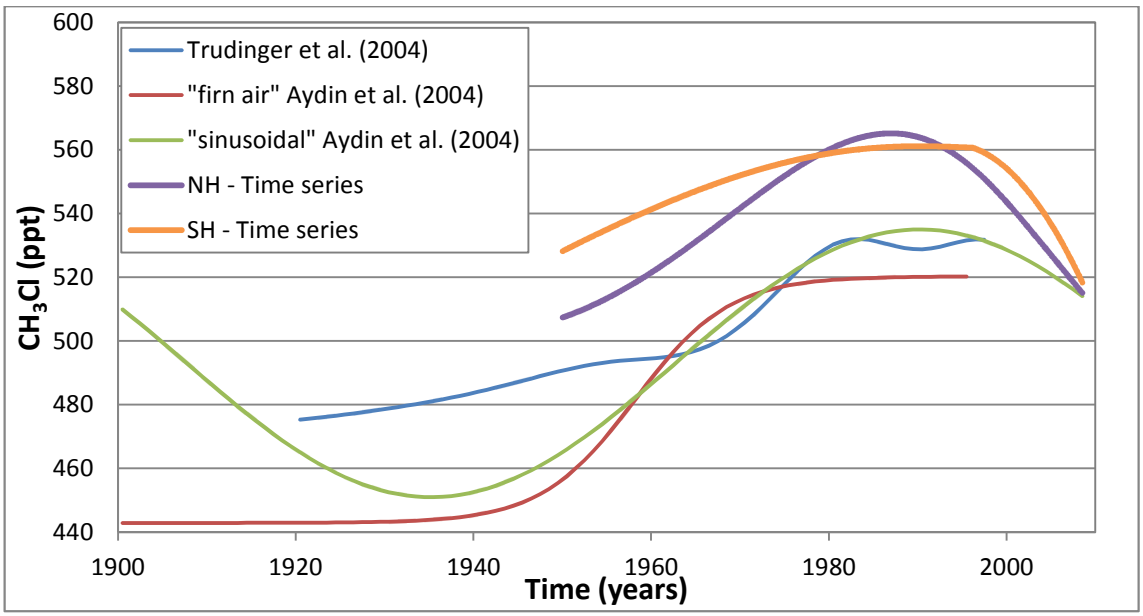

Figure 3.7:. Northern hemispheric time series from this study (purple line – Figure 3.2) and the southern hemispheric time series from this study (orange lines – Figure 3.3) compared with the southern hemispheric CH_3Cl atmospheric mixing ratio time series from selected previous studies obtained from firn air and ice cores data; *Trudinger et al.* (2004) (blue line), "firn air" history *Aydin et al.* (2004) (red line) and ''sinusoidal'' history *Aydin et al.* (2004) (green line)

Figure 3.7 shows there is a good general agreement between the different studies. There is an offset between the absolute mixing ratios, which is most likely due to a calibration scale offset of ~ 4 % between the two studies. For example, a comparison of calibration scale by *Cox et al.* (2003) showed a difference between 2 different studies.

Trudinger et al. (2004) explained much of this variation in the CH_3Cl budget as a result of emissions from biomass burning. The authors assessed the biomass burning emissions with the use of a two-box atmospheric model (*Trudinger et al.*, 2004). The model used time variation of the sources such as biomass burning, coal combustion, waste incineration and industry. Coal combustion was scaled with the time evolution of CO_2 emissions due to estimated solid fuel uses from *Marland et al.* (2003). Emissions due to biomass burning were scaled using the method of *Reeves* (2003) which scales emission estimates by global population, with 10 % of the present-day value held constant. Global population data for *Trudinger et al.* (2004) came from the United Nations *Chamie et al.* (1999). However, unlike *Aydin et al.* (2004), the other large sources of CH_3Cl such as tropical plants and oceans remained relatively constant with in the model. The results from the *Trudinger et al.* (2004) model suggest that the time series derived in this study could be caused by biomass burning emissions increasing at similar rate to human population growth until around 1980. However, after 1980, the firn reconstruction shows a reduced growth rate for CH_3Cl mixing ratio while the biomass burning source, following population, drives the modelled mixing ratios higher. Rather little is known about the

variation in global emissions of CH_3Cl from biomass burning over the last century. However, *Duncan et al.* (2003) has estimated biomass burning emissions of CO from satellite measurements between 1979 - 2000. These estimated emissions show that there is no general trend for emissions during this period, but there is a significant interannual variability, with a very large peak in 1998. The results from *Trudinger et al.* (2004) show that most of this variation in CH_3Cl atmospheric mixing ratio could be caused by an increase in biomass burning source increasing in a similar way to population until 1980, then becoming more stable (apart from some high burning years). The decrease in CH_3Cl observed after 1998 may be due to a period of recovery after the large biomass burning event in 1997–1998 (*Simmonds et al.*, 2004). Alternatively, this increase in mixing ratios could have resulted from one or more source(s) also varying in a manner similar to population growth (e.g. increased industrial / agricultural and/or some other anthropogenically influenced source). However *Aydin et al.* (2004) reported that it was unlikely that anthropogenic emissions were responsible for the increase in atmospheric CH_3Cl mixing ratios derived during the 20th century, because the CH_3Cl atmospheric mixing ratio time series did not show any correlation with the temporal pattern of emissions from coal combustion during the 20th century (*Keeling*, 1994).

There is also be evidence of natural variability in the flux of CH_3Cl. *Aydin et al.* (2004) observed an oscillating pattern in the atmospheric mixing ratio of CH_3Cl over the lasted 300 years (green line - Figure 3.7 – only between 1900 and 2008). If the atmospheric CH_3Cl mixing ratio time series is sinusoidal, then it is unclear what the underlying causes of these regular cycles are. However, the cycles seem to predate significant industrial activity, thus *Aydin et al.* (2004) indicate that a natural variability may reflect climate-driven changes in the CH_3Cl budget. The apparent dominance of tropical plants as a CH_3Cl source (*Yokouchi et al.*, 2002), resulted in *Aydin et al.* (2004) speculating that such variability could arise from changes in tropical flora as a response to changes in climate. The cycles may also point to changes in the atmospheric lifetime of CH_3Cl. The largest atmospheric sink of CH_3Cl is through oxidation with the OH radical (*Montzka et al.*, 2010). Therefore any cycles in the OH budget could result in a similar cycle in CH_3Cl mixing ratios. Although there is currently no evidence of a cycle in the global OH budget, *Prinn et al.* (2005) reported OH concentrations in 2003–2004 as comparable to those in 1979, with a derived global averaged OH linear trend of 0.2 % year^{-1} during this period. Analysis of global average OH levels indicates a small maximum around 1989 and a minimum around 1998 (6 % drop in OH between 1997–1999) (*Montzka et al.*, 2010). There have been observations of strong centennial-scale climatic oscillations in atmospheric gases. However, this has not yet been observed for CH_3Cl, during the late Holocene from Greenland ice cores

(*Meeker and Mayewski*, 2002 and *Appenzeller et al.*, 1998). These variations appear to reflect large-scale atmospheric circulation changes associated with the North Atlantic Oscillation. Hundred year periodicities are also apparent in other climate proxy records during the last thousand years (*Briffa et al.*, 2001 *Mann et al.*, 1998 and *Overpeck et al.*, 1997). *Gleissberg* (1966) suggested that variability in solar activity may provide the forcing for climate change on such time scales, but as yet there is no direct evidence for this mechanism.

The general agreement between the *Aydin et al.* (2004) ''sinusoidal'' history and the time series derived in this study during the 20th century indicates that the CH_3Cl time series are consistent with preindustrial variability, without including any anthropogenic contributions to the atmospheric budget. This result suggests there may not be a significant industrial or agricultural contribution to CH_3Cl levels in the modern atmosphere. If CH_3Cl in the atmosphere continues to oscillate as suggested in the past by the *Aydin et al.* (2004) ''sinusoidal'' history, then the CH_3Cl burden may decrease by up to 10 % over the next half century. However since ca. 2000 the *Aydin et al.* (2004) ''sinusoidal'' history does not accurately reproduce the decline in atmospheric mixing ratio observed in the current study by the NEEM firn air and Cape Grim measurements as well as the observation from Barrow (updated from - *Khalil and Rasmussen*, 1999b). This indicates that either the "sinusoidal" forcing on CH_3Cl mixing ratios has not been effecting the global abundance, or that this forcing has now stopped or that the current sources and sinks are now counteracting this "sinusoidal" forcing.

3.2.3 Emissions of CH_3Cl

The 'global' annual emission of CH_3Cl was estimated using the atmospheric time series in Figure 3.5 and with the use of a 1 - box model, further details of the emission estimate process are given in the methods chapter (Section 2.5.4). These annual emission estimates are shown in Figure 3.8.

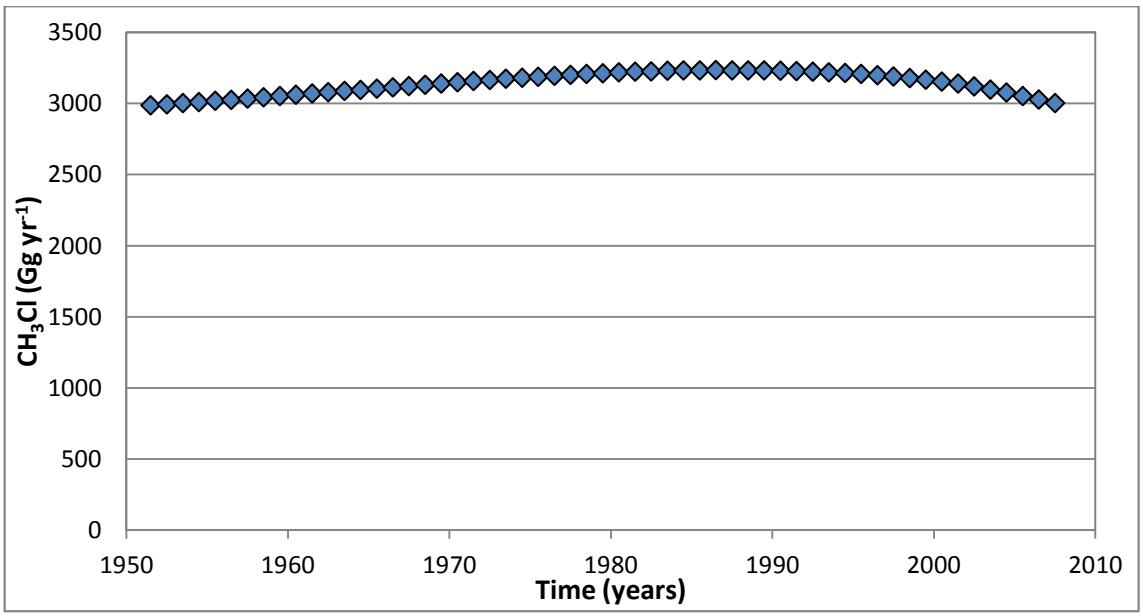

Figure 3.8: Annual emission of CH_3Cl based on the atmospheric time series in Figure 3.5.

Figure 3.8 shows that the emissions of CH_3Cl rose from 3000 Gg yr^{-1} in 1950 to a peak of 3200 Gg yr^{-1} in 1986 before progressively declining to 3000 Gg yr^{-1} in 2007 this is a decline of around 7 % from the peak emission. These emissions estimates generally agree with the global emissions estimates report by *Montzka et al.* (2010) of between 2844 and 5508 Gg yr^{-1}. However, as stated earlier this study does under estimate the global mixing ratio due to the strong tropical emissions of CH_3Cl (*Montzka et al.* 2010). There means that it is likely that the emissions estimates are an under estimate of the global emission rate. It should also be noted that there are still uncertainties in the strength and sources of CH_3Cl emissions, therefore these atmospheric time series may point to an as yet unidentified anthropogenic source or an indirect effect of human activities on natural sources and sinks, for example those caused by changes in land use patterns and agricultural practices (*Aydin et al.* 2004).

3.3 Very Short-Lived (VSL) chlorinated substances

The VSL chlorine substances are defined as chlorinated trace gases whose local lifetimes are comparable to, or shorter than, the tropospheric transport timescales and that have non-uniform tropospheric abundances (*Montzka et al.*, 2010). Generally, VSL chlorine substances are considered to be compounds that have atmospheric lifetimes of less than 6 months.

Based on a limited number of observations, very short-lived source gases account for 55 (38–80) ppt chlorine in the middle of the tropical tropopause layer (*Montzka et al.*, 2010). Approximately 40 ppt of the chlorine from source gases is from anthropogenic VSLs emissions (e.g. $CHCl_3$ and CH_2Cl_2) (*Montzka et al.*, 2010). The amount of chlorine from a VSL source

substance that reaches the stratosphere depends on the location of the emissions as well as atmospheric removal and transport processes (*Montzka et al.*, 2010). Therefore, there are uncertainties in quantifying the full impact of VSL chlorine-containing compounds on stratospheric ozone.

In this section, I will report the atmospheric time series of the mixing ratios of the VSL chlorine substances: $CHCl_3$, CH_2Cl_2, CCl_2CCl_2, CH_2ClCH_2Cl, C_2H_5Cl and $CHClCCl_2$. Firn air samples collected in Greenland were used to reconstruct a northern hemispheric time series. Samples collected in Antarctica, as well as observations from archived samples taken at the Cape Grim baseline air pollution station were used to reconstruct a southern hemispheric time series. These two time series are then used to calculate emission rates for the VSL chlorine substances.

3.3.1 Background information on $CHCl_3$

Chloroform (trichloromethane, $CHCl_3$) is the second most abundant organic source of natural chlorine to the atmosphere after methyl chloride and is an important source of tropospheric chlorine. The globally averaged mixing ratio of chloroform at the earth's surface was calculated as 7.0 ± 1.5 ppt in 2008 (*Montzka et al.*, 2010). It is used almost exclusively in the production of HCFC-22 and fluoropolymers, but is also released as a by-product from chlorine bleaching in the paper and pulp industry and from water chlorination (*Worton et al.*, 2006).

"Top-Down" average annual global emission were calculated to be 315-373 Gg yr^{-1} for 2001 (*Worton et al.*, 2006) and 370 ± 120 Gg yr^{-1} between 2000-2004 (*Xiao*, 2008). About 75 % of these emissions are natural in origin (*Montzka et al.*, 2010). The largest single source appears to be the open oceans (contributing 168 ± 106 $Ggyr^{-1}$, (*Xiao*, 2008)), from a yet undefined biological process (*Khalil et al.*, 1999). However sources from macroalgae in the coastal regions of the ocean appear not to contribute much to the total release (*Baker et al.*, 2001).

Table 3.3: Annual emissions of atmospheric $CHCl_3$ in Gg yr^{-1}.

Source	**Emissions** (*Xiao*, 2008)	**Emissions** (*Keene et al.*, 1999)	**Emissions** (*Worton et al.*, 2006)	**Emissions** (*McCulloch*, 2003)
Reference year	2000-2004	1990	2001	(not given)
Oceans	168 ± 106	361		360 ± 90
Soils	136 ± 56	202		220 ± 100
Industry	64.5	65	79-108	66 ± 23
Biomass burning	1.97 ± 1.83	2		
Total	370 ± 120	630	315-373	660 ± 220

Soil processes are the next most important natural source for $CHCl_3$ formation. The worlds soils emit about 136 ± 56 Gg yr^{-1} of $CHCl_3$ (*Xiao*, 2008), and it is produced naturally in the top layers of soil when an oxidising agent acts on an organic material in the presence of chloride ions (*Hoekstra et al.*, 1998b *Hoekstra et al.*, 1998a and). Rice fields and termite bearing soils have also been identified as a $CHCl_3$ sources (*Khalil et al.*, 1998). Other natural sources, mainly volcanic and geological, account for less than 20 Gg yr^{-1} (*McCulloch*, 2003).

Industrial sources of $CHCl_3$ total 65-108 Gg yr^{-1} (*Xiao*, 2008, *Worton et al.*, 2006 and *McCulloch*, 2003) and are predominantly the result of using strong oxidizing agents on organic material in the presence of chloride ions, which is a direct parallel with the natural processes occurring in soils. $CHCl_3$ is produced as a by-product during the delignification of wood and other cellulose pulps and the bleaching of paper by chlorine. *Juuti et al.* (1996) identified that other chlorine-containing oxidants used in these processes (such as chlorine dioxide, ClO_2) also generate $CHCl_3$. Chloroform is produced when water is treated with chlorine through the haloform reaction involving humic compounds (*Larson and Weber*, 1994). With its relatively low solubility in water and relatively high vapour pressure, $CHCl_3$ generated in water can be expected to partition into the atmosphere (*Ballschmiter*, 1992).

Xiao (2008) and *O'Doherty et al.* (2001) estimated around 62 % of total $CHCl_3$ emissions originate from the Northern Hemisphere. Chloroform is only estimated to contribute < 10 ppt (*McCulloch*, 2003) to stratospheric chlorine as a result of its short tropospheric lifetime of 149 days (*Montzka et al.*, 2010). $CHCl_3$ is degraded in the troposphere through oxidation by OH to phosgene ($COCl_2$) a small percentage of which reaches the stratosphere where it can participate in ozone destruction (*Kindler et al.*, 1995). Chloroform is also removed by anaerobic and aerobic soil microorganisms, although not important to the global $CHCl_3$ mixing ratio, this can have a profound effect on the local concentration in the soil that cannot equilibrate into the atmosphere (*McCulloch*, 2003).

Chloroform has been observed in the environment over many years: in air (*O'Doherty et al.*, 2001 and *Murray and Riley*, 1973), water (*Zok et al.*, 1998) and soil pores (*Hoekstra et al.*, 1998a). The globally averaged mixing ratio of chloroform at the Earth's surface has been reported to be 18.5 ppt between 1986 and 1994 (*Khalil and Rasmussen*, 1999a). The mixing ratio is estimated to have contributed ca. 60 ppt chlorine to the lower troposphere, and about 40 ppt chlorine to the total troposphere (*Khalil and Rasmussen*, 1999a). Later measurements from the AGAGE network between 1994 and 1998 show a much lower global average baseline mixing ratio of 8.9 ± 0.1 ppt with no appreciable trend during this period (*O'Doherty et al.*,

2001). Since 2000, annual averaged $CHCl_3$ mixing ratios have remained approximately constant, suggesting little change in the fraction arising from industrial emissions (*Montzka et al.*, 2010). The globally averaged mixing ratio of $CHCl_3$ at the Earth's surface was 7.0 ± 1.5 ppt in 2008. This was only a −0.02 ± 0.09 ppt change in mixing ratio from the 2007 value (*Montzka et al.*, 2010).

Long term time series of atmospheric chloroform mixing ratio have been assessed through the analysis of air trapped in firn from both the Arctic and Antarctic (*Worton et al.*, 2006 and *Trudinger et al.*, 2004). The detail of these firn air sites can be found in Table 3.1 and Chapter 2.

The *Trudinger et al.* (2004) reconstruction of southern hemispheric $CHCl_3$ mixing ratios in the atmosphere shows an increase from about 1930, to ca. 1970, with $CHCl_3$ mixing ratios reaching a maximum around 1990 before then decreasing (Figure 3.9). The mixing ratio around 1940 was ~3.9 ppt and the maximum (mean annual) mixing ratio was over 6.5 ppt in ca. 1990 (*Trudinger et al.*, 2004). Between 1986 and 1994, *Khalil and Rasmussen* (1999) made measurements of atmospheric $CHCl_3$ mixing ratios directly from the atmosphere at a number of sites including Cape Grim and Antarctica. Their records show consistently higher mixing ratios than the firn or AGAGE records, but this may be due to a difference in calibration scale (*Cox et al.*, 2003).

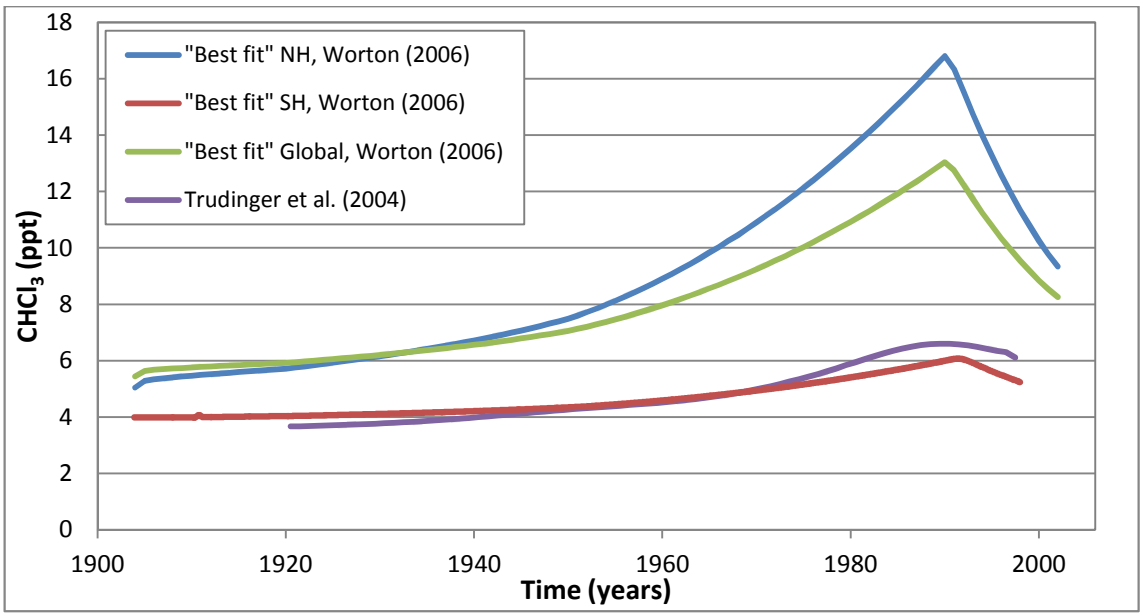

Figure 3.9: The atmospheric time series of chloroform during the 20th century from the "best fit" modelled global (green line), northern hemispheric (NH, blue line), and southern hemisphere (SH, red line) by *Worton et al.* (2006) and the southern hemisphere atmospheric time series (purple line) by *Trudinger et al.* (2004).

Worton et al. (2006) collected firn air samples at the North Greenland Ice core Project (NGRIP), Greenland, Devon Island (DI), Canada, Dronning Maud Land (DML), Antarctica and Dome Concordia (Dome C), Antarctica sites (Chapter 2).

Worton et al. (2006) generated the atmospheric mixing ratios for the locations of the firn sites with the use of a 2-D atmospheric chemistry transport model, detailed in *Reeves* (2003). To validate these atmospheric mixing ratios, a firn physical transport model (*Rommelaere et al.*, 1997) was used to interpolate atmospheric time series into firn concentration depth profiles. By varying the magnitudes of anthropogenic and natural emissions of $CHCl_3$ in the atmospheric model, *Worton et al.* (2006) produced four scenarios that matched the firn profiles. These profiles are referred to as the "best fit" time series.

These four "best fit" scenarios incorporate either 4 or 5 times the reported paper and pulp emissions by *Aucott et al.* (1999), double the reported water chlorination and other industrial emissions by *Aucott et al.* (1999) and natural emissions based on *Khalil et al.* (1999). These modelled calculations suggest anthropogenic emissions accounted for ca. 14 - 20 % of total $CHCl_3$ emissions in 1950, and increased to 41 - 50 % of total emissions at the peak in global mixing ratios around 1990. Anthropogenic emissions subsequently decreased to ~ 19 % of total emissions in 2001 (*Worton et al.*, 2006). This decrease was attributed mostly to a reduction in paper and pulp manufacture, from the 1990s. When the "best fit" scenarios were modelled a global background mixing ratio of ~5.4 pptv was derived for the start of the 20th century

(Figure 3.9). The atmospheric mixing ratios of $CHCl_3$ was then shown to increase to a global background maximum of 13.0 pptv in 1990, before decreasing in the atmosphere.

There is agreement between the atmospheric time series derived by the different studies. For example, the southern hemispheric time series derived by *Worton et al.* (2006) correlates with the southern hemispheric time series derived by *Trudinger et al.* (2004).

Worton et al. (2006) estimated an average global mixing ratio of 10.4 pptv $CHCl_3$ between 1994 – 1998, which is higher than the 8.9 ± 0.1 pptv measured by the AGAGE network (*O'Doherty et al.*, 2001). The rate of decline during this period, (-0.42 pptv yr^{-1} (*Worton et al.*, 2006)) is slightly outside the errors of the estimated decrease during the same period measured by the AGAGE network (*O'Doherty et al.*, 2001).

3.3.2 Results and discussion of $CHCl_3$

In the current study, I will report firn air measurement of $CHCl_3$ from a number of northern and southern hemispheric firn air records, as well as southern hemispheric observations from the Cape Grim baseline air pollution station. These measurements have then been used to derive the atmospheric time series of $CHCl_3$ mixing ratios. The time series of atmospheric $CHCl_3$ mixing ratios were derived using the LGGE method, which is described in more detail in the methods chapter. These new atmospheric time series are then compared with previous atmospheric time series estimated by *Worton et al.* (2006). The time series obtained and the output from the inverse model for the northern and southern hemisphere site are shown alongside the measured concentration of $CHCl_3$ with depth at northern hemispheric firn sites (NEEM, NGRIP and DI) and southern hemispheric (DML) firn sites in Figures 3.10 and 3.11, respectively.

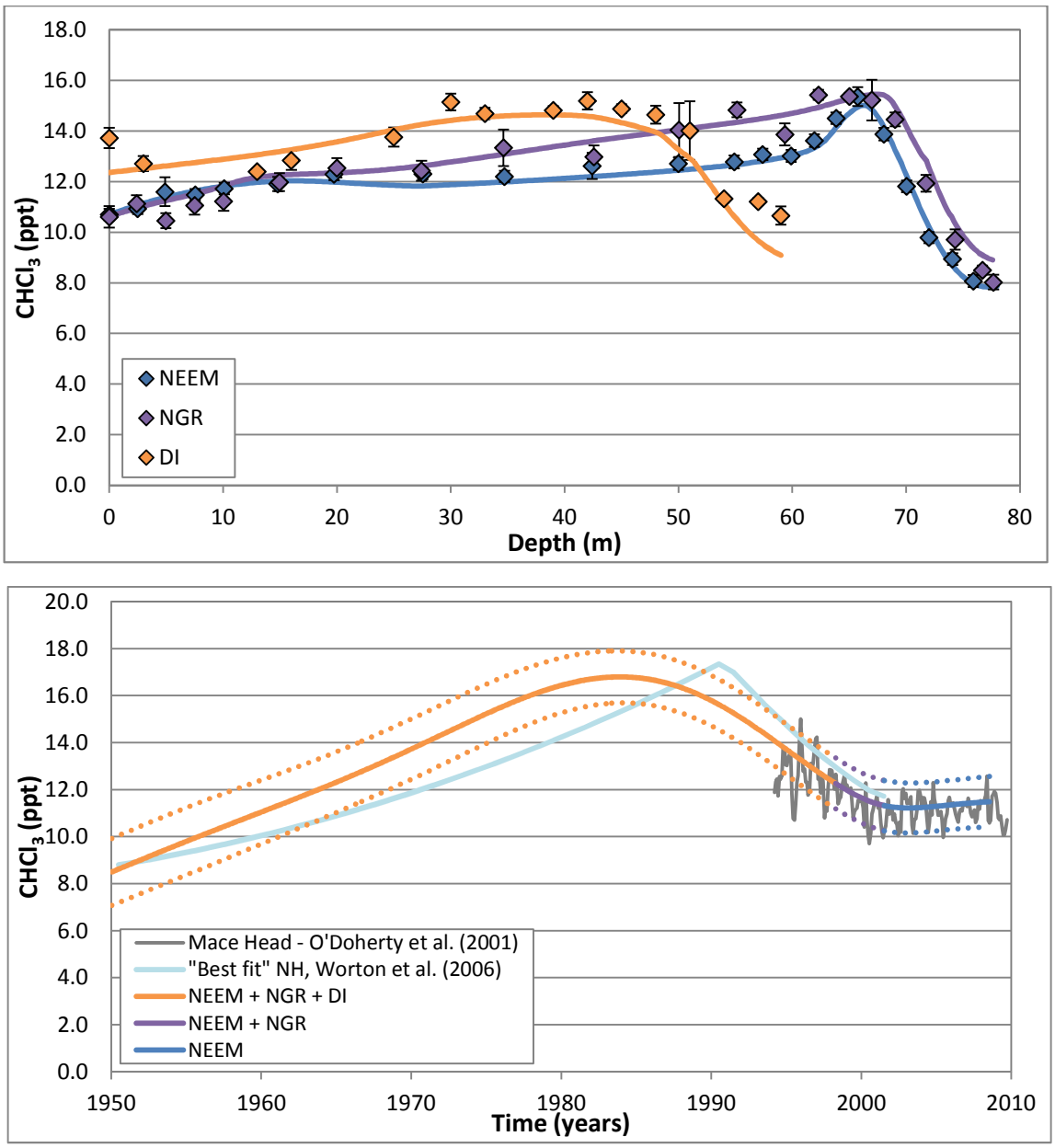

Figure 3.10: Top panel, depth profiles of northern hemispheric $CHCl_3$ concentration with depth at the; NEEM firn site (blue points), NGRIP firn site (purple points) and the DI firn site (yellow points), compared with model simulations based on the atmospheric time series indicated in the bottom panel with a seasonal cycle of 28 % added to the time series. The error bars represent the 1 σ of the measurements. Bottom panel, Atmospheric time series derived by a multi-site inversion modelling of the NEEM, NGRIP and DI firn air measurements (solid line) using the LGGE method. The time series derived by the NEEM, NGRIP and DI - yellow line, NEEM and NGRIP – purple line and NEEM only – blue line. The dashed lines represent the uncertainties envelope of the time series (as described Figure 2.10). Observations of atmospheric $CHCl_3$ from the Mace Head observation station updated from *O'Doherty et al.* (2001) (grey line) and the "Best fit" northern hemispheric time series derived by *Worton et al.* (2006) (light blue line) are shown as comparisons.

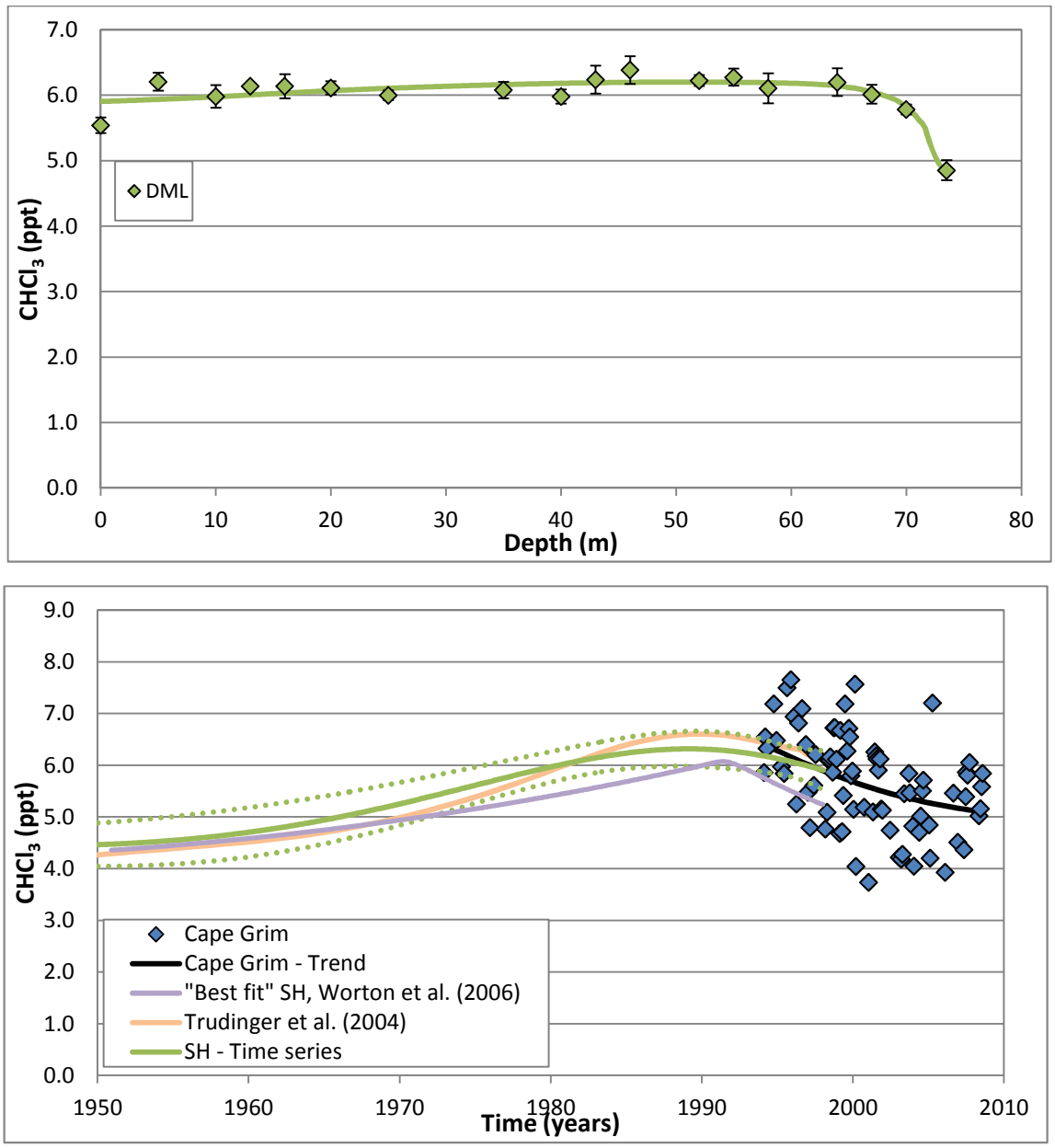

Figure 3.11: Top panel, depth profiles of southern hemispheric $CHCl_3$ concentration with depth at the DML firn site (green points), compared with model simulations based on the atmospheric time series indicated in the bottom panel with a seasonal cycle of 28 % added to the time series. The error bars represent the 1 σ of the measurements. Bottom panel, atmospheric time series derived by a single site inversion modelling of the DML firn air measurements (solid line) using the LGGE method. The dashed lines represent the uncertainties envelope of the time series (as described Figure 2.10). Also the mixing ratios of $CHCl_3$ as a function of time as measured in air samples collected in the southern hemisphere (blue points, from Cape Grim). The black line is a sigmoid expression fitted through the Cape Grim time series in order to derive growth rates and emissions. The "Best fit" southern hemispheric time series derived by *Worton et al.* (2006) (light purple line) and the time series derived by *Trudinger et al.* (2004) (light orange line)are shown as comparisons.

The ambient air measurements (shown as depth = 0 m) were collected at the NEEM site in July 2008. These ambient air measurements had an average mixing ratio of 10.70 ± 0.23 ppt and represent the latest northern hemispheric measurements of $CHCl_3$ in this study. The ambient air measurements were collected at the DML site in the December 1997 during the firn air drilling. These ambient air measurements have an average mixing ratio of 5.54 ± 0.12 ppt and are the latest southern hemispheric measurements from the firn air sites in this study.

With a total atmospheric lifetime of 149 days (*Montzka et al.*, 2010), $CHCl_3$ should have a short enough lifetime for there to be a seasonal cycle in its atmospheric mixing ratio. *O'Doherty et al.* (2001) observed a seasonal cycle in the atmospheric mixing ratio of $CHCl_3$ that appears to be consistent with the removal by reaction with OH, However, it also appears that the cycle is effected by the seasonality in $CHCl_3$ emissions. *O'Doherty et al.* (2001) observed a seasonal cycle with an amplitude of 23 % of the mean mixing ratio. *Worton et al.* (2006) modelled the seasonal cycle of $CHCl_3$ using a 2-D atmospheric chemistry transport model (*Reeves*, 2003), by assigning a seasonal variation to each source and sink. *Worton et al.* (2006) calculated a seasonal cycle of around 28 % of the mean mixing ratio. This seasonal cycle can be seen in the variations in the $CHCl_3$ concentration in the shallowest part of the firn columns, as described in *Kaspers et al.* (2004) and *Sturges et al.* (2001). This is also supported by the detrended Cape Grim observations which are shown in Figure 3.12.

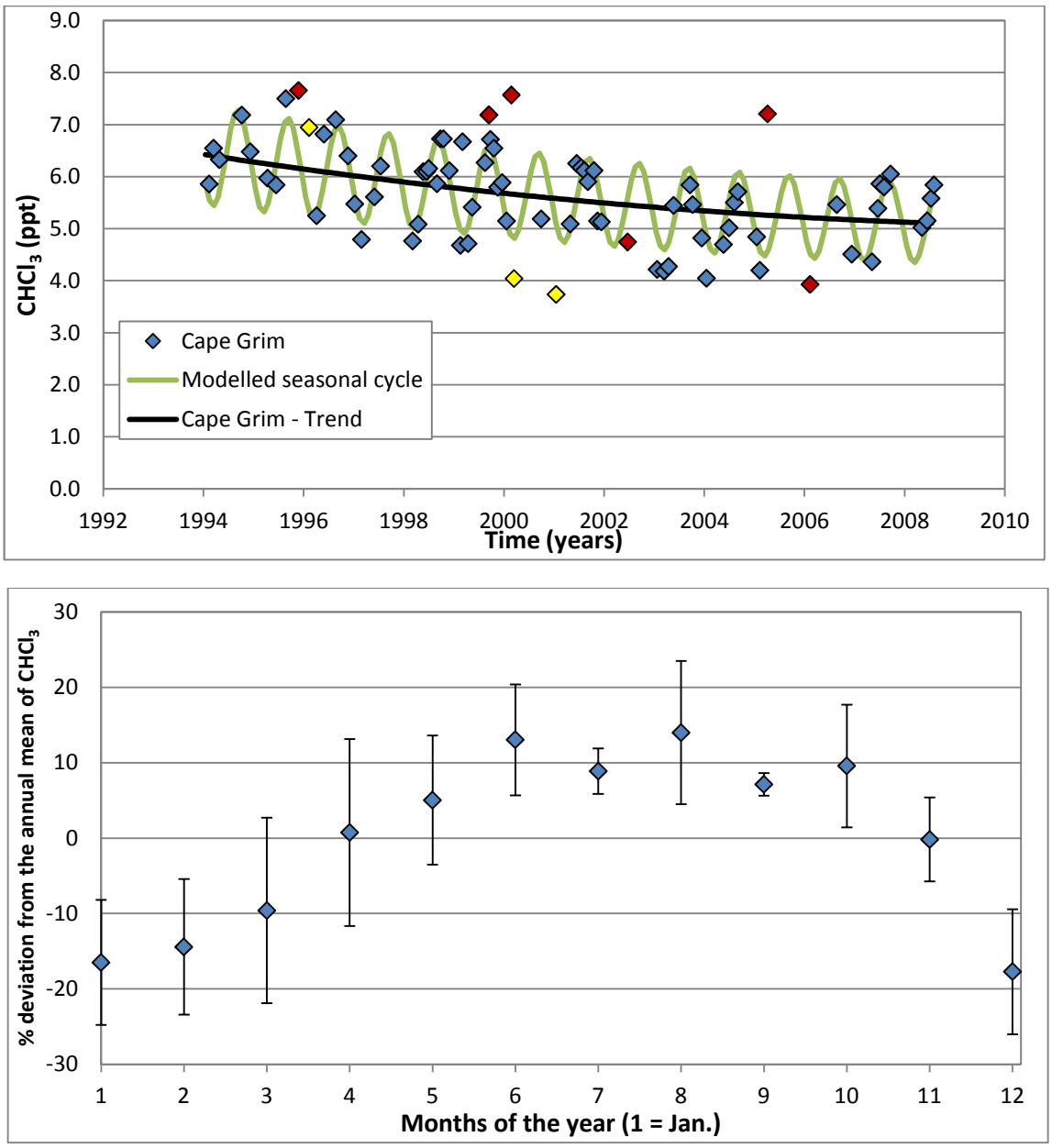

Figure 3.12: Top panel, atmospheric mixing ratios of $CHCl_3$ as a function of time from observations of archived samples taken at Cape Grim (blue points). A polynomial expression fitted through the Cape Grim time series in order to detrend the data is shown by a black line and a modelled seasonal cycle based on that observed in the bottom panel (green line). Data points more than 3 standard deviations away from the mean were taken as outliers and removed from the seasonal cycle calculation (yellow points). Six unreliable samples were also removed from the seasonal cycle calculation (red points) (see Figure 3.4 for more details). Bottom panel, percentage deviation from the annual mean $CHCl_3$ mixing ratio based on the Cape Grim observations (top panel), taken as the mean of the observations made in a particular calendar month (between 3 - 8 data points). The error bars represent the 1 σ of the measurements.

The seasonal patterns of the Cape Grim observations were determined by using the same method described in section 3.2.2. Figure 3.12 shows that there is a seasonal cycle in the atmospheric mixing ratio of $CHCl_3$. The amplitude of the seasonal cycle is taken as the difference between the average of the winter (June, July and August) and the summer

months (Decembers, January and February) average mixing ratios. The Cape Grim observation indicates a seasonal cycle with an total amplitude of 28 % of the annual mean mixing ratio in the southern hemisphere. This would represent a southern hemispheric seasonal cycle with an amplitude of 1.43 ppt in 2008. This seasonal cycle agrees with that observed by *Worton et al.* (2006) and *O'Doherty et al.* (2001).

Figures 3.10 and 3.11 indicate that the mixing ratio of $CHCl_3$ was 8.5 ppt in the northern hemisphere and 4.5 ppt in the southern hemisphere in 1950. After the 1950s, the time series show a sustained growth in both hemispheres until the mid-1980s in the northern hemisphere and around 1990 in the southern hemisphere. Average growth rates during this period were 0.25 ppt yr^{-1} or 2.0 % yr^{-1} in the northern hemisphere and 0.05 ppt yr^{-1} or 0.9 % yr^{-1} in the southern hemisphere. The greater increase in the northern hemisphere reflects a larger contribution of northern hemispheric anthropogenic emissions of $CHCl_3$ to the global mixing ratio. *Xiao* (2008) estimated 62 % of global $CHCl_3$ emissions originate from the northern hemisphere. The peak in the northern hemisphere atmospheric mixing ratio occurred at 16.8 ppt in 1984 which is double the 1950 mixing ratio. In contrast the peak in the southern hemisphere atmospheric mixing ratio occurred at 6.3 ppt in 1988 which is around 1.5 times the 1950 mixing ratio. The results also indicate that there has been a doubling of $CHCl_3$ concentration over the last century consistent with *Worton et al.* (2006) and *Trudinger et al.* (2004). After the observed peak the atmospheric mixing ratios in both hemispheres deceased to 11.3 ppt in mid-2002 in the northern hemisphere and 5.9 ppt in January 1998 in the southern hemisphere. January 1998 is the drill date of the DML firn air, and therefore represents the most recent data point in the current study for $CHCl_3$ derived from firn air in the southern hemisphere.

Southern hemispheric measurements of $CHCl_3$ mixing ratios have been observed from 1994 onwards at the Cape Grim baseline air pollution station. Figure 3.11 shows that these observations are in general agreement with the firn derived southern hemispheric time series, although there may be a number of outlying points. Growth rates were inferred for the Cape Grim observations by fitting a three parameter sigmoid expression to the data set (the black line in Figure 3.11). Figure 3.10 indicates that there is good general agreement between the time series derived in the current study and the “best fit” northern hemispheric time series modelled by *Worton et al.* (2006). Although the time series in the current study has been smoothed compared to that of *Worton et al.* (2006). This result validates the findings of *Worton et al.* (2006), and shows that previously anthropogenic emission estimates have been underestimated. This is especially true for emissions from the pulp and paper industry, which

was underestimated by 4-5 fold by *Aucott et al.* (1999). Also Figure 3.11 indicates that there is general agreement between the time series derived in the current study and the southern hemispheric time series derived by *Worton et al.* (2006) and *Trudinger et al.* (2004). This indicates that the anthropogenic emissions of $CHCl_3$ increased relative to human population increases up until 1990.

Since 2002, the atmospheric mixing ratio has remained almost constant in both hemispheres the mixing ratio was estimated as 11.5 ppt in the northern hemisphere and 5.1 ppt in the southern hemisphere by mid-2008. With the growth rate during this period being only 0.02 ppt yr^{-1} in the northern hemisphere and -0.06 ppt yr^{-1} in the southern hemisphere, this suggest there has been little change in the emissions of $CHCl_3$ during this period. The atmospheric mixing ratio of $CHCl_3$ in mid-2008 is larger than the 1950 mixing ratio, which suggests that there are still significant anthropogenic emissions.

The 'global' averaged atmospheric time series of $CHCl_3$ was estimated between 1950 and 2008 (the drill date of the NEEM site). This 'global' average time series was derived by averaging the northern and southern time series (Figures 3.10 and 3.11). The southern hemispheric time series was derived using both the firn derived time series and the Cape Grim time series. These two southern hemispheric time series were averaged for the years that are covered by both.

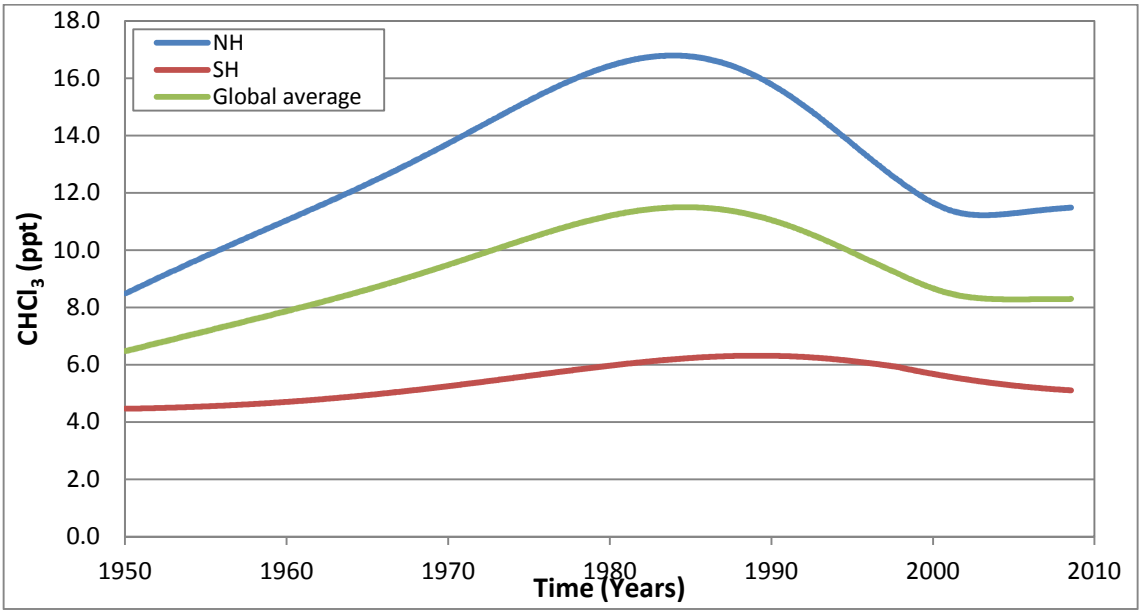

Figure 3.13: Northern hemispheric atmospheric time series of $CHCl_3$ derived from Arctic firn air (blue line). Southern hemispheric atmospheric time series of $CHCl_3$ derived from Antarctic firn and Cape Grim observation (red line). 'Global' atmospheric time series of $CHCl_3$ derived as the average between the northern and southern hemispheric time series (green line).

Figure 3.13 indicates that 'global' mixing ratio of $CHCl_3$ increased from 6.5 ppt in 1950 to a maximum of 11.5 ppt in 1985. In mid-2008 the 'global' mixing ratio was 8.3 ppt and the growth rate was 0.01 ppt yr^{-1} in 2007. This is consistent the 'global' observations from the AGAGE network which reported a mixing ratio of 7.0 ± 1.5 ppt in 2008 (*Montzka et al.*, 2010). Figure 3.13 also indicates that the northern hemispheric time series of atmospheric $CHCl_3$ agrees with the time series in atmospheric $CHCl_3$ observed at the Mace Head observation station since 1994 (Updated from *O'Doherty et al.*, 2001).

3.3.3 Background information on CH_2Cl_2

Dichloromethane or methylene chloride (CH_2Cl_2) is a very short-lived source gas and a known source of chlorine to the tropical tropopause layer (TTL) (*Montzka et al.*, 2010). CH_2Cl_2 is a highly volatile solvent which finds application in a wide variety of industrial and commercial processes. The global average mole fraction of dichloromethane was estimated as ca. 22.1 ± 6.7 ppt in 2008 (*Montzka et al.*, 2010). The corresponding tropospheric chlorine burden was approximately 0.25 Tg Cl (*Xiao*, 2008).

About 70 % of CH_2Cl_2 emissions are anthropogenic in origin (*Montzka et al.*, 2010). CH_2Cl_2 is principally used are as a paint remover, in foam production and foam blowing applications, as a solvent and degreaser, in fumigation, and even as an extraction solvent in the decaffeination of coffee (*Cox et al.*, 2003). Natural emissions of this compound include production from both the open and costal ocean and biomass burning (*Keene et al.*, 1999).

Estimated industrial emissions (from audited sales) data were about 519 ± 32 Gg yr^{-1} for the years 1999-2003 (*Simmonds et al.*, 2006), and *Xiao* (2008) estimated rates of 430 ± 12 Gg yr^{-1} for a similar time period between 2000-2004. Both these estimates are lower than the 580 Gg yr^{-1} given by *McCulloch et al.* (1999a). There has been a steady decline in emission rates of about 12 Gg yr^{-2} between 1988 and 1996 (*McCulloch et al.*, 1999a). *Xiao* (2008) shows that in the years 2000-2004, emissions from the Southeast Asian region increased, with the region becoming a significant source of CH_2Cl_2 emissions. In contrast, emissions from North America have reduced in recent years.

A model analysis of the atmospheric data by *Simmonds et al.* (2006) indicates that more than 90% of the emissions originate from the Northern Hemisphere, which further indicates their predominantly industrial origin. Industrial inventories support this model and indicate that 1% of industrial emissions are from the Southern Hemisphere (*McCulloch et al.*, 1999a). However, other anthropogenic and natural sources are likely to contribute to CH2Cl2 mixing ratios in the atmosphere. The nature and magnitude of natural CH_2Cl_2 sources are not well known, but

some natural emissions sources include the ocean (*Keene et al.*, 1999 and *Khalil et al.*, 1999) with estimated emissions of 190 Gg yr^{-1}.

Emissions of CH_2Cl_2 from the oceans show well-established seasonal variations. Greater emissions have been modelled for the tropical oceanic regions compared with higher latitudes (*Xiao*, 2008), probably related to the higher sea surface temperature. Recent work by *Moore* (2009) suggests that the apparent supersaturation of this gas in higher latitude waters is an artifact of circulation and mixing. In this sense, the observed surface supersaturation of the gas would likely have resulted from the recent decline of this gas in the atmosphere (*Simmonds et al.*, 2006) with the ocean gradually re-equilibrating, and not necessarily the result of production in the ocean. Studies by *Keene et al.* (1999) and *Khalil et al.* (1999) conclude that oceanic emissions of dichloromethane could account for about 25 % of the total emissions to the atmosphere.

An estimate of biomass burning to global atmospheric CH_2Cl_2 was given as 7 % by *Keene et al.* (1999) later supported by *Xiao* (2008). *Lobert et al.* (1999) estimated emissions due to biomass burning of about 50 Gg yr^{-1}. However, these values have been questioned by *Simmonds et al.* (2006) on the basis of much lower (by two orders of magnitude) biomass burning emission factors observed from Australian wild fires.

The major atmospheric removal process for CH_2Cl_2 is destruction by OH, with a resultant atmospheric lifetime of 144 days (*Montzka et al.*, 2010). Compared to longer-lived chlorocarbons, this significantly lowers the likelihood of CH_2Cl_2 reaching the stratosphere where it could damage the ozone layer. *Graedel and Keene* (1996) estimate that about 2 % of CH_2Cl_2 emissions reach the stratosphere. Because of its low impact on stratospheric ozone, it is not regulated by the Montreal Protocol. However, it is classified as a hazardous air pollutant and a toxic volatile organic compound in regional air quality inventories (*Simmonds et al.*, 2006).

Atmospheric measurements of CH_2Cl_2 extending back in time are quite limited. AGAGE measurements began in 1998 at Mace Head, Ireland and Cape Grim, Tasmania (*Simmonds et al.*, 2006 and *Cox et al.*, 2004). CH_2Cl_2 has increased significantly in recent years in both hemispheres, having previously fallen from 1995 (when records began) to about 2000 (updated from *Simmonds et al.*, 2006). In the northern hemisphere, mean surface mixing ratios in 2008 are similar to those previously observed in the mid-1990s. The growth rate between 2007 and 2008 increased by 8.1 ± 2.3 % yr^{-1} to give a global average of 22.1 ± 6.7 ppt (*Montzka et al.*, 2010).

Elkins (2001) reported mixing ratios of CH_2Cl_2 of approximately 20–40 ppt between 1995–1997 at Niwot Ridge, values 20 % greater at higher northern latitudes (e.g., Barrow), and markedly less (8 – 12 ppt) in the southern hemisphere. Between the years 1998 – 2004, mixing ratios in the northern and southern hemispheres were about 30.8 ± 0.2 ppt and 8.74 ± 0.03 ppt, respectively (*Simmonds et al.*, 2006), which gives an inter-hemispheric contrast with a factor of around 3.5. This large inter-hemispheric difference reflects the significant contribution of anthropogenic emissions in the Northern Hemisphere. This is supported by *Montzka et al.* (2010) who report 93 % of global emissions are from the northern hemisphere

Trudinger et al. (2004) reconstructed Southern Hemispheric mixing ratios of dichloromethane to pre-1940 through the study of firn air. The reconstruction shows a steep increase in mixing ratios from ca. 1960, peaking around 1990, then decreasing (*Trudinger et al.*, 2004) (Figure 3.14). The rate of change in the most recent years of the reconstruction matches well with the rate of change of the Cape Grim record (*Trudinger et al.*, 2004).

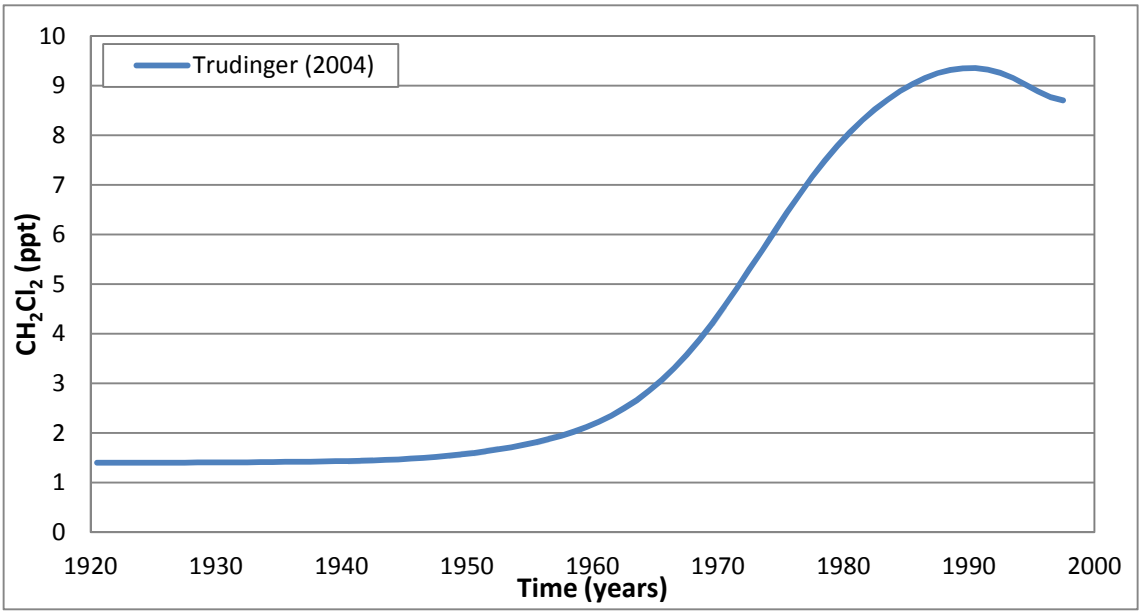

Figure 3.14: The atmospheric time series of dichloromethane during the 20th century from the synthesis time series based on *Trudinger et al.* (2004).

3.3.4 Results and discussion of CH_2Cl_2

In the current study, I will report firn air measurement of CH_2Cl_2 from a number of northern and southern hemispheric firn air records, as well as southern hemispheric observations from the Cape Grim baseline air pollution station. These measurements have then been used to derive the atmospheric time series of CH_2Cl_2 mixing ratios. The time series of atmospheric CH_2Cl_2 mixing ratios were derived using the LGGE method, which is described in more detail in the methods chapter. These new atmospheric time series are then compared with previous atmospheric time series estimated by *Trudinger et al.* (2004). The time series obtained and the output from the inverse model for the northern and southern hemisphere site are shown alongside the measured concentration of CH_2Cl_2 with depth at northern hemispheric firn sites (NEEM, NGRIP and DI) and southern hemispheric (DC and DML) firn sites in Figures 3.15 and 3.16, respectively.

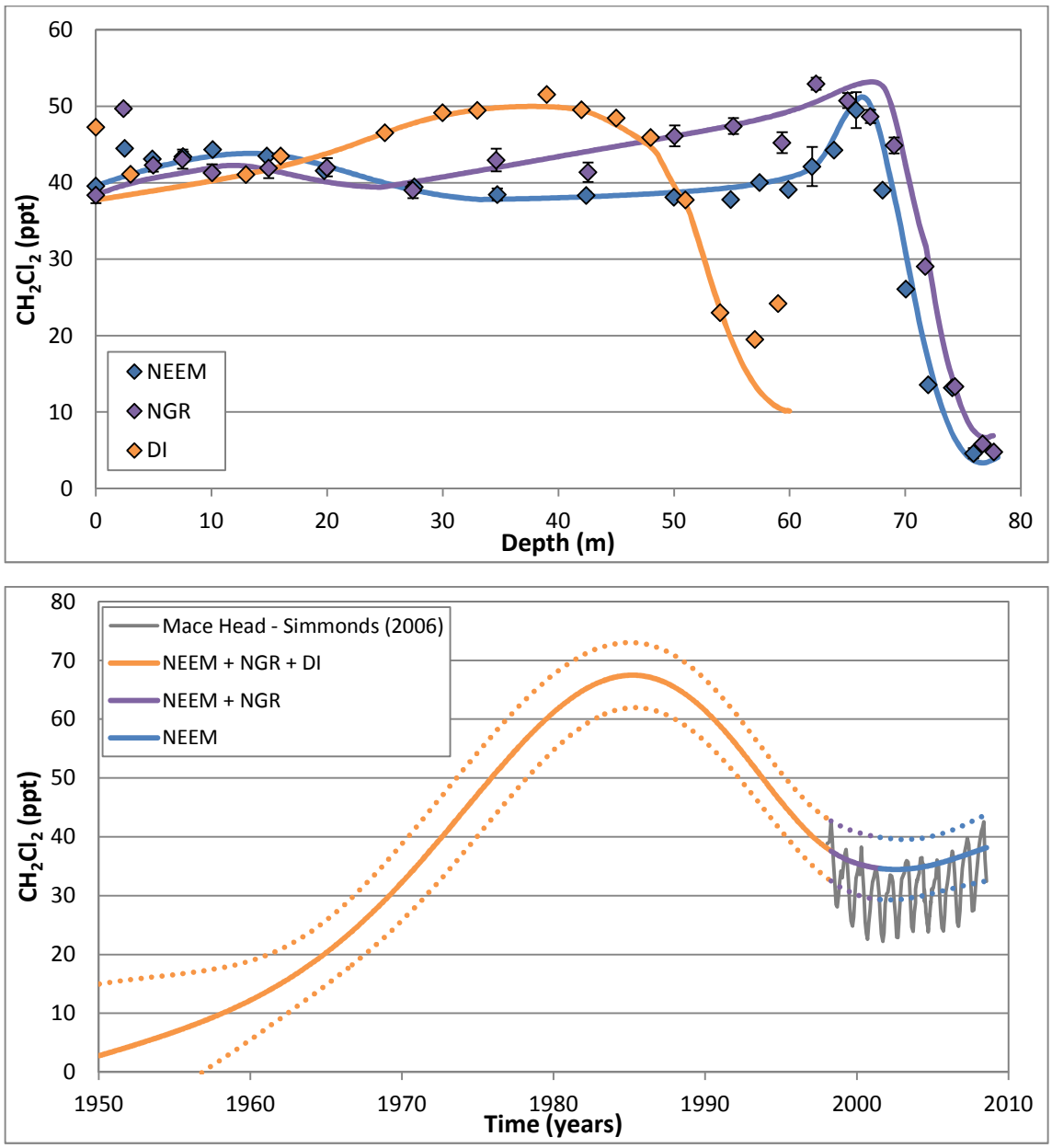

Figure 3.15: Top panel, depth profiles of northern hemispheric CH_2Cl_2 concentration with depth at the; NEEM (blue points), NGRIP (purple points) and the DI (yellow points), compared with model simulations based on the atmospheric time series indicated in the bottom panel with a seasonal cycle of 46 % added to the time series. The error bars represent the 1 σ of the measurements. Bottom panel, Atmospheric time series derived by a multi-site inversion modelling of the NEEM, NGRIP and DI firn air measurements (solid line) using the LGGE method. As the firn sites have different drill dates the LGGE method derives an atmospheric time series using all of the firn sites up to the drill date of a firn site, after which the atmospheric time series is derived using the remaining sites. The time series derived are illustrated by the NEEM, NGRIP and DI - yellow line, NEEM and NGRIP – purple line and NEEM only – blue line. The dashed lines represent the uncertainties envelope of the time series (as described Figure 2.10). Observations of atmospheric CH_2Cl_2 updated from *Simmonds et al.* (2006) (grey line) are shown for comparative purposes.

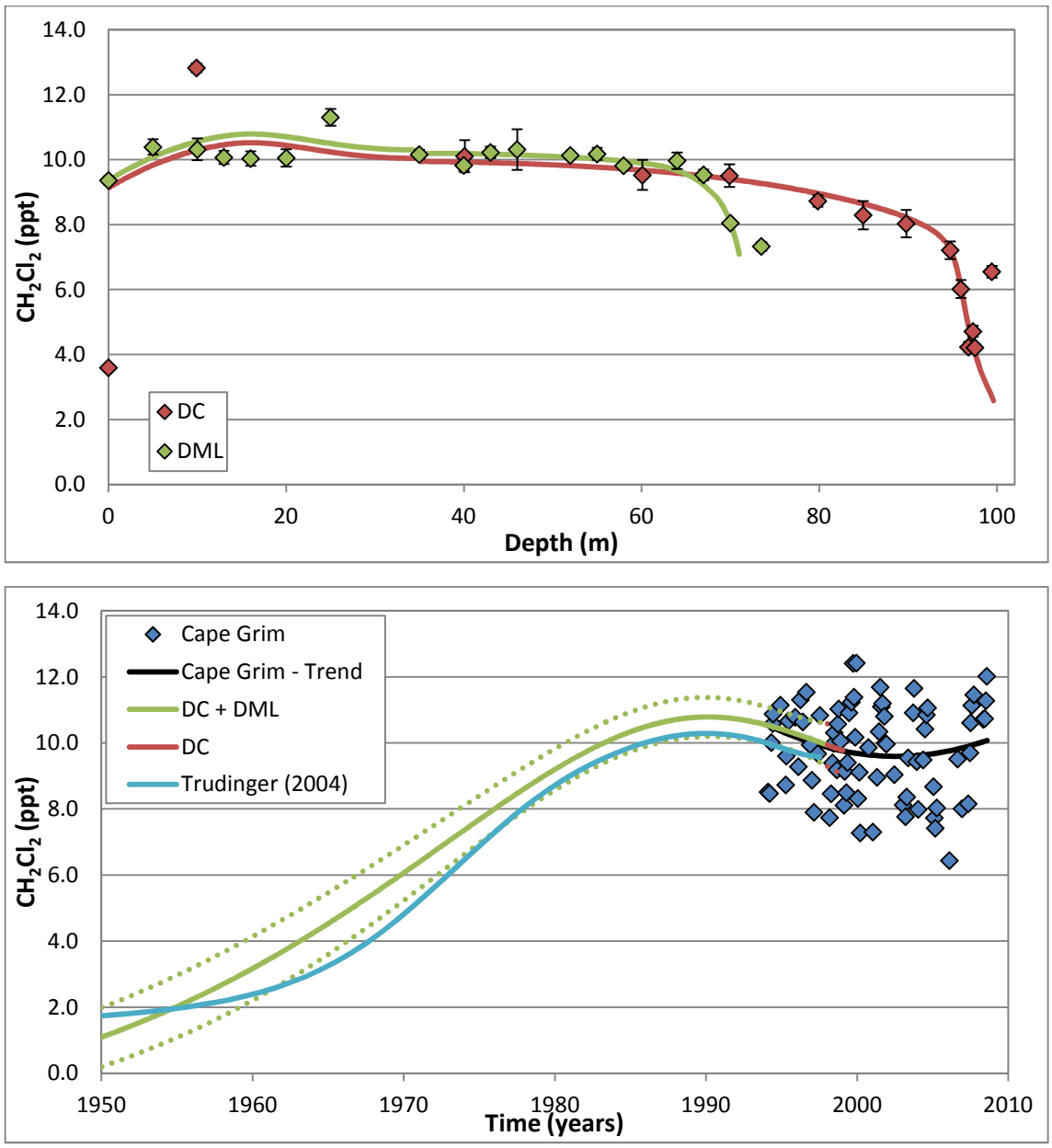

Figure 3.16: Top panel, depth profiles of southern hemispheric CH_2Cl_2 concentration with depth at the; DC (red points) and the DML (green points), compared with model simulations based on the atmospheric time series indicated in the bottom panel with a seasonal cycle of 46 % added to the time series. The error bars represent the 1 σ of the measurements. Bottom panel, Atmospheric time series derived by a multi-site inversion modelling of the DC and DML firn air measurements (solid line) using the LGGE method. The time series derived by the DC and DML - green line and DC only – red line. The dashed lines represent the uncertainties envelope of the time series (as described Figure 2.10). Also the mixing ratios of CH_2Cl_2 as a function of time as measured in air samples collected in the southern hemisphere (blue points, from Cape Grim, Tasmania, 41°S, 145° E). The black line is a sigmoid expression fitted through the Cape Grim time series in order to derive growth rates and emissions. The southern hemispheric time series (light blue line) derived by *Trudinger et al.* (2004) is show for comparative purposes.

The ambient air measurements (shown as depth = 0 m) were collected at the NEEM site in July 2008 during firn air drilling. These measurements have an average mixing ratio of 39.6 ± 0.4 ppt and are the latest northern hemispheric measurements of CH_2Cl_2 in this study. The

ambient air measurements were collected at the DML site in the December 1997 during the firn air drilling. These air measurements have an average mixing ratio of 9.4 ± 0.1 ppt and are the latest southern hemispheric measurement from the firn air sites in this study. This is because the DC ambient air measurements are much lower than the other DC measurement and therefore are like to be an outlining data point.

CH_2Cl_2 has a significant atmospheric sink as a result of its reaction with the hydroxyl radical (OH) (*Montzka et al.,* 2010). The atmospheric lifetime of CH_2Cl_2 with respect to OH is 144 days (*Montzka et al.,* 2010). This should be short enough for there to be a seasonal cycle in CH_2Cl_2 atmospheric mixing ratio compared with other trace gases with similar lifetimes. This seasonal cycle can be seen in the variations in CH_2Cl_2 concentration in the shallowest part of the firn columns, that would have reflected the seasonality in the OH atmospheric mixing ratios that has been described in *Kaspers et al.* (2004) and *Sturges et al.* (2001). This is also supported by the detrended Cape Grim observations which are shown in Figure 3.17.

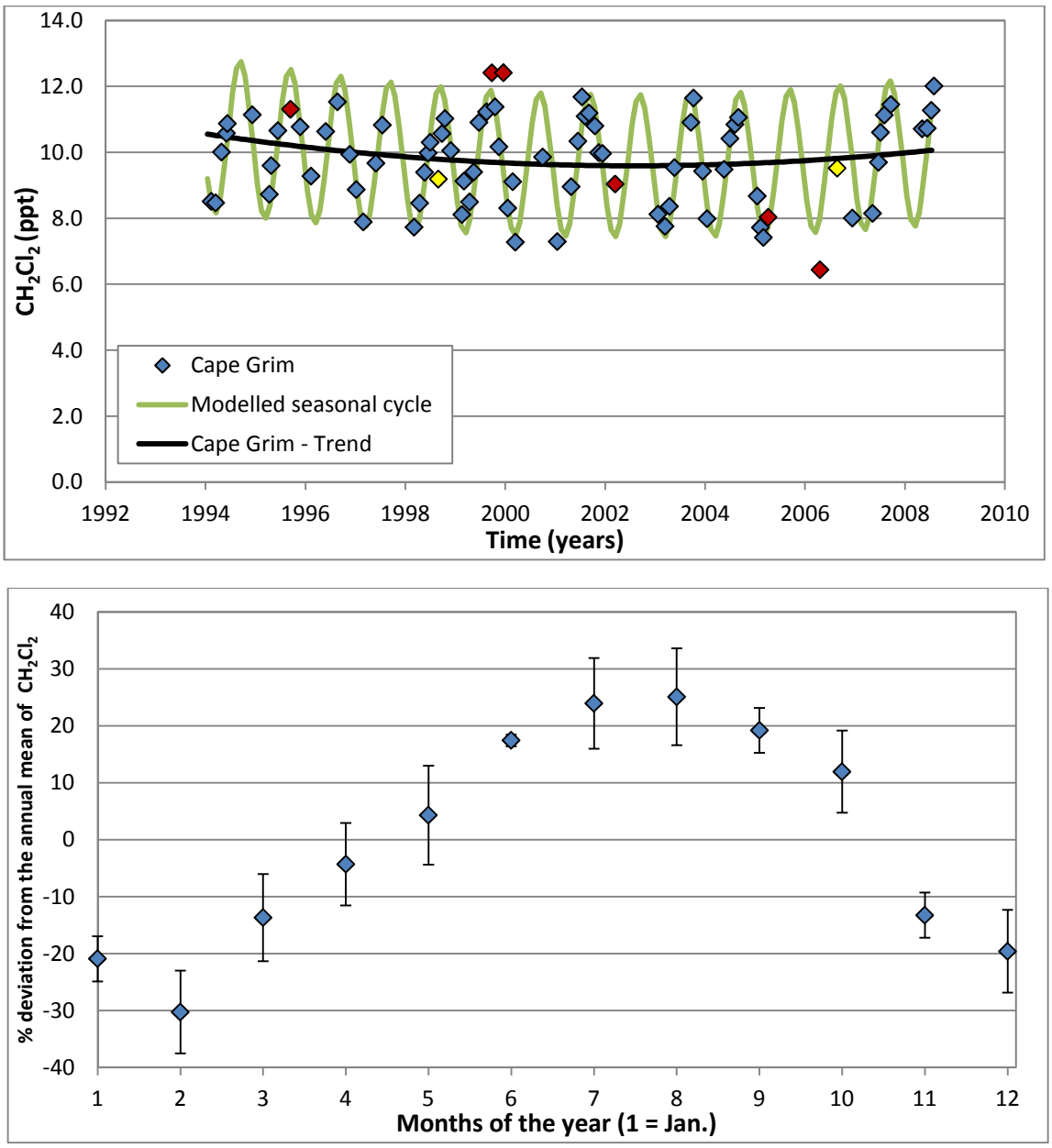

Figure 3.17: Top panel, Atmospheric mixing ratios of CH_2Cl_2 as a function of time from observations of archived samples taken at Cape Grim (blue points). A polynomial expression fitted through the Cape Grim time series in order to detrend the data (black line). A modelled seasonal cycle based on the seasonal cycle observed in the bottom panel (green line). Data points more than 3 standard deviations away from the mean were taken as outliers and removed from the seasonal cycle calculation (yellow points). Six unreliable samples were also removed from the seasonal cycle calculation (red points) (see Figure 3.4 for more details). Bottom panel, percentage deviation from the annual mean CH_2Cl_2 mixing ratio based on the Cape Grim observations (top panel), taken as the mean of the observations made in a particular calendar month (between 3 - 8 data points). The error bars represent the 1 σ of the measurements.

The seasonal patterns of the Cape Grim observations were determined by using the same method stated earlier (section 3.2.2). Figure 3.17 shows that there is a seasonal cycle in the atmospheric mixing ratio of CH_2Cl_2. The amplitude of the seasonal cycle is taken as the difference between the average of the winter months (June, July and August) and summer

months (Decembers, January and February). Therefore, the Cape Grim observation indicates a seasonal cycle with an amplitude of 46 % of the annual mean mixing ratio in the southern hemisphere. This would represent a southern hemispheric seasonal cycle with an amplitude of 5.5 ppt in 2008. This seasonal cycle agrees with that observed by *Montzka and Elkins* (2006) with an amplitude of 48 %. *Montzka and Elkins* (2006) observed the seasonal cycle from measurements of CH_2Cl_2 from the Barrow observation station. Barrow is a long term observation research station in the northern hemisphere run as part of the NOAA/ESRL's Global Monitoring Division and is located at 71.3°N, 156.6°W and 11 m a.s.l.

Figures 3.15 and 3.16 indicate that the 1950 mixing ratios of CH_2Cl_2 were 2.8 ppt in the northern hemisphere and 1.1 ppt in the southern hemisphere. After 1950, the time series show a sustained growth in both hemispheres until the mid-1980s in the northern hemisphere and around 1990 in the southern hemisphere. The average growth rates during this period were 1.8 ppt yr^{-1} in the northern hemisphere and 0.2 ppt yr^{-1} in the southern hemisphere. This greater value for the northern hemisphere reflects the significant contribution of northern hemispheric anthropogenic emissions of CH_2Cl_2 to the global mixing ratio. *Montzka et al.* (2010) report that 93 % global CH_2Cl_2 emissions are from the northern hemisphere. The peak in the northern hemisphere atmospheric mixing ratio occurred in 1985 at 67.4 ppt, whereas the peak in the southern hemisphere atmospheric mixing ratio occurred in 1990 at 10.8 ppt. These measurements are in general agreement with the southern hemispheric time series derived by *Trudinger et al.* (2004) (light blue line Figure 3.16), although the southern hemispheric atmospheric time series derived in this study is ~ 10 % larger that the *Trudinger et al.* (2004) time series. This difference is likely due to a calibration scale offset between the two studies. A comparison of calibration scales by *Simmonds et al.* (2006) observed an 8.8 ± 4%, increase in the NOAA measurements compared with AGAGE.

After the peak in atmospheric mixing ratios in both hemispheres, there was a continual decease until a mixing ratio of 34.5 ppt in mid-2002 in the northern hemisphere and 9.8 ppt in January 1999 in the southern hemisphere. January 1999 is the drill date of the Dome C firn air and therefore represents the end of the southern hemispheric time series. Southern hemispheric measurements of CH_2Cl_2 mixing ratios have been made from 1994 onwards at the Cape Grim baseline air pollution station. Figure 3.16 shows that these observations are in general agreement with the firn derived southern hemispheric time series, although there may be a number of outlying points. Growth rates were inferred for the Cape Grim observations by fitting a three parameter sigmoid expression to the data set (the black line in Figure 3.16). The Cape Grim time series shows a continuation of the decreasing trend in the southern

hemisphere down to a mixing ratio of 9.6 ppt in mid-2002. This is in agreement with the northern hemispheric time series. However, since 2002 the atmospheric mixing ratio has started to increase again in both hemispheres reaching 38.2 ppt in the northern hemisphere and 10.1 ppt in the southern hemisphere by mid-2008. The growth rate during this period has also increased year-on-year from 0.12 ppt yr^{-1} in 2003 up to 0.87 ppt yr^{-1} 2007 in the northern hemisphere and from 0.01 ppt yr^{-1} in 2003 up to 0.12 ppt yr^{-1} 2007 in the southern hemisphere, which suggests this increase is likely to continue in the future.

The turnaround in the atmospheric time series of CH_2Cl_2 occurs at around 34 ppt in the northern hemisphere and around 10 ppt in the southern hemisphere. This is much larger than the 1950 levels measured in the current study. This would suggest that this increase is due to an increased in anthropogenic emissions as it is unlikely that natural emission rates have increased by this amount. If the major source of CH_2Cl_2 emissions is anthropogenic in origin, it is unclear if either a previously known source has increased emissions rate or if there is a new source. The northern hemispheric time series of atmospheric CH_2Cl_2 agrees with the time series observed at Mace Head since 1998 (Figure 3.15) (Updated from *Simmonds et al.*, 2006). Again the difference in absolute mixing ratio is likely due to a calibration difference between the two studies.

The 'global' averaged atmospheric time series of CH_2Cl_2 was estimated between 1950 and 2008 by averaging the northern and southern time series (Figure 3.18). The southern hemispheric time series was estimated using both the firn derived time series and the Cape Grim time series. These two time series were averaged for the years that are covered by both.

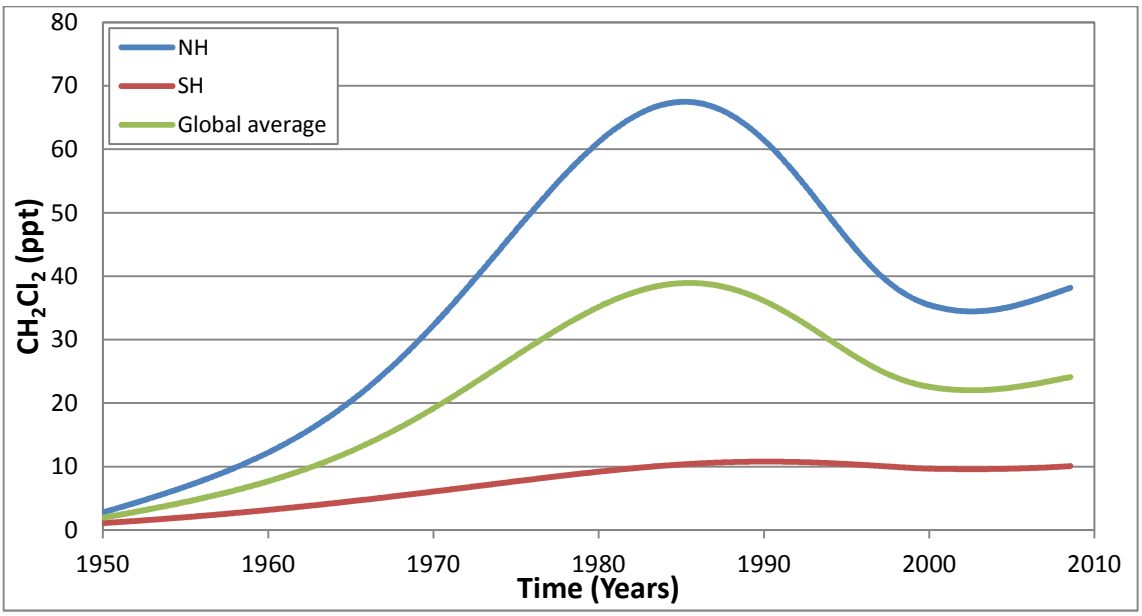

Figure 3.18: Northern hemispheric atmospheric time series of CH_2Cl_2 derived from Arctic firn air (blue line). Southern hemispheric atmospheric time series of CH_2Cl_2 derived from Antarctic firn and Cape Grim observation (red line). 'Global' atmospheric time series of CH_2Cl_2 estimated as the average between the northern and southern hemispheric time series (green line).

Figure 3.18 indicates that 'global' mixing ratio of CH_2Cl_2 increased from 2.0 ppt in 1950 to a maximum of 39.0 ppt in 1985. In mid-2008 the 'global' mixing ratio was 24.1 ppt with a growth rate of 0.5 ppt yr^{-1} in 2007. These 'global' observations are in good general agreement with the global observation from the AGAGE network which observed a mixing ratio of 22.1 ± 6.7 ppt in 2008 (*Montzka et al.*, 2010).

The firn modelling method developed at LGGE derives atmospheric time series for the northern and southern hemisphere independently. This means that the model assumes that there is no relationship between the two time series; therefore, a 2 box was used to validate the two time series. The 2 box model uses the northern hemisphere as an input and then derives a southern hemispheric time series using the inter-hemispheric mixing time (1.34 years) and an atmospheric lifetime of 144 days (*Montzka et al.*, 2010). This modelled southern hemispheric time series was then compared with the atmospheric time series derived from the southern hemispheric firn air measurements (Figure 3.19). However this method makes the assumption that all emissions of CH_2Cl_2 are in the northern hemisphere, with zero emissions in the southern hemisphere, consistent with *Simmonds et al.* (2006) who indicated that > 90 % of the emissions emanate from the northern hemisphere and *McCulloch et al.* (1999), who indicated that only 1 % of industrial emissions are in the southern hemisphere. More details on this model can be found in section 2.5.5.

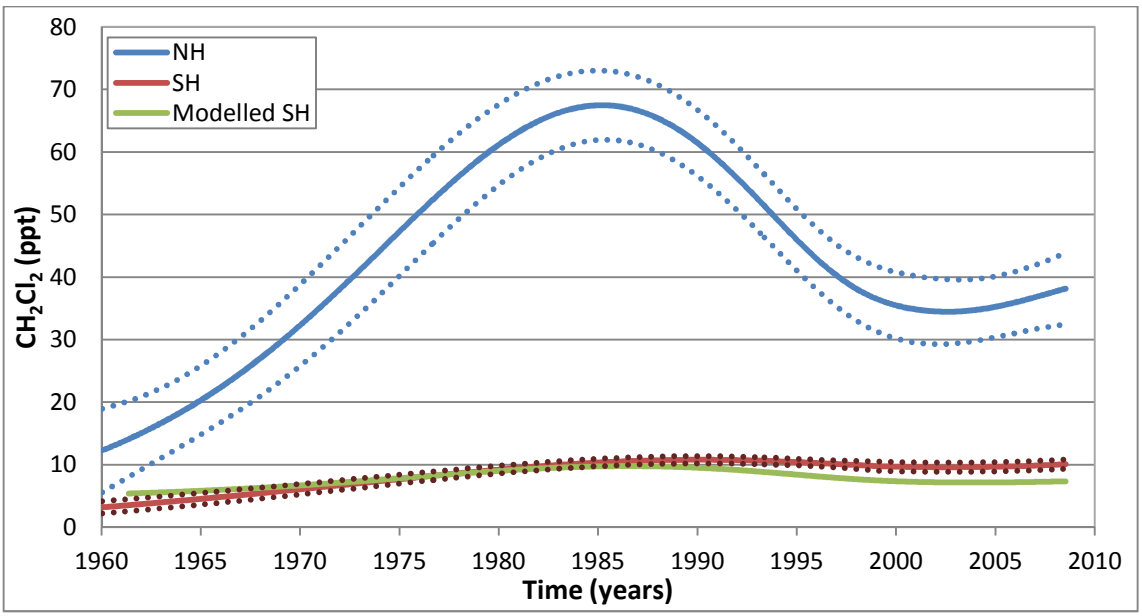

Figure 3.19: Northern hemispheric atmospheric time series of CH_2Cl_2 derived from Arctic firn air (blue lines). Southern hemispheric atmospheric time series of CH_2Cl_2 derived from Antarctic firn and Cape Grim observations (red lines). The dotted lines represent the uncertainty of the atmospheric time series as stated in Figures 3.15 and 3.16. Modelled southern hemispheric time series derived using the 2 box model (green line).

Figure 3.19 shows that there is good agreement between the calculated and observed southern hemispheric CH_2Cl_2 atmospheric time series. Both time series have similar growth rates between the mid-1950 and the peak in atmospheric CH_2Cl_2 in late 1980. However, Figure 3.19 does indicate that the decline after the 1980s was greater in the northern hemisphere, suggesting that since 1990, southern hemispheric emissions have increased relative to those in the northern hemispheric.

3.3.5 Background information on CCl_2CCl_2

This section will report the atmospheric time series of the atmospheric mixing ratios of perchloroethylene (tetrachloroethene, "dry-cleaning fluid", CCl_2CCl_2). Firn air samples collected in Greenland were used to reconstruct a northern hemispheric history of CCl_2CCl_2 atmospheric mixing ratios. Firn air samples collected in Antarctic were used to reconstruct a southern hemispheric history of CCl_2CCl_2 atmospheric mixing ratios. CCl_2CCl_2 was also detected and quantified in air samples from the Cape Grim baseline air pollution station in the southern hemisphere (Tasmania, 41°S, 145°E) from archived samples dating back to 1979.

Nearly 100 % of CCl_2CCl_2 emissions are anthropogenic in origin (*Montzka et al.*, 2010). Its principal uses are in dry-cleaning applications, in the textile industry and in vapour degreasing of metals (*Phillips*, 2006). Also, small but significant quantities of CCl_2CCl_2 is emitted in the “flue

gas" from coal-fired power plants (*Garcia et al.*, 1992). It has also been used as an intermediate in the manufacture of HFC-134a and related refrigerants (*Montzka et al.*, 2010). This dominance of its anthropogenic production source makes it a useful tracer for urban/industrial activities (*Blake et al.*, 2003). In terms of natural sources, biomass burning is thought to contribute < 1 % to total global emissions of CCl_2CCl_2 (*Montzka et al.*, 2010).

Reaction with OH is the primary atmospheric sink of CCl_2CCl_2 (*Montzka et al.*, 2010). The unsaturated nature of CCl_2CCl_2 with its C=C double bond makes it readily susceptible to degradation by OH and O_3. *Rudolph et al.* (1996) noted that CCl_2CCl_2 reacts about 300 times faster with Cl atoms than with OH, although tropospheric levels of Cl are too small for this to be a significant atmospheric sink. *Simpson et al.* (2003) have suggested that CCl_2CCl_2 undergoes cirrus-activated depletion in the upper troposphere. It has also been estimated that about 5 % of CCl_2CCl_2 in the atmosphere is converted into trichloroacetic acid (CCl_3COOH, TCA), via an alternate pathway involving Cl atoms (*McCulloch*, 2002). The atmospheric lifetime of CCl_2CCl_2 is 90 days (*Montzka et al.*, 2010). This lifetime is shorter than the inter-hemispheric mixing time of ~ 1 yr (*Seinfeld et al.*, 1998) and CCl_2CCl_2 consistently shows a strong inter-hemispheric gradient, with higher mixing ratios in the northern hemisphere (*Simpson et al.*, 2004).

CCl_2CCl_2 has been declared a hazardous air pollutant under the U.S. Clean Air Act Amendments of 1990 because of potential health and environmental impacts (*Kleiman and Prinn*, 2000). In the UK, releases of CCl_2CCl_2 are controlled under the Surface Water Regulations and Pollution Prevention and Control Regulations. Voluntary reductions of industrial CCl_2CCl_2 emissions began in the U.S. in 1991, and increased solvent recycling and lower production rates of CFC-113 (the principal derivative of CCl_2CCl_2) have helped reduce industrial emissions (*Simpson et al.*, 2004).

Atmospheric mixing ratios of CCl_2CCl_2 have been observed by a number of different studies (*Laube et al.*, 2008 *Clerbaux and Cunnold et al.*, 2006 and *Schauffler et al.*, 1999) summarised in Table 3.4. Observations range from 1.2–3.8 ppt in the marine boundary layer (*Clerbaux and Cunnold et al.*, 2006) to 0.1–1.0 ppt in the tropical tropopause (*Laube et al.*, 2008).

Table 3.4: Summary of available observations of CCl_2CCl_2 from the marine boundary layer (MBL) to the tropical tropopause layer (TTL) based on *Montzka et al.* (2010).

Region	Marine Boundary Layer	Upper Troposphere	Lower TTL	level of *zero* radiative *heating* (LZRH)	Upper TTL	Tropical Tropopause
Ref.	*Clerbaux and Cunnold et al.* (2006)	*Schauffler et al.* (1999)	*Laube et al.* (2008)	*Clerbaux and Cunnold et al.* (2006)	*Clerbaux and Cunnold et al.* (2006)	*Laube et al.* (2008)
Height range (km)	0-~2	10-12	12-14	14.5-15.5	15.5-16.5	16.5-17
CCl_2CCl_2 (ppt)	1.2–3.8	0.7–1.8	0.8–1.5	0.4–1.3	0.3–0.9	0.1–1.0

Long term observations of CCl_2CCl_2 have been made by *Simpson et al.* (2004) since 1989 and have been up dated by *Montzka et al.* (2010) from a number of remote surface locations around the world. These observations show that the global mean annual CCl_2CCl_2 mixing ratio has decreased almost monotonically from 6.3 ± 0.6 ppt in 1989 (*Simpson et al.*, 2004) to about 1.7 ± 0.7 in 2008 (*Montzka et al.*, 2010). The northern hemispheric mixing ratio was 13.9 ± 0.5 ppt in 1989 and deceased to 6.5 ± 0.2 ppt in 2002 (*Simpson et al.*, 2004). However, in recent years this declining trend has levelled off with the 2007 – 2008 growth rate being 0.01 ± 0.00 ppt yr^{-1} (*Montzka et al.*, 2010). *Dimmer et al.* (2001) observed an average baseline mixing ratio of 4.26 ± 0.84 ppt during the 1998 CHAOS cruise in the north eastern Atlantic and Arctic Oceans (April–May 1998); during a separate field campaign (July–September 1997) at Ny-Ålesund (Norwegian Arctic) a much lower mixing ratio of 1.77 ± 0.07 ppt was reported. Between March 1998 to January 1999 high frequency CCl_2CCl_2 measurements have been observed by *Kleiman and Prinn* (2000) for the north eastern United States with clean background CCl_2CCl_2 levels around 2 ppt and polluted levels up to 90 ppt. CCl_2CCl_2 exhibits a strong interhemispheric gradient (*Rudolph et al.*, 1996 and *Wang et al.*, 1995) with an estimated tropospheric mixing ratio of 5 – 15 ppt in the northern hemisphere and 0.7 – 1.5 ppt in the southern hemisphere (*Ko and Poulet*, 2003). It is likely that significant calibration differences exist between the measurements of CCl_2CCl_2 made by different laboratories, with *Simmonds et al.* (2006) noting a 10 % difference between NOAA and AGAGE measurements of CCl_2CCl_2. To date, no intercomparison exercises have been published for atmospheric mixing ratios of CCl_2CCl_2.

Estimates of total global and industrial emissions of CCl_2CCl_2 have been calculated in a number of different studies (*Simmonds et al.*, 2006, *Simpson et al.*, 2004 and *McCulloch et al.*, 1999a).

These studies show that emissions estimate derived from a "top-down" analysis of atmospheric observations are similar to independently estimated industrial emissions derived from recorded inventories. Also, a model analysis of the atmospheric observation of CCl_2CCl_2 by *Simmonds et al.* (2006) indicates that > 90 % of the emissions emanate from the northern hemisphere. Industrial inventories by *McCulloch et al.* (1999), indicate that only 1 % of emissions from industrial sources originate in the southern hemisphere, and suggests that other sources such as biomass burning might contribute to the total atmospheric CCl_2CCl_2 mixing ratios.

3.3.6 Results and discussion of CCl_2CCl_2

In the current study, I report firn air measurement of CCl_2CCl_2 from a number of northern and southern hemispheric firn air records, as well as southern hemispheric observations from the Cape Grim baseline air pollution station. These measurements have then been used to derive the atmospheric time series of CCl_2CCl_2 mixing ratios. The time series of atmospheric CCl_2CCl_2 mixing ratios were derived using the LGGE method, which is described in more detail in the methods chapter. The time series obtained and the output from the inverse model for the northern and southern hemisphere site are shown alongside the measured concentration of CCl_2CCl_2 with depth at northern hemispheric firn sites (NEEM, NGRIP and DI) and southern hemispheric (DML) firn sites in Figures 3.20 and 3.21, respectively.

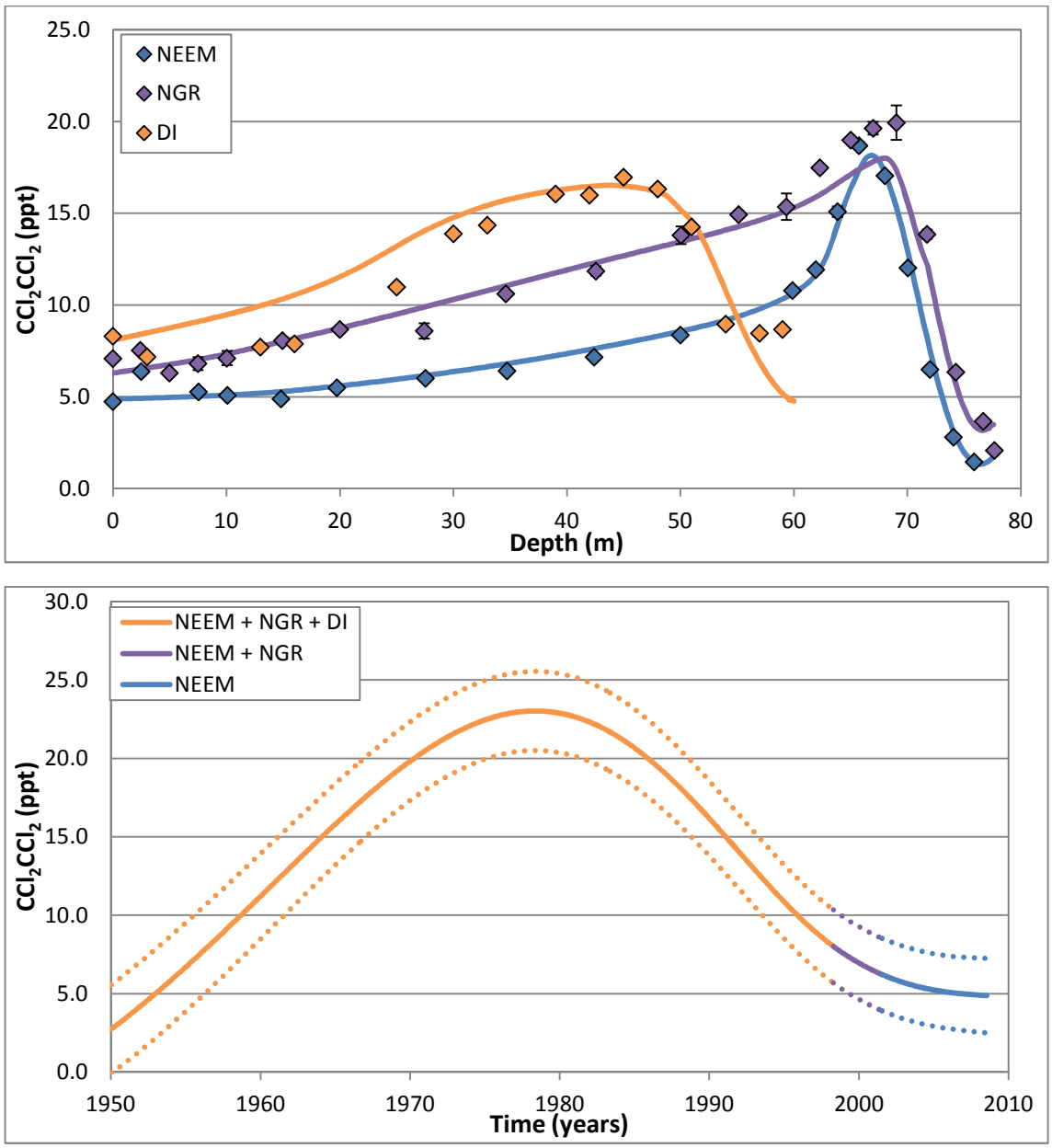

Figure 3.20: Top panel, depth profiles of northern hemispheric CCl_2CCl_2 concentration with depth at; NEEM (blue points), NGRIP (purple points) and DI (yellow points), compared with model simulations based on the atmospheric time series indicated in the bottom panel. The error bars represent the 1 σ of the measurements. Bottom panel, atmospheric time series derived by a multi-site inversion modelling of the NEEM, NGRIP and DI firn air measurements (solid line) using the LGGE method. As the firn sites have different drill dates the LGGE method derives an atmospheric time series using all of the firn sites up to the drill date of a firn site, after this the atmospheric time series is derived using the remaining sites. The time series derived by the NEEM, NGRIP and DI - yellow line, NEEM and NGRIP – purple line and NEEM only – blue line. The dashed lines represent the uncertainties envelope of the time series (as described Figure 2.10).

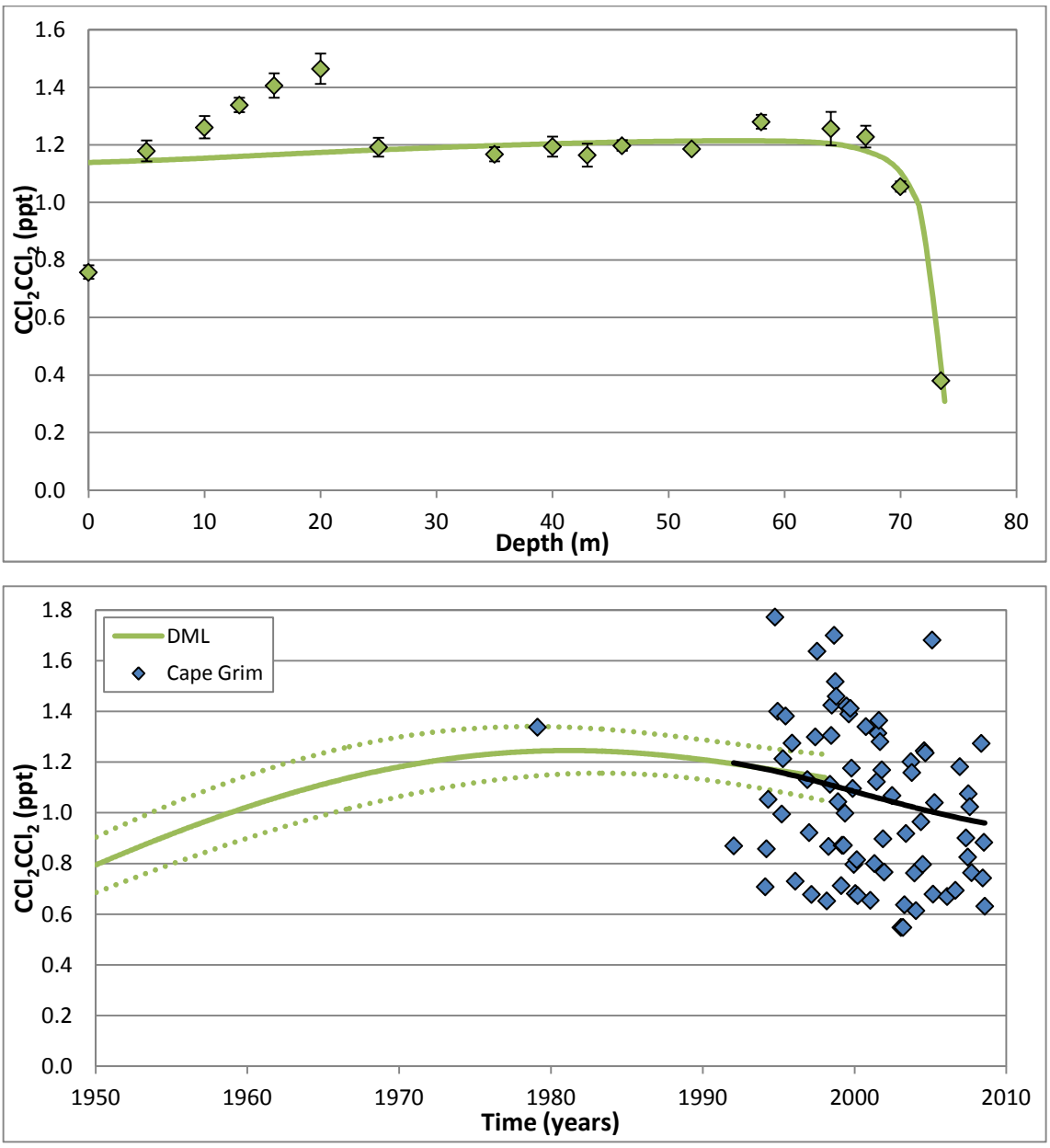

Figure 3.21: Top panel, depth profiles of southern hemispheric CCl_2CCl_2 concentration with depth at the DML firn site (green points), compared with model simulations based on the atmospheric time series indicated in the bottom panel. The error bars represent the 1 σ of the measurements. Bottom panel, atmospheric time series derived by a single site inversion modelling of the DML firn air measurements (solid line) using the LGGE method. The time series derived by the DML firn air - green line. The dashed lines represent the uncertainties envelope of the time series (as described Figure 2.10). The mixing ratios of CCl_2CCl_2 as a function of time as measured in air samples collected in the southern hemisphere (blue points, from Cape Grim, Tasmania, 41°S, 145° E). The black line is a sigmoid expression fitted through the Cape Grim observation in order to derive growth rates and emissions.

The ambient air measurements (shown as depth = 0 m) were collected at the NEEM site in July 2008 during the firn air drilling. These ambient air measurements have an average mixing ratio of 4.75 ± 0.05 ppt and are the latest northern hemispheric measurements of CCl_2CCl_2 in this study. The ambient air measurements were collected at the DML site in the December 1997

during the firn air drilling; they have an average mixing ratio of 0.76 ± 0.02 ppt and are the latest southern hemispheric measurement from the firn air sites in this study.

With a total atmospheric lifetime of 90 days (*Montzka et al.*, 2010), CCl_2CCl_2 should have a short enough lifetime for there to be a seasonal cycle in its atmospheric mixing ratio, compared with other trace gases with similar lifetimes. *Wang et al.* (1995) observed a seasonal cycle in the northern hemisphere with an amplitude of 14 ppt in 1990, but did not observe any apparent seasonal variations in the southern hemisphere. In additions, *Simmonds et al.* (2006) observed a seasonal cycle for CCl_2CCl_2 with an amplitude of about 40% of the mean mixing ratio. However, even with this relatively large seasonal cycle, there are no signs of variations in the mixing ratio of CCl_2CCl_2in the shallowest part of the firn columns, that would have reflected the seasonality in the OH atmospheric mixing ratios previously described in *Kaspers et al.* (2004) and *Sturges et al.* (2001). However, *Kaspers et al.* (2004) only observed this variation for CH_3Cl which has a larger atmospheric mixing ratio and seasonal cycle. Although this cannot be taken as evidence that there is no seasonality in the CCl_2CCl_2 atmospheric mixing ratio, either the amplitude of seasonality is not large enough to be recorded in the firn air measurements or decrease in CCl_2CCl_2 mixing ratio is masking any seasonality.

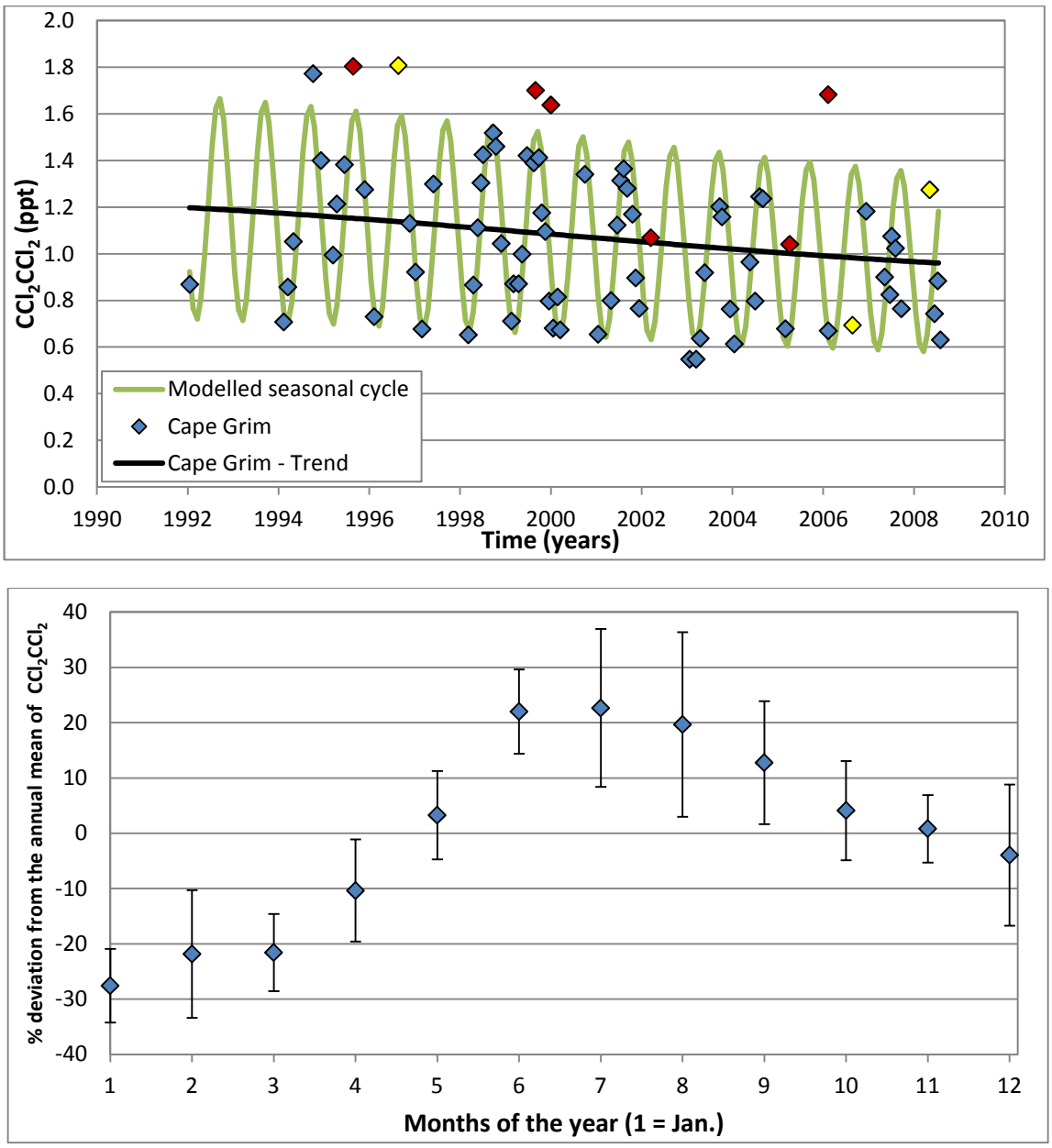

Figure 3.22: Top panel, atmospheric mixing ratios of CCl_2CCl_2 as a function of time from observations of archived samples taken at Cape Grim (blue points). A polynomial expression fitted through the Cape Grim time series in order to detrend the data (black line). A modelled seasonal cycle based on the seasonal cycle observed in the bottom panel (green line). Data points more than 3 standard deviations away from the mean were taken as outliers and removed from the seasonal cycle calculation (yellow points). Six unreliable samples were also removed from the seasonal cycle calculation (red points) (see Figure 3.4 for more details). Bottom panel, percentage deviation from the annual mean CCl_2CCl_2 mixing ratio based on the Cape Grim observations (top panel), taken as the mean of the observations made in a particular calendar month (between 3 - 8 data points). The error bars represent the 1 σ of the measurements.

The seasonal patterns of the Cape Grim observations were determined by using the same method stated in section 3.2.2. Figure 3.22 shows that there is a seasonal cycle in the atmospheric mixing ratio of CCl_2CCl_2. The amplitude of the seasonal cycle is taken as the difference between the average of the winter (June, July and August) and summer months

(Decembers, January and February). The Cape Grim observation indicates a seasonal cycle with an amplitude of 40 % of the annual mean mixing ratio in the southern hemisphere. This would represent a southern hemispheric seasonal cycle with an amplitude of 0.4 ppt in 2008. This seasonal cycle agrees, with the observation by *Simmonds et al.* (2006).

Figures 3.20 and 3.21 indicate that the 1950 mixing ratios of CCl_2CCl_2 were 2.8 ppt in the northern hemisphere and only 0.8 ppt in the southern hemisphere. As CCl_2CCl_2 originates principilly from anthropogenic sources this indicates that significant anthropogenic emissions of this compound must have started before 1950. After 1950, the time series show a sustained growth in both hemispheres until around 1980. The average growth rate during this period was 0.7 ppt yr^{-1} in the northern hemisphere and 0.002 ppt yr^{-1} in the southern hemisphere. The peak in the northern hemisphere atmospheric mixing ratio occurred at 23.0 ppt in 1978, whereas the peak in the southern hemisphere atmospheric mixing ratio occurred at 1.2 ppt in 1981. After the peak around 1980, the atmospheric mixing ratio have decreased until the drill dates of the firn sites (NH = 2008 and SH = 1999).

Measurements of CCl_2CCl_2 mixing ratios have been made from 1979 onwards at the Cape Grim baseline air pollution station. Figure 3.21 shows that these observations are in good general agreement with the firn air derived southern hemispheric time series, although there are a number of outlying points. Growth rates were inferred for the Cape Grim observations by fitting a three parameter sigmoid expression to the data set (the black line in Figure 3.21). The average growth rate during this period was -0.6 ppt yr^{-1} in the northern hemisphere and -0.01 ppt yr^{-1} in the southern hemisphere. This decline in the atmospheric mixing ratios during this period is consistent with the long term measurements of *Simpson et al.* (2004) who observed a decline in CCl_2CCl_2 atmospheric mixing ratios since their observations began in 1989. *Simpson et al.* (2004) observed a northern hemispheric mixing ratio of 13.9 ± 0.5 ppt in 1989 whereas in the current study, the mixing ratio was 16.7 ppt in 1989. Also, in the Arctic regions, *Dimmer et al.* (2001) observed an average baseline mixing ratio of 1.77 ± 0.07 ppt (July–September 1997) at Ny-Ålesund (Norwegian Arctic) which is much lower mixing ratio than the 8.6 ppt observed in the current study. This offset of ~ 16 % in the absolute mixing ratio is likely to be a result of significant calibration differences. *Simmonds et al.* (2006) observed a 10 % calibration differences between the AGAGE and NOAA scales.

The decline in atmospheric mixing ratios occurred before controls were introduced on emissions in the early 1990s (*Kleiman and Prinn*, 2000) suggesting that emissions were falling before they were officially controlled. However, in recent years, this decline has slowed with

CCl_2CCl_2 remaining somewhat constant since around 2006. In the northern hemisphere in 2007, the mixing ratio was 5.0 ppt with a growth rate of -0.09 ppt yr^{-1}; this is 22 % of the peak mixing ratio. In the southern hemisphere in 2007 the mixing ratio was 1.0 ppt with a growth rate of -0.01 ppt yr^{-1}; representing 78 % of the peak mixing ratio. This levelling off is in agreement with recent trends observed by (*Montzka et al.*, 2010). Also, the greater percentage decline in CCl_2CCl_2 in the northern hemisphere and the large interhemispheric ratio shows that CCl_2CCl_2 emissions are dominated by northern hemispheric anthropogenic emissions. This agrees with the model analysis by *Simmonds et al.* (2006) who indicated that > 90 % of the emissions emanate from the northern hemisphere. It should also be noted that these growth rates and peak timing represent only the best estimates and contain considerable uncertainties within the envelopes shown in Figures 3.20 and 3.21.

The 'global' averaged atmospheric time series of CCl_2CCl_2 was derived between 1950 and 2008 (the drill date of the NEEM site) by averaging the northern and southern time series (Figure 3.23). Using the method described in section 3.2.2.

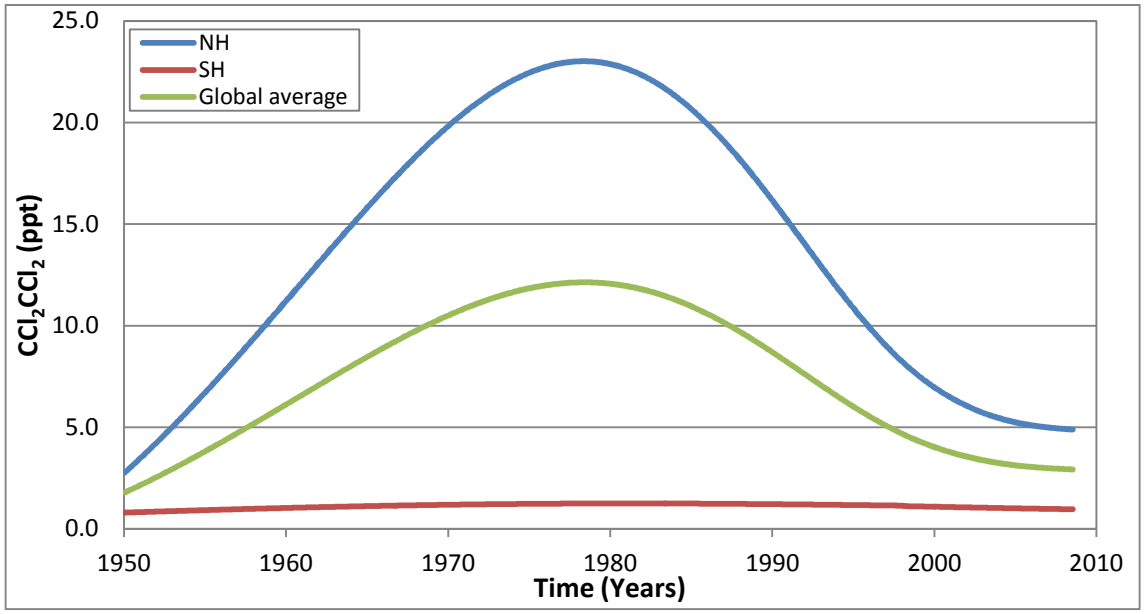

Figure 3.23: northern hemispheric atmospheric time series of CCl_2CCl_2 derived from Arctic firn air (blue line). Southern hemispheric atmospheric time series of CCl_2CCl_2 derived from Antarctic firn and Cape Grim observation (red line). 'Global' atmospheric time series of CCl_2CCl_2 derived as the average between the northern and southern hemispheric time series (green line).

Figure 3.23 indicates that 'global' mixing ratio of CCl_2CCl_2 increased from 1.9 ppt in 1950 to a maximum of 12.1 ppt in 1978, before declining to 2.9 ppt in mid-2008. These 'global' mixing ratios are higher than the global observations made by *Simpson et al.* (2004) and *Montzka et al.* (2004); this offset is likely to result from significant calibration differences between the two studies.

A 2-box model used the northern hemisphere time series as an input to derive a southern hemispheric time series using the inter-hemispheric mixing time (1.34 years) and an atmospheric lifetime of 90 days (*Montzka et al.*, 2010).This modelled southern hemispheric time series was then compared with the atmospheric time series derived from the southern hemispheric firn air measurements (Figure 3.24). More details on this model can be found in sections 2.5.5 and 3.3.4.

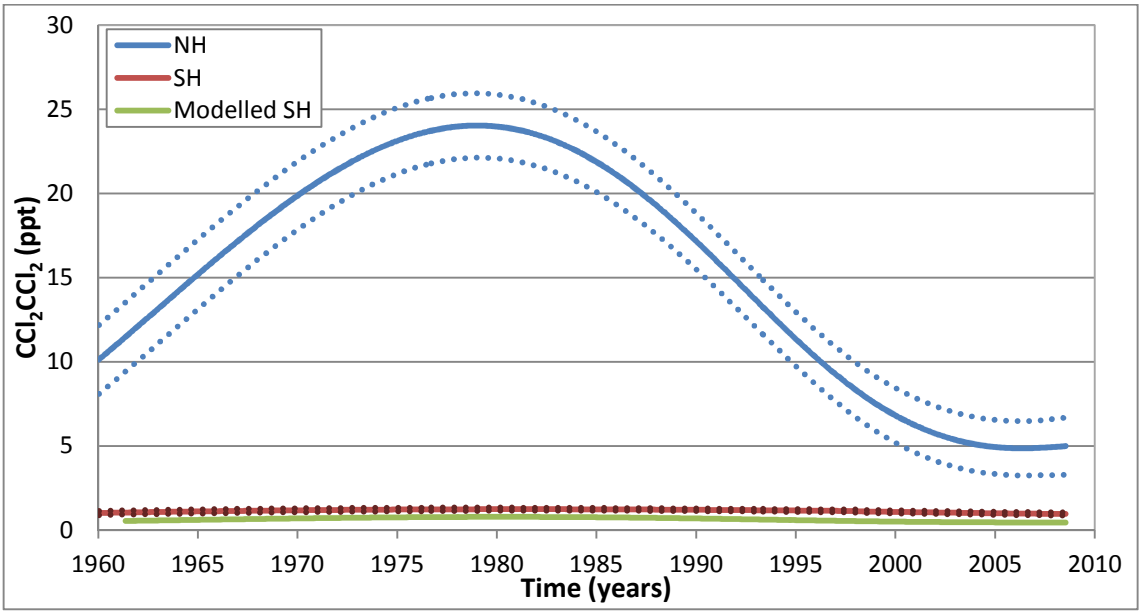

Figure 3.24: Northern hemispheric atmospheric time series of CCl_2CCl_2 derived from Arctic firn air (blue lines). Southern hemispheric atmospheric time series of CCl_2CCl_2 derived from Antarctic firn and Cape Grim observation (red lines). The dotted lines represent the uncertainty of the atmospheric time series as stated in Figures 3.20 and 3.21. The modelled southern hemispheric time series derived using the 2 box model (green line).

As can be seen from Figure 3.24, there is good general agreement between the calculated and observed southern hemispheric CCl_2CCl_2 atmospheric time series. Although there is a slight difference with the observed time series being marginally higher than the modelled time series. Although this is likely due a small error in the atmospheric lifetime and/or transport times, it may indicate a significant southern hemispheric source of CCl_2CCl_2. *McCulloch et al.* (1999) suggest that biomass burning might provide the largest source of CCl_2CCl_2 in the southern hemispheric. However, a greater number of observations are needed to validate if there is a significant source and whether it derives from a biomass source.

3.3.7 Background information on CH_2ClCH_2Cl, C_2H_5Cl and $CHClCCl_2$

In this section I will discuss the atmospheric time series of a number of VSL **chlorocarbons**: 1,2 dichloroethane (CH_2ClCH_2Cl), chloroethane (C_2H_5Cl) and trichloroethene ($CHClCCl_2$). All of these VSL chlorocarbons originate principally from anthropogenic sources. CH_2ClCH_2Cl is used in the

production of polymers and rubbers and is also used as a solvent, as a fumigant and as a food additive as a result of its use in extracting spices (*Phillips*, 2006). It was also historically widely used as a lead scavenger in antiknock gasoline (*Phillips*, 2006). CH_2ClCH_2Cl was first used in antiknock gasoline in the 1940's when it replaced around 50 % of CH_2BrCH_2Br in gasoline, in a new mixture known as "motor fluid" (*Otto and Montreuil*, 1976). This "motor fluid" contains 61 % $(CH_3CH_2)_4Pb$, 18 % CH_2BrCH_2Br, 19 % CH_2ClCH_2Cl, and 2 % dye (*Otto and Montreuil*, 1976). After the 1940's this became the primary lead additive fluid sold worldwide (*Thomas et al.*, 1997). The U.S. Environmental Protection Agency (EPA) began reducing the use of leaded petrol in 1973 (*Santodonato et al.*, 1985 and *Fishbein*, 1980), and as a result, CH_2ClCH_2Cl use as a fuel additive declined rapidly.

Sources of atmospheric C_2H_5Cl are not well known. It is used in the manufacture of ethyl cellulose, dyes, and pharmaceuticals as well as being used as a refrigerant, flame retardant and as a topical anesthetic (*Montzka et al.*, 2010). It was also formerly used as a starter compound for the production of tetraethyl lead ($(CH_3CH_2)_4Pb$) (*Low et al.*, 2003). As well as these anthropogenic sources, *Williams et al.* (1999) have observed a very small level of natural emission of C_2H_5Cl from cows.

$CHClCCl_2$ was first widely produced in the 1920s where it was used to extract vegetable oils from plant materials. Since then it has been used by the food industry in the decaffeination of coffee and the preparation of flavouring extracts from hops and spices as well as the production of 100% ethanol (*Phillips*, 2006). From the 1930s through the 1970s, it was used as a volatile anaesthetic in both Europe and North America (*Fenton*, 2000). It was phased out in developed countries as an anaesthetic in the 1960s by the introduction of halothane (Section 4.4.2), although as of 2000, it was still in use as an anaesthetic in Africa (*Fenton*, 2000). $CHClCCl_2$ has also been used as a dry cleaning solvent, although it was widely replaced by CCl_2CCl_2 in the 1950s.

The major use of $CHClCCl_2$ has been as a degreaser for metal parts in industry (*Montzka et al.*, 2010), although its demand as a degreaser began to decline in the 1950s in favour of the less toxic CH_3CCl_3 (*Phillips*, 2006). Under the terms of the Montreal Protocol (*González et al.*, 2006) CH_3CCl_3 production has been phased out in most of the world, and as a result $CHClCCl_2$ has experienced some resurgence in use as a degreaser (*Phillips*, 2006). $CHClCCl_2$ is also used in the manufacture of a range of fluorocarbon refrigerants such as HFC 134a (*Phillips*, 2006). The main sink of atmospheric CH_2ClCH_2Cl, C_2H_5Cl and $CHClCCl_2$ is through the reaction with the hydoxyl (OH) radical (*Montzka et al.*, 2010).

Atmospheric mixing ratios of CH_2ClCH_2Cl and $CHClCCl_2$ have been observed by a number of different studies (*Laube et al.*, 2008 *Clerbaux and Cunnold et al.*, 2006 and *Schauffler et al.*, 1999), summarised in Table 3.5.

Table 3.5: Summary of available observations of CH_2ClCH_2Cl and $CHClCCl_2$ (in ppt) from the marine boundary layer (MBL) to the tropical tropopause layer (TTL) based on *Montzka et al.* (2010).

Region	Marine Boundary Layer	Upper Troposphere	Lower TTL	LZRH	Upper TTL	Tropical Tropopause
Ref.	*Clerbaux and Cunnold et al.* (2006)	*Schauffler et al.* (1999)	*Laube et al.* (2008)	*Clerbaux and Cunnold et al.* (2006)	*Clerbaux and Cunnold et al.* (2006)	*Laube et al.* (2008)
Height range (km)	0- ~2	10-12	12-14	14.5-15.5	15.5-16.5	16.5-17
CH_2ClCH_2Cl	0.7 – 14.5	1.9 – 5.4	1.9 – 4.1	1.6 – 4.9	1.2 – 4.0	0.6 – 4.3
$CHClCCl_2$	0.05 – 2.00	0.00 – 2.02	0.00 – 0.16	0.00 – 0.17	0.00 – 0.05	0.00 – 0.17

The background mixing ratio of CH_2ClCH_2Cl in the northern hemispheric was observed as <1 to 24 ppt between 1982 and 1985 (*Class and Ballschmiter*, 1987) and a background mixing ratio for the southern hemisphere was given as <1 ppt for the same period (*Class and Ballschmiter*, 1987). However, the large interhemispheric ratio does suggest a predominantly anthropogenic source at that time. In 2008, the atmospheric mixing ratio was taken to be approximately 6 ± 6 ppt (*Montzka et al.*, 2010). C_2H_5Cl was claimed to be detected in Los Angeles air (*Pellizzari et al.*, 1976), but was not quantified.

Low et al. (2003) observed a northern hemispheric mixing ratio of C_2H_5Cl of 2.6 ppt and a southern hemispheric mixing ratio of 1.6 ppt between 1996 and 1999. This indicates that there might be a significant, presumably nonindustrial, source to sustain this observed southern hemispheric abundance. In addition, higher values have also been noted in the tropical marine boundary layer, also indicative of a natural source (*Low et al.*, 2003). C_2H_5Cl was not quantified, but was estimated to be in the order of 1.5 ppt in the upper tropical troposphere (*Montzka et al.*, 2010). *The AGAGE* global network observed a global atmospheric mixing ratio of $CHClCCl_2$ of 0.19 ± 0.19 ppt in 2007 and 0.28 ± 0.28 in 2008 (*Montzka et al.*, 2010). However the short atmospheric lifetime of $CHClCCl_2$ means that the global mixing ratio should be seen rather as an approximation than a defined global value (*Montzka et al.*, 2010). Emission rates of CH_2ClCH_2Cl and $CHClCCl_2$ have been calculated by *McCulloch et al.* (1999), *Class and Ballschmiter* (1987) and *Singh et al.* (1983).

3.3.8 Results and discussion of CH_2ClCH_2Cl, C_2H_5Cl and $CHClCCl_2$

In the current study, I report firn air measurement of CH_2ClCH_2Cl, C_2H_5Cl and $CHClCCl_2$ from a number of northern hemispheric firn air records. The NEEM measurements are a new set of data obtained during this study whereas the NGRIP measurements have previously been measured at the University of East Anglia. These measurements have then been used to derive northern hemispheric time series of atmospheric mixing ratios. The time series of atmospheric CH_2ClCH_2Cl, C_2H_5Cl and $CHClCCl_2$ mixing ratios were derived using the LGGE method, which is described in more detail in the methods chapter. The time series obtained and the output from the inverse model (Figure 3.25 and 3.26) are shown alongside the measured concentration of CH_2ClCH_2Cl and C_2H_5Cl with depth at the NEEM firn sites in Figure 3.25, and the measured concentration of $CHClCCl_2$ with depth at the NGRIP firn sites in Figure 3.26.

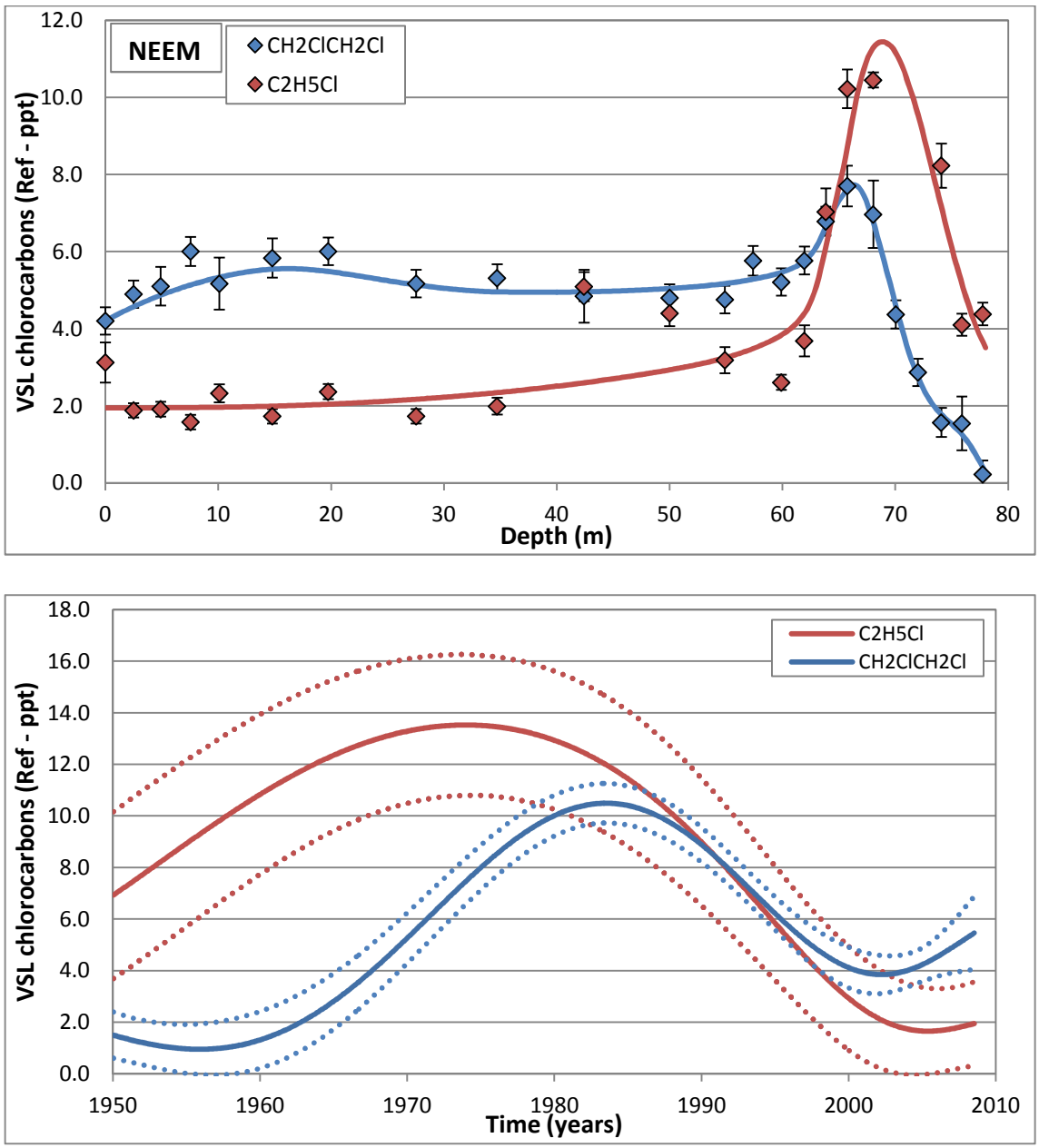

Figure 3.25: Top panel, measured concentration of northern hemispheric CH_2ClCH_2Cl (blue points) and C_2H_5Cl (red points) with depth at the NEEM firn site, compared with model simulations based on the atmospheric time series indicated in the bottom panel with a seasonal cycle with an amplitude of 60 % added to the CH_2ClCH_2Cl time series. The error bars represent the 1 σ of the measurements. Bottom panel, atmospheric time series derived by a single site inversion modelling of the NEEM firn air measurements CH_2ClCH_2Cl (blue line) and C_2H_5Cl (red line) using the LGGE method. The dashed lines represent the uncertainties envelope of the time series (as described Figure 2.10). The reference scale is used to scale the NEEM data to previous observations. This was achieved by scaling the CH_2ClCH_2Cl data so that the 2008 mixing ratio equals 6 ppt (*Montzka et al.*, 2010) and the C_2H_5Cl data so that the 1999 mixing ratio equals 2.6 ppt (*Low et al.*, 2003).

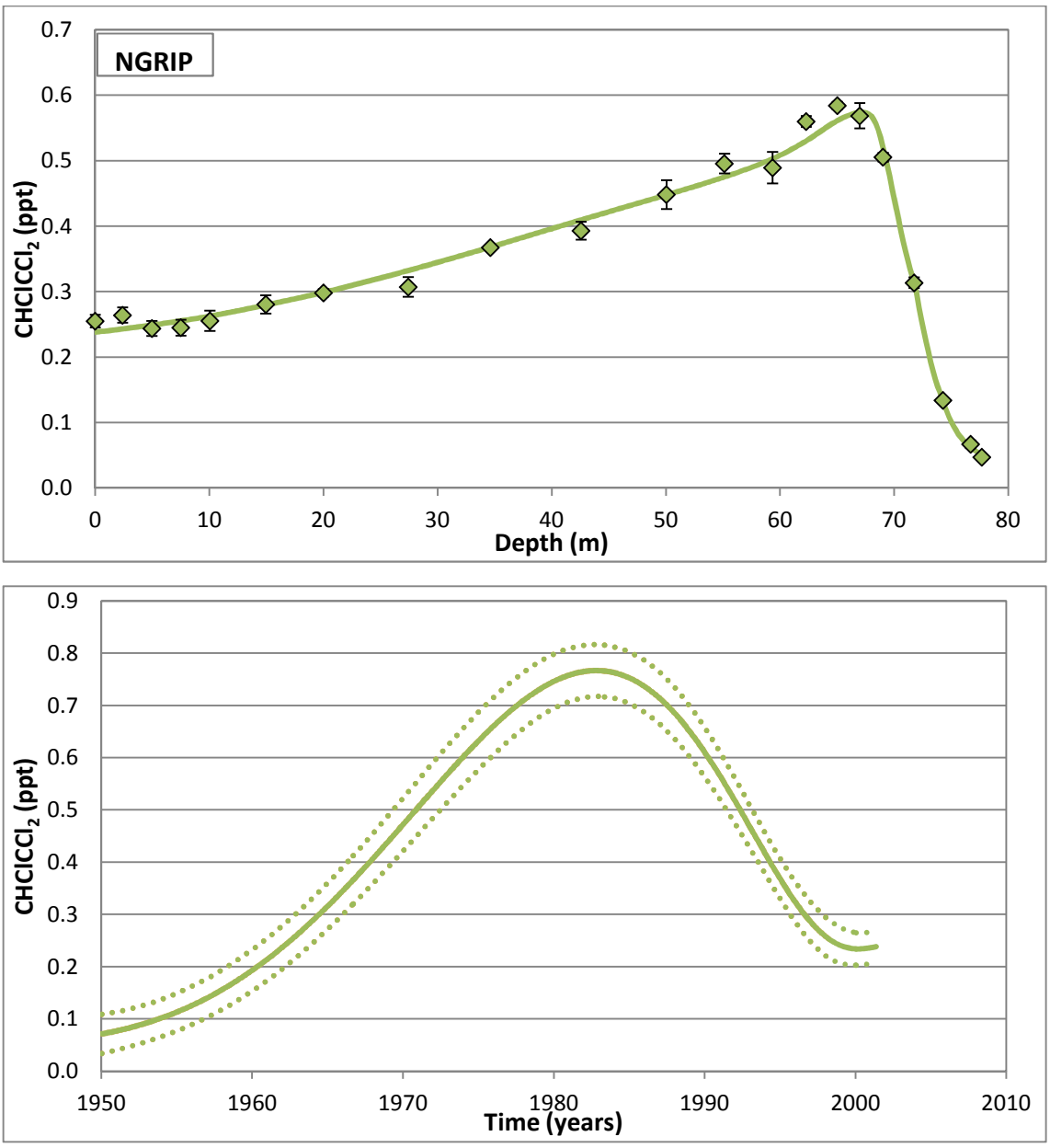

Figure 3.26: Top panel, measured concentration of northern hemispheric $CHClCCl_2$ (green points) with depth at the NGRIP firn site, compared with model simulations based on the atmospheric time series indicated in the bottom panel. The error bars represent the 1 σ of the measurements. Bottom panel, atmospheric time series derived by a single site inversion modelling of the NGRIP firn air measurements $CHClCCl_2$ (green line) using the LGGE method. The dashed lines represent the uncertainties envelope of the time series (as described Figure 2.10).

Figure 3.25 and 3.26 shows that CH_2ClCH_2Cl, C_2H_5Cl and $CHClCCl_2$ at the NEEM and NGRIP firn air observations have good measurement precision. All of the VSL chlorocarbons have a significant atmospheric sink as a result of reactions with the hydroxyl radical (OH) (*Montzka et al.*, 2010). The local atmospheric lifetime of bromo-chloro methanes are given as: CH_2ClCH_2Cl – 65 days, C_2H_5Cl – 39 days, and $CHClCCl_2$ – 4.9 days (*Montzka et al.*, 2010). This should be short enough for there to be a seasonal cycle in their atmospheric mixing ratio compared with other trace gases with similar lifetimes. This seasonal cycle can be seen in variations in

concentrations in the shallowest part of the firn columns for CH_2ClCH_2Cl, which would have reflected the seasonality in the OH atmospheric mixing ratios previously described by *Kaspers et al.* (2004) and *Sturges et al.* (2001). However, there are no signs of variation in C_2H_5Cl and $CHClCCl_2$ concentrations in the shallowest part of the firn columns. Although this does not mean that there is no seasonality in the C_2H_5Cl and $CHClCCl_2$ atmospheric mixing ratio, the amplitude of seasonality might not be large enough to be recorded in the firn air measurements or a general decrease in C_2H_5Cl and $CHClCCl_2$ mixing ratio could mask any seasonality.

The seasonal cycle of CH_2ClCH_2Cl was calculated by adding seasonal cycles with increasing amplitudes to the atmospheric time series in Figure 3.25 until the time series derived the lowest error with the firn air measurements. The error was calculated as the square root of the sum of the squares of the difference between the model and the observations. This method derived a seasonal cycle for CH_2ClCH_2Cl with an amplitude of 60 % of the annual mean mixing ratio, which results in a seasonal cycle with an amplitude of 3.6 ppt in 2008. This indicates that CH_2ClCH_2Cl does have a large amplitude in its seasonal cycle in terms of the percentage to the annual mean mixing ratio; this result is consistent with the size of the amplitudes observed from other compounds with similar atmospheric lifetimes (*Atlas and Ridley*, 1996).

Figure 3.25 indicates that the 1950 mixing ratio of CH_2ClCH_2Cl was 1.5 ppt in the northern hemisphere. CH_2ClCH_2Cl was first used in antiknock gasoline in the 1940's (*Otto and Montreuil*, 1976). Therefore, it is expected that there would be a significant atmospheric mixing ratio of CH_2ClCH_2Cl by 1950. After 1960, the time series show a sustained growth until 1983 when the atmospheric mixing ratio was 10.5 ppt. The average growth rate during this period was 0.4 ppt yr^{-1}. This increase in atmospheric mixing ratio is consistent with the use of CH_2ClCH_2Cl in antiknock gasoline which was extensively used from the 1940s up to the mid-1970s when its use was banned (*Santodonato et al.*, 1985 and *Fishbein*, 1980). However, the atmospheric mixing ratios continued to increase after the decrease in use of antiknock gasoline which suggests that other emissions source(s) might be governing atmospheric mixing ratios. Since 1983, mixing ratios have deceased continually reaching a mixing ratio of 3.9 ppt in mid-2001. During this period, the average growth rate was -0.4 ppt yr^{-1}. However, since 2001 the atmospheric mixing ratio shows evidence of increasing and reached 5.4 ppt in mid-2008. The growth rate during this period also increased year-on-year from 0.03 ppt yr^{-1} in 2002 up to 0.4 ppt yr^{-1} 2007, which suggests that this increase is likely to continue in the future.

It is unclear what is causing this current increase in CH_2ClCH_2Cl mixing ratios, either a previously known source has increased its emissions rate or there might be a new source of atmospheric CH_2ClCH_2Cl. Figure 3.25 also indicates that the 1950s mixing ratio of C_2H_5Cl was 7.1 ppt which indicates that there must be a significant pre-1950 source. After the 1950 the time series show a sustained growth until 1973 when the atmospheric mixing ratio was 13.5 ppt. The average growth rate during this period was 0.3 ppt yr^{-1}. These measurements agree with the phasing out of leaded petrol in the U.S. and Europe in the early 1970s (*Santodonato et al.*, 1985 and *Fishbein*, 1980). After a peak in the early 1970s, the atmospheric mixing ratios decrease until the drill data of the firn sites in the mid-2008. The average growth rate during this period was -0.4 ppt yr^{-1}. However, in recent years this decline has stopped with C_2H_5Cl mixing ratios remaining somewhat constant. In the northern hemisphere the decline stopped in 2005 at a mixing ratio of 1.7 ppt, which represents 13 % of the peak mixing ratio (Figure 3.25). These results indicate that the atmospheric mixing ratio of C_2H_5Cl is likely to be very strongly linked to its use in leaded petrol.

Figure 3.26 shows that the 1950 mixing ratio of $CHClCCl_2$ was 0.1 ppt in the northern hemisphere. This is in good general agreement with the introduction of $CHClCCl_2$ in many industrial processes in the 1920s (*Phillips*, 2006). After 1950, the time series show a sustained growth until 1983 when the atmospheric mixing ratio was 0.8 ppt. The average growth rate during this period was 0.02 ppt yr^{-1}. Since 1983, mixing ratios have deceased continually to 0.2 ppt in mid-2001. During this period, the average trend was -0.03 ppt yr^{-1}. However, in recent years the rate of decline in the atmospheric mixing ratio has decreased to -0.002 ppt yr^{-1} in 2000. This atmospheric time series is very similar to that of CH_2ClCH_2Cl and may suggest a similar emissions source or related emissions rates between the two compounds. The CH_2ClCH_2Cl time series shows an increase in mixing ratios after 2001. However, the $CHClCCl_2$ time series only go to 2001 therefore, it is unclear if there has been an increase in the mixing ratio in recent years. Nonetheless the AGAGE network do observe an increase in mixing ratio between 2007 and 2008 (*Montzka et al.*, 2010) which suggest that there is similar emissions sources between these two compounds. It should also be noted that these growth rates and peak timing represent only the best estimates and contain considerable uncertainties within the envelopes shown in Figures 3.25 and 3.26.

3.3.9 Emissions of the VSL chlorinated substances

Annual emissions of $CHCl_3$, CH_2Cl_2, CCl_2CCl_2, CH_2ClCH_2Cl, C_2H_5Cl and $CHClCCl_2$ were derived using the atmospheric time series in Figures 3.13, 3.18, 3.23, 3.25 and 3.26 with use of a 1 - box model, further details of the emission estimate process are given in the methods chapter. These annual emission estimates are shown in Figure 3.27, 3.28, 3.29 and 3.30.

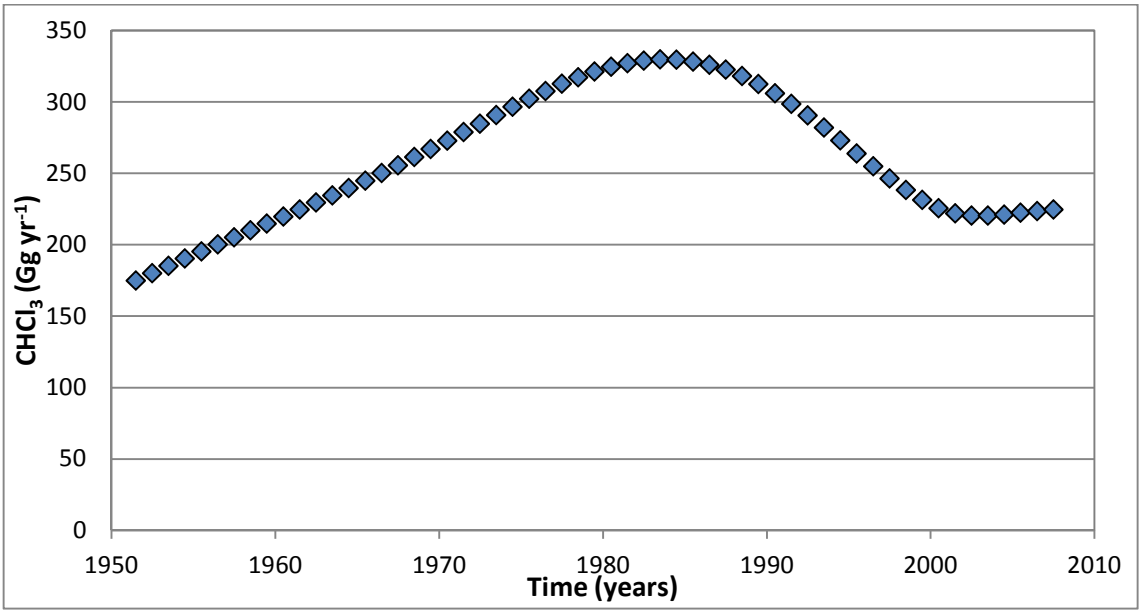

Figure 3.27: Annual emission of $CHCl_3$ based on the atmospheric time series in Figure 3.13.

Figure 3.27 shows that the emissions of $CHCl_3$ rose from 175 Gg yr^{-1} in 1950 to a peak of 330 Gg yr^{-1} in 1985 before progressively declining to 220 Gg yr^{-1} in 2002; this represents ~67 % of peak emissions. In recent years, emissions have remained almost constant with an average of 225 Gg yr^{-1} emitted between 2000 and 2007. The $CHCl_3$ emissions associated with the *Worton et al.* (2006) "best fit" scenario are shown in Table 3.6.

Table 3.6: Comparison of anthropogenic and estimated global $CHCl_3$ emissions for 1950, 1990 and 2001 based on *Worton et al.* (2006)

Year	Emissions (Gg yr^{-1}) (*Worton et al.*, 2006)		Anthropogenic Contribution (%)	Emissions (Gg yr^{-1}) Current study
	Anthropogenic	Global		
1950	46–55	270–335	14–20	175
1990	193–226	417–506	41–50	300
2001	91–93	315–373	25–29	220

Table 3.6 shows that the emissions estimate derived by *Worton et al.* (2006) are larger than emissions estimate derived in the current study. *Worton et al.* (2006) did note that by invoking a more northerly transport in their model would result in a slight reduction of the estimated

magnitude of their estimated emissions. The differences between the two emissions estimates suggest that the assumptions (Section 2.5.4) used in the model in the current study do not represent the emissions of $CHCl_3$. In the current study the emission modelling does not take into account the global location of the emissions. Therefore, as the model does not take into account any loss of atmospheric $CHCl_3$ before it reaches the polar regions, it under estimates the emission rate at the source. The time series of the emission rates do, however agree between the two studies. The emission rate is within the 32 % uncertainty of the reported 460 Gg yr^{-1} for 1990 reported by *McCulloch* (2003) and *Keene et al.* (1999). Table 3.6 also shows that the contribution from anthropogenic sources dropped since 1990. This suggests that the decline shown in the time series (Figure 3.10 and 3.11) is most likely due to declines in anthropogenic emissions. This decline is largely due to reduced emissions from the pulp and paper industry which became undetectable in ~ 2001 (*Worton et al.*, 2006). Therefore, the almost constant global emissions after 2001 results mainly from emissions from the pulp and paper industry and no longer effecting the global emissions. It also indicates that there has been little change in the other sources during this period, which agrees with the findings of *Montzka et al.* (2010). If the decline in $CHCl_3$ emissions after 1985 was assumed to be entirely due to the paper and pulp industry and that all the other emissions sources remained constant during this period, it can be calculated that at its peak in 1985, the paper and pulp industry was responsible for emitting 109 Gg yr^{-1} of $CHCl_3$.

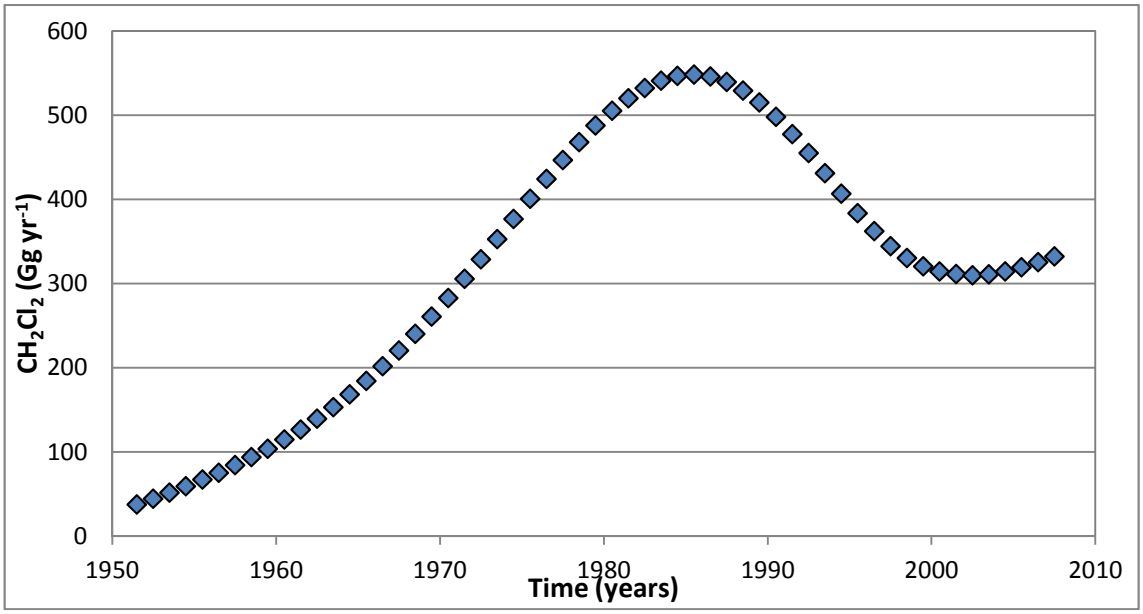

Figure 3.28: Annual emission of CH_2Cl_2 based on the atmospheric time series in Figure 3.18.

Figure 3.28 shows that the emissions of CH_2Cl_2 rose from 38 Gg yr^{-1} in 1950 to a peak of 550 Gg yr^{-1} in 1985 before progressively declining to 310 Gg yr^{-1} in 2002. This is around 57 % of the

peak emissions. In recent years, emissions have started to increase up to 330 Gg yr^{-1} estimated in 2007. These emission estimates agree with the estimates of industrial emissions by *Trudinger et al.* (2004) who report an increase from 1930 up to a peak of 650 Gg yr^{-1} by ~ 1990. There have been a number of assessments of the location of the global industrial emissions of CH_2Cl_2. Table 3.7 shows a comparison between 1990 emission rates by *Keene et al.* (1999) and 2000-2004 emission rates by *Xiao* (2008) from different global regions.

Table 3.7: Comparison of averaged surface flux values from industrial sources from different regions during 1990 by *Khalil et al.* (1999) and during 2000-2004 by *Xiao* (2008).

Region	***Keene et al.* (1999) 1990 (Gg yr^{-1})**	***Xiao* (2008) 2000 - 2004 (Gg yr^{-1})**
Europe	184	42
North America	168	95
South East Asia	118	195
Rest of the World	111	98
Global Industrial	581	430
Total Global Emission	**836**	**629**

Table 3.7 shows that the emission estimates in the current study are lower than the total global emissions estimated by *Xiao* (2008) and *Khalil et al.* (1999). It also shows that between 1990 and 2000-2004 the global industrial emissions decreased from 580 Gg yr^{-1} to 430 Gg yr^{-1}. This decrease is mainly down to a reduction in emissions from Europe and North America during this period. However, during the same period, emissions from South East Asia rose significantly to become the major industrial source region of CH_2Cl_2. Therefore, the current increase in CH_2Cl_2 is most likely a result of increased emissions from South East Asia.

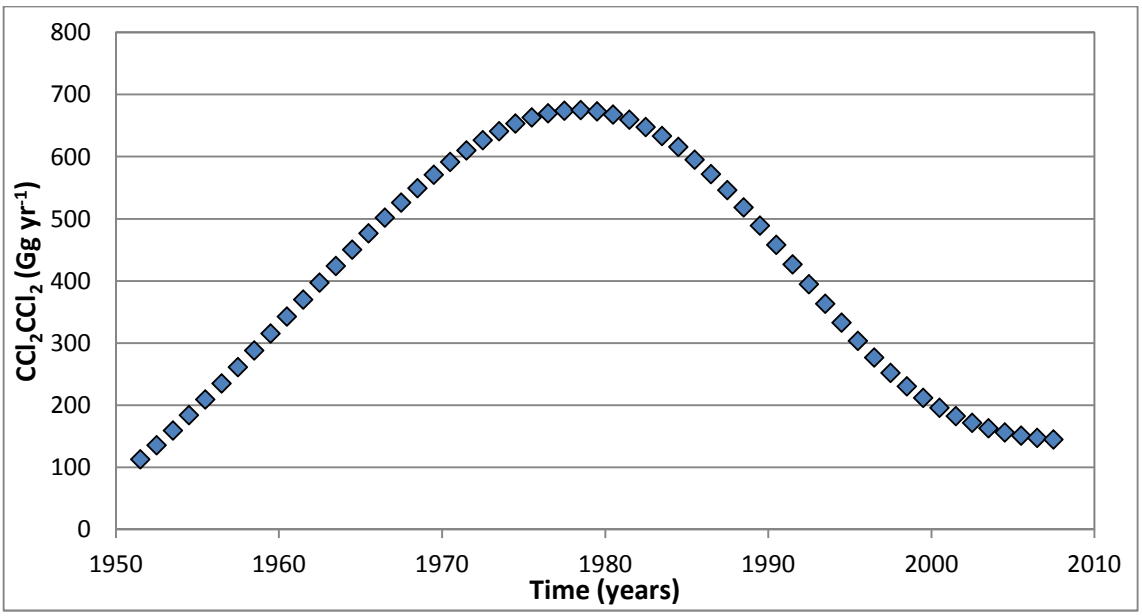

Figure 3.29: Northern hemispheric emission of CCl_2CCl_2 based on the atmospheric time series in Figure 3.23.

Figure 3.29 shows that emissions of CCl_2CCl_2 rose year-on-year from the 1950s to the late 1970s, peaking at 360 Gg yr^{-1} in ca. 1978 before progressively declining to 87 Gg yr^{-1} in 2007, representing around 25 % of the peak emission. These emissions estimate generally agree with the modelled average annual emission between 1999 to 2003 of 228 Gg yr^{-1} (*Simmonds et al.*, 2006), and the industrially derived global emission estimates of 268 ± 27 Gg yr^{-1} for 1999 and 2000, (*McCulloch et al.*, 1999a). Although it is significantly larger than the emission estimates of 366 Gg yr^{-1} in 1990 reported by *McCulloch et al.* (1999).

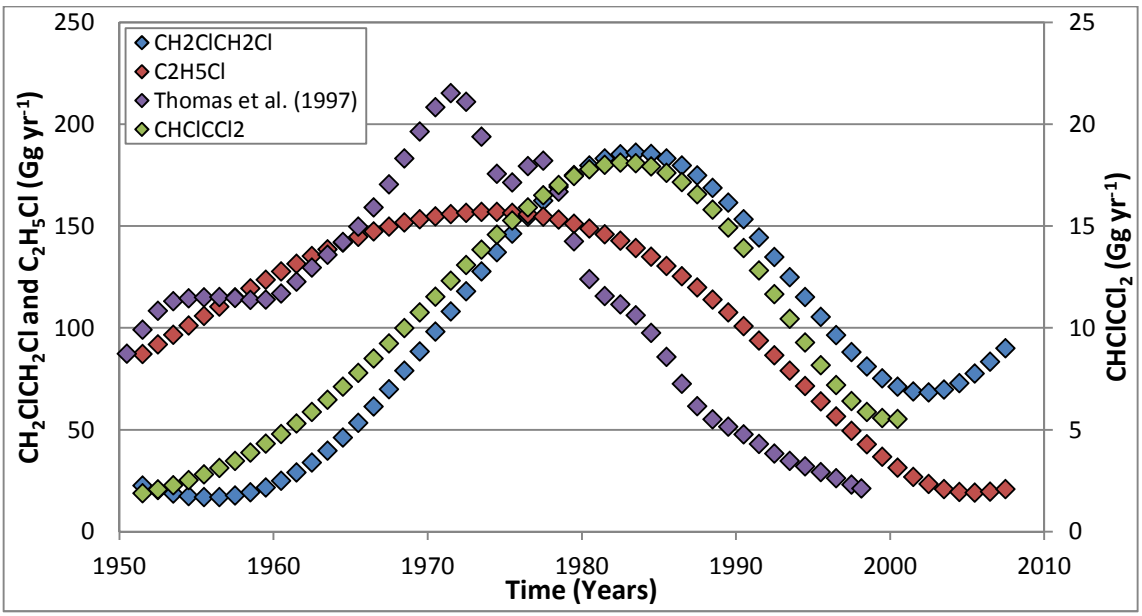

Figure 3.30: Annual emission of CH_2ClCH_2Cl (blue points), C_2H_5Cl (red points) and $CHClCCl_2$ (green points) based on the atmospheric time series in Figure 3.25 and 3.26. Annual emission of bromine from leaded petrol based on *Thomas et al.* (1997) are given as a comparison (purple points).

Figure 3.30 shows that estimated emissions of C_2H_5Cl rose year-on-year from 87 Gg yr^{-1} in 1950 to a peak of 160 Gg yr^{-1} in 1972 before progressively declining to 21 Gg yr^{-1} in 2007, representing around 13 % of the peak emission. These emissions estimates are in general agreement with the reported temporal trend of leaded petrol emissions in the United States, which declined rapidly between 1971 and 1991 (*Penkett et al.*, 1995). In addition they agree well with the bromide emissions from leaded petrol given by *Thomas et al.* (1997) (Figure 3.30). The authors estimated bromine emissions from lead petrol based on the world use of lead in petrol and on petrol scavenger formulations (*Thomas et al.*, 1997). However, the estimated emissions from the firn air derived time series are smoothed due to diffusion within the firn as well as the smoothing factors in the firn model process. This will result in the emissions from the firn time series smoothing some features such as the timing and the value of the peak emission. These estimated emissions in the current study are in general agreement with the time series of emission estimates of CH_2BrCH_2Br (Figure 5.14), which indicates they might share a common emissions source most likely to be the emissions from leaded petrol (*Thomas et al.*, 1997 and *Otto and Montreuil*, 1976).

Figure 3.30 shows that the emissions of CH_2ClCH_2Cl rose from 17 Gg yr^{-1} in 1955 to a peak of 170 Gg yr^{-1} in 1983, before progressively declining to 68 Gg yr^{-1} in 2002 this is around ~40 % of the peak emission. In recent years emissions have started to increase. These estimates are less than the northern hemispheric emissions deduced by *Class and Ballschmiter* (1987) be in the range of 400-500 Gg yr^{-1} between 1982 and 1985, representing about 3-4 % of the global

production of > 12000 Gg yr^{-1} reported (*Schulze et al.*, 1985) during this period. The emissions are also less than the global emissions of 534 Gg yr^{-1} reported by *Singh et al.* (1983) based on numbers from *Bauer* (1979) for the year 1981. Figure 3.30 also shows that the emissions of $CHClCCl_2$ rose from 2 Gg yr^{-1} in 1950 to a peak of 18 Gg yr^{-1} in ca. 1982, before progressively declining to 6 Gg yr^{-1} in 2000 this is ~35 % of the peak emission. As a result of the similarity in emissions rates between CH_2ClCH_2Cl and $CHClCCl_2$ it is highly likely that they are emitted from similar sources.

3.4 Equivalent effective stratospheric chlorine of the chlorocarbons

When chlorine and bromine atoms are released from the degradation of ODSs in the stratosphere, they combine to form the inorganic chlorine and bromine containing compounds that belong to the chemical groups called total inorganic chlorine (Cl_y) and inorganic bromine (Br_y). Some ODSs, such as methyl chloride and methyl bromide, and a number of other halogen-containing gases, do also have natural sources. Therefore there is a natural background in Cl_y and Br_y produced from ODSs which have significant natural sources (*Montzka et al.*, 2010). The combination of Cl_y and Br_y in the stratosphere represents the potential for halogens to destroy ozone. A measure of this potential is defined as equivalent stratospheric chlorine (ESC) which is calculated using Equation 1 (*Eyring et al.*, 2007).

$$ESC = Cl_y + \alpha \cdot Br_y \quad \text{– (Equation 1)}$$

where the units are stratospheric mixing ratio and α is the weighting factor that accounts for the greater effectiveness of bromine in ozone destruction compared to the effectiveness of chlorine on a per atom basis.

Although the relative effectiveness of bromine compared with chlorine for ozone depletion is treated as a single, fixed quantity, it represents a globally integrated result with sensitivity to many factors, including the kinetic parameters for chlorine and bromine species, the amount of inorganic bromine and inorganic chlorine in the background atmosphere, and atmospheric transport. In addition, it varies with altitude, latitude and total emissions of halogen gases at the Earth's surface. In the lower stratosphere, α is estimated to be 60 and around 5 in the upper stratosphere at mid-latitudes ((*Montzka et al.*, 2010 and *Sinnhuber et al.*, 2009), and a value of 65 is used for Antarctic regions (*Montzka et al.*, 2010). In the current study I selected a value of 60 for the weighting factor. For fluorine, the relative effectiveness compared with chlorine for ozone destruction is negligibly small (*Blake et al.*, 1997).

There is a lack of direct measurements of Cl_y and Br_y which makes it difficult to derive ESC directly from observations. Therefore, an approximation of the spatial and temporal distributions of Cl_y and Br_y are generally used. This approximation uses the time series measurements of ODS surface concentrations combined with estimated rates at which individual gases release their halogens into the stratosphere (fractional release rates), as well as estimates of the age of air parcels, which is taken as the time elapsed since air parcels entered the stratosphere at the tropical tropopause. Using these estimates in Equation (1) yields equivalent effective stratospheric chlorine (EESC) (Equation 2) (*Clerbaux and Cunnold et al.*, 2006). Therefore EESC provides a simple index that relates the time evolution of surface mixing ratios of ODSs with the ozone-destructive ability of stratospheric halogens that come from these source gases (*Montzka et al.*, 2010).

$$EESC(t) = f_{CFC-11}\left[n_{i,Cl}\frac{f_i}{f_{CFC-11}}\rho_{i,entry} + \alpha \cdot n_{i,Br}\frac{f_i}{f_{CFC-11}}\rho_{i,entry}\right] \quad \text{- Equation 2}$$

where $f_{CFC\text{-}11}$ is the fractional release factor of CFC-11, n_i is the number of chlorine or bromine atoms in the source gas, f_i / $f_{CFC\text{-}11}$ represents the relative fractional release and $\rho_{i,entry}$ is the tropospheric mixing ratio of source gas i when it entered the stratosphere.

The distributions of species in the stratosphere depend on the competition between local photochemical removal processes and transport processes that carry the material from the entry point through, and out of, the stratosphere. Once a halogen source gas is in the stratosphere, halogen atoms can be released through photolysis or chemical reactions. The fractional release factor, $f_i(x,y,z,t)$ is calculated as the fraction of halocarbon (*i*) converted to an inorganic form by some time at a given location in the stratosphere (Equation 3) (*Montzka et al.*, 2010).

$$f_i(x,y,z,t) = \frac{\rho_{i,entry} - \rho_i(x,y,z,t)}{\rho_{i,entry}} \quad \text{- Equation 3}$$

where $\rho_i(x,y,z,t)$ denotes the mixing ratio of the halocarbon at a given stratospheric location (x,y,z) at time t, and ρ_i,entry is the mixing ratio of species i in the air parcel when it entered the stratosphere.

The relative fractional release term used in Equation 2 is the ratio f_i / $f_{CFC\text{-}11}$, which is a measure of the local fractional release of inorganic halogen compounds relative to the fractional release of CFC-11. Conceptually, the fractional release factor should be globally integrated. However, a more limited range of measured correlations representing mid to high latitudes, where ozone is highly sensitive to changes in the local photochemical removal rate, is generally used

(*Schauffler et al.*, 2003). Currently there are no calculated values of fractional release for the VSL chlorocarbons. Therefore, in the current study these will be estimated (Table 3.8).

Table 3.8: Fractional release values of the chlorocarbons and CFC-11

Compound	f_{cfc-11}	f_i	f_i / f_{CFC-11}
CH_3Cl	0.47	0.44#	0.94
$CHCl_3$	0.47	1.00	2.13
CH_2Cl_2	0.47	1.00	2.13
CCl_2CCl_2	0.47	1.00	2.13
CH_2ClCH_2Cl	0.47	1.00	2.13
C_2H_5Cl	0.47	1.00	2.13
$CHClCCl_2$	0.47	1.00	2.13

Montzka et al. (2010)

The VSL chlorocarbons release chlorine atoms very quickly after they have entered the stratosphere due to their high photolysis rate and reactivity to the OH radical (*Montzka et al.*, 2010). This means that chlorine is released very quickly, and an estimated fractional release factor of 1.0 is used in this study. This is consistent with *Montzka et al.* (2010), which recommends a unit fractional release value for any VSLS. It is also supported by observations by *Wamsley et al.* (1998), who reported that short-lived species are seen to have been fully degraded at altitudes below the mid-stratosphere.

To retain the simplicity of the EESC index, the stratospheric entry mixing ratio for a given time is calculated assuming a simple time lag (Γ) from the surface observations (*Montzka et al.*, 2010). In this study Γ was taken to be 3 years (typical of the lower, midlatitude stratosphere (*Montzka et al.*, 2010)) to obtain a value appropriate for relating to midlatitude-averaged ozone loss. This assumption is used for CH_3Cl in the current study, so that they are consistent with EESC estimations derived by *Montzka et al.* (2010). However, this assumption is likely to be an overestimate of the EESC contribution for shorter-lived compounds like $CHCl_3$, whose abundance will be reduced before reaching the tropopause. In this study a reduction factor is used to account for this decline in mixing ratio between the surface and the tropopause. These reduction factors are calculated by taking the fraction between the surface mixing ratios and the mixing ratios at the tropopause observed in previous studies. These reduction factors can be found in Table 3.9. It should be noted that all EESC estimates in the current study are for mid-latitude and mid-stratosphere values. The estimated EESC for CH_3Cl would be greater in the polar regions, due to more chlorine being released, as a result of the increase mean age of

the air (*Newman et al.*, 2007). However, as I have assumed a fractional release value of one for the VSL chlorocarbons, their estimated EESC will not increase in the polar regions.

Table 3.9: Reduction factors of chlorocarbons based on *Montzka et al.* (2010)

Compounds	Surface mixing ratio (ppt)	Mixing ratio at the tropopause (ppt)	Reduction factor
$CHCl_3$	7.8	4.9	0.63
CH_2Cl_2	17.5	12.6	0.72
CCl_2CCl_2	1.8	0.5	0.28
CH_2ClCH_2Cl	3.7	2.0	0.54
C_2H_5Cl	2.6	1.5	0.58
$CHClCCl_2$	0.5	0.03	0.06

There are a number of limitations to the concept of EESC, due to the uncertainties, in the transport time, the efficiency of stratospheric halogen released from the source gas and the spatial and temporal dependencies of the bromine efficiency for ozone destruction versus chlorine (*Newman et al.*, 2007). The EESC concept also does not account for changes in the atmospheric emissions and mixing ratios of other relevant constituents that can also affect ozone (e.g. CO_2 and methane) (*Daniel et al.*, 2010).

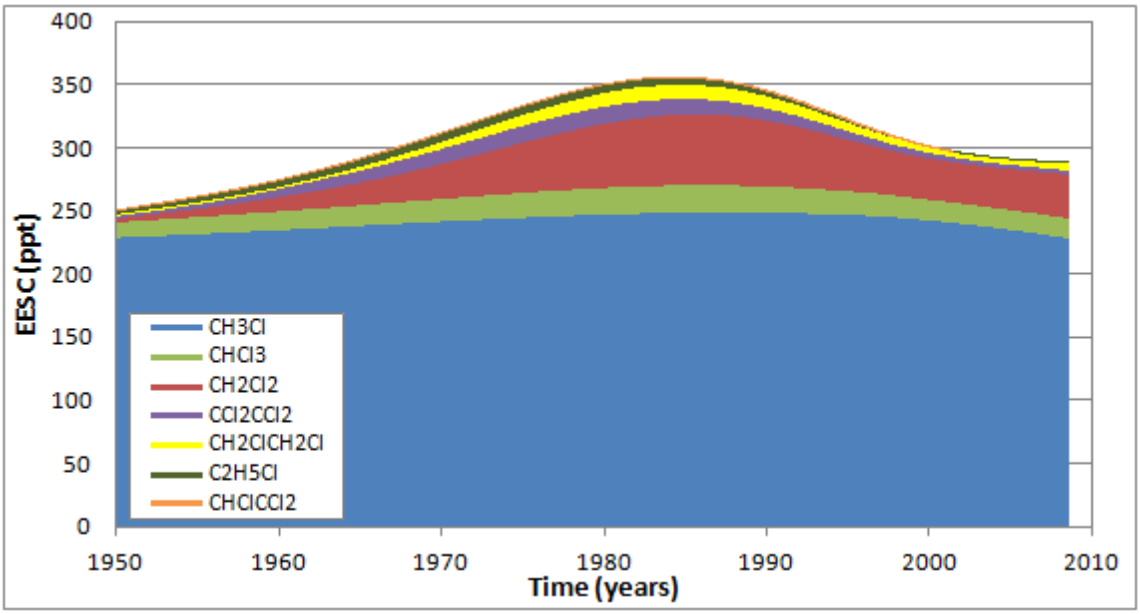

Figure 3.31: Equivalent effective stratospheric chlorine emitted since 1950 from CH_3Cl (blue area), $CHCl_3$ (light green), CH_2Cl_2 (red area), CCl_2CCl_2 (purple area), CH_2ClCH_2Cl (yellow area), C_2H_5Cl (dark green area) and $CHClCCl_2$ (orange area).

Figure 3.31 indicates that in 2008 these chlorocarbons had a combined total of 290 ppt EESC. This is ~17 % of the 1700 ppt total EESC in 2008 from inorganic halogen calculated for the midlatitude stratosphere from surface measurements (*Montzka et al.*, 2010) and ~19 % of the 1500 ppt total EESC in 2008 from anthropogenic sources including the halogenated ODS and N_2O modelled by *Daniel et al.* (2010).

Figure 3.31 also shows that the EESC of the chlorocarbons peaked at 356 ppt in 1984 before decreasing by 20 % to its 2008 value. This peak in EESC occurred nearly 15 years before the peak in total EESC from inorganic halogen, which occurred in 1997 and is important because the EESC value in 1980 is used as an important benchmark for ozone recovery (*Montzka et al.*, 2010). Therefore, these chlorocarbons were likely to be having a significant effect on the ozone layer around this time. In 1980, the EESC value from these chlorocarbons was 350 ppt which is around 29 % of the 1200 ppt EESC value used in the last Scientific Assessment of Ozone Depletion as the 1980 benchmark for mid-latitude stratosphere from surface measurements (*Montzka et al.*, 2010).

Between 1990 and 2004, the observed declines in EESC values was mainly a result of the decline in the shorter-lived gases CH_3CCl_3 and CH_3Br (*Clerbaux and Cunnold et al.*, 2006). This is also the period of the greatest decrease in EESC from the chlorocarbons. However, between 2005 and 2008, no single chemical class dominated the decline in the total combined abundance of ozone-depleting halogen (Table 3.10) (*Montzka et al.*, 2010).

Table 3.10: Changes in EESC values between 2005 and 2008 based on *Montzka et al.* (2010)

Compounds	Change in EESC 2005 -2008 (ppt)
CFCs	-17
CH_3CCl_3	-20
CH_3Br	-24
CCl_4	-10
Halons	-4
HCFCs	+6
Chlorocarbons#	-2

This study

Table 3.10 shows that the chlorocarbons observed in this study have decreased only slightly between 2005 and 2008 especially compared to the other halogenated compounds. This is a result of the increase in the EESC mixing ratio of CH_2Cl_2 and CH_2ClCH_2Cl during this period. Therefore, these chlorocarbons are likely to have a significant effect on future changes of total EESC. Figure 3.31 shows that CH_3Cl has the largest EESC of the chlorocarbons with 227 ppt in mid-2008. This is in good general agreement with the findings of *Montzka et al.* (2010) who observed that CH_3Cl has the greatest effect on the stratospheric ozone of the chlorocarbons.

As well as equivalent effective stratospheric chlorine, it is important to assess the stratospheric chorine injected as source gases from the chlorocarbons. This was calculated by reducing the surface chlorine mixing ratios by the reduction factors in Table 3.9. The 2008 stratospheric chlorine contributions from the chlorocarbons source gases are shown in Table 3.11.

Table 3.11: Stratospheric chlorine from the chlorocarbons

Compounds	Stratospheric chlorine in 2008 (ppt)
CH_3Cl	517
$CHCl_3$	16
CH_2Cl_2	35
CCl_2CCl_2	3
CH_2ClCH_2Cl	6
C_2H_5Cl	1
$CHClCCl_2$#	0.04
Total VSL chlorocarbons	61
Total chlorocarbons	580

Stratospheric chlorine in 2001 (ppt)

Table 3.11 shows that the VSL chlorocarbons provide 61 ppt of stratospheric chlorine in 2008 from source gases. This includes the 2001 stratospheric chlorine from $CHClCCl_2$, although this

contributed only 0.04 ppt or 0.1 % to the total. This observation agrees with *Montzka et al.* (2010) who estimated that the VSLS chlorine source gases, including unmeasured species (this includes C_2H_5Cl), account for about 55 (38–80) ppt at the tropical cold point tropopause.

However, it is important to note that, the observations in the current study are from polar regions, and not the tropics. This means that the EESC values are likely to be an underestimate for compounds like CH_3Cl that have strong emissions rates in the tropics. It should also be noted that the EESC in the current study might be an underestimate as the calculation does not account for any product gas injection from the VSL chlorocarbons. *Aschmann et al.* (2009) modelled transport of VSL halogenated compounds into the lower stratosphere and estimated that product gas injection could account for an addition 30 % of stratospheric halogen from VSL halogenated compounds. *Hossaini et al.* (2010) and *Sinnhuber and Folkins* (2005), indicated that the ratio of product gas injection to source gas injection is greater for VSL compounds containing more halogen atoms.

3.5 Summary

In this chapter, I have reported observations of the chlorocarbons from northern and southern hemispheric firn air, with the resulting derived atmospheric time series from the mid-20th century up until mid-2008. Table 3.12 summarises the atmospheric time series, growth rates, emissions and EESC for the compounds reported in this study.

I have provided the first detailed northern hemispheric atmospheric time series from 1950 to 2008 for CH_3Cl, CH_2Cl_2, CCl_2CCl_2, CH_2ClCH_2Cl, C_2H_5Cl and $CHClCCl_2$. I have shown that all of these compounds had significant atmospheric mixing ratios in 1950. Since 1950, all of the reported gases have shown significant growth before a steady decline.

Even though the VSl chlorocarbons have small atmospheric mixing ratios, I have shown that they do significantly add to the stratospheric loading of ozone-depleting halogenated compounds. Currently, these compounds contribute 61 ppt of the stratospheric chlorine from source gases, with CH_2Cl_2 and CH_2ClCH_2Cl mixing ratios currently are increasing in the atmosphere.

These results also indicate that it would be desirable to minimise future anthropogenic emissions and that further studies should include observations from global ground-based networks, are needed to improve the understanding of the emission processes, patterns and the global distribution of the chlorocarbons.

Table 3.12: Summary of the chlorocarbons.

Compound	1950 mixing ratio	Mid–2008 mixing ratio (ppt)	2007 Growth rate (ppt yr^{-1})	Maximum annual emission (Gg yr^{-1})	Date of maximum annual emission	2008 Equivalent effective stratospheric chlorine (ppt)	Key Finding
CH_3Cl[#]	518	517	-4.3	3200	1986	227	A significant decline in emissions since 1990
$CHCl_3$[#]	6.5	8.3	0.005	330	1983	16	Mixing ratio currently stable
CH_2Cl_2[#]	2.0	24.1	0.5	550	1985	35	Mixing ratio currently increasing
CCl_2CCl_2[#]	1.8	2.9	-0.05	680	1978	3	Emissions are dominated by northern hemispheric anthropogenic emissions
CH_2ClCH_2Cl[†]	1.5	5.5	0.4	190	1983	6	Mixing ratio currently increasing
C_2H_5Cl[†]	6.9	1.9	0.1	160	1973	1	Emissions strongly reflected its use in leaded petrol
$CHClCCl_2$[†]	0.07	0.2*	-0.002[Θ]	18	1982	0.04[¥]	Similar emissions source as CH_2ClCH_2Cl

'Global'

† Northern Hemisphere

* Mid–2001 mixing ratio (ppt)

Θ 2000 Growth rate (ppt yr^{-1})

¥ 2001 Equivalent effective stratospheric chlorine (ppt)

Chapter 4: Analysis of bromocarbons from firn extracted from both Arctic and Antarctic firn sites

4.1 Introduction

In this study firn air samples collected from the North Greenland Eemian Ice Drilling (NEEM), were measured for a number of brominated compounds by GC- MS. These observations along with measurements from previous firn air measurements from other northern hemispheric firn sites, North Grip (NGRIP) and Devon Island (DI), as well as from southern hemispheric firn sites, Dronning Maud Land (DML) and Dome Concordia (DC), were used to reconstruct the atmospheric time series of these compounds. These histories were derived with the help of a 1-dimensional firn diffusion model and iterative dating techniques. In this chapter these atmospheric time series for the brominated compounds are discussed.

The brominated compounds I measured are all part of the group of chemicals known as the bromocarbons. They include: the short-lived brominated substances (lifetimes of greater than 6 months but less than a few years, e.g. CH_3Br), the very short-lived (VSL) brominated substances (lifetimes of less than 6 months, e.g. $CHBr_3$ and CH_2Br_2) and the fully anthropogenic brominated compounds (e.g. Halons and $CF_3CHBrCl$). These compounds originate from both natural and/or anthropogenic origins and are important for the bromine chemistry of the atmosphere (*Montzka et al.*, 2010). It is generally accepted that reactive bromine compounds, could be playing a significant role in controlling the composition of the global atmosphere. In recent decades, stratospheric ozone depletion has been largely driven by increases in the atmospheric concentrations of a number of anthropogenic halogen compounds. These anthropogenic compounds are now regulated by the Montreal Protocol and a number of them have now show signs of decline in their atmospheric abundances (*González et al.*, 2006).

Bromine is much less abundant in the atmosphere than chlorine (*Montzka et al.*, 2010). Nonetheless, its ability to deplete stratospheric ozone is 45 to 69 times more efficient on a per atom basis (*Sinnhuber et al.*, 2006). This means that reactions involving bromine contribute about half of the seasonal polar ozone loss and about 45 % of the long-term column loss at northern midlatitudes (*Sinnhuber et al.*, 2006). Therefore, release of just a few parts per trillion of additional bromine into the atmosphere can result in a significantly larger loss of stratospheric ozone (*Salawitch et al.*, 2005) particularly under enhanced aerosol loading (*Montzka et al.*, 2010). *Feng et al.* (2007), used an atmospheric chemical transport model to calculate that an additional 5 ppt of bromine from short-lived species can result in mid-latitude column ozone decreases by about 10 Dobson units (DU).

Compared with the stratosphere, the current understanding of the role of bromine in the global troposphere is not as well known. It has been observed for a number of years that

brominated compounds are responsible for sporadic and rapid ozone depletion in the polar boundary layer (e.g. *Barrie et al.*, 1988). In the last few years modelling studies by *von Glasow et al.* (2004) and *Yang et al.* (2005) have argued that bromine compounds, including both the bromocarbons as well as the inorganic salts, can have an important influence on global tropospheric ozone and oxidising capacity.

The principal objective of this study is to provide atmospheric time series of the bromocarbons, this will include the first full reconstruction atmospheric histories of the VLS bromocarbons; CH_2Br_2, CH_2BrCH_2Br, C_2H_5Br, CH_2BrCl, $CHBr_2Cl$ and $CHBrCl_2$ and the short lived fully anthropogenic bromocarbon; $CF_3CHBrCl$. These reconstructions of time series are then compared with ambient atmospheric observations or measurements from air archives.

This study provides insights into the growth rates of these compounds, the 1930 mixing ratios of the compounds with natural emissions, and the date of first significant atmospheric abundance of the compounds that are fully anthropogenic in origin. Also emissions estimated from the growth rates will be obtained, as well as assessing the effect these ozone depleting substances have on the stratospheric ozone budget, by estimating their equivalent effective stratospheric chlorine.

This chapter consists of detailed discussion of each individual bromocarbon species. Each subsection has its own background information on the compound, results and discussion on atmospheric time series from the firn data and estimating emissions from the reconstructed time series. At the end of the chapter, the equivalent effective stratospheric chlorine of the individual compounds are calculated.

4.2 Methyl Bromide

Methyl bromide (bromomethane, CH_3Br) is an organic halogenated compound that is a colourless and non-flammable gas with chemical properties that are quite similar to those of methyl chloride. CH_3Br is also a recognized ozone-depleting chemical as it is a major source of stratospheric bromide (*Montzka et al.*, 2010) and is currently the most abundant brominated gas regulated by the Montreal Protocol (*Montzka et al.*, 2010).

4.2.1 Background information on CH_3Br

CH_3Br differs from most of the other "long-lived" ozone depleting gases because it has significant natural and anthropogenic sources. The main anthropogenic sources of CH_3Br include fumigation of soils for planting and agricultural products for import and export, biomass burning from human activities and automobile emissions as a result of burning leaded gasoline (*Montzka et al.*, 2010). It is believed that the oceans are the largest natural source for atmospheric CH_3Br (*Montzka et al.*, 2010), but further studies are needed to confirm this.

Many studies have observed net fluxes of CH_3Br from isolated, terrestrial ecosystems. For example *Dimmer et al.* (2001) measured net fluxes of CH_3Br from Irish peatlands, *Varner et al.* (1999) measured net fluxes from New Hampshire wetlands and *Rhew et al.* (2001) and *Rhew et al.* (2000) studied the net fluxes of CH_3Br from salt marshes and shrublands. Chemical information for CH_3Br is given Table 4.1.

Table 4.1: Chemical information for CH_3Br based on *Montzka et al.* (2010).

Compound	Lifetime (Days)	ODP (Relative to CFC-11)	2008 mixing ratio (ppt)	2007-2008 Growth rate (ppt yr^{-1})
CH_3Br	292	0.66	7.4	-0.3

4.2.2 Results and discussion of CH_3Br

Figure 4.1 shows the measured concentration of CH_3Br with depth at the NEEM northern hemispheric firn sites.

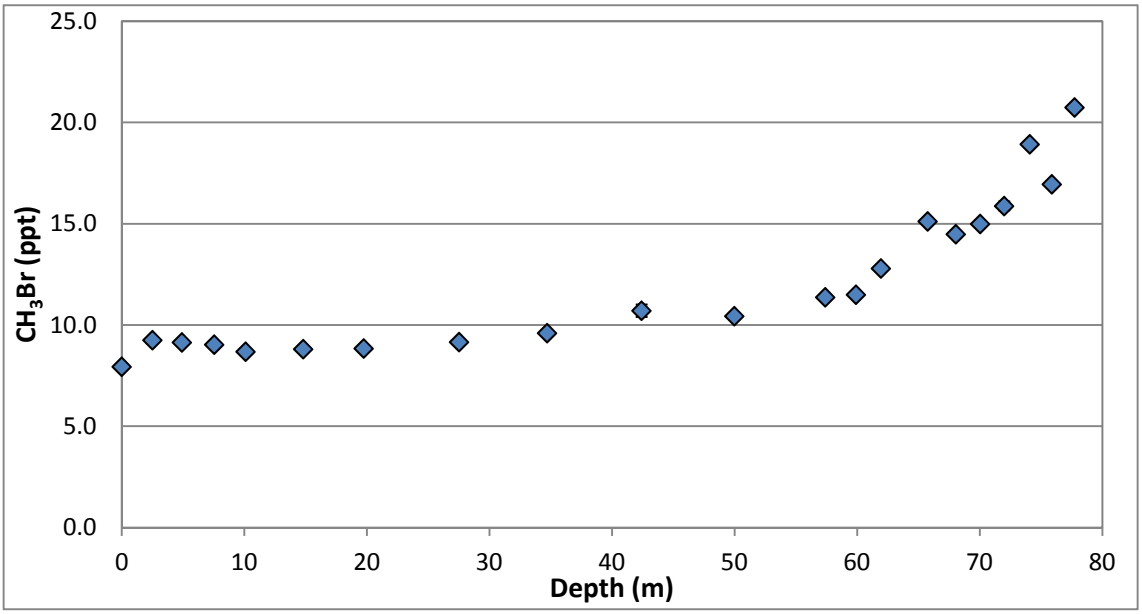

Figure 4.1: measured concentration of CH_3Br with depth at the NEEM firn site (blue points). The error bars represent the 1 σ of the measurements.

The firn air profile of CH_3Br shows that concentration increase by 11.5 ppt between the surface and the bottom of the firn profile, representing a 125 % increase. This does not agree the atmospheric time series observed by *Trudinger et al.* (2004) with an increase in mixing ratios from about 1950 to 1980, then a period of roughly stable concentration to 1990, followed by an increase during part of the 1990s. Since the 1990s atmospheric measurements show a decline in mixing ratios until 2008 (*Montzka et al.*, 2010, *Simmonds et al.*, 2004 and *Yokouchi et al.*, 2002). Therefore this firn profile is likely a result of the production of CH_3Br within the firn column and not a representation of the atmospheric time series of the compound. Production of CH_3Br has been observed in Greenland snowpack by *Swanson et al.* (2002), who suggest that the photochemistry associated with the surface snowpack environment plays an important role in the oxidative capacity of the local atmospheric boundary layer, and influences the post-depositional chemistry of CH_3Br. This means that I was not able to derive an atmospheric time series for CH_3Br in this study.

4.3 Very Short-Lived (VSL) brominated substances

The VSL bromine substances are defined as brominated trace gases whose local lifetimes are comparable to, or shorter than, the tropospheric transport timescales and that have non-uniform tropospheric abundances (*Montzka et al.*, 2010). Generally, VSL bromine substances are considered to be those compounds that have atmospheric lifetimes of less than 6 months. In 2008, total bromine in the stratosphere was 22.5 ppt (*Montzka et al.*, 2010), this stratospheric bromine budget cannot be explained simply by the breakdown of the short and long lived bromine compounds of methyl bromide and the halons. Therefore, the very short-lived bromine compounds are needed to balance the bromine budget in the lower stratosphere (*Montzka et al.*, 2010 *Dorf et al.*, 2006 and *Pfeilsticker et al.*, 2000). The amount of bromine from a VSL source substance that reaches the stratosphere depends on the location of the emissions as well as atmospheric removal and transport processes (*Montzka et al.*, 2010). Therefore, there are substantial uncertainties in quantifying the full impact of VSL bromine-containing compounds on stratospheric ozone.

In this section I will report the atmospheric time series of the mixing ratios of VSL bromine substances: CH_2Br_2, CH_2BrCH_2Br, C_2H_5Br, CH_2BrCl, $CHBr_2Cl$, $CHBrCl_2$ and $CHBr_3$. Firn air samples collected in Greenland were used to reconstruct northern hemispheric time series. Firn air samples collected in Antarctica, as well as observations from archived samples taken at the Cape Grim baseline air pollution station were used to reconstruct southern hemispheric time series. These time series will then be used to calculate emission rates for the VSL bromine substances.

4.3.1 Background information on CH_2Br_2

To date dibromomethane (CH_2Br_2) has only been showed to be emitted into the atmosphere from natural sources (*Montzka et al.*, 2010 *Worton et al.*, 2006 and *Yokouchi et al.*, 2005). These include ice algae (*Sturges et al.*, 1993b), and macroalgae/phytoplankton (*Tokarczyk and Moore*, 1994, *Moore and Tokarczyk*, 1993, *Sturges et al.*, 1993b and *Manley et al.*, 1992).

All of these sources are emitted predominantly from the oceans, with a combination of both open ocean sources (*Tokarczyk and Moore*, 1994) and coastal waters (*Clerbaux and Cunnold et al.*, 2006). Recent studies have emphasized the potential importance of coastal water emissions (*Liang et al.*, 2010, *Butler et al.*, 2007 and *Clerbaux and Cunnold et al.*, 2006). Conversely, *Palmer and Reason* (2009) considered tropical coastal sources to be unimportant based on a supposition that seaweeds are largely absent from the tropics. However, relatively high mixing ratios of CH_2Br_2 have been measured by *Yokouchi et al.* (2005), being emitted from

algal-colonized tropical shores. It has not yet been unequivocally proven that macroalgae account for all coastal emissions, as *O'Brien et al.* (2009) detected elevated mixing ratios of CH_2Br_2 without evidence of significant macroalgae in coastal waters off the tropical Atlantic. In addition, *Quack et al.* (2007) have suggested that CH_2Br_2 might originate naturally as part of biologically mediated reductive hydrogenolysis of $CHBr_3$.

Oceanic emissions of CH_2Br_2 are potentially influenced by changes in seawater temperature, pH, wind speed, mixed layer depth, light penetration, nutrient supply, the depth of biotic production and the depth of degradation of trace gases (*Montzka et al.*, 2010, *Schmittner et al.*, 2008 and *Kloster et al.*, 2007). *Quack et al.* (2007) showed that CH_2Br_2 concentrations, around the Mauritanian upwelling off West Africa are enhanced in colder, nitrogen-enriched and deeper waters.

Anthropogenic sources of CH_2Br_2 cannot be ruled out, there is evidence from a few published data sets on interhemispheric ratios (*Atlas et al.*, 1993 and *Penkett et al.*, 1985) and measurements during arctic haze pollution episodes (*Rasmussen and Khalil*, 1984). However *Worton et al.* (2006) did not find any significant 20^{th} century trends in CH_2Br_2 mixing ratios, which leads to the conclusion that it is largely emitted from natural sources. The main destruction of atmospheric CH_2Br_2 is via reactions with the OH radical, but also through photolysis (*Montzka et al.*, 2010), the resultant local lifetime of CH_2Br_2 is 123 days (*Montzka et al.*, 2010).

Estimates of global oceanic emissions of CH_2Br_2 have been calculated in a number of different studies (e.g. *Liang et al.*, 2010 *Butler et al.*, 2007 and *Warwick et al.*, 2006) and give a range of 270 – 57 Gg Br yr^{-1} (Table 4.2).

Table 4.2: Fluxes of bromine from CH_2Br_2 in Gg Br yr^{-1}.

Reference	Global	Open Ocean	Coastal
Butler et al. (2007)	280	50	230
Liang et al. (2010)	57	34	23
Warwick et al. (2006)	100		

The data in Table 4.2 emphasizes the potential importance of coastal oceans to the global emissions of CH_2Br_2. However these values should be treated with caution as a result of large variation in emissions from coastal zones (*Butler et al.*, 2007).

Some studies suggest significant regional "hotspots" in the tropics and subtropics (*Palmer and Reason*, 2009 and *Kerkweg et al.*, 2008), especially in the west Pacific Ocean near Indonesia. This is consistent with Butler et al. (2007), who estimated that 40% of CH_2Br_2 emissions

originated from the Pacific (24% from the tropical Pacific, and 40% in total from the tropics), compared with 20% from the Atlantic.

Atmospheric mixing ratios of CH_2Br_2 have been observed by a number of different studies (*Laube et al.*, 2008 *Clerbaux and Cunnold et al.*, 2006 and *Schauffler et al.*, 1999a), which are summarised in Table 4.3.

Table 4.3: Observations of CH_2Br_2 from the marine boundary layer (MBL) to the tropical tropopause layer (TTL) based on *Montzka et al.* (2010).

Region	Marine Boundary Layer	Upper Troposphere	Lower TTL	LZRH	Upper TTL	Tropical Tropopause
Ref.	*Clerbaux and Cunnold et al.* (2006)	*Schauffler et al.* (1999)	*Laube et al.* (2008)	*Clerbaux and Cunnold et al.* (2006)	*Clerbaux and Cunnold et al.* (2006)	*Laube et al.* (2008)
Height range (km)		10-12	12-14	14.5-15.5	15.5-16.5	16.5-17
CH_2Br_2 (ppt)	0.7 – 1.5	0.63 – 1.21	0.77 – 1.15	0.59 – 0.99	0.43 – 0.83	0.3 – 0.86

Observations of CH_2Br_2 range from 0.7 – 1.5 ppt in the marine boundary layer (*Clerbaux and Cunnold et al.*, 2006) to 0.3 – 0.86 ppt in the tropical tropopause (*Laube et al.*, 2008). Inter hemispheric observations have been made by *Carpenter et al.* (2003) from Mace Head, Ireland (1.76 ppt in September, 1998) and Cape Grim, Tasmania (0.33 ppt in January-February, 1999). These data indicate that southern hemisphere mixing ratios are 20 % lower than northern hemisphere mixing ratios. However, it should be noted that Mace Head is strongly influenced by emissions from local macroalgae (*Carpenter et al.*, 2003). *Atlas and Ridley* (1996), observed CH_2Br_2 at Mauna Loa, Hawaii (20°N, 156°W) in 1992 with an average mixing ratio of 0.79 ppt.

A 20th century time series for CH_2Br_2 has been derived by *Worton et al.* (2006) from Arctic firn air taken from the NGRIP drill site and by *Sturges et al.* (2001) from Antarctic firn air taken from the DML and DC sites. These studies show no significant change in atmospheric mixing ratios during this period. *Worton et al.* (2006) observed a constant northern hemispheric atmospheric mixing ratio of 1.00 ppt with a seasonal cycle with an amplitude of 0.15 ppt. In contrast *Sturges et al.* (2001) observed a constant northern hemispheric atmospheric mixing ratio of 0.83 ppt with a seasonal cycle of 1.2 ppt.

4.3.2 Results and discussion of CH_2Br_2

In the current study, I will report firn air measurement of CH_2Br_2 from a number of northern and southern hemispheric firn air records, as well as southern hemispheric observations from the Cape Grim baseline air pollution station. These measurements have then been used to derive the atmospheric time series of CH_2Br_2 mixing ratios. The time series of atmospheric CH_2Br_2 mixing ratios were derived using the direct firn modelling method developed at Laboratoire de Glaciologie et Géophysique de l'Environnement (LGGE) Grenoble. These new atmospheric time series are then compared with previous atmospheric time series estimated by *Worton et al.* (2006) and *Sturges et al.* (2001). The time series obtained and the output from the inverse model for the northern and southern hemisphere site are shown alongside the measured concentration of CH_2Br_2 with depth at northern hemispheric firn sites (NEEM and NGRIP) and southern hemispheric (DC and DML) firn sites in Figures 4.2 and 4.3, respectively.

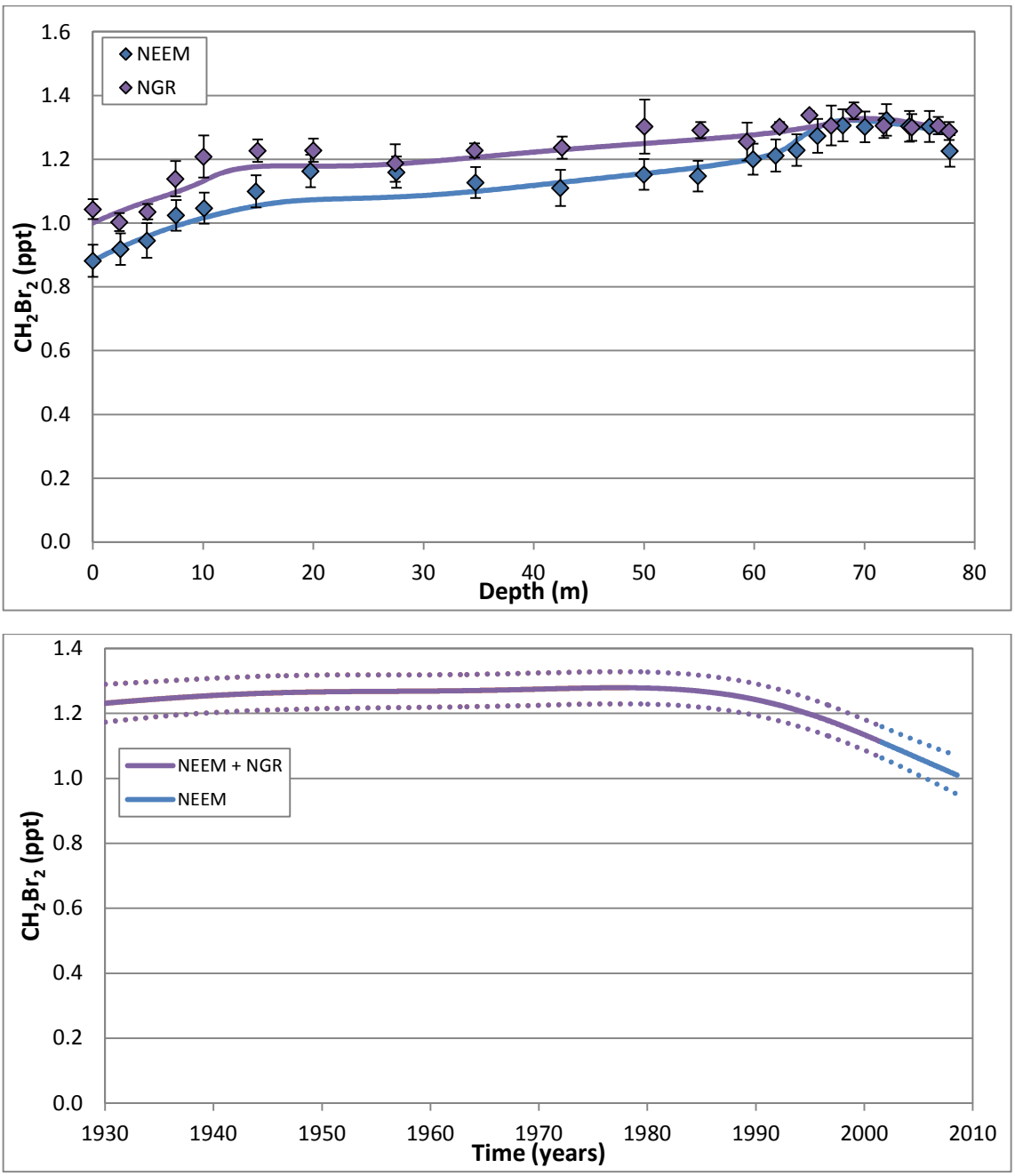

Figure 4.2: Top panel, depth profiles of northern hemispheric CH_2Br_2 concentration with depth at the; NEEM firn site (blue points) and the NGRIP firn site (purple points), compared with model simulations based on the atmospheric time series indicated in the bottom panel with a seasonal cycle of 12 % added to the time series. The error bars represent the 1 σ of the measurements (see methods chapter for more details). Bottom panel, Atmospheric time series derived by a multi-site inversion modelling of the NEEM and NGRIP firn air measurements (solid line) using the LGGE method. As the firn sites have different drill dates the LGGE method derives an atmospheric time series using all of the firn sites up to the drill date of a firn site, after this the atmospheric time series is derived using the remaining sites. The time series derived by NEEM and NGRIP firn air – Purple line and NEEM only firn air – blue line. The dashed lines represent the uncertainties envelope of the time series (as described Figure 2.10).

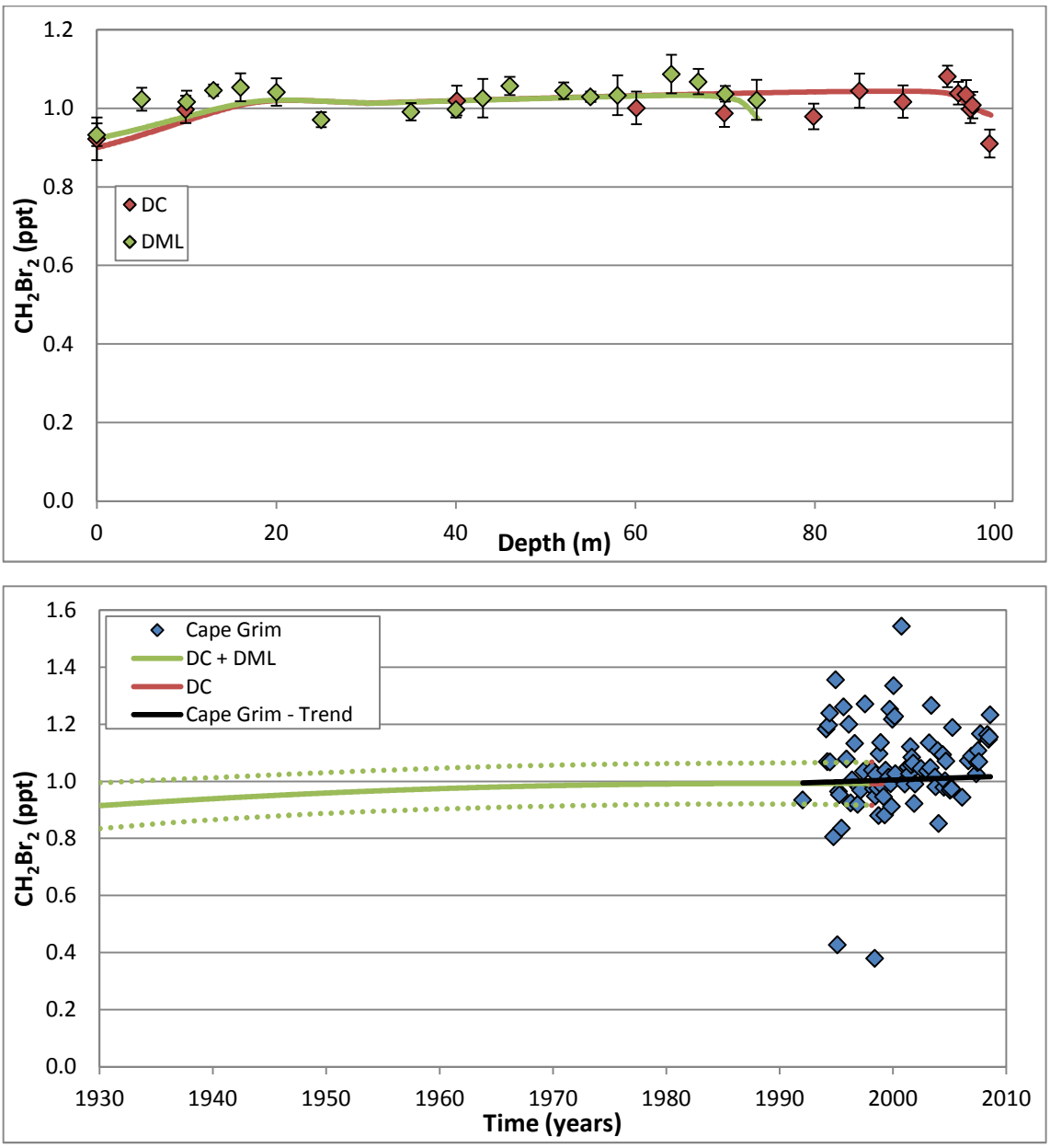

Figure 4.3: Top panel, depth profiles of southern hemispheric CH_2Br_2 concentration with depth at the DC firn site (red points) and the DML firn site (green points), compared with model simulations based on the atmospheric time series indicated in the bottom panel with a seasonal cycle of 12 % added to the time series. The error bars represent the 1 σ of the measurements. Bottom panel, Atmospheric time series derived by a multi-site inversion modelling of the DC and DML firn air measurements (solid line) using the LGGE method. The time series derived by the DC and DML (green line) and DC only (red line). The dashed lines represent the uncertainties envelope of the time series (as described Figure 2.10). Also the mixing ratios of CH_2Br_2 as a function of time as measured in air samples collected in the southern hemisphere (blue points, from Cape Grim). The black line is a polynomial expression fitted through the Cape Grim time series in order to derive growth rates and emissions, based on the method used by *Laube et al.* (2012) and *Sturges et al.* (2012).

Ambient air measurements (depth, 0 m) were collected at the NEEM site on three different days (16, 17, 27 July 2008) during the firn air drilling. These ambient air measurements have an average mixing ratio of 0.882 ± 0.050 ppt and are the most recent northern hemispheric measurements of CH_2Br_2 in this study. The ambient air measurements were collected at the DC site on the 28 December 1998 during firn air drilling. These ambient air measurements have an average mixing ratio of 0.992 ± 0.054 ppt and represent the most recent southern hemispheric measurement from the firn sites in this study.

CH_2Br_2 has a significant atmospheric sink as a result of its reaction with the hydroxyl radical (OH) (*Montzka et al.*, 2010). The local lifetime of CH_2Br_2 with respect to OH is 123 days, (*Montzka et al.*, 2010), which results in a total local lifetime of 123 days (*Montzka et al.*, 2010). This enables a seasonal cycle in the CH_2Br_2 atmospheric mixing ratio. This seasonal cycle can be seen in the variations in CH_2Br_2 concentration in the shallowest part of the firn columns, which would likely have reflected the seasonality in the OH atmospheric mixing ratios described in *Kaspers et al.* (2004) and *Sturges et al.* (2001). This is supported by the Cape Grim observations from the current study (Figure 4.4).

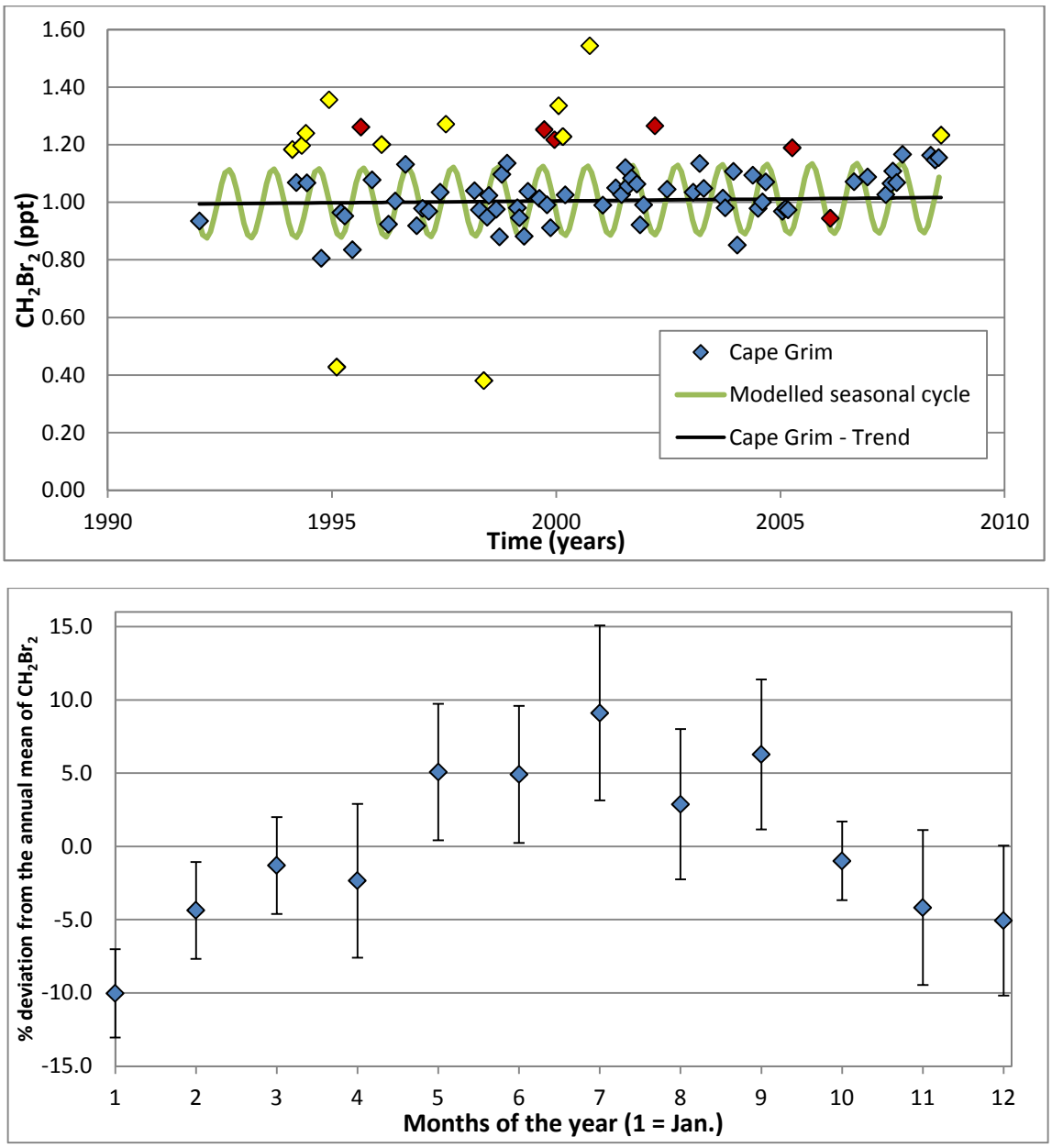

Figure 4.4: Top panel, Atmospheric mixing ratios of CH_2Br_2 as a function of time from observations of archived samples taken at Cape Grim (blue points). A polynomial expression fitted through the Cape Grim time series in order to detrend the data (black line). A modelled seasonal cycle based on the seasonal cycle observed in the bottom panel (green line). Data points more than 3 standard deviations away from the mean were taken as outliers and removed from the seasonal cycle calculation (yellow points). Six unreliable samples were also removed from the seasonal cycle calculation (red points) (see Figure 3.4 for more details). Bottom panel, percentage deviation from the annual mean CH_2Br_2 mixing ratio based on the detrended Cape Grim observations (top panel), taken as the mean of the observations made in a particular calendar month (between 3 - 8 data points). The error bars represent the 1 σ of the measurements.

The seasonal patterns of the Cape Grim observations were determined by using a polynomial expression fitted through the data to subtract cycles of periods longer than 12 months, which includes long-term time series. A polynomial expression was used an not a 12 month moving average filter as used by *Khalil and Rasmussen* (1999) because the Cape Grim data was not

measured for every month so that the moving averaged did not remove cycles of periods shorter than 12 months. The resulting time series after the subtraction by long term trends was averaged for each of the 12 months over the years when measurements were taken. However data points more than 3 standard deviations away from the mean are taken as outliers and removed from the seasonal cycle calculation. The result is 12 indices which represent an estimate of the CH_2Br_2 seasonal cycle (Figure 4.4).

Figure 4.4 shows that there is a seasonal cycle in the atmospheric mixing ratio of CH_2Br_2. The amplitude of the seasonal cycle is taken as the difference between the average of the winter months (June, July and August) and the average of the summer months (Decembers, January and February). Therefore the detrended Cape Grim observation indicates a seasonal cycle with an amplitude of 12 % of the annual mean mixing ratio in the southern hemisphere. This would represent a southern hemispheric seasonal cycle with an amplitude of 0.12 ppt in 2008. *Worton et al.* (2006) observed a 12 % seasonal cycle in the northern hemispheric NGRIP firn air, which agrees with the findings in this study. However long-term observations at Summit Greenland observe a seasonal cycle with an amplitude of 41 % (personal communication with Steve Montzka). Although using this seasonal cycle in the firn modeling (Figure 4.2) I was not able to reproduce the variation in the upper part of the firn profile.

Figures 4.2 and 4.3 indicates that the 1930 atmospheric mixing ratio of CH_2Br_2 was 1.2 ppt in the northern hemisphere and 0.9 ppt in the southern hemisphere. After the 1930s the time series show a period of stable atmospheric mixing ratios in both hemispheres. This stable atmospheric mixing ratio continued in the southern hemisphere up to 1999 when the Dome C firn air was abstracted.

Measurements of CH_2Br_2 mixing ratios have been made from 1992 onwards at the Cape Grim baseline air pollution station. Figure 4.2 shows that these observations are in general agreement with the firn derived southern hemispheric time series, although there are a number of outlying points. Growth rates were inferred for the Cape Grim observations by fitting a polynomial expression to the data set (the black line in Figure 4.3) similar to the method presented in *Laube et al.* (2012) and *Sturges et al.* (2012). These results are in agreement with the findings of *Sturges et al.* (2001) who observed no significant trends in the southern hemispheric atmospheric mixing ratios as well as *Worton et al.* (2006) who observed no significant trends in the northern hemisphere.

However in the northern hemisphere (Figure 4.2) mixing ratios remained approximately constant for the 1930s till the early 1990s. Since 1990 atmospheric mixing ratios have been

shown to decrease from 1.3 ppt in 1990 to 1.0 ppt in mid-2008, which is 79 % of the peak mixing ratio. The average change during this period was -0.01 ppt yr^{-1}. However, the rate of this decrease has been increasing in recent years from -0.007 ppt yr^{-1} in 2000 to -0.015 ppt yr^{-1} in 2007. The firn air used for current analyses was collected in July 2008. Therefore, an average growth rate cannot be provided for 2008, but mixing ratios continued to show a decrease. It should also be noted that these growth rates and peak timing represent only the best estimates and contain considerable uncertainties within the envelopes shown in Figures 4.2 and 3. It is currently unclear if this decline is due to a decrease in atmospheric mixing ratios in the northern hemisphere or is some process with the firn that is resulting in a increase in concentration in the upper part of the firn column. More studies are needed to validate this finding.

It is also unclear what might be causing the observed decline in northern hemispheric CH_2Br_2 mixing ratio since 1990. In 2008, the northern hemispheric mixing ratio (1.0 ppt, Figure 4.2) decreased to the same abundant as the southern hemispheric mixing ratio (1.0 ppt, Figure 4.5), which may suggest that a northern hemispheric anthropogenic source has declined in recent years. However, it may also imply a decline in the natural sources of CH_2Br_2 in the northern hemisphere.

The 'global' averaged atmospheric time series of CH_2Br_2 was derived between 1930 and June 2008 (the drill date of the NEEM site) by averaging the northern and southern time series Figure 4.5. The southern hemispheric time series was derived using both the firn derived time series and the Cape Grim time series. These two time series were averaged for the years that are covered by both.

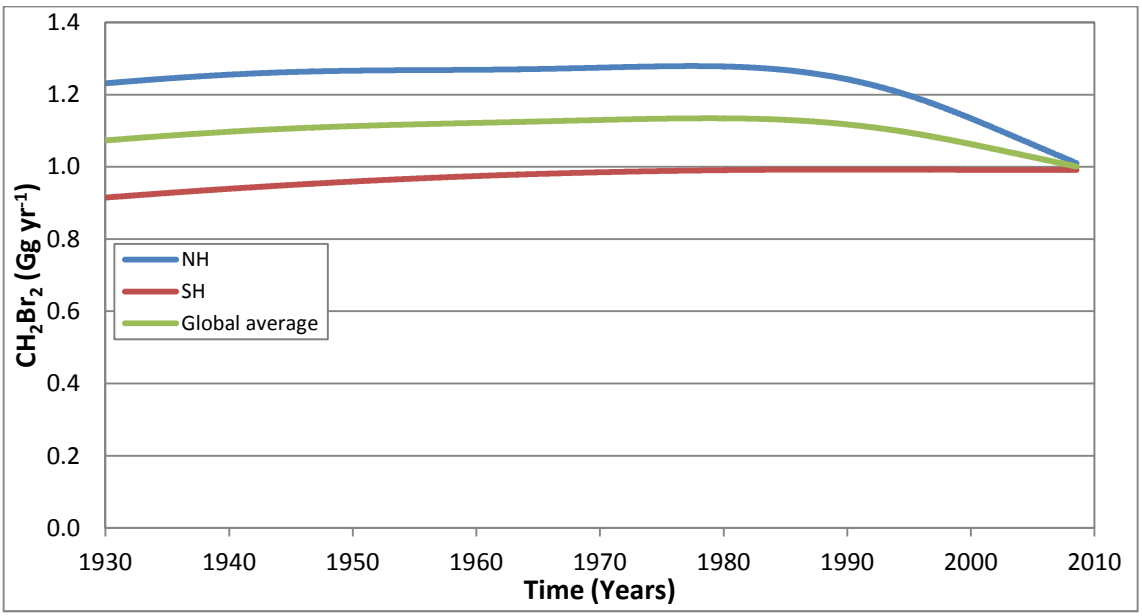

Figure 4.5: Northern hemispheric atmospheric time series of CH_2Br_2 derived from Arctic firn air (blue line). Southern hemispheric atmospheric time series of CH_2Br_2 derived from Antarctic firn and Cape Grim observation (red line). 'Global' atmospheric time series of CH_2Br_2 shown as the average between the northern and southern hemispheric time series (green line).

Figure 4.5 indicates that the global mixing ratio of CH_2Br_2 remain stable at 1.1 ppt between 1930 and 1990, before declining to 1.0 ppt in 2008. These 'global' mixing ratios are in general agreement with those observed by *Clerbaux and Cunnold et al.* (2006) of between 0.7 – 1.5 in the marine boundary layer.

4.3.3 Background information on CH_2BrCH_2Br

This section will report the first atmospheric time series of the atmospheric mixing ratios of 1,2-dibromoethane (CH_2BrCH_2Br, Ethylene Dibromide (EDB) and trade names Bromofume / Dowfume). CH_2BrCH_2Br has mainly anthropogenic sources, but it does have a few natural sources. Its main use is as an additive in leaded petrol where it acts as a "scavenger" that converts lead oxides in cars to lead halides (*Fishbein*, 1980). This additive has been used since 1925 (*Randi*, 1952), in a fuel known as "aviation fluid". In the 1940s, CH_2ClCH_2Cl was used to replace around 50 % of CH_2BrCH_2Br and this new mixture was termed "motor fluid" (*Otto and Montreuil*, 1976). However, "aviation fluid" continued to be used as an automobile fuel in some countries (e.g. the Soviet Union) and only as aviation gasoline in others. During this period the U.S. consumption of aviation gasoline was only about 0.25 % of its consumption of automobile petrol (*Thomas et al.*, 1997). In 1978, 90 % of the CH_2BrCH_2Br production went into the additives used in leaded petrol (*Santodonato et al.*, 1985). The U.S. Environmental Protection Agency (EPA) implemented legislation in 1973 to reduce the use of leaded petrol (*Santodonato et al.*, 1985 and *Fishbein*, 1980), and as a result, since the 1970's, CH_2BrCH_2Br use

as a fuel additive declined rapidly from 121 ktonnes in 1971 to 24 ktonnes in 1991 in the USA (*Penkett et al.*, 1995).

In the 1970s and early 1980s, the second largest application of CH_2BrCH_2Br was as a soil fumigant to protect against insects, pests, and nematodes in citrus, vegetable, and grain crops and as a fumigant for turf, particularly on golf courses (*Phillips*, 2006). However, in 1984, EPA banned the use of it as a soil and grain fumigant, thus eliminating this market for manufacturers in the US (*Santodonato et al.*, 1985). Currently, other minor applications include treatment of felled logs for bark beetles, termite control, control of wax moths in beehives, spot treatment of milling machinery, Japanese beetle control in ornamental plants, and as a chemical intermediate for dyes, resins, waxes, and gums (*Phillips*, 2006). Small amounts of CH_2BrCH_2Br have been used in the manufacture of vinyl bromide, which is used as a flame retardant (*Phillips*, 2006). It also has a source from the release from industrial processing facilities (*Roper. W*, 1992). Natural sources of CH_2BrCH_2Br induce production by a large number of macroalgae such as kelp (*Baker et al.*, 2001 and *Laturnus et al.*, 1996). The main destruction of atmospheric CH_2BrCH_2Br is via reactions with the OH radical (*Montzka et al.*, 2010), and the resultant local lifetime of CH_2BrCH_2Br is 70 days (*Montzka et al.*, 2010).

CH_2BrCH_2Br has previously been detected in the atmosphere by *Pratt et al.* (2000), *Brodzinsky et al.* (1997), *Khalil and Rasmussen* (1985) and *Berg et al.* (1984). During 1981, observations from 676 sites in US, recorded a mean mixing ratio of 26 ppt with a range of 0 – 130 ppt (*Brodzinsky et al.*, 1997). Whereas observations from urban areas in the 1990s indicated a mixing ratio of around 5 ppt (*Pratt et al.*, 2000). At high latitudes, mixing ratios have been measured at 1 ppt at the South Pole (*Khalil and Rasmussen*, 1985), whilst observations from 8 sites in the Arctic during March and April of 1983 measured an average mixing ratio of 11 ± 10 ppt (*Berg et al.*, 1984). A stratospheric mixing ratio for CH_2BrCH_2Br was determined as being around 32 ppt in March 1983 above Baffin Bay near Thule, Greenland (70 °N) (*Berg et al.*, 1984). In the tropics *Laube et al.* (2008) have suggested unidentified peaks in their chromatogram from air sampled at 15.2 km that point towards the presence of CH_2BrCH_2Br.

Currently there is not a fully publicly available report on the worldwide production, sales or emission of CH_2BrCH_2Br, although data is available for the United States. In the 1970s, production of CH_2BrCH_2Br in the United States averaged 127 Gg yr^{-1} (*Phillips*, 2006). The production volume in 1974 was 151 Gg yr^{-1}, and in 1979 was 130 Gg yr^{-1} (*Phillips*, 2006). After the increase in government regulations and restrictions in the 1970s, the production of

CH_2BrCH_2Br, steadily decreased. By 1982, U.S. production of CH_2BrCH_2Br had fallen to 77 Gg yr^{-1} (*Phillips*, 2006), following which data has not been available.

The annual world use of bromine in gasoline has been estimate by *Thomas et al.* (1997), based on world use of lead in gasoline and on gasoline scavenger formulations. Bromine in gasoline peaked in the early 1970s at about 170 ± 20 Gg, before declining to 100 ± 11 in 1980, 40 ± 5 Gg in 1990 and 23 ± 2.5 Gg in 1995 (*Thomas et al.*, 1997). Southern hemisphere use was relatively constant at 9 ± 1 Gg yr^{-1} between 1970 - 1985, and dropped to 6.6 ± 0.7 Gg yr^{-1} by 1990 and 4.3 Gg yr^{-1} by 1995 (*Thomas et al.*, 1997).

4.3.4 Results and discussion of CH_2BrCH_2Br

In this study, I report firn air measurement of CH_2BrCH_2Br from a number of northern and southern hemispheric firn air records. These measurements have then been used to derive the atmospheric time series of CH_2BrCH_2Br mixing ratios. The time series of atmospheric CH_2BrCH_2Br mixing ratios were derived using the LGGE method, which is described in more detail in the methods chapter. The time series obtained and the output from the inverse model for the northern and southern hemisphere sites alongside the measured concentration of CH_2BrCH_2Br with depth at northern hemispheric firn sites (NEEM, NGRIP and DI) and Southern Hemispheric (DML) firn sites are shown in Figures 4.6 and 4.7, respectively.

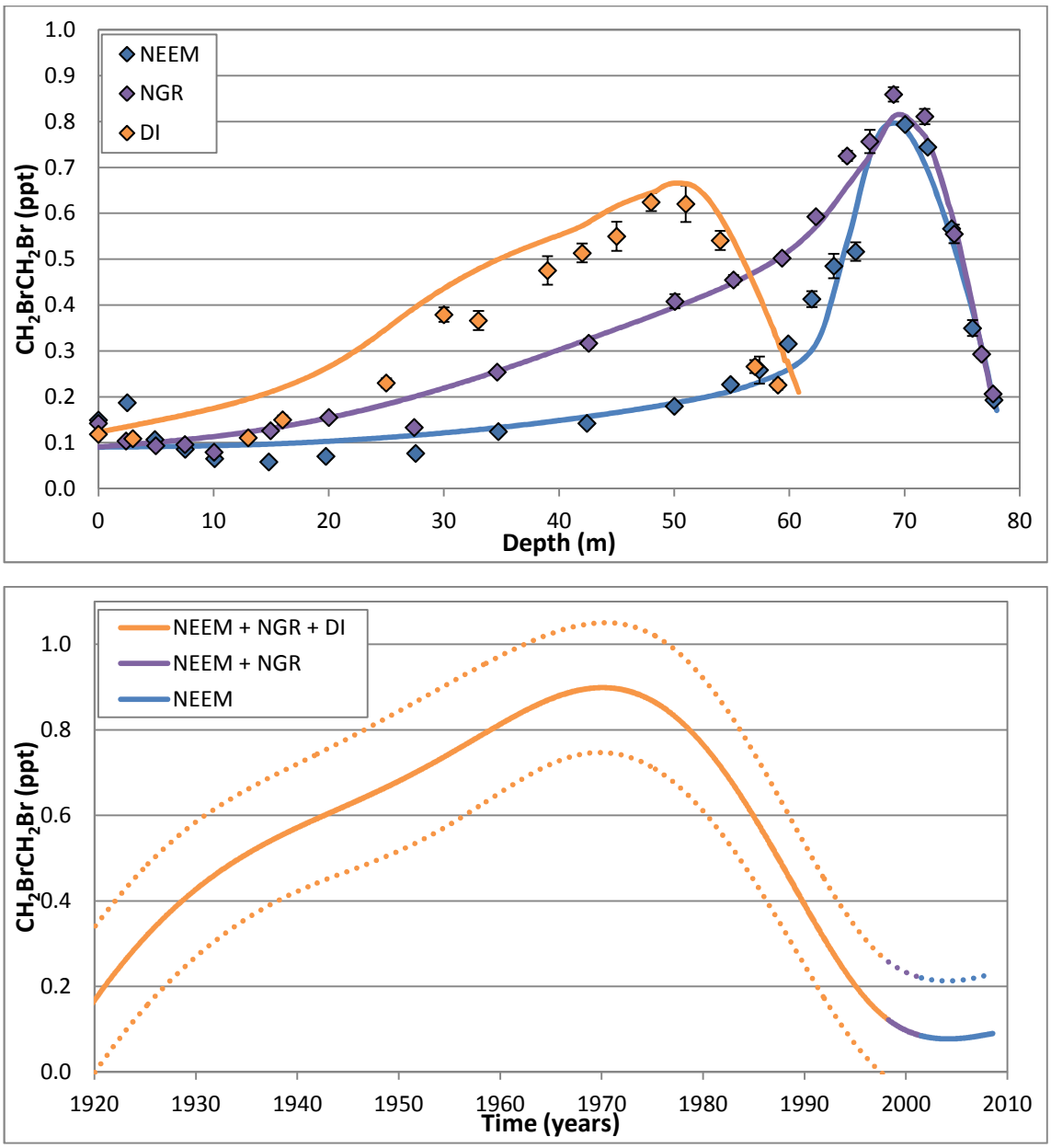

Figure 4.6: Top panel, depth profiles of northern hemispheric CH_2BrCH_2Br concentration with depth at the NEEM firn site (blue points), NGRIP firn site (purple points) and the DI firn site (yellow points), compared with model simulations based on the atmospheric time series indicated in the bottom panel. The error bars represent the 1 σ of the measurements. Bottom panel, Atmospheric time series derived by a multi site inversion modelling of the NEEM, NGRIP and DI firn air measurements (solid line) using the LGGE method. As the firn sites have different drill dates the LGGE method derived an atmospheric time series using all of the firn sites up to the drill date. After this the atmospheric time series is derived using the remaining sites. The time series derived by the NEEM, NGRIP and DI (yellow line), NEEM and NGRIP (purple line) and NEEM only (blue line). The dashed lines represent the uncertainties envelope of the time series (as described Figure 2.10).

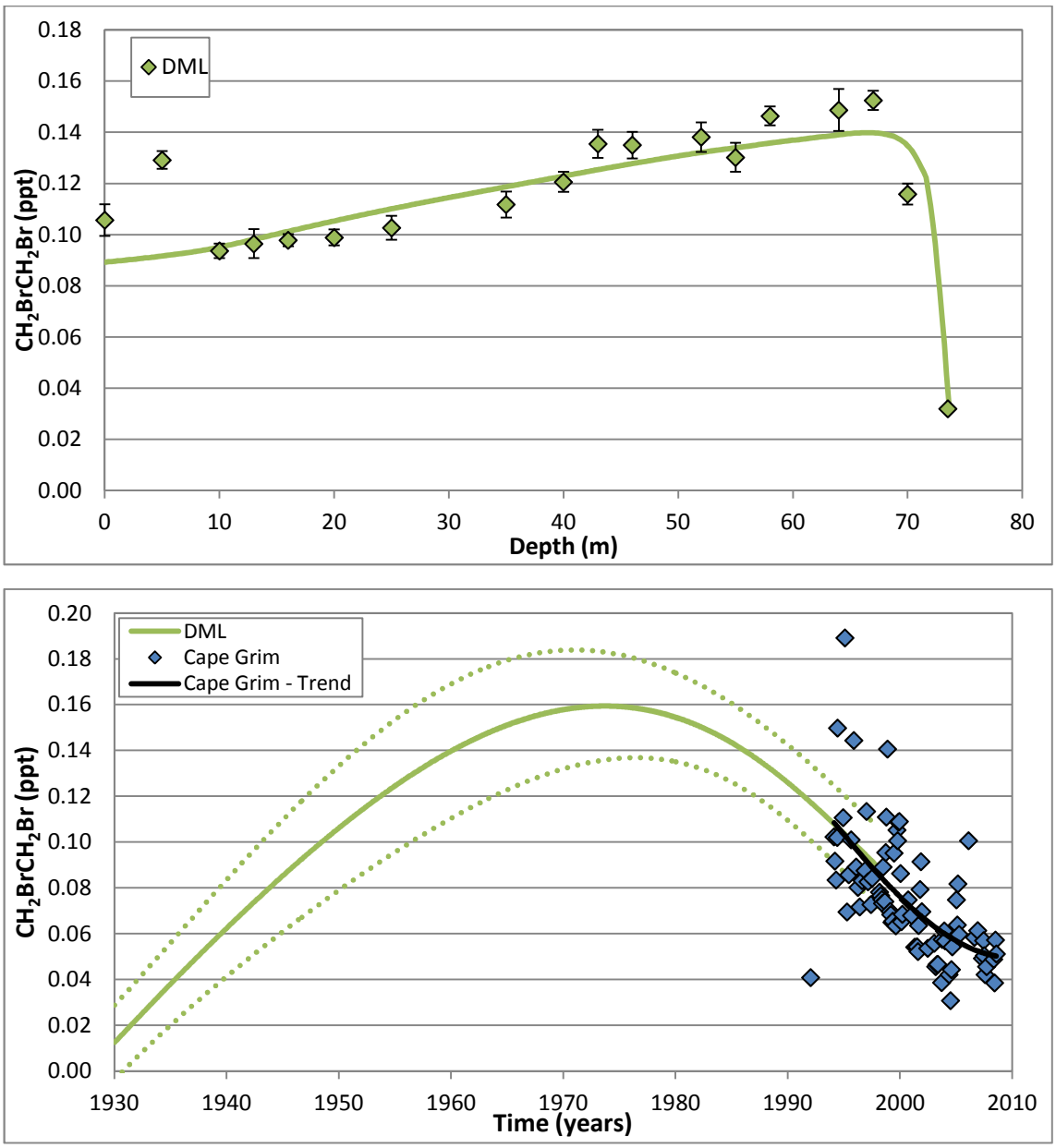

Figure 4.7: Top panel, depth profile of southern hemispheric CH_2BrCH_2Br concentration with depth at the DML firn site (green points), compared with model simulations based on the atmospheric time series indicated in the bottom panel. The error bars represent the 1 σ of the measurements. Bottom panel, atmospheric time series derived by a single site inversion modelling of the DML firn air measurements (solid line) using the LGGE method. The time series is derived by the DML (green line). The dashed lines represent the uncertainties envelope of the time series (as described Figure 2.10). The mixing ratios of CH_2BrCH_2Br as a function of time measured in air samples collected in the southern hemisphere (blue points, from Cape Grim). The black line is a polynomial expression fitted through the Cape Grim time series in order to derive growth rates and emissions.

The ambient air measurements (depth, 0 m) were collected at the NEEM during July 2008. These ambient air measurements have an average mixing ratio of 0.149 ± 0.007 ppt and are the most recent northern hemispheric measurements of CH_2BrCH_2Br in this study. The ambient air measurements were collected at the DC site on the 28 December 1998 during the firn air drilling. These ambient air measurements have an average mixing ratio of 0.117 ± 0.007 ppt and represents the most recent southern hemispheric measurement from the firn sites in this study.

CH_2BrCH_2Br has a significant atmospheric sink as a result of its reaction with the hydroxyl radical (OH) (*Montzka et al.*, 2010). The local lifetime of CH_2BrCH_2Br is 70 days (*Montzka et al.*, 2010). This should be short enough for there to be a seasonal cycle in CH_2BrCH_2Br atmospheric mixing ratio compared with other trace gases with similar lifetimes (i.e. CH_2Br_2). However there are no signs of variations in CH_2BrCH_2Br concentration in the shallowest part of the firn columns, that would have reflected the seasonality in the OH atmospheric mixing ratios as has been described in *Kaspers et al.* (2004) and *Sturges et al.* (2001). This does not necessarily mean that there is no seasonality in the CH_2BrCH_2Br atmospheric mixing ratio as the amplitude of seasonality might not be large enough to be recorded in the firn air measurements and/or the general decrease in CH_2BrCH_2Br mixing ratio could mask patterns of seasonality. This is supported by the detrended Cape Grim observations which are shown in Figure 4.8.

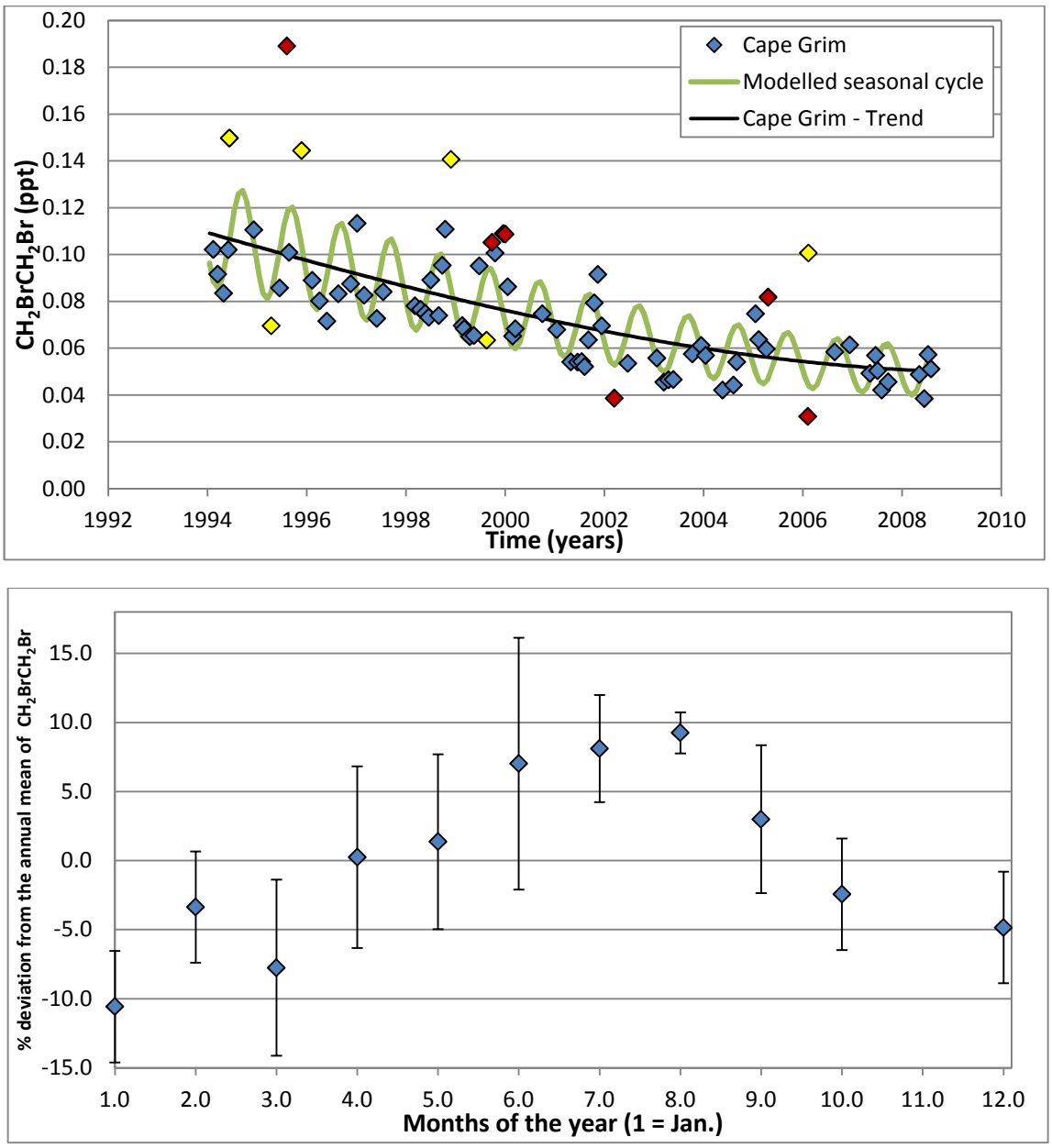

Figure 4.8: Top panel, Atmospheric mixing ratios of CH_2BrCH_2Br as a function of time from observations of archived samples taken at Cape Grim (blue points). A polynomial expression fitted through the Cape Grim time series in order to detrend the data (black line). A modelled seasonal cycle based on the seasonal cycle observed in the bottom panel (green line). Data points more than 3 standard deviations away from the mean were taken as outliers and removed from the seasonal cycle calculation (yellow points). Six unreliable samples were also removed from the seasonal cycle calculation (red points) (see Figure 3.4 for more details). Bottom panel, percentage deviation from the annual mean CH_2BrCH_2Br mixing ratio based on the detrended Cape Grim observations (top panel), taken as the mean of the observations made in a particular calendar month (between 3 - 8 data points). The error bars represent the 1 σ of the measurements.

The seasonal patterns of the Cape Grim observations were determined by using the same method that has been stated earlier. I show in Figure 4.8 that there is a seasonal cycle in the atmospheric mixing ratio of CH_2BrCH_2Br. The amplitude of the seasonal cycle is taken as the differences between the average of the winter months (June, July and August) and the average

of the summer months (December, January and February). Therefore, the detrended Cape Grim observation indicates a seasonal cycle with an amplitude of 21 % of the annual mean in the southern hemisphere. This would suggest a southern hemispheric seasonal cycle with an amplitude of 0.01 ppt in 2008.

Figures 4.6 indicate that the 1920 mixing ratio of CH_2BrCH_2Br was 0.17 ppt in the northern hemisphere. Whereas Figures 4.7 indicate that the 1930 mixing ratio of CH_2BrCH_2Br was 0.01 ppt in the southern hemisphere. The first reported use of CH_2BrCH_2Br was as an additive in leaded petrol in 1925 (*Randi*, 1952). This agrees with the period of a sustained growth in the mixing ratio of CH_2BrCH_2Br in both hemispheres up until the early 1970s. The average growth rates during this period were 0.01 ppt yr^{-1} or 1.8 % yr^{-1} in the northern hemisphere and 0.004 ppt yr^{-1} or 3.7 % yr^{-1} in the southern hemisphere.

The peak in the northern hemisphere atmospheric mixing ratio occurred in 1970 at 0.90 ppt, whereas the peak in the southern hemisphere atmospheric mixing ratio occurred in 1973 at 0.16 ppt. These measurements in general agree with the phasing out of leaded petrol in the U.S. and Europe in the early 1970s (*Santodonato et al.*, 1985 and *Fishbein*, 1980). After the peak in the early 1970s, atmospheric mixing ratios in both hemispheres have been shown to decrease until the drill date of the firn sites (NH = 2008 and SH = 1999). Measurements of CH_2BrCH_2Br mixing ratios have been made from 1994 onwards at the Cape Grim baseline air pollution station. Figure 4.7 shows that these observations are in general agreement with the firn derived southern hemispheric time series, although there are a number of outlying points. Growth rates were inferred for the Cape Grim observations by fitting a three parameter polynomial expression to the data set (the black line in Figure 4.7) similar to the method presented in *Laube et al.* (2012) and *Sturges et al.* (2012). The average growth rates during this period were -0.03 ppt yr^{-1} in the northern hemisphere and -0.003 ppt yr^{-1} in the southern hemisphere. However, in recent years this decline has stopped, with CH_2BrCH_2Br mixing ratios remaining somewhat constant. In the northern hemisphere, the decline stopped in 2004 at a mixing ratio of 0.08 ppt, which is 8 % of the peak mixing ratio (Figure 4.6). This is a return to the mixing ratios of the 1920 and may suggest that CH_2BrCH_2Br is currently at its natural background level. In the southern hemisphere, this decline stopped in 2006 at 0.05 ppt, representing 33 % of the peak mixing ratio (Cape Grim time series – Figure 4.7). It should also be noted that these growth rates and peak timings, represent only the best estimates and contain considerable uncertainties within the envelopes shown in Figures 4.6 and 4.7.

I derived the 'global' averaged atmospheric time series of CH_2BrCH_2Br between 1930 and 2008 (the drill date of the NEEM site) by averaging the northern and southern time series (Figure 4.9). The southern hemispheric time series was derived using both the firn derived time series and the Cape Grim time series. These two time series were averaged for years covered by both.

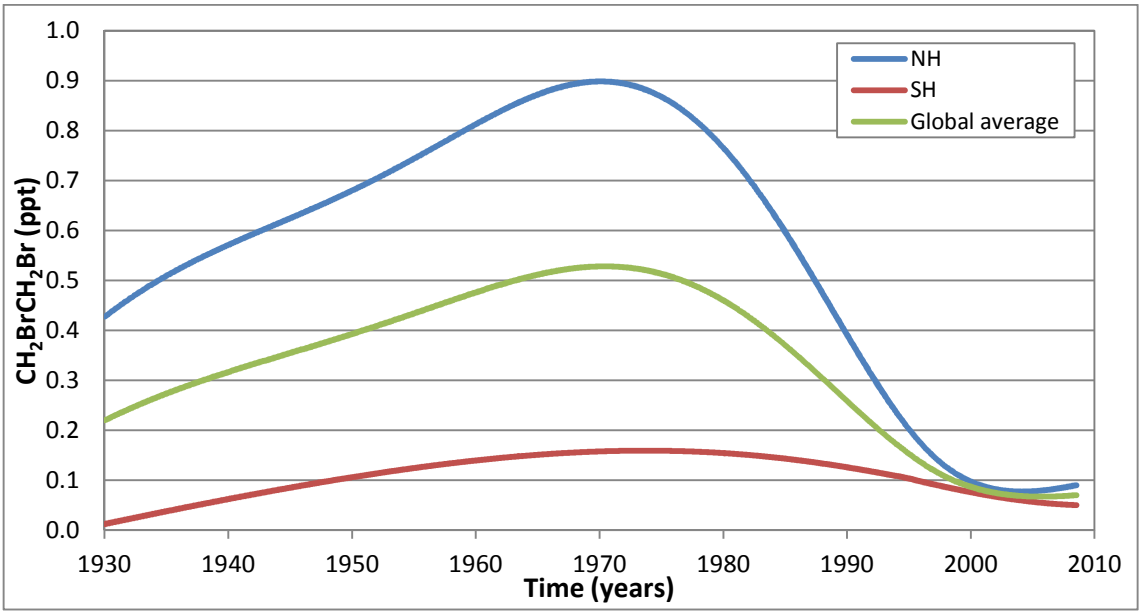

Figure 4.9: Northern hemispheric atmospheric time series of CH_2BrCH_2Br derived from Arctic firn air (blue line). Southern hemispheric atmospheric time series of CH_2BrCH_2Br derived from Antarctic firn and Cape Grim observation (red line). 'Global' atmospheric time series of CH_2BrCH_2Br derived as the average between the northern and southern hemispheric time series (green line).

Figure 4.9 indicates that the 'global' mixing ratio of CH_2BrCH_2Br was ~ 0.1 ppt in 2008, which is 13 % of the peak mixing ratio. These 'global' mixing ratios are much lower than the mixing ratios observed by *Pratt et al.* (2000), *Brodzinsky et al.* (1997), *Khalil and Rasmussen* (1985) and *Berg et al.* (1984) which suggest a mixing ratios of around 5 ppt in urban areas (*Pratt et al.*, 2000) and 1 ppt at the South Pole (*Khalil and Rasmussen*, 1985). This difference is most likely a result of differences in the calibration scales used between studies.

4.3.5 Background information on C_2H_5Br

This section reports the northern hemispheric time series of the atmospheric mixing ratios of Bromoethane (ethyl bromide, C_2H_5Br). C_2H_5Br is a bromine-containing very short-lived source gas with predominately anthropogenic sources. *Carpenter et al.* (2000) observed emissions from 10 species of brown, red, and green macroalgae collected in the intertidal or subtidal zones off the west coast Ireland. Very small emissions of C_2H_5Br have also been observed from

cattle (*Williams et al.*, 1999) and volcanic gases (*Phillips*, 2006), as well as being released by the species of seaweed *Sargassum fucales* (*Class and Ballschmiter*, 1988).

The main anthropogenic sources of C_2H_5Br are from use as an ethylating agent in organic synthesis and as a solvent in the chemical and pharmaceutical industries (*Phillips*, 2006). It has also been used as a refrigerant and as a flame retardant (*Low et al.*, 2003), as well as being part of a blend with halon-2402 (*Montzka et al.*, 2010). C_2H_5Br has been historically used as an anesthetic, but widespread use for this purpose has now been stopped (*Phillips*, 2006). *Carpenter et al.* (1999) suggested that there is a correlation between CH_3Br and C_2H_5Br emissions and may be a result of similar emission rate from macroalgae. The main destruction of atmospheric C_2H_5Br is via reactions with the OH radical (*Montzka et al.*, 2010), with a resultant local lifetime of 41 days (*Montzka et al.*, 2010).

Currently the worldwide production, sales or emission of C_2H_5Br are not well known. Although U.S. production has been estimated as >0.45 Mg yr^{-1} in 1972 and 1.36 Mg yr^{-1} in 1975 (*Phillips*, 2006). An upper limit to the global emissions of C_2H_5Br is estimated at 1.4 ± 0.4 Gg for 2000 (*Low et al.*, 2003).

Atmospheric mixing ratios of C_2H_5Br have been observed by a number of different studies (*Low et al.*, 2003, *Pfeilsticker et al.*, 2000, *Carpenter et al.*, 1999, *Class and Ballschmiter*, 1988 and *Shah and Singh*, 1988). *Low et al.* (2003) observed atmospheric mixing ratios of C_2H_5Br at coastal and inland sites in California between 1996 and 1999. The observed median ambient mixing ratio averaged during this period was <0.3 ± 0.4 ppt (*Low et al.*, 2003). Higher variability was seen at urban sites which suggests there might be significant sources of C_2H_5Br in polluted air. A median northern hemispheric mixing ratio of 0.3 ± 0.1 ppt was observed from a number of Pacific Ocean transects taken between 1996 and 1999, with a median southern hemispheric mixing ratio of less than 0.2 ppt (*Low et al.*, 2003). These observations are in general agreement with *Carpenter et al.* (1999) who observed a mean of 0.23 ppt, with a range between 0.09 to 0.49 ppt in May 1997 at Mace Head.

In the upper atmosphere, whole air samplers on board balloons observed C_2H_5Br mixing ratios of 0.11 ppt just above the Arctic tropopause (9.5 km) in early 1999 (*Pfeilsticker et al.*, 2000). In addition *Laube et al.* (2008) suggested unidentified peaks in their chromatogram from air sampled at 15.2km pointed towards the presence of C_2H_5Br. *Pfeilsticker et al.* (2000) reported a decrease in C_2H_5Br by an order of magnitude in mixing ratio from 9 km to 16 km. Also modelled C_2H_5Br concentrations by *Hossaini et al.* (2012) have shown that C_2H_5Br is sufficiently long-lived to be potentially an important carrier of bromine to the stratosphere. Simulations

show, regardless of the surface mixing ratios ~ 70 – 73 % of surface bromine from C_2H_5Br at the surface in the tropics can reach the lower stratosphere (*Hossaini et al.*, 2012).

4.3.6 Results and discussion of C_2H_5Br

In this study, I report firn air measurement of C_2H_5Br from a number of northern hemispheric firn air records. These measurements have then been used to derive the atmospheric time series of C_2H_5Br mixing ratios. This time series was derived using the LGGE method, which is described in more detail in the methods chapter. The time series obtained and the output from the inverse model for the northern hemisphere sites alongside the measured concentration of C_2H_5Br with depth at northern hemispheric firn sites (NEEM, and NGRIP) are shown in Figure 4.10.

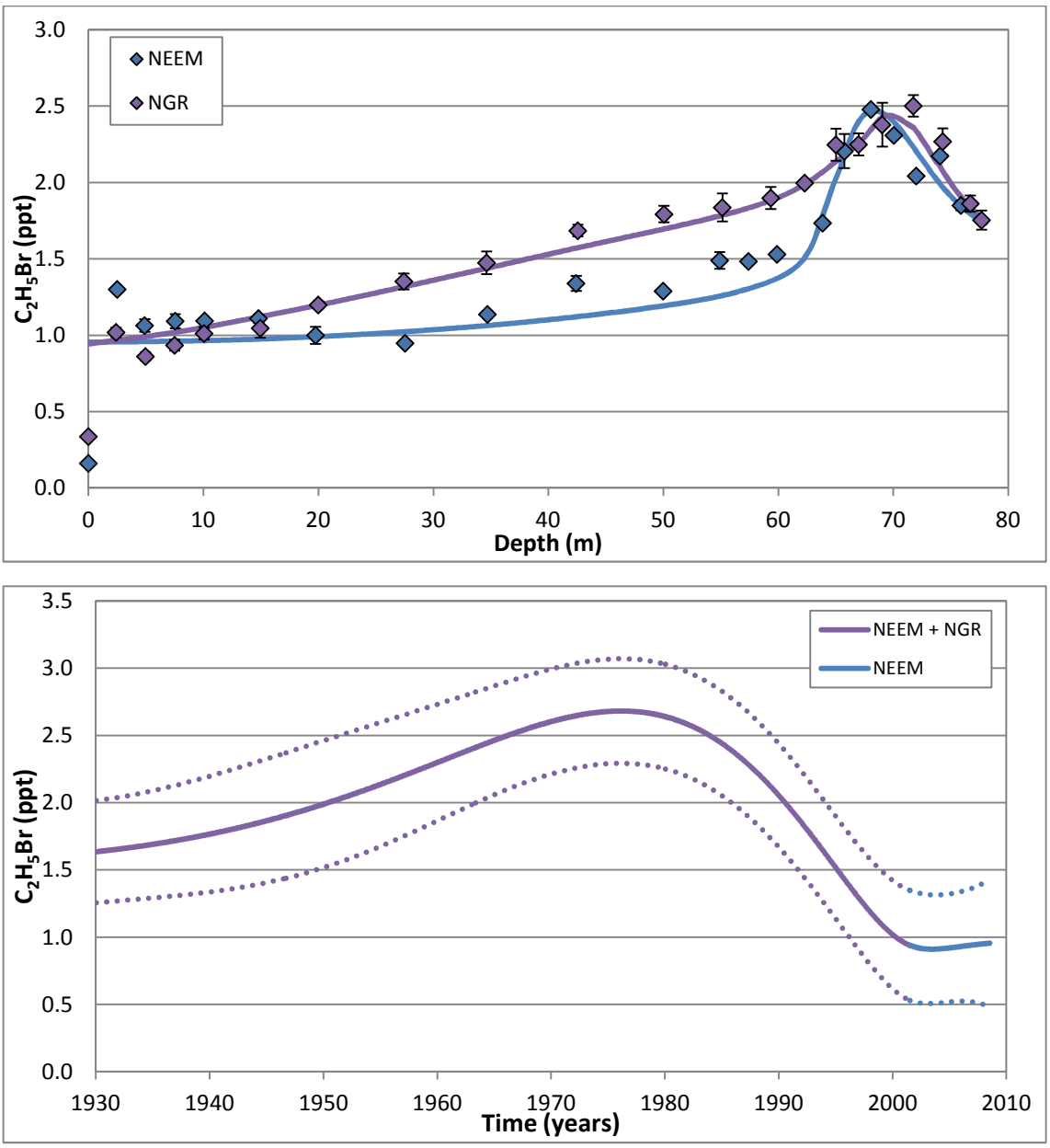

Figure 4.10: Top panel, depth profiles of northern hemispheric C_2H_5Br concentration with depth at the NEEM firn site (blue points) and the NGRIP firn site (purple points), compared with model simulations based on the atmospheric time series indicated in the bottom panel. The error bars represent the 1 σ of the measurements. Bottom panel, Atmospheric time series derived by a multi-site inversion modelling of the NEEM and NGRIP firn air measurements (solid line) using the LGGE method. As the firn sites have different drill dates the LGGE method derives an atmospheric time series using all of the firn sites up to the drill date of a firn site, after this the atmospheric time series is derived using the remaining sites. The time series derived by NEEM and NGRIP (purple line) and NEEM only (blue line). The dashed lines represent the uncertainties envelope of the time series (as described Figure 2.10).

C_2H_5Br has a significant atmospheric sink as a result of its reaction with the hydroxyl radical (OH) (*Montzka et al.*, 2010). With the total local lifetime of C_2H_5Br is 41 days (*Montzka et al.*, 2010). As stated earlier this should be short enough for there to be a variation in the upper part of the firn column. However there are no signs of variations in the C_2H_5Br concentration in the shallowest part of the firn columns. Although this does not necessarily mean that there is

no seasonality in the C_2H_5Br atmospheric mixing ratio, as the amplitude of the seasonality might not be large enough to be detected in the firn air measurements, or the general decrease in C_2H_5Br mixing ratio could be masking any seasonality. There might also be a local contaminate at the drill sites that could also be masking any seasonality.

Figure 4.10 indicates that the 1930 mixing ratio of C_2H_5Br was 1.6 ppt in the northern hemisphere. As the worldwide production, sales and emissions of C_2H_5Br are not well known and it is unclear when anthropogenic sources emissions began. Therefore, this 1930 mixing ratio cannot be taken as the natural background. After 1930s, the time series show a sustained growth until the mid-1970s, with the average growth rate during this period calculated as 0.02 ppt yr^{-1} or 1.1 % yr^{-1}. The peak in the northern hemisphere atmospheric mixing ratio occurred at 2.7 ppt in 1976. After this peak, atmospheric mixing ratio decreased to 0.9 ppt in the early 2000s, which is 35 % of the peak mixing ratio. During this period the average growth rate was -0.08 ppt yr^{-1}. However in recent years, this decline has stopped with C_2H_5Br mixing ratios remaining somewhat constant (Figure 4.10), with the atmospheric mixing ratio being 1.0 ppt in 2008. This time series does not match the atmospheric time series of CH_3Br observed by the NOAA and AGAGE network (*Montzka et al.*, 2010). This indicates that there is not a correlation between CH_3Br and C_2H_5Br emissions as suggested by *Carpenter et al.* (1999). It should also be noted that these growth rates and peak timing represent only the best estimates and contain considerable uncertainties within the envelopes as shown in Figure 4.10. It should also be noted that this atmospheric time series do not agree with previous atmospheric measurements of C_2H_5Br of $< 0.3 \pm 0.1$ ppt in 1999 (*Low et al.*, 2003) and 0.23 ppt in 1997 (*Carpenter et al.*, 1999). The difference between this study and previous measurements are most likely due to a difference in calibration scales.

4.3.7 Background information on CH_2BrCl, $CHBr_2Cl$ and $CHBrCl_2$

The bromo-chloro methanes consist of three compounds; bromochloromethane (methylene bromochloride, CH_2BrCl), dibromochloromethane ($CHBr_2Cl$) and bromodichloromethane ($CHBrCl_2$). All of the bromo-chloro methanes originate from both natural and anthropogenic sources (*Worton et al.*, 2006). They have been formerly used as flame retardant and are currently used as a laboratory reagents (*Phillips*, 2006). $CHBr_2Cl$ was also used as an intermediate in chemicals manufacturing (*Phillips*, 2006), whereas $CHBrCl_2$ has been used as a solvent for fats and waxes and because of its high density, for mineral separation. CH_2BrCl was invented for use in fire extinguishers by the Germans during the mid-40s and was used up until the late 1960s, being officially banned by the US by the National Fire Protection Association (NFPA) for use in fire extinguishers in 1969 (*Phillips*, 2006). Due to its ozone depletion

potential, its production was banned from January 2002 by the Montreal Protocol on Substances that Deplete the Ozone Layer (*González et al.*, 2006). $CHBr_2Cl$ and $CHBrCl_2$ are formed through so called "haloform" reactions, which revolve around the bromide substitution of chloroform. *Lepine and Archambault* (1992) have shown through the analysis of pre and post treated water, that these compounds can be generated with the chlorination of water. *Worton et al.* (2006) calculated that there is a significant emission from the chlorination of seawater used as cooling water in coastal power stations and estimate this source to contribute $\sim$ 10 % to the global budgets.

The main natural source of the bromo-chloro methanes is from biogenic emissions (*Carpenter et al.*, 1999, *Ekdahl et al.*, 1998 *Sturges et al.*, 1993a and *Class and Ballschmiter*, 1988). $CHBrCl_2$ has been been reported from soils through the process of natural chlorination of organic matter with bromide substitution (*Hoekstra et al.*, 1998). High atmospheric mixing ratios have been observed within the marine boundary layer in regions of high oceanic productivity (*Clerbaux and Cunnold et al.*, 2006). The main sink of atmospheric CH_2BrCl, $CHBr_2Cl$ and $CHBrCl_2$ is through the reaction with the hydoxyl (OH) radical (*Montzka et al.*, 2010). However, there is a minor, but not insignificant sink from photolysis in the troposphere (*Montzka et al.*, 2010).

Atmospheric mixing ratios of CH_2BrCl, $CHBr_2Cl$ and $CHBrCl_2$ have been observed by a number of different studies (e.g. *Laube et al.*, 2008, *Clerbaux and Cunnold et al.*, 2006 and *Schauffler et al.*, 199a), summarised in Table 4.4. Recorded observations range from 0.1 – 0.9 ppt in the marine boundary layer (*Clerbaux and Cunnold et al.*, 2006) to 0.00 – 0.14 ppt in the tropical tropopause (*Laube et al.*, 2008). The sum of CH_2BrCl, $CHBr_2Cl$, and $CHBrCl_2$ contributes about 0.5 ppt of bromine to the upper troposphere and lower TTL. Near the tropical tropopause the total contribution of these source gases declines to about 0.2 ppt (*Montzka et al.*, 2010).

Table 4.4: Summary of available observations of bromo-chloro-methanes from the marine boundary layer (MBL) to the tropical tropopause layer (TTL) based on *Montzka et al.* (2010).

Region	Marine Boundary Layer	Upper Troposphere	Lower TTL	LZRH[#]	Upper TTL	Tropical Tropopause
Ref.	*Clerbaux and Cunnold et al.* (2006)	*Schauffler et al.* (1999)	*Laube et al.* (2008)	*Clerbaux and Cunnold et al.* (2006)	*Clerbaux and Cunnold et al.* (2006)	*Laube et al.* (2008)
Height range (km)		10 - 12	12-14	14.5 - 15.5	15.5 - 16.5	16.5 - 17
CH_2BrCl (ppt)	0.4 – 0.6	0.03 – 0.16	0.13 – 0.16	0.08 – 0.13	0.1 – 0.12	0.05 – 0.11
$CHBr_2Cl$ (ppt)	0.1 – 0.8	0.01 – 0.36	0.06 – 0.15	0.03 – 0.11	0.01 – 0.11	0.00 – 0.14
$CHBrCl_2$ (ppt)	0.1 – 0.9	0.02 – 0.28	0.18 – 0.22	0.12 – 0.18	0.11 – 0.14	0.03 – 0.12

level of zero clear-sky radiative heating

A 20th century time series for the bromo-chloro methanes has been observed by *Worton et al.* (2006) from Arctic firn air taken from the NGRIP drill site in Greenland. Longer term time series have also been determined for the southern hemisphere from the analysis of firn air at two Antarctic sites, DML and DC (*Sturges et al.*, 2001). *Sturges et al.* (2001) found no evidence for any significant temporal trends in the southern hemisphere mixing ratio of these compounds. The *Worton et al.* (2006) NGRIP firn profiles indicate that the annual mean atmospheric mixing ratio of CH_2BrCl has remained constant since ~ 1950 and thus imply that anthropogenic sources are insignificant. There is evidence of a few data points in the deepest firn with relatively high concentrations which could be the result of post deposition effects and which might have complicated the interpretation of results. In contrast, *Worton et al.* (2006) observed an increase in the concentrations of $CHBr_2Cl$ and $CHBrCl_2$ in the direction of the surface within the firn column. This observed behaviour can be explained by an increase in the atmospheric mixing ratios of $CHBr_2Cl$ and $CHBrCl_2$ since ~1950. The authors observed that this increase in atmospheric mixing ratios levelled off in about 1992 (*Worton et al.*, 2006).

4.3.8 Results and discussion of CH_2BrCl, $CHBr_2Cl$ and $CHBrCl_2$

In this study I report firn air measurement of CH_2BrCl, $CHBr_2Cl$, and $CHBrCl_2$ from a number of northern hemispheric firn air records. The NEEM measurements are a new set of data obtained in this study whereas the NGRIP measurements are taken from *Worton et al.* (2006). These measurements have then been used to derive the atmospheric time series of CH_2BrCl, $CHBr_2Cl$, and $CHBrCl_2$ mixing ratios. These were derived using a new iterative modelling approach as based on the method described in *Trudinger* (2002). However, it has the added advantage that it can be used for atmospheric time series that have increased monotonically up to a peak mixing ratio before decreasing monotonically. More details on this method are given in the methods chapter. The time series obtained and the output from the model for the NEEM site are shown in Figure 4.11 alongside the measured concentration of CH_2BrCl, $CHBr_2Cl$, and $CHBrCl_2$ with depth at northern hemispheric firn sites (NEEM and NGRIP).

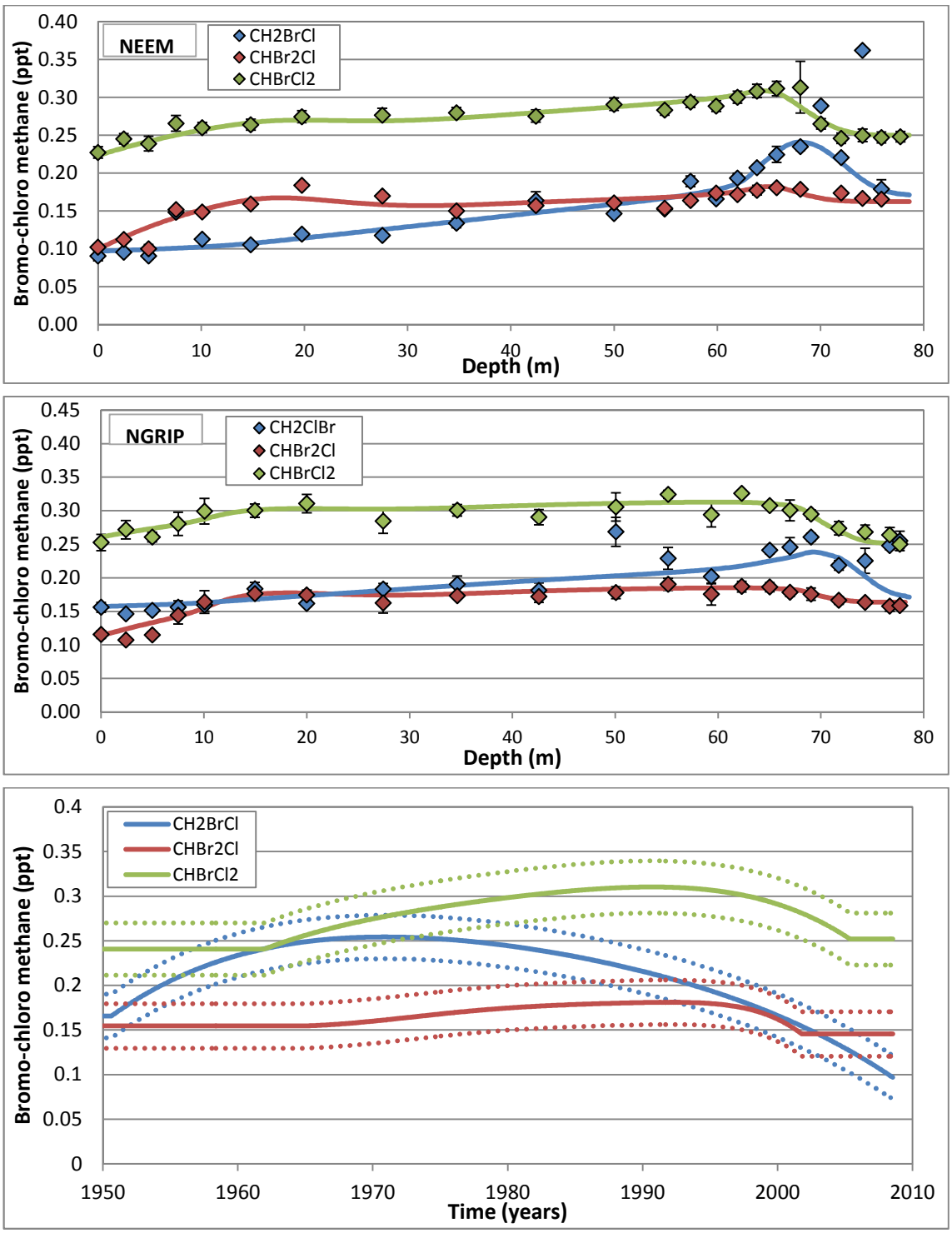

Figure 4.11: Top and middle panel, measured concentration of northern hemispheric CH_2BrCl (blue points), $CHBr_2Cl$ (red points) and $CHBrCl_2$ (green points) with depth at the NEEM firn site (top) and NGRIP firn site (middle, taken from *Worton et al.* (2006)), compared with model simulations based on the atmospheric time series indicated in the bottom panel with a seasonal cycle (Table 4.5) added to the time series. The error bars in top and middle panels represent the 1 σ of the measurements. Bottom panel, atmospheric time series based on the NEEM and NGRIP firn air measurements CH_2BrCl (blue line), $CHBr_2Cl$ (red line) and $CHBrCl_2$ (green line) using the new iterative method. The dashed lines consist of the sum of a) the firn air model maximum and minimum runs obtained by adding and subtracting the 1 σ measurement to/from the firn data and b) the maximum deviation of the actual mixing ratios from the polynomial fitted to derive the time series.

Figure 4.11 shows that there is one outlying point in the CH_2BrCl NEEM data at 70.04 m. The ambient air measurements (shown as depth = 0 m) were collected at the NEEM site during July 2008. These ambient air measurements have average mixing ratios of: CH_2BrCl - 0.16 ± 0.01 ppt, $CHBr_2Cl$ - 0.12 ± 0.01 ppt, and $CHBrCl_2$ - 0.25 ± 0.01 ppt, represent the most recent measurements of the bromo-chloro methanes in this study.

All of the bromo-chloro methanes have a significant atmospheric sink as a result of their reaction with the hydroxyl radical (OH) (*Montzka et al.*, 2010). The local atmospheric lifetime of bromo-chloro methanes are given as: CH_2BrCl – 137 days, $CHBr_2Cl$ – 59 days, and $CHBrCl_2$ – 78 days (*Montzka et al.*, 2010). This should be short enough for there to be a seasonal cycle in their atmospheric mixing ratio compared with other trace gases with similar lifetimes. However there are no signs of variations in the CH_2BrCl concentration in the shallowest part of the firn columns. Although this does not necessarily mean that there is no seasonality in the CH_2BrCl atmospheric mixing ratio, as the amplitude in seasonality might not be large enough to be recorded in the firn air measurements especially as it has small atmospheric mixing ratio and has a relatively long lived. This is support by the findings of *Yokouchi et al.* (1996) who observed a seasonal cycles for CH_2BrCl, of 5 % at the Alert Arctic observation station. The seasonal cycle of the bromo-chloro methanes was calculated by adding seasonal cycles with increasing amplitudes to the atmospheric time series in Figure 4.14, until the time series derives the lowest error with the firn air measurements. Where the error was calculated as the square root of the sum of the squares of the difference between the model and the observations. Seasonal cycle information for the bromo-chloro methanes is shown in Table 4.5.

Table 4.5: Seasonal cycle of the bromo-chloro methanes

Compound	Amplitude of seasonal cycle (% of the annual mean mixing ratio)	Amplitude of seasonal cycle in 2008 (ppt)	Amplitude of seasonal cycle from *Worton et al.* (2006) (% of the annual mean mixing ratio)
CH_2BrCl	0	0	0
$CHBr_2Cl$	55	0.08	60
$CHBrCl_2$	40	0.1	44

Table 4.5 shows that both $CHBr_2Cl$ and $CHBrCl_2$ have a large amplitude in their seasonal cycle in terms of the percentage to the annual mean mixing ratio and they general agree with *Worton et al.* (2006). This agrees with the findings of *Yokouchi et al.* (1996) who observed a seasonal cycles for $CHBr_2Cl$, of 66 % at the Alert Arctic observation station. These seasonal cycle also

general agreement with the seasonal cycles of 60 % - $CHBr_2Cl$ and 35 % - $CHBrCl_2$ observed by *Atlas and Ridley* (1996) at the Mauna Loa observatory although this is located in a tropical region.

Figure 4.11 indicates that the 1950 mixing ratio of CH_2BrCl was 0.17 ppt in the northern hemisphere. As CH_2BrCl has been used in fire extinguishers since the 1940s, these 1950 mixing ratios cannot be taken as natural background. After the 1950 the time series show a sustained growth until 1970 when the atmospheric mixing ratio reached 0.25 ppt. The average growth rate for CH_2BrCl during this period was 0.01 ppt yr^{-1}. This time series is consistent with the previously discussed use of CH_2BrCl in fire extinguishers. Since 1970, mixing ratios have deceased continually up to 0.10 ppt in mid-2008 when the firn was extracted. During this period, the average atmospheric growth rate was -0.004 ppt yr^{-1} or -2.1 % yr^{-1} with the growth rate in 2007 being -0.009 ppt yr^{-1} or -8.7 % yr^{-1}. This decline in the atmospheric mixing ratio agrees with the total banning of production of CH_2BrCl in January 2002, by the Montreal Protocol on Substances that Deplete the Ozone Layer (*González et al.*, 2006). The 2008 atmospheric mixing ratio is less than the 1950 mixing ratio, which suggests that I have not observed the natural background mixing ratio for CH_2BrCl in this study. Also it is likely that in the future the atmospheric mixing ratio will continue to decline until it approaches the natural background mixing ratio.

Figure 4.11 indicates that the atmospheric time series of both $CHBr_2Cl$ and $CHBrCl_2$ are very similar. Both compounds increase in the later part of the 20th century from their natural background (1950) mixing ratio by between 18 to 28 %. This is consistent with the findings of *Worton et al.* (2006) who observed an increase of between 16 – 24 % in the concentrations of $CHBr_2Cl$ and $CHBrCl_2$ from firn air records at the NGRIP site in Greenland. *Worton et al.* (2006) also observed that the increase in atmospheric mixing ratios levelled off at ~1992, which again agrees with the findings in this study. Since 1992, the mixing ratios of both compounds deceased continually until they reached approximately natural background levels. A comparison between the nature of the observed changes in the atmospheric time series of $CHBr_2Cl$ and $CHBrCl_2$ indicates that there is likely to be a similar source driving their atmospheric mixing ratios. This could result from emissions from the chlorination of seawater used as cooling water in coastal power stations. This emission source was estimated to contribute ~ 10 % to the global budget of these compounds in 2000 (*Worton et al.*, 2006). However it remains unclear what has caused emissions to decline since 1992, as there are no signs of a decrease in water chlorination during this period (*Worton et al.*, 2006).

4.3.9 Background information on $CHBr_3$

Bromoform ($CHBr_3$) is an organic halogenated compound which has chemical properties that are quite similar to those of chloroform. $CHBr_3$ is a recognized ozone-depleting chemical as it is a source of stratospheric bromine (*Montzka et al.*, 2010). The anthropogenic sources of $CHBr_3$ are small in comparison to natural sources. Small emissions of $CHBr_3$ occur from chlorination of drinking water and power plant cooling water (*Worton et al.*, 2006). In the past, it was used as a solvent, sedative and flame retardant, but now it is mainly used as in laboratory reagent (*Phillips*, 2006). It has also been used as a heavy liquid floatation agent in mineral separation and a purification of materials such as quartz (*Phillips*, 2006). The largest natural source of atmospheric $CHBr_3$ is from the ocean (*Montzka et al.*, 2010). Oceanic emissions originate from either the open ocean or coastal regions (*Montzka et al.*, 2010). While numerous studies have identified coastal macroalgae as significant source of $CHBr_3$ in coastal regions (*Clerbaux and Cunnold et al.*, 2006). Although, it has not been unequivocally proven that macroalgae account for all such coastal emissions. Close to shore in Cape Verde in the tropical Atlantic, *O'Brien et al.* (2009) detected elevated mixing ratios of $CHBr_3$ without evidence of significant macroalgae on the local shore.

The atmospheric mixing ratio of $CHBr_3$ in 2008 was 1.5 (*Montzka et al.*, 2010) which is around 20 % of the atmospheric mixing ratio of $CHBr_3$. Although $CHBr_3$ provides 4.5 ppt of Br to the atmosphere which is around 60 % of the atmospheric Br provided by CH_3Br.

4.3.10 Results and discussion of $CHBr_3$

This gas is of large importance to the global bromine budget. Therefore I measured $CHBr_3$ concentrations in this study from NEEM firn air samples. The variation in concentration with depth is shown in Figure 4.12.

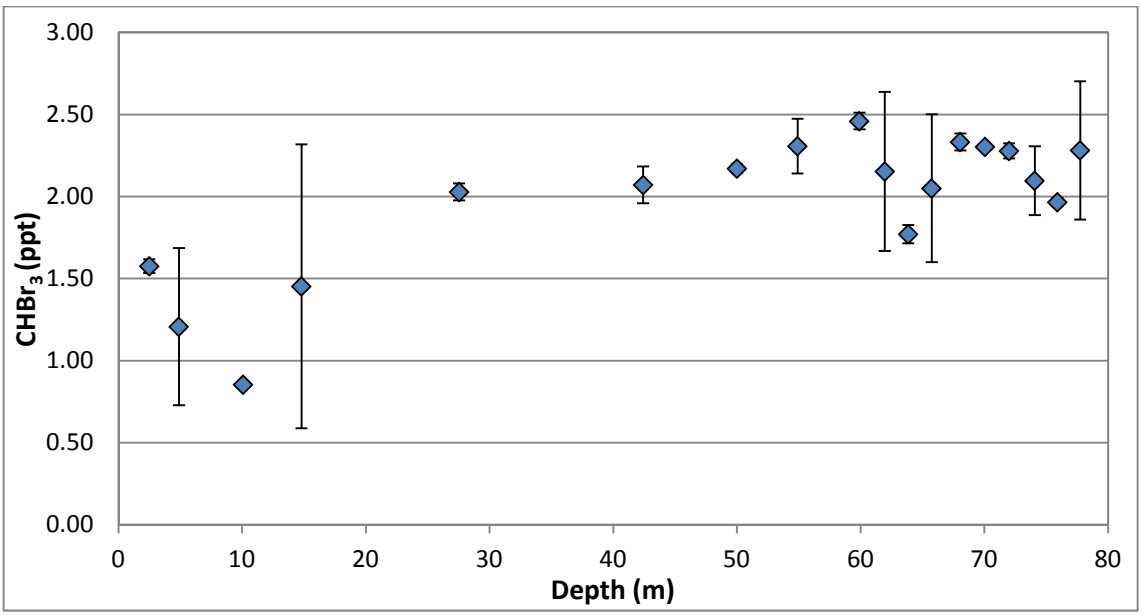

Figure 4.12: Top panel, measured concentration of $CHBr_3$ with depth at the NEEM firn site (blue points). The error bars in both panels represent the 1 σ of the measurements.

The firn air profile of $CHBr_3$ concentrations shows a scattered profile (Figure 4.12). As a result of extensive testing at different pre-concentration volumes and concentrations, I discovered that $CHBr_3$ was not consistently being fully flushed off the trap and onto the column of the GC-MS. Therefore, data from the GC-MS used in this study did not produce accurate measurements of $CHBr_3$ concentrations and I have not derive an atmospheric time series for this compound in this study.

4.3.11 Emissions of the VSL brominated substances

I dervied the annual emissions for the VSL bromine substances (CH_2Br_2, CH_2BrCH_2Br, C_2H_5Br, CH_2BrCl, $CHBr_2Cl$, $CHBrCl_2$) using the atmospheric time series in Figures 4.5, 4.9, 4.10 and 4.11 using the 1 - box model described in methods chapter. These annual emissions estimates are shown in Figures 4.13, 4.14, 4.15 and 4.16 respectively. These emissions are derived by assuming that there is: a constant atmospheric lifetime (i.e. a homogeneous OH field), a constant total mass of the atmosphere of 5.1 x 10^{18} kg, instantaneous mixing in the atmosphere and the difference between annually averaged atmospheric mixing ratio is wholly due to emissions rates.

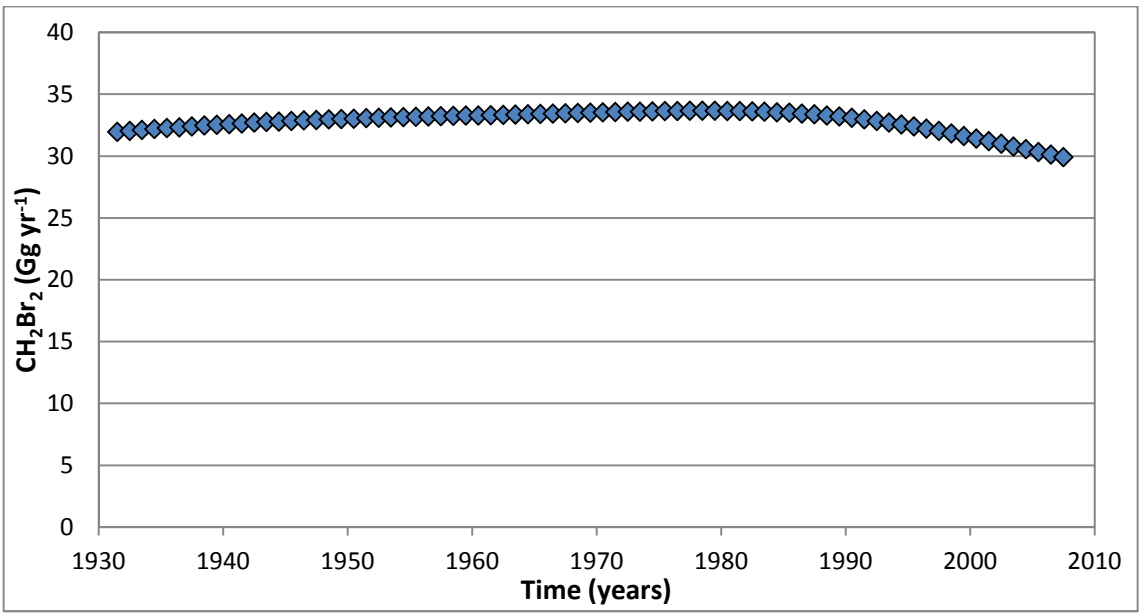

Figure 4.13: Annual emissions of CH_2Br_2 based on the atmospheric time series in Figure 4.5.

Figure 4.13 shows that estimated emissions of CH_2Br_2 rose slightly from ~33 Gg yr^{-1} in 1951 to a peak of ~34 Gg yr^{-1} in 1980 before progressively declining to ~33 Gg yr^{-1} by 2007, representing around 89 % of the peak emission. These emissions estimates are in general agreement with the global emissions derived by *Kurylo and Rodriguez* (1999) of 58 Gg yr^{-1} and *Liang et al.* (2010) of 57 Gg yr^{-1}. Although it is much less than 280 Gg yr^{-1} and 100 Gg yr^{-1} reported by *Butler et al.*, (2007) and *Warwick et al.*, (2006), respectively. However, it is worth noting that there are large uncertainties associated with the estimates, of *Butler et al.* (2007) and *Warwick et al.* (2006), notably due to the large variability in emissions from coastal zones.

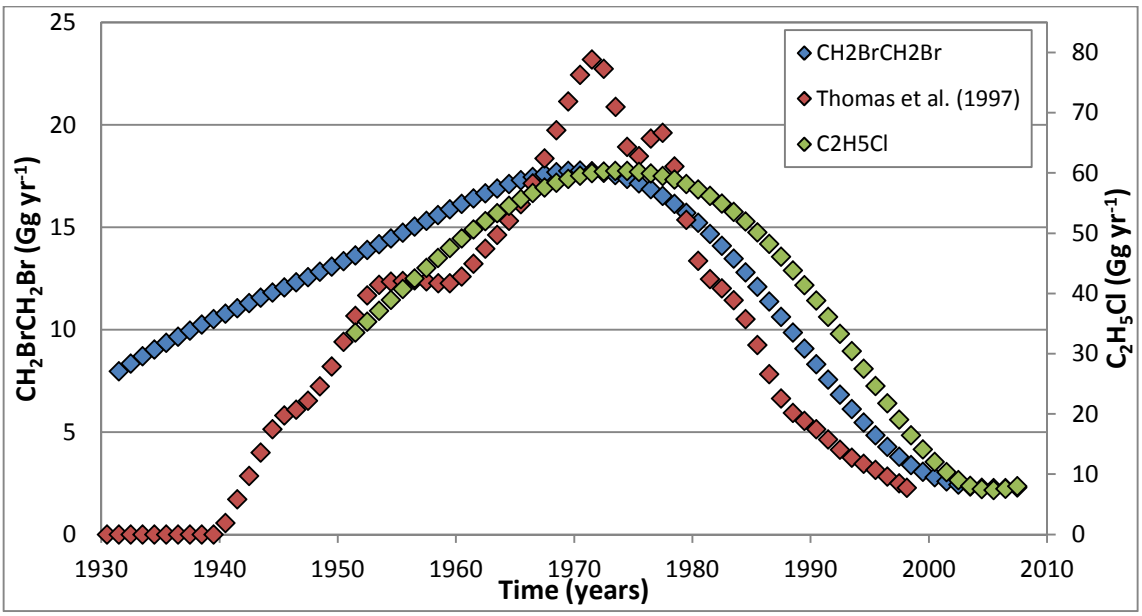

Figure 4.14: Annual emission of CH_2BrCH_2Br (blue points) based on the atmospheric time series in Figure 4.9. The annual Br emission based on *Thomas et al.* (1997) is given as a comparison (red points). The C_2H_5Cl emissions derived in this study (green points) are also included as a comparison.

Figure 4.14 shows that estimated emissions of CH_2BrCH_2Br rose year-on-year from ~14 Gg yr^{-1} in 1951 to a peak in 1970 of ~18 Gg yr^{-1} before progressively declining to ~2 Gg yr^{-1} in 2007, representing around 13 % of the peak emission. These emissions estimates are in general agreement with the reported temporal trend of CH_2BrCH_2Br use as an additive in leaded petrol in the United States, which declined rapidly between 1971 and 1991 (*Penkett et al.*, 1995). In addition they agree well with the bromide emissions from leaded petrol given by *Thomas et al.* (1997) (Figure 4.14). The authors estimated bromine emissions from lead petrol based on the world use of lead in petrol and on petrol scavenger formulations (*Thomas et al.*, 1997). I derived the CH_2BrCH_2Br emission estimate by assuming that 14 % of bromine emissions from leaded petrol are in the form of CH_2BrCH_2Br. However, the estimated emissions from the firn air derived time series are smoothed due to diffusion within the firn as well as the smoothing factors in the firn model process. This will result in the emissions from the firn time series smoothing some features such as the timing and the value of the peak emission. These estimated emissions in the current study are in general agreement with the time series of emission estimates of C_2H_5Cl (Figure 4.14), which indicates they might share a common emissions source most likely to be the emissions from leaded petrol (*Thomas et al.*, 1997 and *Otto and Montreuil*, 1976).

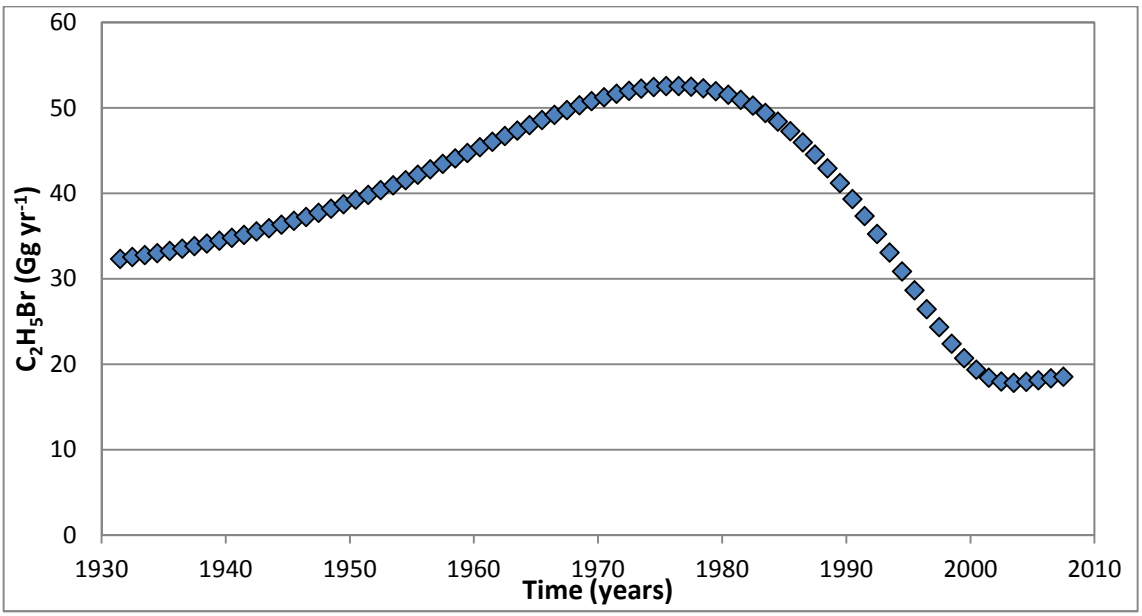

Figure 4.15: Annual emission of C_2H_5Br based on the atmospheric time series in Figure 4.10.

Figure 4.15 shows that estimated emissions of C_2H_5Br rose slightly from ~40 Gg yr^{-1} in 1951 to a peak of ~53 Gg yr^{-1} in 1976 before progressively declining to ~18 Gg yr^{-1} in 2001 representing ~35 % of the peak emission. In recent years, emissions have remain somewhat constant at ~19 Gg yr^{-1}. These estimated emissions are higher than the global emissions derived by *Low et al.* (2003) of 1.4 ± 0.4 Gg for 2000. As stated earlier, this is most likely due to calibration differences between the studies.

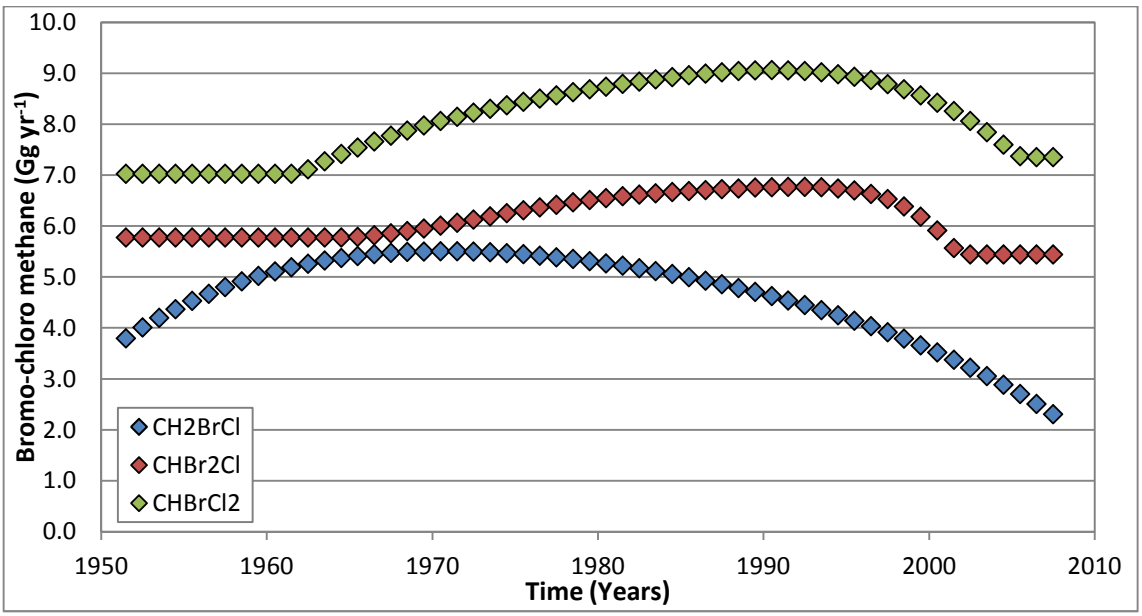

Figure 4.16: Annual emission of CH_2BrCl (blue points), $CHBr_2Cl$ (red points) and $CHBrCl_2$ (green points) based on the atmospheric time series in Figure 4.11.

Figure 4.16 shows that emissions of CH_2BrCl rose year-on-year from ~4 Gg yr^{-1} in 1951 to a peak of ~6 Gg yr^{-1} in 1970. This is larger than the estimate of 4.54 x 10^5 Gg yr^{-1} production rate in the US in 1972 based on manufactures' reports (*Phillips*, 2006). However this estimate was based on production from one country, and was reported as a likely under-estimate of the true US production, as not all emissions sources were reported (*Phillips*, 2006). After 1970, emissions progressively declined to ~2 Gg yr^{-1} in 2007, representing around 40 % of the peak emission. These emissions estimates are in general agreement with the reported temporal trend of CH_2BrCl use in fire extinguishers (*Phillips*, 2006). The estimated emissions of $CHBr_2Cl$ rose from ~6 Gg yr^{-1} to a peak of ~7 Gg yr^{-1} in 1992, which is similar to the emissions of $CHBrCl_2$ which rose from ~7 Gg yr^{-1} to a peak of ~9 Gg in 1992 yr^{-1}. After 1992, both emissions rates decreased to ~5 Gg yr^{-1} ($CHBr_2Cl$) and ~7 Gg yr^{-1} ($CHBrCl_2$) by 2007. As a result of the similarity in emissions rates between $CHBr_2Cl$ and $CHBrCl_2$ it is highly likely that they are emitted from similar sources. However, it should be noted that the emissions estimated from the firn air derived time series are smoothed due to diffusion within the firn as well as the smoothing factors in the firn model process. This will result in the emissions from the current time series will smooth some features such as the timing and the value of the peak emission.

4.4 Halothane ($CF_3CHBrCl$)

This section reports the first measurements of the atmospheric mixing ratio of 2-bromo-2-chloro-1,1,1-trifluoroethane (Halon-2311, Halothane, Fluorothane, $CF_3CHBrCl$). $CF_3CHBrCl$ has been used widely for a number of years as a general anaesthetic gas for both humans (*Bovill*, 2008) and animals (*Riviere and Papich*, 2009), used widely in operating theatres, dentist and veterinary rooms as well as in animal research laboratories and is still stated as a core medicine in the World Health Organization's "Essential Drugs List" (*WHO*, 2011). Concern has been expressed over the use of $CF_3CHBrCl$ because of its potential for stratospheric ozone destruction (*Norreslet et al.*, 1989 and *Fox et al.*, 1975), although its contribution to the total global warming potential of the atmosphere is either small (*Bosenberg*, 2011 *Ishizawa*, 2011 and *Brown et al.*, 1989) or negative if the indirect global warming potential is calculated. As it is the only widely used inhalational anaesthetic agent to contain a bromide atom, it has the largest ozone depletion potentials (ODP) of any anaesthetic compounds (*Brown et al.*, 1989).

Firn air samples collected in Greenland (NEEM, NGRIP and DI) were used to reconstruct a northern hemispheric time series of $CF_3CHBrCl$ atmospheric mixing ratios. Firn air samples collected from the Antarctic (DC and DML) were used to reconstruct a southern hemispheric time series. $CF_3CHBrCl$ was also detected and quantified in air samples from the Cape Grim baseline air pollution station in the southern hemisphere from archived samples dating back to 1978. Furthermore these atmospheric histories have been used to validate the atmospheric lifetime of $CF_3CHBrCl$. This is important because in recent years there have been a number of different atmospheric lifetimes calculated (*Montzka et al.*, 2010, *McCulloch*, 2000, *Langbein et al.*, 1999 and *Brown et al.*, 1989).

4.4.1 Background information on $CF_3CHBrCl$

It has been noted that more than 80% of inhalation anaesthetic agents are exhaled unchanged by the patient (*Shiraishi and Ikeda*, 1990) and therefore can be emitted into the lower atmosphere (*Norreslet et al.*, 1989). The production of $CF_3CHBrCl$ has also been identified as a possible source to the atmospheric mixing ratio (*Phillips*, 2006). The main sink of atmospheric $CF_3CHBrCl$ is through the reaction with the hydoxyl (OH) radical (*Montzka et al.*, 2010). There is a minor, but not insignificant sink from photolysis in the troposphere and stratosphere (*Bilde et al.*, 1998).

$CF_3CHBrCl$ was first synthesized by C. W. Suckling of Imperial Chemical Industries *Homan et al.*, 2010) in 1951 and was first used clinically by M. Johnstone in the U.K. in 1956 and then in the U.S. in 1958 (*Bunker and Forrest*, 1969). By 1960, $CF_3CHBrCl$ was the most widely used general

anaesthic agent used in humans in the western world (*Riviere and Papich*, 2009). In the period between 1960 and the mid-1980s, $CF_3CHBrCl$ was given to many millions of adult and paediatric patients as well as animals worldwide. Use of $CF_3CHBrCl$ was phased out during the 1980s for adults and the 1990s for paediatric patients as different anesthetic agents became more popular (*Bovill*, 2008). In recent years, its common use as an anaesthetic has been largely replaced by newer volatile anaesthetics, and as a result, its commercial availability is becoming more limited (*Riviere and Papich*, 2009). However, $CF_3CHBrCl$ retains some use in veterinary surgery and is popular in developing countries because of its lower cost (*Phillips*, 2006).

$CF_3CHBrCl$ has previously been detected in the atmosphere by *Ensminger* (1998). During an air sampling campaign in France between 1981 and 1985, 22 of the 2013 air samples recorded $CF_3CHBrCl$ (*Ensminger*, 1988). Highly elevated mixing ratios (0.08 - 9.19 ppm) have been measured in the personal air samples of 13 veterinarians during 38 surgical procedures (*Potts and Craft*, 1988). Currently there is not a fully publicly available report on the worldwide production, sales or emission of $CF_3CHBrCl$. Although the average annual consumption rate has been given 342 kg yr^{-1} by the University Hospital Göttingen during the late 1980s (*Langbein et al.*, 1999), and 426 kg yr^{-1} by the 31 operating theatres of the Grampian Health Board in 1988 (*Hopkins et al.*, 1989). The maximum global capacity to produce $CF_3CHBrCl$ was calculated at 1500 tonnes yr^{-1} by *McCulloch* (2000). Also, manufacturer of $CF_3CHBrCl$ (May and Baker, ICI and BOC Health Care) have been quoted in *Hopkins et al.* (1989) that total annual production did not exceed 1000 tonnes yr^{-1}. However, this production value was only an estimate as precise details were deemed to be commercially sensitive.

Since *Fox et al.* (1975) first published a warning in 1975, concern has been repeatedly expressed about the potential harm that release of $CF_3CHBrCl$ poses to the global environment. $CF_3CHBrCl$ is potentially destructive to stratospheric ozone as well as having a small effect on the total global warming potential of the atmosphere. A number of reports have assessed these potentials by calculating the Ozone Depletion Potentials (ODP), the direct Greenhouse Warming Potentials (GHWP) and the direct Global Warming Potentials (GWP) for $CF_3CHBrCl$ (e.g.*Ishizawa*, 2011, *Langbein et al.*, 1999 and *Brown et al.* ,1989). Also because the significance of $CF_3CHBrCl$ to the stratospheric ozone loss and to the global climate warming depends on the atmospheric lifetime of $CF_3CHBrCl$, a number of studies have calculated this value (Table 4.6).

Table 4.6: Atmospheric lifetimes (τ) and Ozone Depletion Potentials (ODP), of $CF_3CHBrCl$.

Paper	τ (years)	ODP (relative to CFC-11)	ODP (τ = 1 year)† (relative to CFC-11)
Brown et al. (1989)	2.0	0.36	0.18
Langbein et al. (1999)	6.6	1.56	0.24
McCulloch (2000)	3.6	0.7	0.19
Montzka et al. (2010)	1.0		
Bosenberg (2011)	6.6 – 7.0#	1.56	0.22
Ishizawa (2011)	7.0#	0.36	0.05

taken from *Langbein et al.* (1999)
† τ = 1 years is taken from *Montzka et al.* (2010)

As there are a number of different estimate of the atmospheric lifetime of $CF_3CHBrCl$ (Table 4.6), in this study I used a 1 year lifetime (*Montzka et al.*, 2010). As such, I have re-calculated the ODP from previous studies using a 1 year atmospheric lifetime (Table 4.6). Table 4.6 shows that $CF_3CHBrCl$ has a significant ODP of around 0.2. This suggests that $CF_3CHBrCl$ does have a significant potential for ozone destruction. However, in addition to being a greenhouse gas, $CF_3CHBrCl$ destroys stratospheric ozone, another radiatively important gas. Therefore, a change in ozone radiative forcing due to the addition of $CF_3CHBrCl$ can be attributed to $CF_3CHBrCl$ as an indirect radiative forcing. Stratospheric ozone losses are generally thought to cause a negative radiative forcing, partly cancelling the increased radiative forcing arising from the direct influence of $CF_3CHBrCl$.

4.4.2 Results and discussion of $CF_3CHBrCl$

In this study I report firn air measurement of $CF_3CHBrCl$ from a number of northern and southern hemispheric firn air records, as well as southern hemispheric observations from the Cape Grim baseline air pollution station. These measurements have then been used to derive the atmospheric time series of $CF_3CHBrCl$ mixing ratios. The time series of atmospheric $CF_3CHBrCl$ mixing ratios were derived using the LGGE method, which is described in more detail in the methods chapter. The time series obtained and the output from the inverse model for the northern and southern hemisphere sites alongside the measured concentration of $CF_3CHBrCl$ with depth at northern hemispheric firn sites (NEEM, NGRIP and DI) and Southern Hemispheric (DC and DML) firn sites are shown in Figures 4.17 and 4.18, respectively.

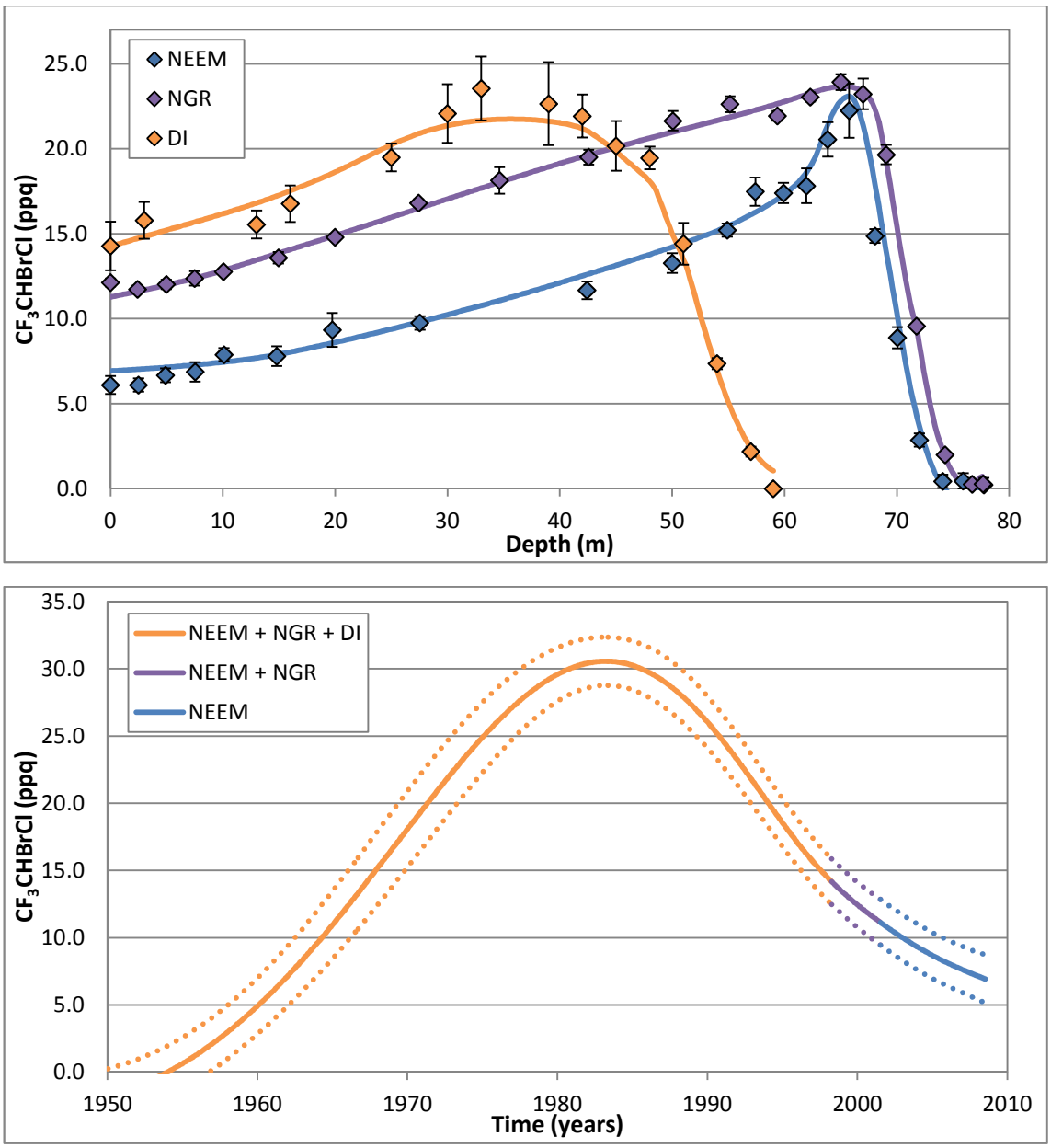

Figure 4.17: Top panel, depth profiles of northern hemispheric $CF_3CHBrCl$ concentration with depth at the NEEM firn site (blue points), NGRIP firn site (purple points) and the DI firn site (yellow points), compared with model simulations based on the atmospheric time series indicated in the bottom panel. The error bars represent the 1 σ of the measurements. Bottom panel, Atmospheric time series derived by a multi-site inversion modelling of the NEEM, NGRIP and DI firn air measurements (solid line) using the LGGE method. As the firn sites have different drill dates the LGGE method derives an atmospheric time series using all of the firn sites up to the drill date of a firn site, after this the atmospheric time series is derived using the remaining sites. The time series derived by the NEEM, NGRIP and DI (yellow line), NEEM and NGRIP (purple line) and NEEM only (blue line). The dashed lines represent the uncertainties envelope of the time series (as described Figure 2.10).

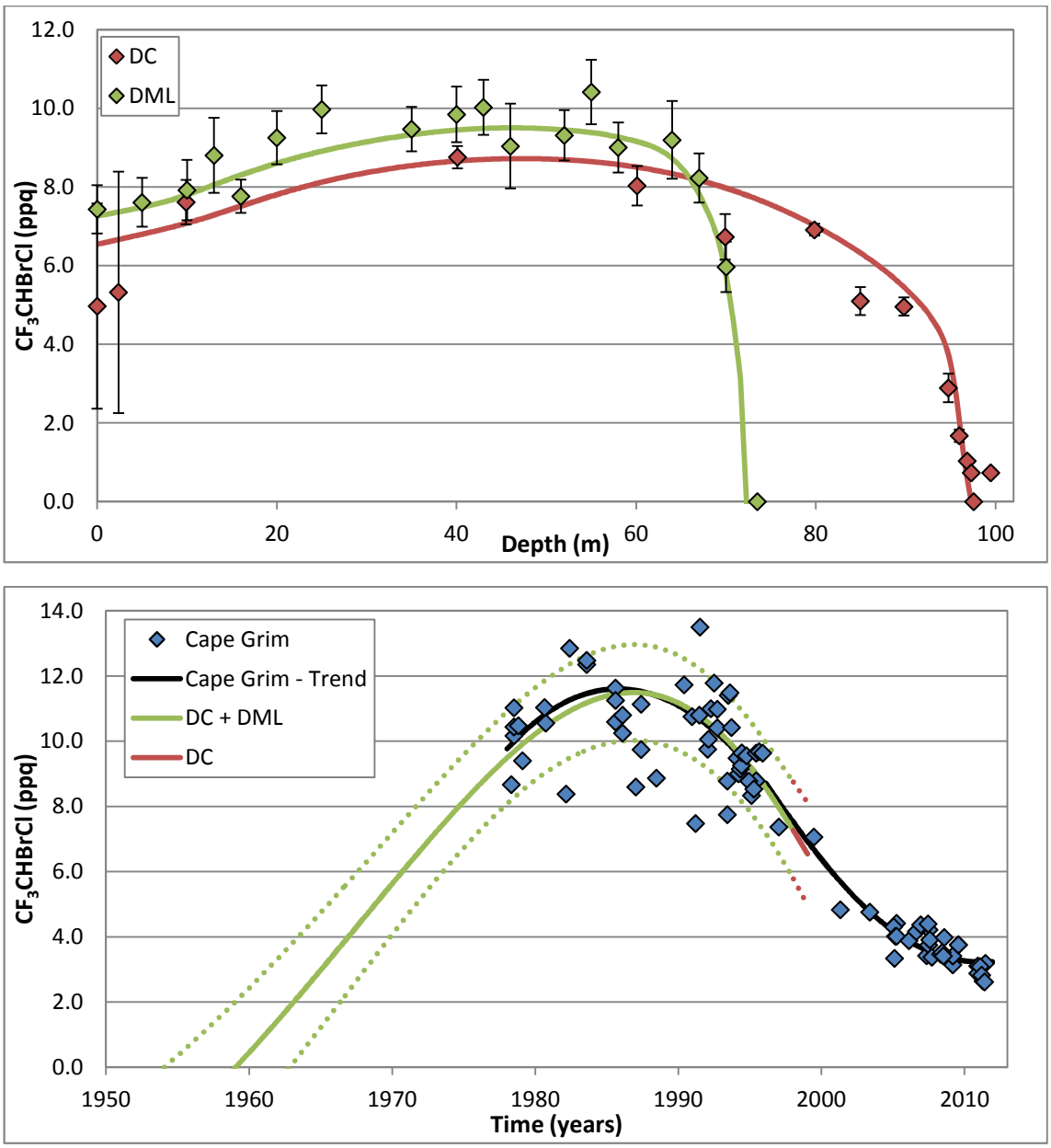

Figure 4.18: Top panel, depth profiles of southern hemispheric $CF_3CHBrCl$ concentration with depth at the DC firn site (red points) and the DML firn site (green points), compared with model simulations based on the atmospheric time series indicated in the bottom panel. The error bars represent the 1 σ of the measurements. Bottom panel, atmospheric time series derived by a multi-site inversion modelling of the DC and DML firn air measurements (solid line) using the LGGE method. The time series derived by the DC and DML - green line and DC only – red line. The dashed lines represent the uncertainties envelope of the time series (as described Figure 2.10). Also the mixing ratios of $CF_3CHBrCl$ as a function of time as measured in air samples collected in the southern hemisphere (blue points, from Cape Grim). The black line is a polynomial expression fitted through the Cape Grim time series in order to derive growth rates and emissions, based on the method used by *Laube et al.* (2012) and *Sturges et al.* (2012).

The ambient air measurements (shown as depth = 0 m) were collected at the NEEM site in July 2008 during the firn air drilling. These ambient air measurements have an average mixing ratio of 6.1 ± 0.5 ppq and are the most recent northern hemispheric measurements of $CF_3CHBrCl$ presented in this study. The ambient air measurements were collected at the DC site in December 1998 during the firn air drilling. These ambient air measurements have an average mixing ratio of 5 ± 2.6 ppq and are the most recent southern hemispheric measurement from the firn air sites presented in this study.

With a total atmospheric lifetime of 1 year (*Montzka et al.*, 2010) $CF_3CHBrCl$ should have a short enough lifetime for there to be a seasonal cycle in its atmospheric mixing ratio, compared with other trace gases with similar lifetimes (e.g. CH_3Cl). However, there are no signs of variations in the $CF_3CHBrCl$ concentration in the shallowest part of the firn columns, that would have reflected the seasonality in the OH atmospheric mixing ratios as described in *Kaspers et al.* (2004) and *Sturges et al.* (2001). Nonetheless, *Sturges et al.* (2001) only observed this variation for VSLS with a lifetime of less than 150 days and *Kaspers et al.* (2004) only observed this variation for CH_3Cl which has a larger atmospheric mixing ratio and seasonal cycle. Although this does not necessarily indicate an absence of seasonality in the $CF_3CHBrCl$ atmospheric mixing ratio, as the amplitude of seasonality might not be large enough to be detected in firn air measurements, alternatively, general decreases in $CF_3CHBrCl$ mixing ratio could mask any seasonality. In this study the seasonal cycle of $CF_3CHBrCl$ was determined by detrending the Cape Grim observations (Figure 4.19).

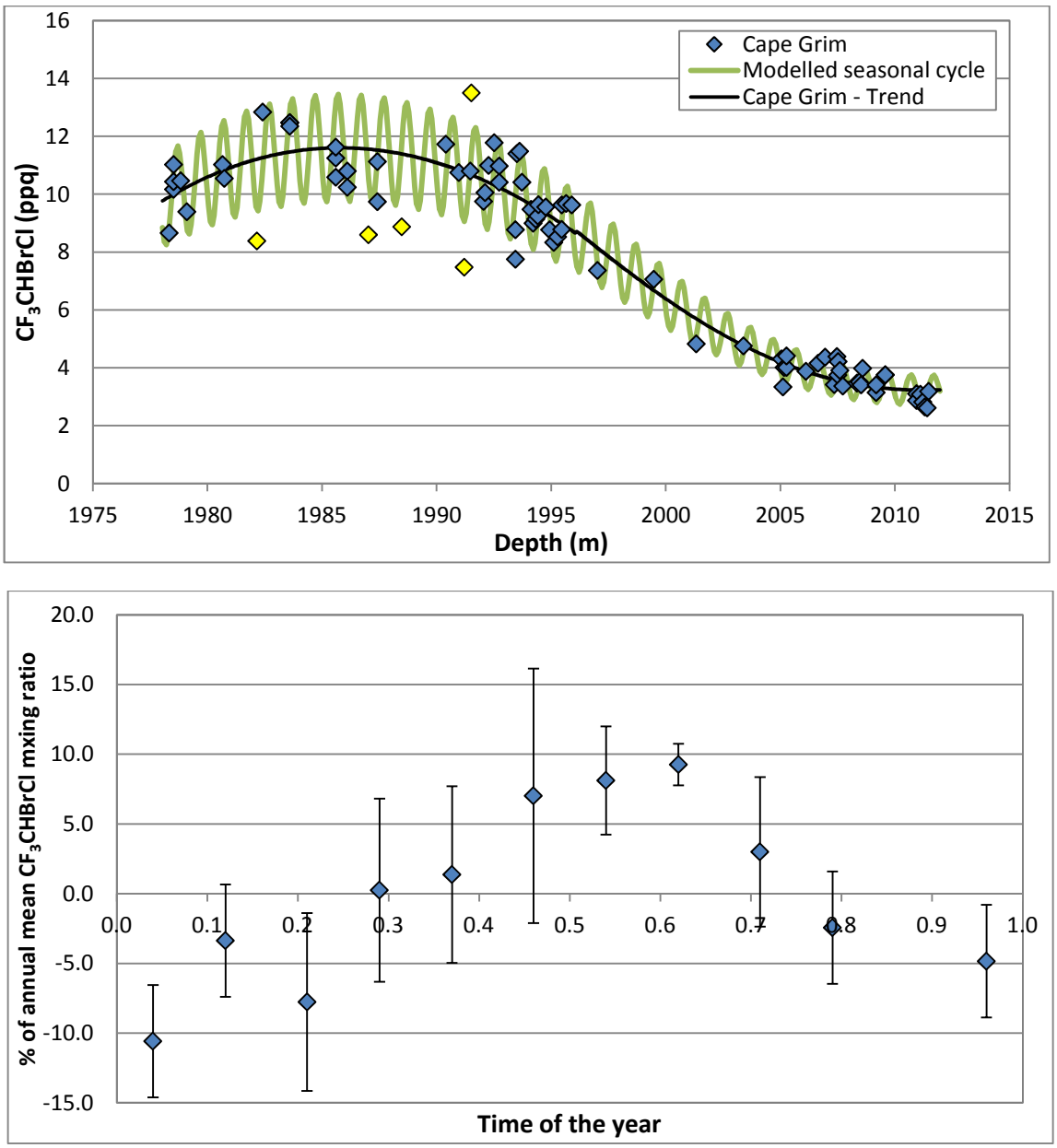

Figure 4.19: Top panel, Atmospheric mixing ratios of $CF_3CHBrCl$ as a function of time from observations of archived samples taken at Cape Grim (blue points). A polynomial expression fitted through the Cape Grim time series in order to detrend the data (black line). A modelled seasonal cycle based on the seasonal cycle observed in the bottom panel (green line). Data points more than 3 standard deviations away from the mean were taken as outliers and removed from the seasonal cycle calculation (yellow points). Bottom panel, percentage deviation from the annual mean $CF_3CHBrCl$ mixing ratio based on the detrended Cape Grim observations (top panel), taken as the mean of the observations made in a particular calendar month (between 3 - 8 data points). The error bars represent the 1 σ of the measurements.

The seasonal patterns of the Cape Grim observations were determined by using the same method that has been stated earlier. Figure 4.19 shows that there is a seasonal cycle in the atmospheric mixing ratio of $CF_3CHBrCl$. The amplitude of the seasonal cycle is taken as the differences between the average of the winter months (June, July and August) and the average of the summer months (Decembers, January and February). Therefore the detrended Cape

Grim observations indicate a seasonal cycle with an amplitude of 16 % of the annual mean in the southern hemisphere. This would represent a southern hemispheric seasonal cycle with an amplitude of 0.5 ppq in 2011.

Figure 4.17 and 4.18 indicate that it is most likely that significant emissions of $CF_3CHBrCl$ started in the mid-1950s in the northern hemisphere, with significant mixing ratios appearing in the southern hemisphere in the late 1950s. These significant southern hemispheric mixing ratios may be as a result of southern hemispheric emission or as a result of northern hemispheric mixing ratios being transported into the southern hemisphere. Thus it remains unclear when southern hemispheric emissions started. This pattern of mixing ratios is in agreement with the first synthesis of $CF_3CHBrCl$ in 1951, and its first clinical use in 1956 (*Bunker and Forrest*, 1969). After the 1960s the time series show a sustained growth of $CF_3CHBrCl$ in both hemispheres until the mid 1980s. The average growth rates during this period were 1.0 ppq yr^{-1} in the northern hemisphere and 0.5 ppq yr^{-1} in the southern hemisphere. Cape Grim observations began in 1978 and Figure 4.18 shows that these observations are in general agreement with the firn derived southern hemispheric time series, although there are a number of outlying points. Growth rates were inferred for the Cape Grim observations by fitting a four parameter polynomial expression to the data set (Figure 4.18) similar to the method presented in *Laube et al.* (2012) and *Sturges et al.* (2012). The peak in the northern hemisphere atmospheric mixing ratio occurred in 1984 at 31 ppq, whereas the peak in the southern hemisphere atmospheric mixing ratio occurred in 1986 at 12 ppq. These measurements agree with the phasing out of $CF_3CHBrCl$ in the medical profession in the mid-1980s (*Bovill*, 2008). After the peak in the mid-1980s, atmospheric mixing ratios are shown to decrease until the drill date of the firn sites (NH = 2008 and SH = 1999) and the Cape Grim observations in 2011. The average growth rate during this period was -1.0 ppq yr^{-1} in the northern hemisphere and -0.4 ppq yr^{-1} in the southern hemisphere. The rate of this decrease has been slowing in recent years in the northern hemisphere from -0.8 ppq yr^{-1} in 2000 to -0.5 ppq yr^{-1} in 2007. In the southern hemisphere this rate has decreased from -0.6 ppq yr^{-1} in 2000 to -0.1 ppq yr^{-1} in 2010 as noted in the Cape Grim time series. The firn air itself was collected in July 2008, therefore an average growth rate cannot be provided for 2008, but mixing ratios continued to decrease. It should also be noted that these growth rates and peak timing represent only the best estimates and contain considerable uncertainties within the envelopes shown in Figures 4.17 and 4.18.

The 'global' averaged atmospheric time series of $CF_3CHBrCl$ was calculated between 1950 and 2008 (the drill date of the NEEM site) by averaging the northern and southern time series

Figure 4.20. The southern hemispheric time series used both the firn derived time series and the Cape Grim time series. These two time series were averaged for the years that are covered by both time series (i.e. 1950 - 1977 uses the firn time series only, 1978 - 1999 uses the average between the firn air derived time series and the Cape Grim time series and 2000 – 2008 uses the Cape Grim time series only).

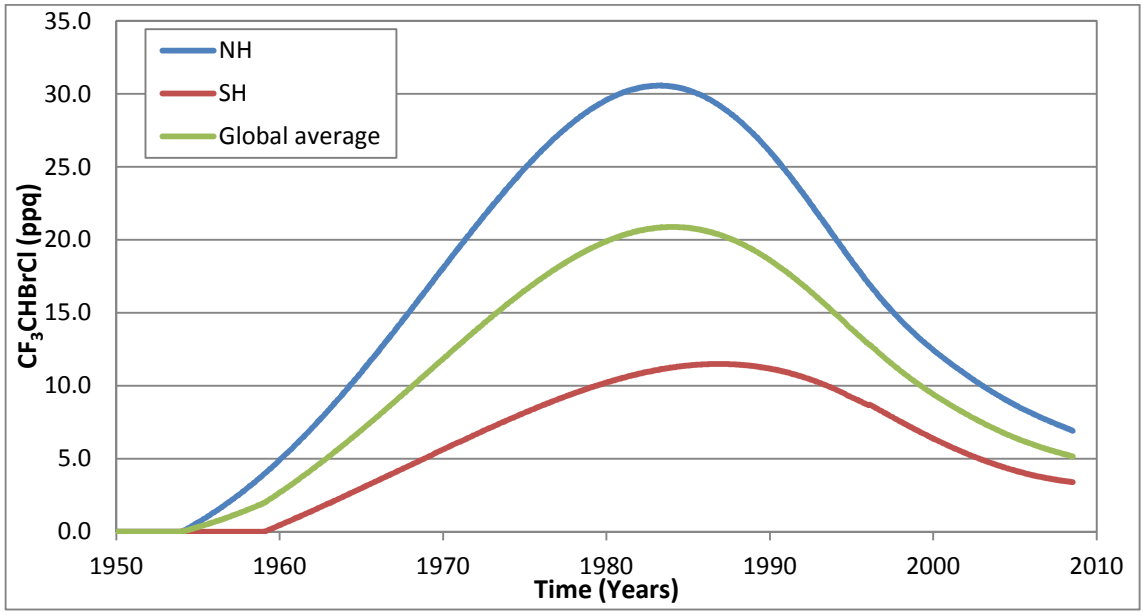

Figure 4.20: Northern hemispheric atmospheric time series of $CF_3CHBrCl$ derived from Arctic firn air (blue line). Southern hemispheric atmospheric time series of $CF_3CHBrCl$ derived from Antarctic firn and Cape Grim observation (red line). 'Global' atmospheric time series of $CF_3CHBrCl$ derived as the average between the northern and southern hemispheric time series (green line).

Figure 4.20 indicates that 'global' mixing ratio of $CF_3CHBrCl$ increased from 0.0 ppq in the mid 1950s to a maximum of 21 ppq in 1984, before declining to 5 ppq in 2008.

The firn modelling method developed at LGGE derives atmospheric time series for the northern and southern hemisphere independently. This means that the model assumes that there is no relationship between the two time series; therefore a 2 box model was used to validate the two time series. The 2 box model uses the northern hemisphere as an input and then derives a southern hemispheric time series using the inter-hemispheric mixing time (1.34 years) and an atmospheric lifetime of 1 year (*Montzka et al.*, 2010). This modelled southern hemispheric time series was then compared with the atmospheric time series derived from the southern hemispheric firn air measurements (Figure 4.21). However, this method makes the assumption that all emissions of $CF_3CHBrCl$ are in the northern hemisphere, with zero emissions in the southern hemisphere. Although $CF_3CHBrCl$ has been used in southern hemispheric hospitals (*Phillips*, 2006), these emissions will have been significantly smaller than

from the larger more developed northern hemispheric hospitals (*Bovill*, 2006). However there is no current estimate of the size of southern hemispheric $CF_3CHBrCl$ emissions.

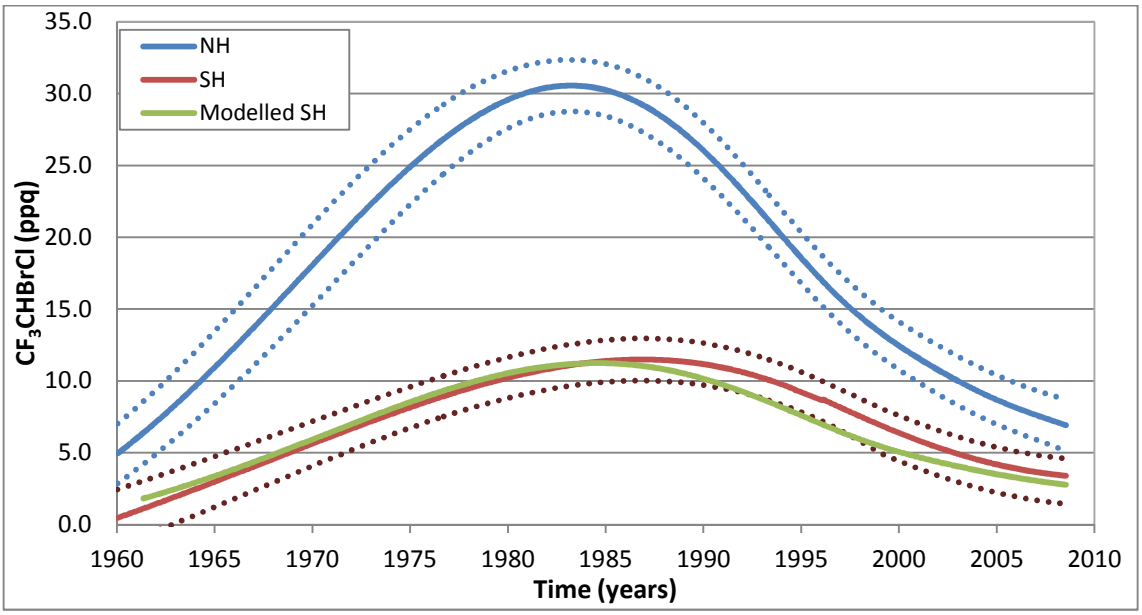

Figure 4.21: Northern hemispheric atmospheric time series of $CF_3CHBrCl$ derived from Arctic firn air (blue lines). Southern hemispheric atmospheric time series of $CF_3CHBrCl$ derived from Antarctic firn and Cape Grim observation (red lines). The dotted lines represent the uncertainty of the atmospheric time series as stated in Figures 4.23 and 4.24. Modelled southern hemispheric time series derived using the 2 box model (green line).

As can be seen from Figure 4.21, there is agreement between the calculated and observed southern hemispheric $CF_3CHBrCl$ atmospheric time series. Both time series have similar growth rates between the mid-1950, and the peak in atmospheric $CF_3CHBrCl$ in the mid-1980s.

However, Figure 4.21 indicates that there is a slight difference between the time series after 1985 with the decline greater in the northern hemisphere. This difference might be due to the model under estimating the lag time between the hemispheres or that after 1985 there has been significant southern hemispheric emissions. These significant southern hemispheric emissions might be a result of $CF_3CHBrCl$ being phased out in northern hemispheric hospitals before southern hemispheric hospitals (*Bovill*, 2008). It is worth noting that a greater number of observations are needed to validate if there is a difference between the atmospheric time series. Figure 4.21 also indicates that the atmospheric lifetime of $CF_3CHBrCl$ is around 1 year (as stated in *Montzka et al.* (2010)), because the model and observed southern hemispheric time series agree when you assume a 1 year atmospheric lifetime.

4.4.3 Emissions of $CF_3CHBrCl$

I derived the 'global' annual emissions of $CF_3CHBrCl$ using the atmospheric time series in Figure 4.20 using the 1 - box model described in the methods Chapter. These annual emissions estimates are shown in Figure 4.22.

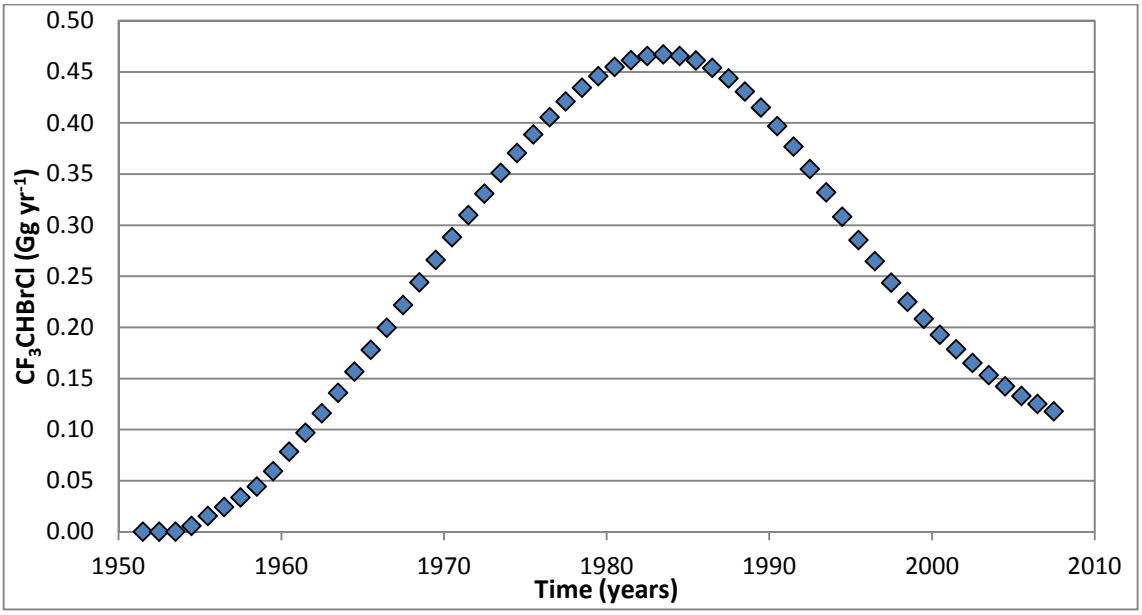

Figure 4.22: Annual emission of $CF_3CHBrCl$ (blue points) based on the atmospheric time series in Figure 4.25.

Figure 4.22 shows that emissions of $CF_3CHBrCl$ rose year-on-year from the 1950s to the 1980s, peaking at ~0.5 Gg yr^{-1} in 1983 before progressively declining to ~0.1 Gg yr^{-1} in 2007, representing ~25 % of the peak emission. These emissions estimates are in general agreement with the reported temporal trend of $CF_3CHBrCl$ use in the medical profession (*Bovill*, 2008). The scale of these emissions estimates generally agree with the upper limit of the total annual production of $CF_3CHBrCl$ of less than 1 Gg yr^{-1} in 1988 as report by May and Baker, ICI and BOC Health Care (*Hopkins et al.*, 1989). The emissions estimates in this study are ~50 % of this upper limit of total annual production.

4.5 Halons (H-1202, H-1211, H-2402 and H-1301)

Halons are a class of chemical compounds that are *fully halogenated* hydrocarbons which contain at least one bromine atom. They are fully-anthropogenic compounds with similar chemical properties to the chlorofluorocarbons (CFCs).

4.5.1 Background information on H-1202, H-1211, H-2402 and H-1301

Halons have been used since the early 1960s as effective gaseous fire-extinguishing agents (*McCulloch*, 1992). The most effective fire extinguishers and therefore the most widely used halons are: Halon-1211 (bromochlorodifluoromethane, Freon 12B1 and $CBrClF_2$), Halon-1301 (bromotrifluoromethane, Freon 13B1 and $CBrF_3$), Halon-1202 (dibromodifluoromethane, Freon 12B2, CBr_2F_2) and Halon-2402 (1,2-dibromotetrafluoroethane, Freon-114B2 and $C_2Br_2F_4$) (*Montzka et al.*, 2010). The key information for the halons are shown in Table 4.7. Halons are a source of stratospheric bromine and therefore they have a potential to destroy ozone. In total, these halons account for about 40 % of the organic bromine that reaches the stratosphere (*Montzka et al.*, 2003, *Pfeilsticker et al.*, 2000 and *Schauffler et al.*, 1999). As such, the production and consumption of H-1301, H-1211 and H-2402 have been regulated under the Montreal Protocol and the subsequent Amendments (*González et al.*, 2006). H-1202 is not covered by the Montreal Protocol or its Amendments, since most of its production is not deliberate (*González et al.*, 2006)

Measurements from firn air samples and atmospheric air samples collected since 1978 have shown that the atmospheric mixing ratios of all 4 of these halons have increased substantially from zero during the latter part of the 20th Century (*Reeves et al.*, 2005, *Fraser et al.*, 1999 and *Butler et al.*, 1998)

Table 4.7: Key information for the halons based on *Montzka et al.* (2010).

Compound	Lifetime (years)	ODP (Relative to CFC-11)	2008 mixing ratio (ppt)	2007-2008 Growth rate (ppt yr^{-1})	2008 Total Br (ppt)
H-1211	16	7.9	4.34	−0.06	4.34
H-1301	65	15.9	3.08	0.05	3.08
H-1202	2.9	1.7	0.027	−0.002	0.054
H-2402	20	13.0	0.44	−0.01	0.88
Total			7.89	-0.02	8.35

Table 4.7 shows that the halons have a combined atmospheric mixing ratio of 7.89 ppt with the largest contribution coming from H-1211. It also shows that currently most of the atmospheric mixing ratios of the halons have stopped increasing (*Montzka et al.*, 2010), with this decline starting in 2005 and its rate increasing year-on-year (*Montzka et al.*, 2010). The only halon to currently increase in the atmosphere is H-1301 which has the largest ODP, although *Montzka et al.* (2010) notes that the growth rate is at a slower rate than observed in 2003–2004.

4.5.2 Results and discussion of H-1202, H-1211, H-2402 and H-1301

In this study measurements of H-1211, H-1202 and H-2402 from the NEEM site have been measured on a negative ion chemical ionization (NICI) mass spectrometer. H-1301 was not measured because it could not be quantified on the NICI mass spectrometer. Figure 4.23 shows the firn measurements for the halons: the atmospheric time series derived by Mike Newland at UEA are given as a comparison and used to validate the firn air measurements. Mike Newland used Cape Grim data and a 2-D atmospheric chemistry-transport model (*Oram et al.*, 2011 and *Laube et al.*, 2010) which has been shown to reproduce well-known emissions of compounds emitted predominantly in the northern hemisphere when constrained by southern hemispheric observations (*Reeves et al.*, 2005). As the atmospheric time series of these species are well known, I did not derive any new time series in this study.

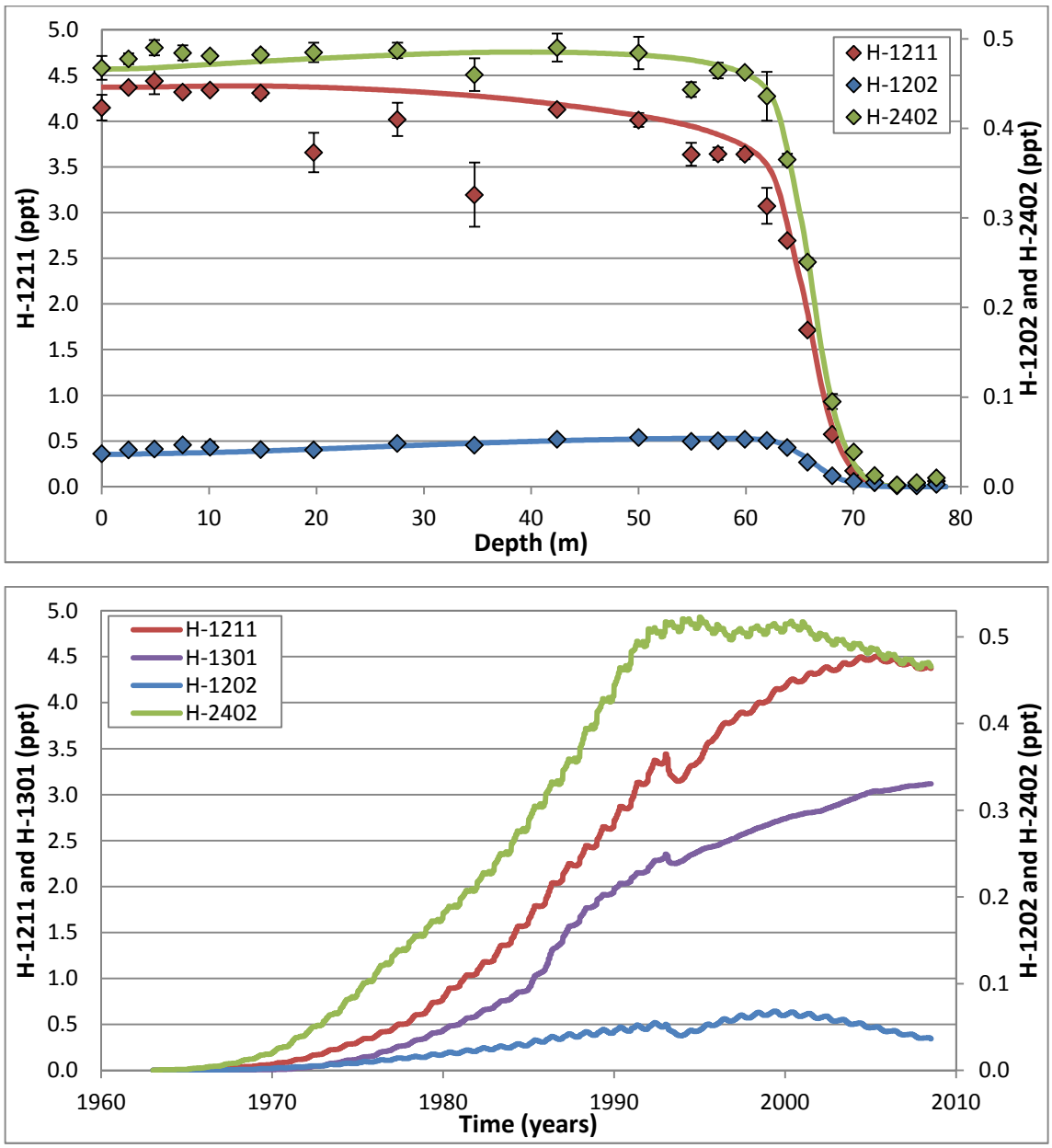

Figure 4.23: Top panel, measured concentration of northern hemispheric H-1202 (blue points), H-1211 (red points) and H-2402 (green points) with depth at the; NEEM firn site compared with model simulations based on the atmospheric time series indicated in the bottom panel. The error bars in both panels represent the 1 σ of the measurements. Bottom panel, atmospheric time series; H-1202 (blue line), H-1211 (red line) and H-2402 (green line), based on Cape Grim data and derived by Mike Newland. The atmospheric time series of H-1301 is given as a comparison.

Figure 4.23 shows that the measurements of the Halon concentrations from the NEEM firn site agrees well with the atmospheric firn sir derived time series derived from the Cape Grim data. Although, there are a number of outlining points in the H-1211 firn profile. The decline in mixing ratios in the 1990s is due to a change in the global distribution of emissions. With a significant increase in south Asian emissions combine with a decrease in north American and Europe emissions. As well as validating the firn air measurements these results show that the 2-D atmospheric chemistry-transport model (*Oram et al.*, 2011 and *Laube et al.*, 2010) is able

to reproduce a northern hemispheric time series from southern hemispheric atmospheric observations.

4.6 Equivalent effective stratospheric chlorine of the bromocarbons

The equivalent effective stratospheric chlorine (EESC) is again used as an approximation of the spatial and temporal distributions of Cl_y and Br_y in the stratosphere. This approximation uses the time series measurements of ODS surface concentrations combined with estimated rates at which individual gases release their halogens into the stratosphere (fractional release rates) and estimates of the age of air parcels, which is taken as the time elapsed since air parcels entered the stratosphere at the tropical tropopause. Therefore, EESC provides a simple index that relates the time evolution of surface mixing ratios of ODSs with the ozone-destructive ability of stratospheric halogens that come from these source gases (*Montzka et al.*, 2010). EESC is explained in more details in Chapter 3.

The distributions of species in the stratosphere depends on the competition between local photochemical removal processes and transport processes that carry the material from the entry point through, and out of, the stratosphere. Once a halogen source gas is in the stratosphere, halogen atoms can be released through photolysis or chemical reactions. The fractional release factor, $f_i(x,y,z,t)$, is calculated as the fraction of halocarbon I converted to an inorganic form by some time at a given location in the stratosphere (*Montzka et al.*, 2010). Currently, there are no calculated values of fractional release for the VSL bromocarbons and $CF_3CHBrCl$. Therefore in this study these will be estimated (Table 4.8).

Table 4.8: fractional release values of the bromocarbons and CFC-11

Compound	$f_{cfc\text{-}11}$ #	f_i	f_i / $f_{CFC\text{-}11}$
CH_2BrCH_2Br	0.47	1.00	2.13
CH_2Br_2	0.47	1.00	2.13
C_2H_5Br	0.47	1.00	2.13
CH_2BrCl	0.47	1.00	2.13
$CHBr_2Cl$	0.47	1.00	2.13
$CHBrCl_2$	0.47	1.00	2.13
$CF_3CHBrCl$	0.47	0.62	1.32

Montzka et al. (2010)

The VSL bromocarbons release bromine atoms very quickly after they have entered the stratosphere, due to their high photolysis rate and reactivity to the OH radical (*Montzka et al.*,

2010). This means that all of the bromine will be released very quickly and they have an estimated fractional release factor of 1.00 in this study. In comparison, $CF_3CHBrCl$ has a slightly longer atmospheric lifetime, therefore, the fractional release factor for Halon 1211 is used as an approximation. Halon 1211 is used because it a similar chemical compound to $CF_3CHBrCl$ and therefore likely to release its halogen atom at a similar rate. To retain the simplicity of the EESC index, the stratospheric entry mixing ratio for a given time is calculated assuming a simple time lag (Γ) from the surface observations (*Montzka et al.*, 2010). In this study Γ was taken to be 3 years (typical of the lower, midlatitude stratosphere (*Montzka et al.*, 2010)) to obtain a value appropriate for relating to midlatitude-averaged ozone loss. This assumption is used for $CF_3CHBrCl$ in this study. However using surface mixing ratios, is likely to result in an overestimate of the EESC contribution for shorter-lived compounds like CH_2Br_2, whose abundance will be reduced before reaching the tropopause. In this study, a reduction factor is used to account for this decline in mixing ratio between the surface and the tropopause. These reduction factors are calculated by taking the fraction between the surface mixing ratios and the mixing ratios at the tropopause observed in previous studies. Although, it should be noted these observations are from the tropics where the observations in this study are from polar regions. These reduction factors can be found in Table 4.9.

Table 4.9: Reduction factors of bromocarbons based on *Montzka et al.* (2010)

Compounds	Tropical surface mixing ratio (ppt)	Mixing ratio at the tropical tropopause (ppt)	Reduction factor
CH_2BrCH_2Br	11	5	0.45
CH_2Br_2	1.1	0.58	0.53
C_2H_5Br	0.3	0.11	0.37
CH_2BrCl	0.5	0.08	0.16
$CHBr_2Cl$	0.45	0.07	0.16
$CHBrCl_2$	0.5	0.075	0.15

Table 4.9 indicates that the CH_2Br_2 reduction factor is larger than the 0.3 modelled by *Gettelman et al.* (2009). The concept of EESC does have limitations because of uncertainties in the transport time, in the spatial and temporal dependencies of the bromine efficiency for ozone destruction versus chlorine (which is generally considered a constant), the efficiency of stratospheric halogen release from the source gas, and possible temporal changes in transport times and source gas lifetimes (*Newman et al.*, 2007). It should be noted that the EESC concept also does not explicitly account for changing atmospheric emissions and concentration of

other relevant constituents that can also affect ozone, such as CO_2 and methane (*Daniel et al.*, 2010). This study only calculates EESC from bromocarbon source gas injection and does not take into account any product gas injection from the bromocarbons.

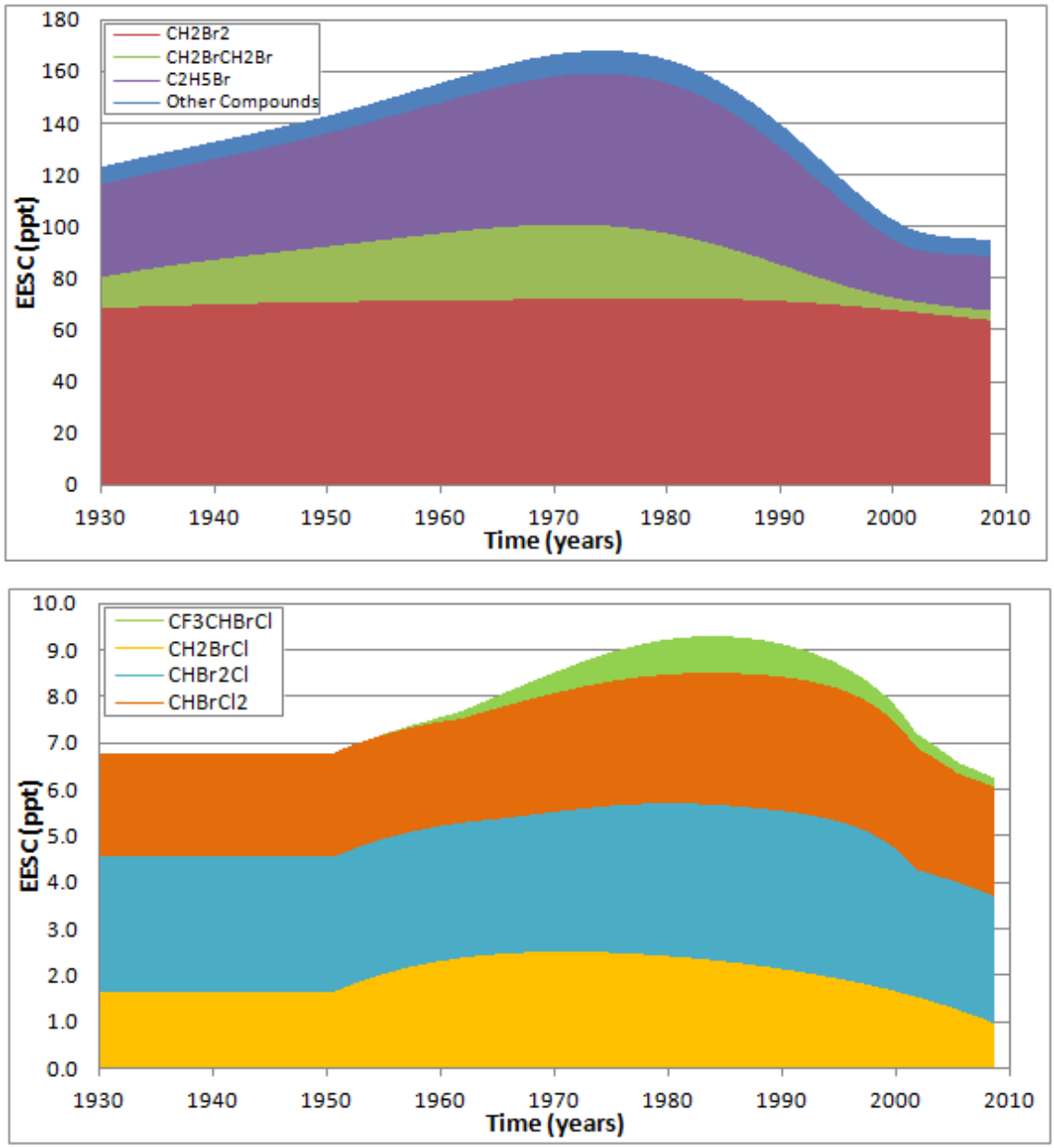

Figure 4.24: Top panel, Equivalent effective stratospheric chlorine mixing ratios since 1930 from CH_2Br_2 (red area), CH_2BrCH_2Br (green area), C_2H_5Br (purple area) and the EESC emitted from the other bromocarbons since 1960 (blue area). Bottom panel, Equivalent effective stratospheric chlorine emitted from the other bromocarbons since 1930 (blue area, top panel) showing the contribution from the individual compounds: CH_2BrCl (yellow area), $CHBr_2Cl$ (light blue area), $CHBrCl_2$ (orange area) and $CF_3CHBrCl$ (light green area).

Figure 4.24 indicates that in 2008, VSL bromocarbons and $CF_3CHBrCl$ had a combined total of 94 ppt of EESC. This is ~6 % of the 1700 ppt total EESC in 2008 from inorganic halogen calculated for the midlatitude stratosphere from surface measurements (*Montzka et al.*, 2010)

and 6 % of the ~1500 ppt total EESC in 2008 from anthropogenic sources including the halogenated ODS and N_2O modelled by *Daniel et al.* (2010).

Figure 4.24 also shows that the EESC of the VSL bromocarbons peaked at 170 ppt in 1974 before decreasing by 43 % to its 2008 EESC. This peak in EESC occurs nearly 25 years before the peak in total EESC from inorganic halogen, which occurred in 1997 (*Montzka et al.*, 2010). This is due to the fact that the anthropogenic sources of the bromocarbons were controlled much earlier than other halogenated compounds (*Santodonato et al.*, 1985), because the bromocarbons emissions where not controlled because of their ozone depletion potential. This peak also occurs before 1980, which is important because the EESC value in 1980 is used as an important benchmark for ozone recovery (*Montzka et al.*, 2010). Therefore, these bromocarbons were having a significant anthropogenic effect on the ozone layer before this important benchmark. In 1980, the EESC value from these VSL bromocarbons was 160 ppt which is around 13 % of the 1200 ppt EESC value used in the last Scientific Assessment of Ozone Depletion as the 1980 benchmark for mid-latitude stratosphere from surface measurements (*Montzka et al.*, 2010).

Before 2004, the observed declines in EESC values was mainly a result of the decline in the shorter-lived gases CH_3CCl_3 and CH_3Br (*Clerbaux and Cunnold et al.*, 2006). This is also the period of the greatest decrease in EESC from the VSL bromocarbons. However between 2005 and 2008, no single chemical class dominated the decline in the total combined abundance of ozone-depleting halogen (Table 4.10) (*Montzka et al.*, 2010).

Table 4.10: Changes in EESC values between 2005 and 2008 based on *Montzka et al.* (2010)

Compounds	Change in EESC 2005 -2008 (ppt)
CFCs	-17
CH_3CCl_3	-20
CH_3Br	-24
CCl_4	-10
Halons	-4
HCFCs	+6
VSL bromocarbons[#]	-0.9

This study

Table 4.10 shows that the VSL bromocarbons observed in this study have decreased only very slightly between 2005 and 2008 especially compared to the other halogenated compounds. Therefore the VSL bromocarbons are not likely to have much effect on future changes of total EESC, unless there is a significant change in their emissions patterns.

Figure 4.24 shows that CH_2Br_2 has the largest EESC of the VSL bromocarbons with 60 ppt in mid-2008. This is in general agreement with the findings of *Montzka et al.* (2010) who observed that CH_2Br_2 has the greatest effect on the stratospheric ozone of the VSL bromocarbons. The VSL bromo-chloro methanes have a total EESC of 6 ppt in mid-2008 with the largest contribution from $CHBr_2Cl$ (3 ppt EESC) $CF_3CHBrCl$ is shown at its peak to contribute 1.0 ppt of EESC in 1985 before declining to 0.2 ppt in mid-2008.

As well as equivalent effective stratospheric chlorine, it is important to assess the stratospheric bromine mixing ratios of the VSL bromocarbons. This was calculated by reducing the surface bromine mixing ratios by the reduction factors in Table 4.9. The 2008 stratospheric bromine contributions from the VSL bromocarbons source gases are shown in Table 4.11 as well as the EESC mixing ratio.

Table 4.11: EESC and stratospheric bromine from the VSL bromocarbons and halothane

Compounds	EESC in 2008 (ppt)	Stratospheric bromine in 2008 (ppt)
CH_2Br_2	63	1.0
CH_2BrCH_2Br	4	0.06
C_2H_5Br	21	0.4
CH_2BrCl	1	0.02
$CHBr_2Cl$	3	0.05
$CHBrCl_2$	2	0.04
$CF_3CHBrCl$	0.2	0.01
$CHBr_3$[#]	16.2	0.27
Total	110	1.9

taken from *Montzka et al.* (2010)

Table 4.11 shows that the VSL bromocarbons provide 1.9 ppt of stratospheric bromine in 2008. This agrees with the *Montzka et al.* (2010) who estimated that the VSLS bromine source gases, including unmeasured species (this includes CH_2BrCH_2Br and C_2H_5Br), account for about 1.5 (0.7–3.4) ppt at the tropical cold point tropopause. Although, the observation in this study where from polar regions and not from the tropics.

It should also be noted that the EESC and stratospheric bromine in the current study might be an underestimate as the calculations do not account for any product gas injection from the VSL bromocarbons. With, *Hossaini et al.* (2010), *Aschmann et al.* (2009) and *Sinnhuber and Folkins* (2005), modelling significant contribution to stratospheric halogen mixing ratios from product gas injection.

4.7 Summary

In this chapter, I have reported observations of the bromocarbons from northern hemispheric and southern hemispheric firn air, and presented the derived atmospheric time series from the mid-20th century up until mid-2008 when the firn air was collected. Table 4.12 summarises the atmospheric time series, growth rates, emissions and EESC for the individual gases covered in this study.

I have provided the first detailed northern hemispheric atmospheric time series from 1930 to 2008 for CH_2Br_2, CH_2BrCH_2Br, C_2H_5Br, CH_2BrCl, $CHBr_2Cl$, $CHBrCl_2$ and $CF_3CHBrCl$. I have shown that all of these compounds apart from $CF_3CHBrCl$ have significant 1930 atmospheric mixing ratios. Since 1930 all of the reported gases have shown significant growth before a decline. The rate of this decline has slowed significantly since 2000.

Even though the bromocarbons have small atmospheric mixing ratios, I have shown that they do significantly add to the destruction of stratospheric ozone from halogenated compounds. This appears especially true before the 1980 bench-make, which means they represent an important set of compounds to the atmospheric chemical composition. Currently, these compounds contributed 94 ppt of EESC to the atmosphere and I suggest this value is unlikely to change significantly in the near future (discussed in more detail in Chapter 6).

These results also indicate that it would be desirable to minimise future anthropogenic emissions and that further studies, which should include observations from global ground-based networks, are needed to improve the understanding of the emission processes, patterns and the global distribution of the bromocarbons.

Table 4.12: Summary of the bromocarbons.

Compound	Modelled 1930 mixing ratio (ppt)	Mid–2008 mixing ratio (ppt)	2007 Growth rate (ppt yr^{-1})	Maximum annual emission (Gg yr^{-1})	Date of maximum annual emission	2008 Equivalent effective stratospheric chlorine (ppt)	Key Finding
CH_2Br_2[#]	1.1	1.0	-0.007	34	1979	63	A small but significant decline in northern hemispheric emissions since 1980
CH_2BrCH_2Br[#]	0.2	0.07	0.001	18	1970	4	The major source is from its use as an additive in leaded petrol
C_2H_5Br[†]	1.6	1.0	0.01	53	1976	21	Emissions have remain constant since 2000
CH_2BrCl[†]	0.17	0.10	-0.009	6	1970	1	Emissions strongly reflected it use in fire extinguishers
$CHBr_2Cl$[†]	0.15	0.15	0.0	7	1992	3	Similar emissions source as $CHBrCl_2$
$CHBrCl_2$[†]	0.24	0.25	0.0	9	1992	2	Similar emissions source as $CHBr_2Cl$
$CF_3CHBrCl$[#]	0.0	0.005	-0.0003	0.5	1984	0.2	Emissions strongly reflected it use in the medical profession

'Global'

† Northern Hemisphere

Chapter 5: Analysis of fluorinated greenhouse gas measurements from firn air extracted at the North Greenland Eemian Ice Drilling site

5.1 Introduction

In this study firn air samples collected from the North Greenland Eemian Ice Drilling (NEEM), were analysed for a number of fluorinated compounds by a GC- MS autospec, and their atmospheric histories were reconstructed with the help of a 1-dimensional firn diffusion model and an iterative dating technique. In this chapter the atmospheric time series of several fluorinated compounds are discussed.

The fluorinated compounds studied in this investigation are all part of the group of chemicals known as the fluorinated greenhouse gases (the so-called "F-Gases") and include the hydrofluorocarbons (HFCs), perfluorocarbons (PFCs) and the fully-fluorinated sulphated compounds. These compounds are very stable, non-toxic and virtually entirely of anthropogenic origins and the HFCs are also used mainly as replacements for the CFCs (*Montzka et al.*, 2010).

Although the fluorinated greenhouse gases do not damage the ozone layer like the CFCs that they replace, they are very effective absorbers of infrared radiation, so that even small amounts of these gases contribute significantly to the radiative forcing of the climate system (*Forster et al.*, 2007). Combined with the fact they are generally long-lived in the atmosphere they have the potential become powerful greenhouse gases. In this chapter, discussions are limited to the following compounds: the fully-fluorinated sulphated gases (SF_6 and SF_5CF_3) the perfluorocarbons (n-C_4F_{10}, n-C_5F_{12}, n-C_6F_{14} and n-C_7F_{16}) and one novel hydrofluorocarbon (HFC-32).

All of these fluorinated greenhouse gases, except SF_5CF_3, are included in the Kyoto Protocol (*deBoer*, 2007) and therefore there is a need to understand how these gases, have evolved over time, identifying the anthropogenic contributions to their atmospheric abundance and to enforce mitigation options to reduce its emissions.

The principal objective of this study is to provide the longest reconstructed atmospheric histories of the PFCs and HFC-32 and also to provide updated trends of the fully-fluorinated sulphated compounds. These reconstructed time series are then compared with atmospheric time series from previous firn air studies and as well as with ambient atmospheric observations and measurements from air archives. This study provides insights into the growth rates of these compounds, the date of first significant atmospheric abundance and emissions estimated from the growth rates obtained, as well as accessing the effect these greenhouse gases have on the atmospheric energy budget by estimating their equivalent CO_2 emissions.

Each subsection in this chapter has its own background information, results and discussion on the atmospheric time series from firn data and estimated emissions predicted from the reconstructed time series. At the end of the chapter, the equivalent CO_2 emissions are calculated for all compounds investigated in this chapter.

5.2 Fully-fluorinated sulphated compounds (SF_6 and SF_5CF_3)

In recent years, the atmospheric growth of a number of fully-fluorinated sulphated and very long lived (τ > 1000 years) greenhouse gases or "super" greenhouse gases, has been studied (e.g. *Levin et al.* (2010) (SF_6) and *Sturges et al.* (2012) (SF_5CF_3)). These gases have exceptionally high Global Warming Potentials (GWPs), on the order of several thousand times that of CO_2, and thus their unconstrained growth would be of considerable concern for the radiative forcing of the atmosphere. In this section, I have analysed the atmospheric time series of SF_6 and SF_5CF_3 and calculate how emission rates have changed over time.

5.2.1 Background information on SF_6

Sulphur hexafluoride (SF_6) is an extremely stable compound. It is essentially an anthropogenic gas as natural emissions are negligible, and is one of the strongest greenhouse gases on a per molecule basis and emissions have been targeted to be collectively reduced under the Kyoto Protocol. The main loss of atmospheric SF_6 is through destruction in the mesosphere (*Montzka et al.*, 2010) with an atmospheric lifetime of 3200 years (*Montzka et al.*, 2010). SF_6, also has a high radiative efficiency (0.52 W m^{-2} ppb^{-1} (*Forster et al.*, 2007)), this results in the largest recorded Global Warming Potential (GWP) (22800 for a 100 year time horizon (*Forster et al.*, 2007)) of any known atmospheric compound.

With a long atmospheric lifetime, around 99 % of all SF_6 emissions have accumulated and remain in the atmosphere. This permits a direct inference of global emissions based on observed changes in atmospheric mixing ratio (*Maiss and Brenninkmeijer*, 1998 and *Maiss and Levin*, 1994). Although, SF_6 has also been used as a tracer to compare and validate atmospheric transport models (*Patra et al.*, 2009 and *Levin and Hesshaimer*, 1996), emissions from this source are negligible. SF_6 is produced for use as an electrical insulating fluid in power distribution equipment (*Levin et al.*, 2010). Also traces of SF_6 have been shown to be produced in the Earth' crust, again emissions from its natural fluxes into the atmosphere are negligible (*Busenberg and Plummer*, 2000).

The industrial production of SF_6 began in 1953 for use as an insulation gas in high voltage installations (*Maiss and Brenninkmeijer*, 1998 and *Ko et al.*, 1993). Since then emissions from

the electricity sector (through leakage and venting) has been the largest source of SF_6 to the atmosphere (*Levin et al.*, 2010), with additional contributions from magnesium production, semiconductor manufacturing as well as other minor sources (*Olivier*, 2005).

Systematic long term measurements of SF_6 began in 1978 with a mixing ratio of 0.6 ppt recorded (*Fraser*, 2004), the lowest reported mixing ratio is, 0.24 ppt in 1976 (*Salas et al.*, 1977). *Butler et al.* (1999) measured SF_6 from firn air extracted from Arctic and Antarctic firn and derive an atmospheric time series from these measurements. This atmospheric time series indicates that it is most likely that significant emissions of SF_6 started in 1960. Since 1960, the SF_6 atmospheric mixing ratios increased monotonically year-on-year (*Forster et al.*, 2007). In 1998, the SF_6 concentration was reported at 4.2 ppt by *Law et al.* (2008). Global average mixing ratios of SF_6 reached 6.4 ppt in 2008 (NOAA, AGAGE (*Levin et al.*, 2010 and *Montzka et al.*, 2010)), with a yearly (2007–2008) increase of 0.2 ppt yr^{-1} (3%) (*Montzka et al.*, 2010), resulting in a contribution to radiative forcing of 3.4 mW m^{-2} by 2008. Global surface SF_6 mixing ratios and the corresponding annual changes have been observed by the AGAGE and NOAA networks. Similar global SF_6 growth rates have been derived from the MIPAS satellite data in 2002 – 2004 (*Stiller et al.*, 2008) and from solar spectroscopy (*Zander et al.*, 2008). Emissions estimate of SF_6 have been derived from a "bottom-up" approach by the Emission Database for Global Atmospheric Research (EDGAR) (*Olivier et al.*, 2010) and a "top-down" observations based approach by *Levin et al.* (2009).

In this study I have derived atmospheric time series of SF_6 from firn air measurements taken at the NEEM firn site (Greenland). Also since SF_6 has a monotonic atmospheric time series and a time series that has been previously published tracking its atmospheric mixing ratio back to zero, these previously observed time series will help to validate both the firn air measurements from the NEEM site as well as the methods used to derive the corresponding atmospheric time series.

5.2.2 Results and discussion of SF_6

An atmospheric time series was derived from the observed concentrations with firn depth profile measured at the NEEM site, using an iterative modelling approach as described in *Trudinger* (2002) as well as in Chapter 2. This method requires essentially no presumptions about the atmospheric time series, other than the compound increases monotonically from negligible abundances to the known present day mixing ratios. The SF_6 mixing ratio time series obtained and the output from the model for the NEEM site are shown in Figure 5.1 alongside the measured concentration of SF_6 with depth.

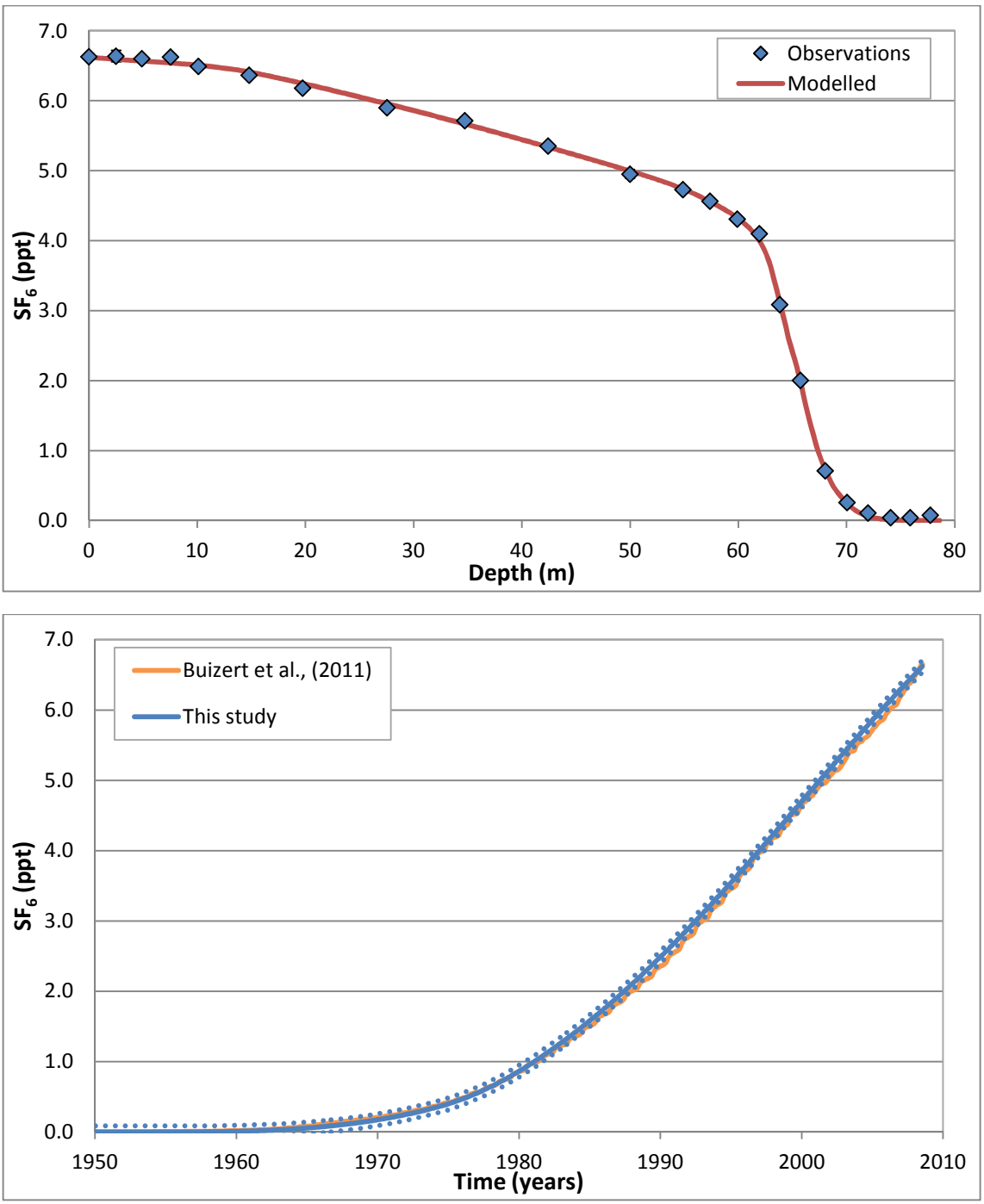

Figure 5.1: Top panel, depth profiles of SF_6 firn air measurements (points), compared with model simulations based on the atmospheric time series indicated in the bottom panel. Although the error bars represent the 1 σ of the measurements (See Chapter 2 for more details), most of the error bars are smaller than the points so cannot be seen. Bottom panel, atmospheric time series based on the NEEM firn air measurements (blue line) using the *Trudinger* (2002) method (See Chapter 2 for more details). The dashed lines consist of the sum of a) the firn air model maximum and minimum runs obtained by adding and subtracting the 1 σ of the measurements to/from the firn data and b) the maximum deviation of the measured mixing ratios from the polynomial fitted used to derive the NH time series. This error analysis is based on *Laube et al.* (2012). The SF_6 atmospheric time series (orange line) from *Buizert et al.* (2011) is given as a comparison.

The atmospheric mixing ratio time series derived in the current study and shown in Figure 5.1 indicate that significant SF_6 emissions (emissions that produce an observable atmospheric mixing ratio) started in the early 1960s. This is consistent with the atmospheric time series produced by *Buizert et al.* (2011) and *Butler et al.* (1999), and agrees with the start of industrial production of SF_6 in 1953 (*Maiss and Brenninkmeijer*, 1998 and *Ko et al.*, 1993). This indicates that SF_6 originates from entirely anthropogenic sources. The derived atmospheric time series shows a sustained growth in mixing ratios SF_6 since the early 1960s until mid-2008 when the firn air was collected (Figure 5.1).

The calculated growth rate accelerated from 0.06 ppt yr^{-1} in 1975 to 0.16 ppt yr^{-1} by 1985 and again to 0.22 ppt yr^{-1} in 1995 (Figure 5.1). This is in general agreement with the atmospheric time series produced by *Buizert et al.* (2011) (orange line – Figure 5.1) which is based on observations made by the N*ational Oceanic and Atmospheric Administration (*NOAA) and *Advanced Global Atmospheric Gases Experiment* (AGAGE) networks. As well as agreeing with the *Levin et al.* (2010) observed atmospheric time series. After 1995, the average growth rate is calculated to have remained comparatively constant (0.23 ppt yr^{-1} in 1996 to 0.22 ppt yr^{-1} in 2007). This is consistent with the introduction of SF_6 emissions controls in 1994 as part of the UNFCCC agreement (*deBoer*, 2007). As the firn air used for the current analysis was collected in July 2008, an average growth rate cannot be provided for 2008. However the mixing ratios indicate a period of increase up to this date.

The global mixing ratios observed from surface measurements and the corresponding annual changes can be found in Table 5.1. The data from a number of different studies are highly consistent, despite a range of different methodologies used (MIPAS satellite data in 2002 – 2004 (*Stiller et al.*, 2008) and from solar spectroscopy (*Zander et al.*, 2008)).

Table 5.1: Mean mixing ratio and growth rates of SF_6

Mixing Ratio (ppt)	Growth Rate (ppt yr^{-1})	Date	Reference
6.4#	0.2#	2007	This Study
6.2	0.3	2007	*Montzka et al.* (2010)
6.2	0.3	2007	*Levin et al.* (2010)
	0.2	2004	*Stiller et al.* (2008)
	0.3	2004	*Zander et al.* (2008)

Northern hemispheric mixing ratios

However, the SF_6 mixing ratio observed in the current study is slightly larger than the global surface mean mixing ratio observed by the AGAGE and NOAA networks (*Levin et al.*, 2010 and *Montzka et al.*, 2010). This is not unexpected result as observations from the NEEM site in the northern hemisphere typically give greater mixing ratios than the global average mixing ratios (*Levin et al.*, 2010). In July 2008, the surface mixing ratio of SF_6 was observed to be 6.62 ppt at the NEEM site. The NEEM observation is consistent with the monthly mean of 6.63 ppt observed at the Barrow, Alaska, Observatory (71.3 N, 156.6 W, elevation: 8m) in the same month (*Hall et al.*, 2012). The northern hemispheric growth rate observed in this study however is less than the *Montzka et al.* (2010) and *Levin et al.* (2010) observed global growth rates. It should also be noted that the growth rates and mixing ratios observed in this study represent only the best estimates and contain considerable uncertainties within the envelopes shown in Figure 5.1.

5.2.3 Background information on SF_5CF_3

Trifluoromethyl sulphur pentafluoride (SF_5CF_3) is a colourless, odourless and incombustible gas under normal conditions. It also possesses a high chemical stability and excellent dielectrical characteristics. SF_5CF_3 was first detected in the atmosphere by *Sturges et al.* (2000) and was shown to be anthropogenic in nature. *Sturges et al.* (2000) suggested that emissions of SF_5CF_3 were related to SF_6, through the possible formation from high energy arc discharge in electrical equipment containing SF_6 as a high voltage dielectric. This suggested source was supported by a number of subsequent studies (e.g. *Solovev et al.*, 2007 and *Huang et al.*, 2005). However, the most up-to-date data shows this process not to be as large as a source as initially reported (*Sturges et al.*, 2012). Current thinking is that the main source of atmospheric SF_5CF_3 is a by-product of the manufacture of certain 3M fluorochemicals (*Sturges et al.*, 2012 and *Santoro*, 2000). SF_5CF_3 is produced during the process of electrochemical fluorination for the production of perfluorooctanyl sulphonate, (PFOS) and other fluoro surfactants used in the manufacture of foams and stain-resist coatings (*Sturges et al.*, 2012).

As SF_5CF_3 is fully-fluorinated, it is very stable thus has a very long atmospheric lifetime of 650 – 950 years (*Montzka et al.*, 2010). Measurements of its infrared absorption cross section show SF_5CF_3 to have a radiative forcing of 0.57 Wm^{-2} ppb^{-1} (*Forster et al.*, 2007). This is the largest radiative forcing, on a per molecule basis, of any gas found in the atmosphere to date (*Sturges et al.*, 2012). This results in a GWP_{100} of 17700 relative to CO_2, with only SF_6 having a higher value (*Forster et al.*, 2007). Therefore, it is important to monitor SF_5CF_3 emissions into the atmosphere in order to prevent an undesirable accumulation of this greenhouse gas. However,

it is worth noting that SF_5CF_3 was calculated to contribute just 0.003 % in 2002 to the total greenhouse effect (*McCulloch*, 2003).

Sturges et al. (2000) demonstrated that the mixing ratio of SF_5CF_3 started to increase in the atmosphere from near zero in the late 1960s. This is consistent with large-scale manufacture of PFOS having begun after 3M acquired the patent for electrochemical fluorination in the 1950s (*Sturges et al.*, 2012). After the 1970s, the SF_5CF_3 mixing ratios increased at a rate of about 0.008 ppt yr^{-1} or 6 % per year until 1999 when the mixing ratio reached 0.12 ppt (*Busenberg and Plummer*, 2008 and *Sturges et al.*, 2000). After 2000, there are mixed reports regarding the SF_5CF_3 atmospheric mixing ratio. *Rosiek et al.* (2007) reported a continuing upward trend between 2001 and 2003 in Krakow, Poland. However, *Busenberg and Plummer* (2008) reported an apparent subsequent slow-down in the growth rate after 2000 from various sites in North America. *Sturges et al.* (2012) reported evidence for an unambiguous decrease in the atmospheric growth rate of SF_5CF_3 starting in 2000 and declining rapidly such that an emission rate of zero or almost zero is inferred after 2003.

These observations are consistent with the phasing-out of 3M PFOS manufacture in 2000 (statement on "3M's Phase Out and New Technologies" (*3M*, 2012)). As well as the overall reduction in greenhouse gas emissions (not just SF_5CF_3) since 1995 (*Santoro*, 2000). The phasing-out of PFOS was supposedly completed in 2002 (*3M*, 2012).

5.2.4 Results and discussion of SF_5CF_3

An atmospheric time series was derived from the observed concentrations with firn depth profile measured at the NEEM site, using an iterative modelling approach as described earlier. The SF_5CF_3 mixing ratio time series obtained and the output from the model for the NEEM site are shown in Figure 5.2 alongside the measured concentration of SF_5CF_3 with depth.

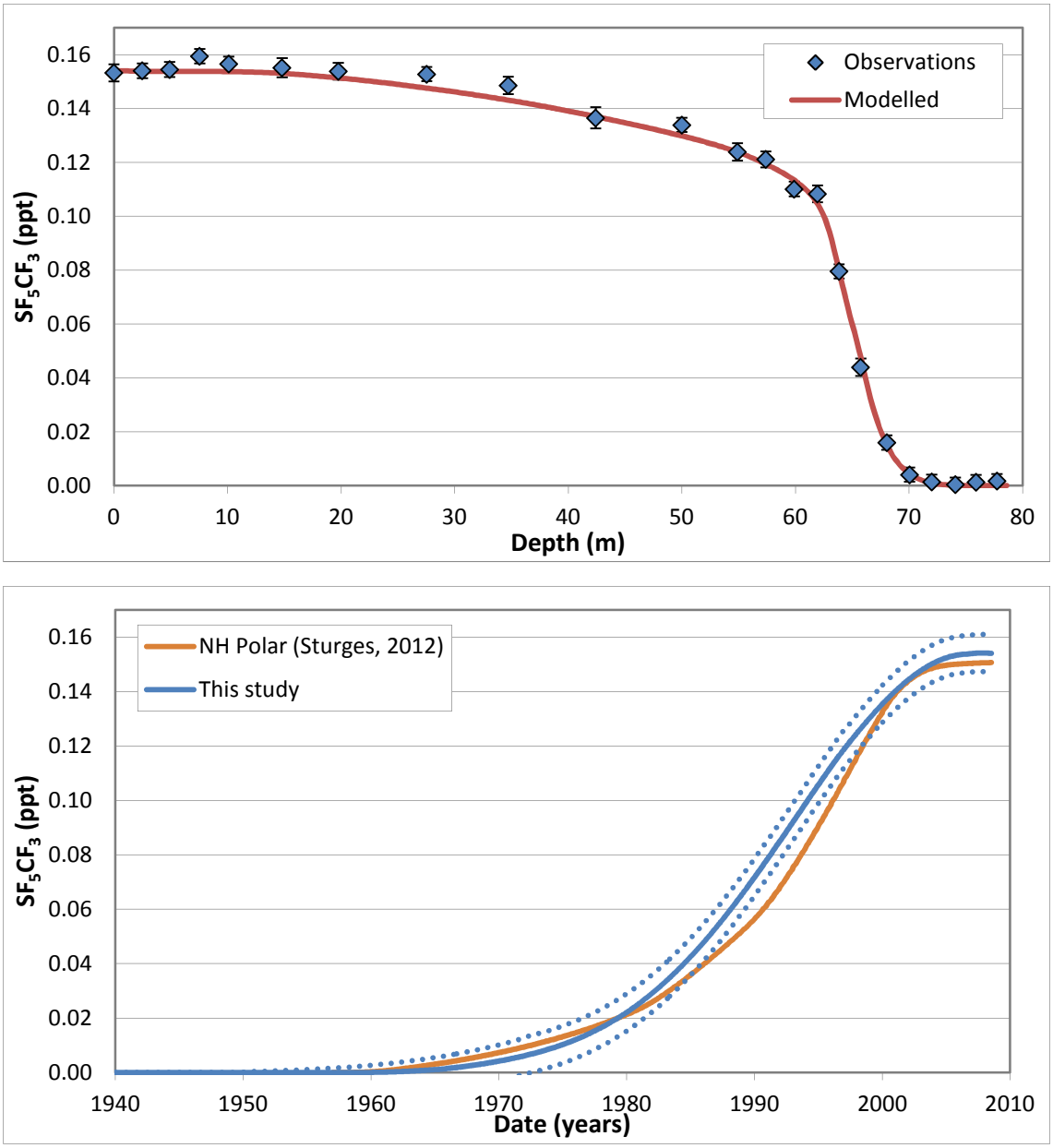

Figure 5.2: Top panel, depth profiles of SF_5CF_3 firn air measurements (points), compared with model simulations based on the atmospheric time series indicated in the bottom panel. The error bars represent the 1 σ of the measurements (See Chapter 2 for more details). Bottom panel, atmospheric time series based on the NEEM firn air measurements (blue line) using the *Trudinger* (2002) method. The dashed lines represent the errors in the time series as described in Figure 5.1. The northern hemispheric polar region atmospheric time series (orange line) from *Sturges et al.* (2012) is given as a comparison.

Figure 5.2 shows that the SF_5CF_3 NEEM firn air data has good measurement precisions and reveals that concentrations were decreasing almost monotonically with increasing depth. The atmospheric mixing ratio time series derived in the current study and shown in Figure 5.2 also indicates that significant SF_5CF_3 emissions (emissions that produce an observable atmospheric mixing ratio) started in the early 1960s. This is in agreement with the large-scale manufacture of PFOS which begun after 3M acquired the patent for electrochemical fluorination in the

1950s. The time series shows a sustained growth of SF_5CF_3 since the early 1960s until around 2000 when the growth rate dramatically decreases.

The average growth rate accelerated from 0.002 ppt yr^{-1} in 1975, to 0.005 ppt yr^{-1} in 1985 to 0.007 ppt yr^{-1} in 1995. This is in general agreement with the atmospheric time series derived by *Sturges et al.* (2012) using a 2-D global atmospheric chemistry-transport model (*Hough*, 1989) to derive a "top-down" emission estimate of SF_5CF_3, fitted to observations made at the Cape Grim observation station (orange line, Figure 5.2). Although, *Sturges et al.* (2012) uses a different data set and a different method to derive their atmospheric time series to this study, both studies uses data that has been measured with the same techniques and placed on the same calibration scale. The atmospheric mixing ratios SF_5CF of during the 1990s observed in the time series derived in this study are slightly higher than the mixing ratios observed during this period in the *Sturges et al.* (2012) time series. This difference likely arises due to the limitations of the firn reconstruction which gives a smoothed trend, especially for reconstructions based on a single site with a limited number of data points and in deep firn where age mixing is strong. These limitations result in the firn reconstruction smoothing the slight step change in growth rates that occurs around 1990 in the *Sturges et al.* (2012) time series. This limitation of the firn method has been highlight in *Laube et al.* (2012).

After 2000, the average growth rate decreased rapidly from 0.005 ppt yr^{-1} in 2000 to 0.0004 ppt yr^{-1} in 2007. In 2008 the mixing ratio of SF_5CF_3 was observed to be 0.15 ppt. It should also be noted that growth rates and mixing ratios derived in the current study represent only the best estimates and contain considerable uncertainties within the envelopes shown in Figure 5.2. However, the observed time series for SF_5CF_3 mixing ratios is generally consistent with *Rosiek et al.* (2007) who reported a continuing upward trend between 2001 and 2003 in Krakow, Poland, and the apparent subsequent slow-down in the growth rate of SF_5CF_3 reported by *Busenberg and Plummer* (2008) from various sites in North America. It is also in agreement with the rate of decline modelled by *Sturges et al.* (2012).

5.2.5 Emissions of the fully-fluorinated sulphated compounds

Annual emissions of SF_6 and SF_5CF_3 were determined from the atmospheric time series detailed in Figure 5.1 and 5.2 with use of a 1 - box model, based on the method used by *Maiss and Brenninkmeijer* (1998) and *Maiss and Levin* (1994) (further details of the emission estimate process are given in Chapter 2). These annual emissions estimates are shown in Figures 5.3 and 5.4.

Emission estimate of SF_6 have been derived from a "top-down" observation-based approach (*Levin et al.*, 2009). *Levin et al.* (2009) used observations from four globally distributed observation stations and from meridional transects over the Atlantic Ocean to produce a global averaged SF_6 mixing ratio. The first temporal derivative of these global atmospheric SF_6 mixing ratios was taken to produce a direct observation-based estimate of global SF_6 emissions. Global annual SF_6 emissions have also been estimated by *Olivier et al.* (2010) using a "bottom-up" approach, based on statistical information on the sources and their global distribution. Both these emission estimates have been compared to the emission estimates derived in this study and are shown in Figure 5.3 as a comparison.

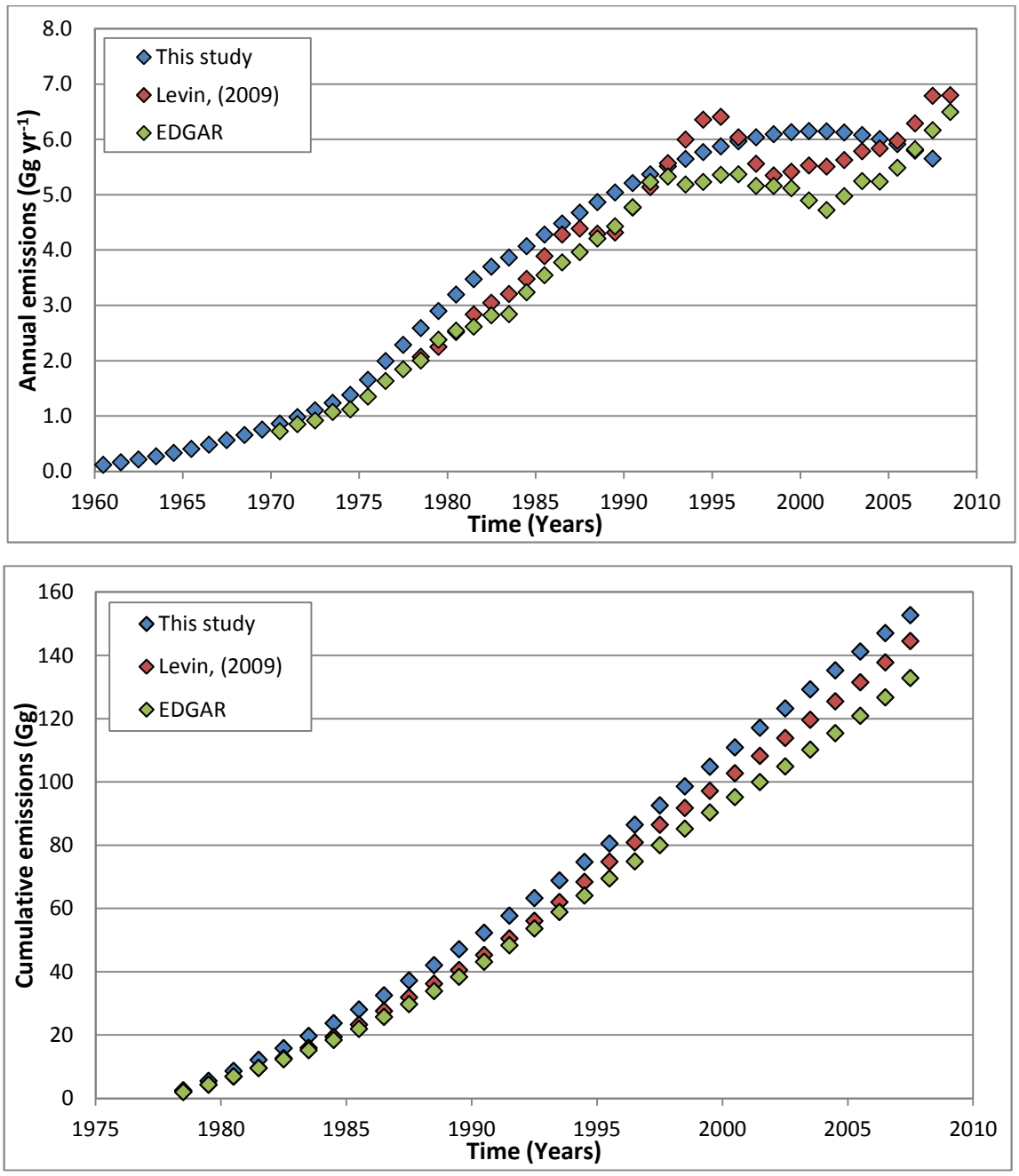

Figure 5.3: Top panel, annual emissions of SF_6 (blue points) based on the atmospheric time series in Figure 5.1. The emissions from *Levin et al.* (2009) (red points) and from EDGAR (*Olivier et al.*, 2010) are given as a comparison. Bottom panel, cumulative emissions since 1978 of SF_6 (blue points) based on the emissions in the top panel. The cumulative emission from *Levin et al.* (2009) (red points) and from EDGAR (*Olivier et al.*, 2010) since 1978 are given as a comparison. *Levin et al.* (2009) start estimating emissions in 1978 therefore the cumulative emissions have been shown since 1978.

Estimates from the current study shows that emissions of SF_6 estimated by this study rose year-on-year from the 1960s to around 1990, increasing from ~ 1 Gg yr^{-1} in 1970 to ~ 5 Gg yr^{-1} in 1990. In 1994, when the United Nations framework convention on climate change (UNFCCC) agreement went into force (*deBoer*, 2007), the growth rate of global SF_6 emissions slowed. Estimated global emissions peak in 1998 at ~6 Gg yr^{-1}. These emission estimates generally agree with the emissions estimates by *Levin et al.* (2009) and EDGAR (*Olivier et al.*, 2010)

(Figure 5.3). However, the emissions produced from the current firn air derived time series are smoothed due to the processes discussed earlier. This results in features such as the timing and the value of the peak emission from the firn air derived time series being smoothed. In addition, *Laube et al.* (2012) notes that the uppermost part of the firn and the surface measurements are of samples which does not fully represent the average composition of the atmosphere. This is due to the fact that the surface measurements are only taken as 'grab' samples and not an observation of the average atmospheric mixing ratio. However, the firn air modelling uses the surface measurements as the average atmospheric of the compound. Therefore a direct comparison cannot be made between the obverted average atmospheric mixing ratio in recent years and the firn air derived atmospheric time series. This could explain why the emissions do not show an increase in 2007 as reported by *Levin et al.* (2009) and EDGAR (*Olivier et al.*, 2010) in which *Levin et al.* (2009) use the average atmospheric mixing ratios of SF_6 and *Olivier et al.* (2010) uses reported industrial emissions. Also as stated earlier the growth rate in 2007 was smaller than observed growth rates from other studies and as the emission estimate is based on the growth rate, this is likely where the discrepancies originates.

The cumulative emissions since 1978 are shown in Figure 5.3. The 1978 start date is used because that is when the *Levin et al.* (2009) emissions estimates begin. The comparison of the cumulative emission since 1978 (Figure 5.3) confirms that there is a generally agreement between the emission estimates. The emission estimate derived in this study are slightly higher than those by *Levin et al.* (2009) and EDGAR (*Olivier et al.*, 2010). Cumulative emission of SF_6 dating back to 1950 (when the firn derived time series begin) show that there has been 170 Gg of SF_6 emissions up to 2007. This indicates that there was 20 Gg of SF_6 emitted between 1950 and 1978.

Emission estimates of SF_5CF_3 derived in the current study are shown in Figure 5.6 for comparative purposes, this data is illustrated alongside the data set of *Sturges et al.* (2012). The emission estimates of SF_5CF_3 of *Sturges et al.* (2012) were derived from a "top-down" observations based approach using Cape Grim data and a 2-D atmospheric chemistry-transport model (*Oram et al.*, 2011 and *Laube et al.*, 2010). This has been proven to reproduce well-known emissions of long-lived compounds emitted mainly in the northern hemisphere when constrained by southern hemispheric observations (*Reeves et al.*, 2005).

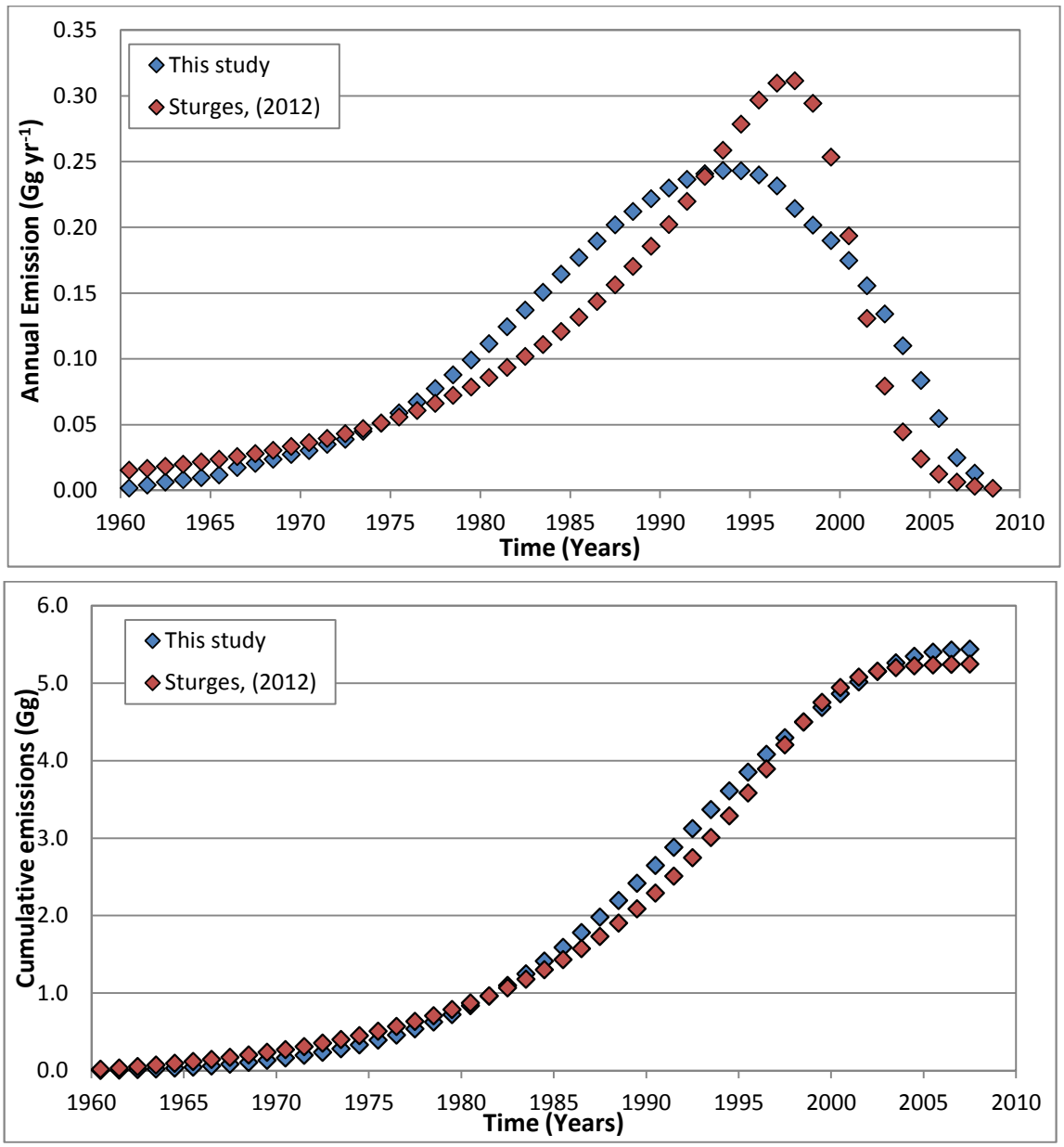

Figure 5.4: Top panel, annual emissions of SF_5CF_3 (blue points) based on the atmospheric time series in Figure 5.2. The annual emissions from *Sturges et al.* (2012) is given as a comparison (red points). Bottom panel, cumulative emission of SF_5CF_3 (blue points) based on the emissions in the top panel. *Sturges et al.* (2012) cumulative emissions are again shown as a comparison.

Figure 5.4 shows that the emissions estimates derived in this study generally agree with the emissions derived by *Sturges et al.* (2012) (Figure 5.4). However the emissions derived from the firn air time series are smoothed due to the processes discussed earlier. This will result in some features such as the timing and the value of the peak emission from the firn air derived time series being smoothed. The emission estimates derived in this study only agree slightly with the emissions report by industry. Industrial emissions are reported to have begun in the 1960s (*3M*, 2012), and phasing-out of emissions in 2000, which was supposedly completed in 2002 (*3M*, 2012). Whereas this studies emission estimates indicate a beginning of phasing-out

around 1995. Again this could be due to the smoothing effect of the firn air derived time series, which will decrease the rate of the rapid decline in industrial emissions.

These results corroborate previous studies that show that there was indeed a rapid decline in emissions between 2000 and 2003 and that current emissions are very small. Though the uncertainties in the observations preclude from determining whether emissions have actually now ceased. Industries having now switched to producing perfluorobutane sulfonate (PFBS), which does not release SF_5CF_3 instead of PFOS which do (*3M*, 2012 and *Renner*, 2006). However a number of companies worldwide continue to manufacture related PFOs (*Renner*, 2006), it appears from the observations, that this occurs without incurring substantial emissions of SF_5CF_3. Comparisons between the key findings of fully-fluorinated sulphated compounds are shown in Table 5.2.

Table 5.2: Comparison of the key findings of the fully-fluorinated sulphated compounds

Compound	Mid -2008 mixing ratio (ppt)	2007 emission estimate (Gg yr^{-1})	Total emission up to 2007 (Gg)
SF_6	6.6	6	170
SF_5CF_3	0.2	0.01	5
Total	6.8	6.01	175

Table 5.2 indicates that SF_6 contributes 97 % of the total emission of the fully-fluorinated sulphated compounds. Table 5.2 also shows that emissions are non-zero and given a large τ we can infer that SF_6 is continuing to increase. Current SF_5CF_3 emissions are almost zero. As such, SF_6 is becoming relatively more important to the energy balance of the atmosphere. Both of these emissions represent an essentially irreversible change to the composition of the Earth's atmosphere.

5.3 Perfluorocarbons (n-C_4 to n-C_7)

Perfluorocarbons (PFCs) are fully fluorinated hydrocarbons which have very long atmospheric lifetimes and very high GWPs in the case of the fluoroalkanes (*Bravo et al.*, 2010 and *Forster et al.*, 2007). Their production and emission are regulated under the Kyoto Protocol to the United Nations Framework Convention on Climate Change (UNFCCC) (*deBoer*, 2007). Due to their long lifetimes and strong absorption in the infrared, PFCs are considered to have a permanent effect on the Earth's radiative budget. In this section, the atmospheric time series of four PFCs; n-decafluorobutane (n-C_4F_{10}), n-dodecafluoropentane (n-C_5F_{12}), n- tetradecafluorohexane (n-

C_6F_{14}) and n-hexadecafluoroheptane (n-C_7F_{16}), are analysed and calculations of their emissions rates over time presented.

5.3.1 Background information on n-C_4F_{10}, n-C_5F_{12}, n-C_6F_{14} and n-C_7F_{16}

The PFCs are very stable compounds and have very long lifetimes in the atmosphere, 2600 years (*n*-C_4F_{10}), 4100 years (*n*-C_5F_{12}) and 3200 years (*n*-C_6F_{14}) (*Forster et al.*, 2007). In addition, they have high radiative efficiencies, 0.33 Wm^{-2} ppb^{-1} (*n*-C_4F_{10}), 0.41 Wm^{-2} ppb^{-1} (*n*-C_5F_{12}) and 0.49 Wm^{-2} ppb^{-1} (*n*-C_6F_{14}) (*Forster et al.*, 2007). These high radiative efficiencies and long lifetimes result in large GWPs of, 8860 (*n*-C_4F_{10}), 9160 (*n*-C_5F_{12}) and 9300 (*n*-C_6F_{14}) on a 100-yr time horizon (*Forster et al.*, 2007). There has not yet been any measurement of GWP for *n*-C_7F_{16}. However, *Laube et al.* (2012) noted that the GWP for *n*-C_7F_{16} is likely to between 8000 and 10000. This means that even comparably small emissions of these PFCs can result in significant and long-lasting effects on atmospheric radiative forcing.

The atmospheric sources of the PFCs in the current investigation are entirely anthropogenic, with *n*-C_4F_{10} and *n*-C_5F_{12} being used or proposed for use as refrigerants, in air conditioning, as fire suppressants and in semiconductor manufacturing (*Olivier et al.*, 2010, *IPCC/TEAP et al.*, 2005, *Mazurin et al.*, 1995 and *Robin and Iikubo*, 1992). The PFCs *n*-C_6F_{14} and *n*-C_7F_{16} have been reported to be used as solvents and as heat transfer fluids (*Waugh et al.*, 2011 *Olivier et al.*, 2010 and *Stone and Springer Jr*, 1995).

Emission estimates of these PFCs have been derived from a “bottom-up” approach by the Emission Database for Global Atmospheric Research (EDGAR) (*Olivier et al.*, 2010) and a “top-down” observations based approach by *Laube et al.* (2012). Theses PFCs were modelled to be first detected in the atmosphere between the late 1960s and early 1970s (*Laube et al.*, 2012). Whereas, *Ivy et al.* (2012) observed n-C_6F_{14} and n-C_7F_{16} in detectable abundances in archived samples from the AGAGE network dated after 1985. The mixing ratios of all of the PFCs have increased monotonically year-on-year from zero to the most recent observation in 2010-2011 (*Ivy et al.*, 2012 and *Laube et al.*, 2012). Both *Ivy et al.* (2012) and *Laube et al.* (2012) observe a slowing down in the growth rates of the PFCs in the atmosphere in the mid-1990s, which relates to a decrease in emissions rates during this period.

5.3.2 Results and discussion of n-C_4F_{10}, n-C_5F_{12}, n-C_6F_{14} and n-C_7F_{16}

An atmospheric time series was derived for, *n*-C_4F_{10}, *n*-C_5F_{12}, *n*-C_6F_{14} and *n*-C_7F_{16} from the measured concentrations at the NEEM firn site and firn depth profile using an iterative modelling approach as described earlier. This measured concentrations and firn depth profile have been taken from *Laube et al.* (2012). The time series obtained and the output from the model for the NEEM site are shown in Figure 5.5 alongside the actual measurements as a function of depth.

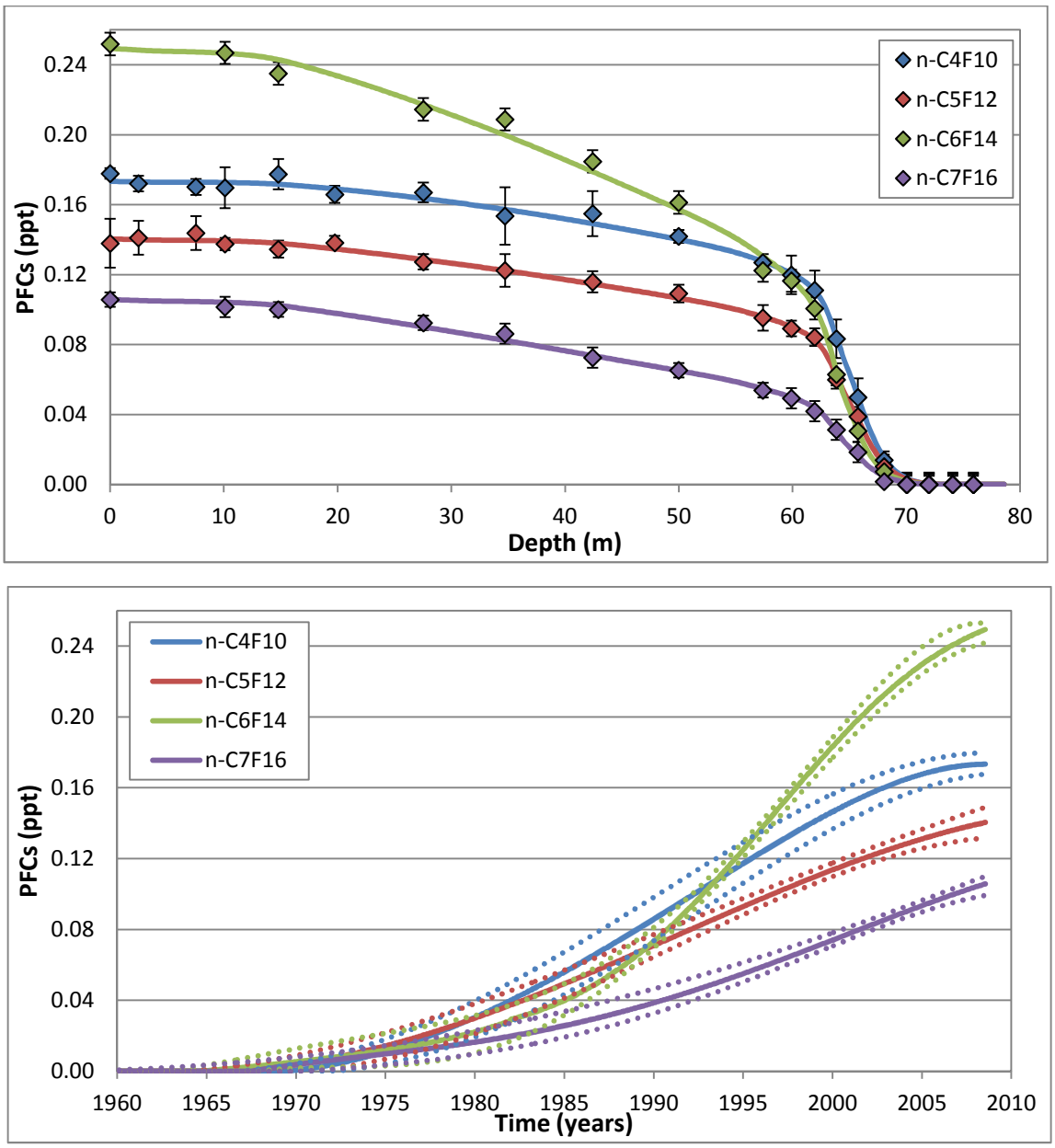

Figure 5.5: Top panel, depth profiles of; n-C_4F_{10} (blue points), n-C_5F_{12} (red points), n-C_6F_{14} (green points) and n-C_7F_{16} (purple points) firn air measurements (measurements taken from *Laube et al.* (2012)), compared with model simulations based on the atmospheric time series indicated in the bottom panel. The error bars represent the 1 σ of the measurements (See Chapter 2 for more details). Bottom panel, atmospheric time series based on the NEEM firn air measurements; n-C_4F_{10} (blue line), n-C_5F_{12} (red line), n-C_6F_{14} (green line) and n-C_7F_{16} (purple line) using the *Trudinger* (2002) method. The dashed lines represent the errors in the time series as described in Figure 5.1.

Figure 5.5 shows that significant *n*-C_4F_{10}, *n*-C_5F_{12}, *n*-C_6F_{14} and *n*-C_7F_{16} emissions (emissions that produce an observable atmospheric mixing ratio) started in the 1960s. This indicates that these PFCs are of entirely anthropogenic origins. The compounds *n*-C_4F_{10} and *n*-C_5F_{12} became detectable in the atmosphere in 1969 and 1966, respectively. This is in agreement with the *n*-C_4F_{10} and *n*-C_5F_{12} atmospheric time series derived by *Ivy et al.* (2012). However, there are discrepancies between the firn air derived time series of this study and those of *Ivy et al.* (2012). In this study the *n*-C_6F_{14} and *n*-C_7F_{16} time series show significant mixing ratio beginning

in 1961 and 1962 respectively, whereas *Ivy et al.* (2012) only detected significant mixing ratios in the late 1960s. The time series in this study show sustained growth of the PFCs since the late 1960s until mid-2008 when the firn air was collected.

The northern hemisphere atmospheric time series derived in this study are in good agreement with the archived record from Cape Grim, Tasmania (*Laube et al.*, 2012). This shows atmospheric mixing ratios of the PFCs increasing monotonically year-on-year from zero until mid-2008. However *Laube et al.* (2012) observed a steep increase in growth rate of *n*-C_6F_{14} in the Cape Grim archive from the late 1980s to the 1990s, which is not shown in the current NEEM time series. This difference is likely a result of the limitations of the current firn air reconstruction which gives a smoothed view of reality, especially for reconstructions based on a single site with a limited number of data points in deep firn where age mixing is strong (*Laube et al.*, 2012). There is good agreement for the mixing ratio abundances and trends for all compounds from 2000 onwards. After 2000, *n*-C_4F_{10}, *n*-C_5F_{12} and *n*-C_6F_{14} show signs of mixing ratios beginning to level off in the atmosphere. In contrast, there is no evidence of *n*-C_7F_{16} mixing ratios of shows no signs of beginning to level off. The atmospheric mixing ratios observed at the NEEM site in mid-2008 are shown in Table 5.3, as well as recent observations from *Ivy et al.* (2012) and *Laube et al.* (2012).

Table 5.3: Recent atmospheric mixing ratio of the PFCs

Reference	This Study	*Laube et al.* (2012)	*Ivy et al.* (2012)
Date	2008.5	2010	2011
Measurement region	Northern Hemisphere	Southern Hemisphere	Global average
n-C_4F_{10}	0.18	0.171	0.18
n-C_5F_{12}	0.14	0.141	0.12
n-C_6F_{14}	0.25	0.253	0.28
n-C_7F_{16}	0.11	0.105	0.12

Table 5.3 shows that the recent atmospheric mixing ratios for the PFCs observed in this study are in general agreement with those observed by *Ivy et al.* (2012) and *Laube et al.* (2012). Growth rates for the PFCs were inferred from the atmospheric time series (Figure 5.5) using the method presented in *Laube et al.* (2012). These growth rates are shown in Figure 5.6.

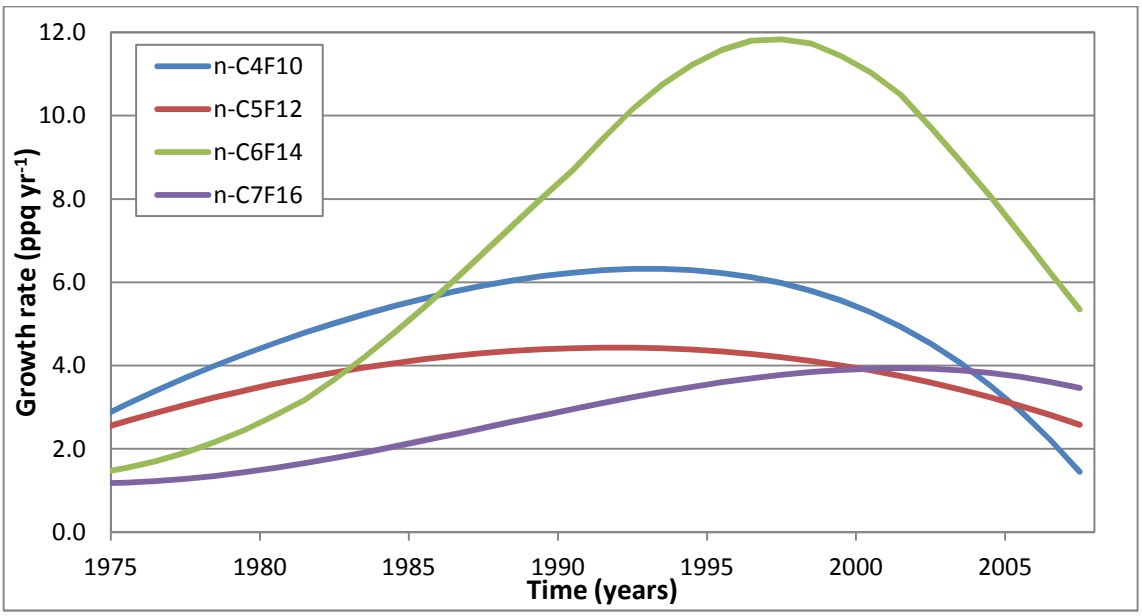

Figure 5.6: Growth rates of, n-C_4F_{10} (blue line), n-C_5F_{12} (red line), n-C_6F_{14} (green line) and n-C_7F_{16} (purple line) based on the atmospheric time series in Figure 5.5.

Figure 5.6 indicates that n-C_4F_{10} growth rates increased from ~5 ppq yr^{-1} (part per quadrillion per year) in 1980 to a maximum of ~6 ppq yr^{-1} in 1993. Since then, growth rate decreased to ~5 ppq yr^{-1} in 2000 reaching ~1 ppq yr^{-1} in 2007. Of the four compounds reported in the current study n-C_4F_{10} has the smallest growth rates since 2005.

Estimated *n*-C_5F_{12} growth rates have increased from ~3 ppq yr^{-1} in 1980 to a maximum of ~4 ppq yr^{-1} in 1991. Since then growth rates have been estimated to have decreased to ~2 ppq yr^{-1} in 2007. This is generally similar to the temporal evolution of *n*-C_4F_{10} and suggests that these two compounds may have been used in similar applications.

Of the four compounds reported here *n*-C_6F_{14} is estimated to have had the highest growth rate of ~12 ppq yr^{-1} in 1997 which increased from ~3 ppq yr^{-1} in 1980, more than double the maximum growth rates of *n*-C_4F_{10} and *n*-C_5F_{12}. Since 1997 growth rates of this compound have decreased but were still comparably high in 2007 at ~5 ppq yr^{-1}. As a consequence *n*-C_6F_{14} became the most abundant of these four PFCs from 1993 onwards (Figure 5.5).

Growth rates of *n*-C_7F_{16} have been estimated to have increased from ~1 ppq yr^{-1} in 1980 to ~4 ppq yr^{-1} in 2001. Since 2001 estimated *n*-C_7F_{16} growth rate have stabilised and is the only one of the four compounds which shows no significant decline in growth rate. The time series of *n*-C_6F_{14} and *n*-C_7F_{16} do not show a strong agreement even though they have been reported to have the same uses (*Waugh et al.*, 2011, *Olivier et al.*, 2010 and *Stone and Springer Jr*, 1995).

5.3.3 Emission of the perfluorocarbons compounds

Three of the four PFCs (*n*-C_4F_{10}, *n*-C_5F_{12} and *n*-C_6F_{14}) show a significant decrease in growth rate since ca. 1995. This can be explained by declining emissions for these PFCs. To validate this the annual emissions of *n*-C_4F_{10}, *n*-C_5F_{12}, *n*-C_6F_{14} and *n*-C_7F_{16} were modelled using the atmospheric time series in Figure 5.5 and with the use of a 1 - box model, this method has been described in more detail earlier and in the methods chapter.

Emissions estimate of these PFCs have been derived from a "bottom-up" approach by the EDGAR (*Olivier et al.*, 2010) and a "top-down" observations based approach by *Laube et al.* (2012). *Laube et al.* (2012) used a similar method to estimate emissions as *Sturges et al.* (2012) (this method has been described in more detail earlier). Similarly to the SF_5CF_3 emissions estimates derived by *Sturges et al.* (2012), *Laube et al.* (2012) uses a different data set and a different method that this study, but both studies use data that have been measured with the same techniques and placed on the same calibration scale. These emissions are shown in Figures 5.7 and 5.8.

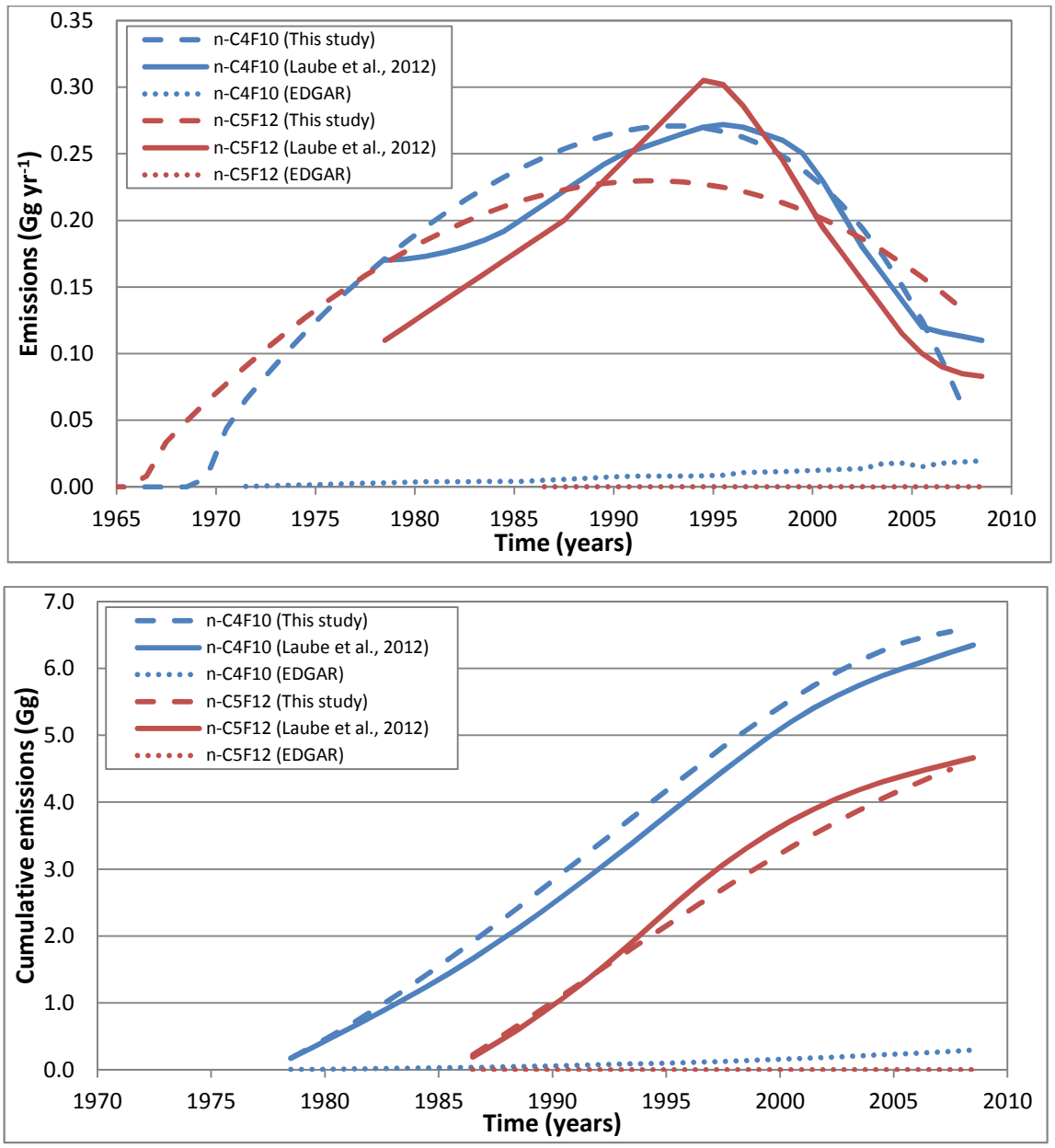

Figure 5.7: Top panel, emissions of n-C_4F_{10} (blue lines) and n-C_5F_{12} (red lines), based on the atmospheric time series in Figure 5.5 (dashed lines). The annual emissions from *Laube et al.* (2012) (solid lines) and from EDGAR (*Olivier et al.*, 2010) (dotted lines) are given as a comparison. Bottom panel, Cumulative emissions since 1978 of n-C_4F_{10} (blue lines) and since 1986 of n-C_5F_{12} (red lines), based on the emissions estimated in this study (top panel) (dashed lines). The cumulative emissions from *Laube et al.* (2012) (solid lines) and from EDGAR (*Olivier et al.*, 2010) (dotted lines) are given as a comparison.

Figure 5.7 shows that estimates of *n*-C_4F_{10} emissions from the current study rose year-on-year from the 1960s to around 1990, peaking at ~0.3 Gg yr^{-1} in 1993 before progressively declining to ~0.1 Gg yr^{-1} in 2007. Emissions of *n*-C_5F_{12} rose year-on-year from the 1960s to around 1990, peaking at ~0.2 Gg yr^{-1} in 1992 before progressively declining to ~0.1 Gg yr^{-1} in 2007. Again the firn and emission modelling has smoothed the emissions estimates, resulting in a flattening of the peak emission and thus effect the timing of the peak emission. The cumulative emissions of *n*-C_4F_{10} since 1978 and since 1986 for *n*-C_5F_{12} are shown in Figure 5.7.

These emission estimates generally agree with the those derived by *Laube et al.* (2012). Figure 5.7 shows that there are huge discrepancies between the "bottom-up" emission database processed by EDGAR (*Olivier et al.*, 2010) and the "top-down" observation based emissions derived by this study and by *Laube et al.* (2012). This might imply that emissions of these two compounds are under-reported by several orders of magnitude in the EDGAR emission database. This is not surprising given that there are only a limited number of countries reporting emissions of *n*-C_4F_{10} and *n*-C_5F_{12} to the EDGAR database (*Olivier et al.*, 2010). This is particularly true in the case of *n*-C_5F_{12} where Romania has been the only country reporting emissions (*Olivier et al.*, 2010).

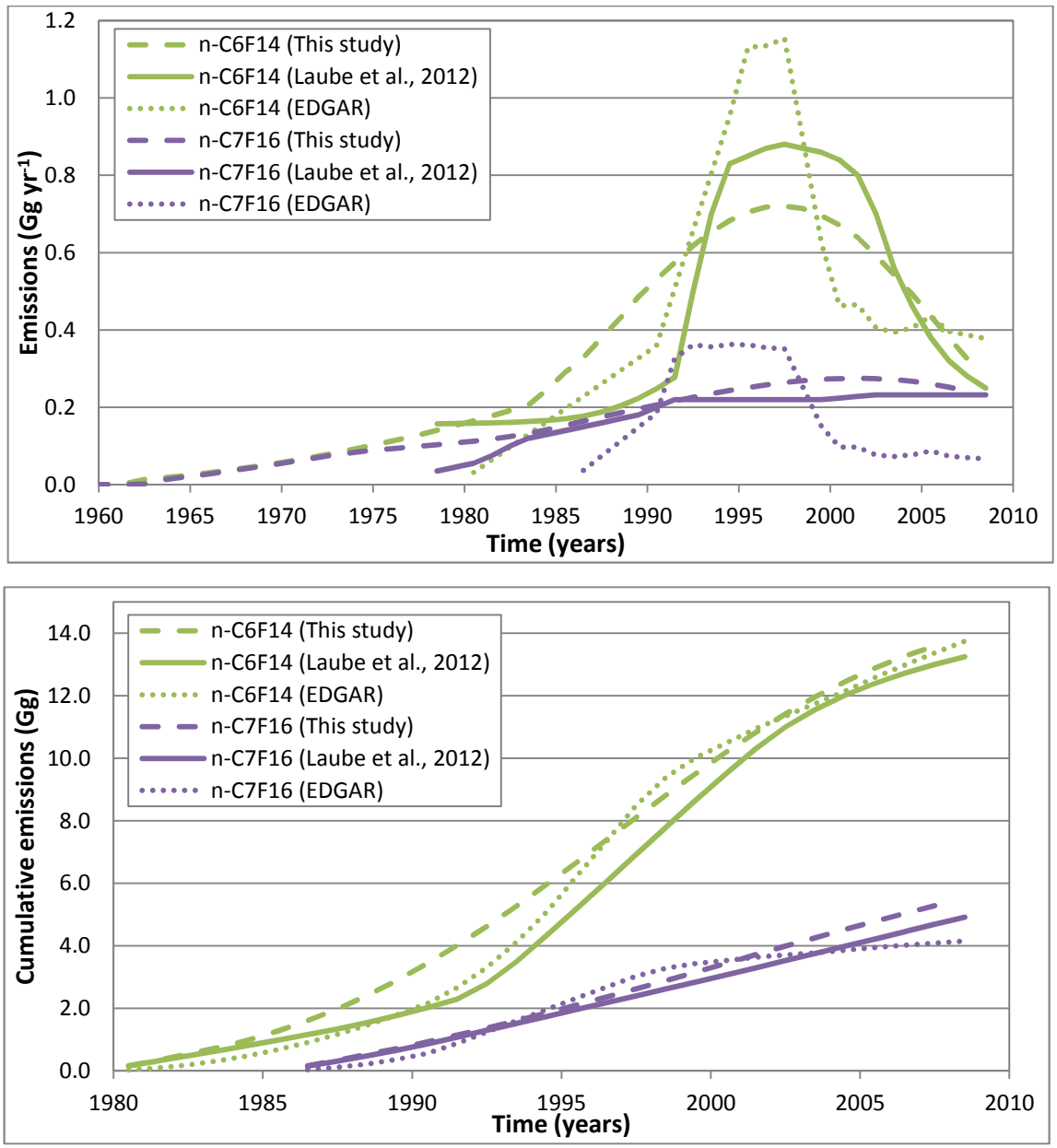

Figure 5.8: Top panel, emissions of n-C_6F_{14} (green lines) and n-C_7F_{16} (purple lines), based on the atmospheric time series in Figure 5.5 (dashed lines). The annual emissions from *Laube et al.* (2012) (solid lines) and from EDGAR (*Olivier et al.*, 2010) (dotted lines) are given as a comparison. Bottom panel, cumulative emission since 1980 of n-C_6F_{14} (green lines) and since 1986 of n-C_7F_{16} (purple lines), based on the emissions estimated in this study (top panel) (dashed lines). The cumulative emission from *Laube et al.* (2012) (solid lines) and from EDGAR (*Olivier et al.*, 2010) (dotted lines) are given as a comparison.

Figure 5.8 shows that estimated emissions of *n*-C_6F_{14} from the current analysis rose year-on-year from the 1960s to the mid 1990s, peaking in 1997 at ~0.7 Gg yr^{-1} before progressively declining to ~0.3 Gg yr^{-1} in 2007. Emissions of *n*-C_7F_{16} rose year-on-year from the 1960s to around 2000, peaking at ~0.3 Gg yr^{-1} in 2001 before declining slightly to ~0.2 Gg yr^{-1} in 2007. The cumulative emissions have been calculated since 1980 for *n*-C_6F_{14} and since 1986 for *n*-C_7F_{16} (Figure 5.8). Figure 5.8 shows that there is reasonable agreement for *n*-C_6F_{14} between the three emission estimates indicating that the emissions sources are well understood and

quantified for this compound. Whereas, also in comparison, *n*-C_7F_{16} shows reasonable agreement between the cumulative emissions (Figure 5.8), however EDGAR annual emissions are up to 60 % higher than the annual emissions estimates from this study and *Laube et al.* (2012) between 1990 and 1999 and up to 75 % lower before and after that period. There are also signs of a slight decline in emissions since 2000, based on current simulations, which is not shown in *Laube et al.* (2012). This decline is small and within the error of the atmospheric time series (Figure 5.5), therefore this decline may not be a true representative of the real emissions and maybe a result of the smoothed firn air derived emissions estimate. The introduction of emission reduction techniques in industrial applications such as the use of alternative chemistries, process optimisation as well as compound destruction, recovery or recycling (*Tsai et al.*, 2002) may have contributed to this decline.

Emissions estimates from the current study indicate that there are significant unknown sources releasing *n*-C_4F_{10} and *n*-C_5F_{12} (and probably *n*-C_7F_{16}) into the atmosphere. However, due to the limited number of countries reporting to the emission data base (*Olivier et al.*, 2010), these discrepancies could well be originating from known applications in countries that have not been reporting these emissions. However it should be noted that even though different methods were used to derive the emissions estimates of the current study and that of *Laube et al.* (2012), the data used has been analysed and placed on the same calibration scale by the same research group.

5.4 Hydrofluorocarbons (HFC-32)

The hydrofluorocarbons (HFCs) are organic compounds that only contain hydrogen and fluorine atoms and have entirely anthropogenic origins. They are second-generation replacements for compounds responsible for the anthropogenic stratospheric ozone depletion. HFCs were virtually unused before 1990 but since then have been increasingly used due to the phase-out of chlorofluorocarbons (CFCs) and also their first-generation replacements (i.e. hydrochlorofluorocarbons, HCFCs, (*Montzka et al.*, 2010)) in, for example, refrigeration and air-conditioning equipment. Therefore, HFCs have become increasingly important to study and measure in the atmosphere. In this study I will investigate only one hydrofluorocarbon, HFC-32 (difluoromethane, CH_2F_2). In this section I analyse the atmospheric time series of HFC-32. This is the first time that a full (tracking back to zero atmospheric mixing ratio) time series has been observed for HFC-32. I then discuss how its emissions rates have changed over time.

5.4.1 Background information on HFC-32

HFC-32 is a colourless, flammable, relatively non-toxic gas used as a replacement for CFCs and HCFCs (*Beukes and Nicolaisen*, 2000). It is mainly used as a refrigerant (*Smith et al.*, 1996) where it replaces HCFC-22, normally as a component of refrigerant mixtures containing HFC-134a and/or HFC-125. This usage typically leads to a slow long-term release of a compound (*Greally et al.*, 2005). HFC-32 also has an important commercial application as a fire extinguisher (*Schwartz et al.*, 1998). This is noteworthy because substances used in extinguisher are chosen specifically to be emitted into the environment during their use. It is also a by-product of the manufacture of other organic compounds (*Blowers and Hollingshead*, 2009).

As HFC-32 does not contain any chlorine, bromine or iodine its ozone depletion potential (ODP) is virtually zero (*Montzka et al.*, 2010). However HFC-32 does have a significant effect on the radiative forcing of the atmosphere. The Intergovernmental Panel on Climate Change states that the GWP_{100} (GWP on a 100 year time horizon) of HFC-32 as 675 relative to CO_2 (*Forster et al.*, 2007). This is in general agreement with *Blowers and Hollingshead* (2009) who have calculated the GWP_{100} of HFC-32 as 698 relative to CO_2 using the scaling factor for short lived halogened compounds described in *Highwood and Shine* (2000).

The main atmospheric sink of HFC-32 is through the reaction with the OH radical and has a OH lifetime of 5.5 years (*Montzka et al.*, 2010). The atmospheric lifetime of HFC-32 is 5.2 years with a stratospheric lifetime of 89 years (*Montzka et al.*, 2010). The atmospheric mixing ratio of HFC-32 was measured as 0.7 ppt at Mace Head (Ireland) in 2004 by the *AGAGE* network (*Greally et al.*, 2005), and increased to 2.7 ppt in 2008 (*Montzka et al.*, 2010). The rate of this atmospheric growth has also been shown to be increasing year on year with the growth between 2005 and 2006 being 0.3 ppt yr^{-1} compared with 0.6 ppt yr^{-1} between 2007 and 2008 (*Montzka et al.*, 2010).

Emission estimates of HFC-32 have been derived from a “bottom-up” approach by the EDGAR (*Olivier et al.*, 2010) and a “top-down” observations based approach by applying the 12-box model to AGAGE measurements (*Montzka et al.*, 2010).

In this work I will report the first atmospheric time series that tracks HFC-32 mixing ratios back to zero. This will be done through the use of firn air measurements taken at the NEEM site.

5.4.2 Results and discussion of HFC-32

An atmospheric time series was derived for HFC-32 from the measured concentrations and firn depth profile using an iterative modelling approach as described earlier. The time series obtained and the output from the model for the NEEM site are shown in Figure 5.9 alongside the actual measurements as a function of depth.

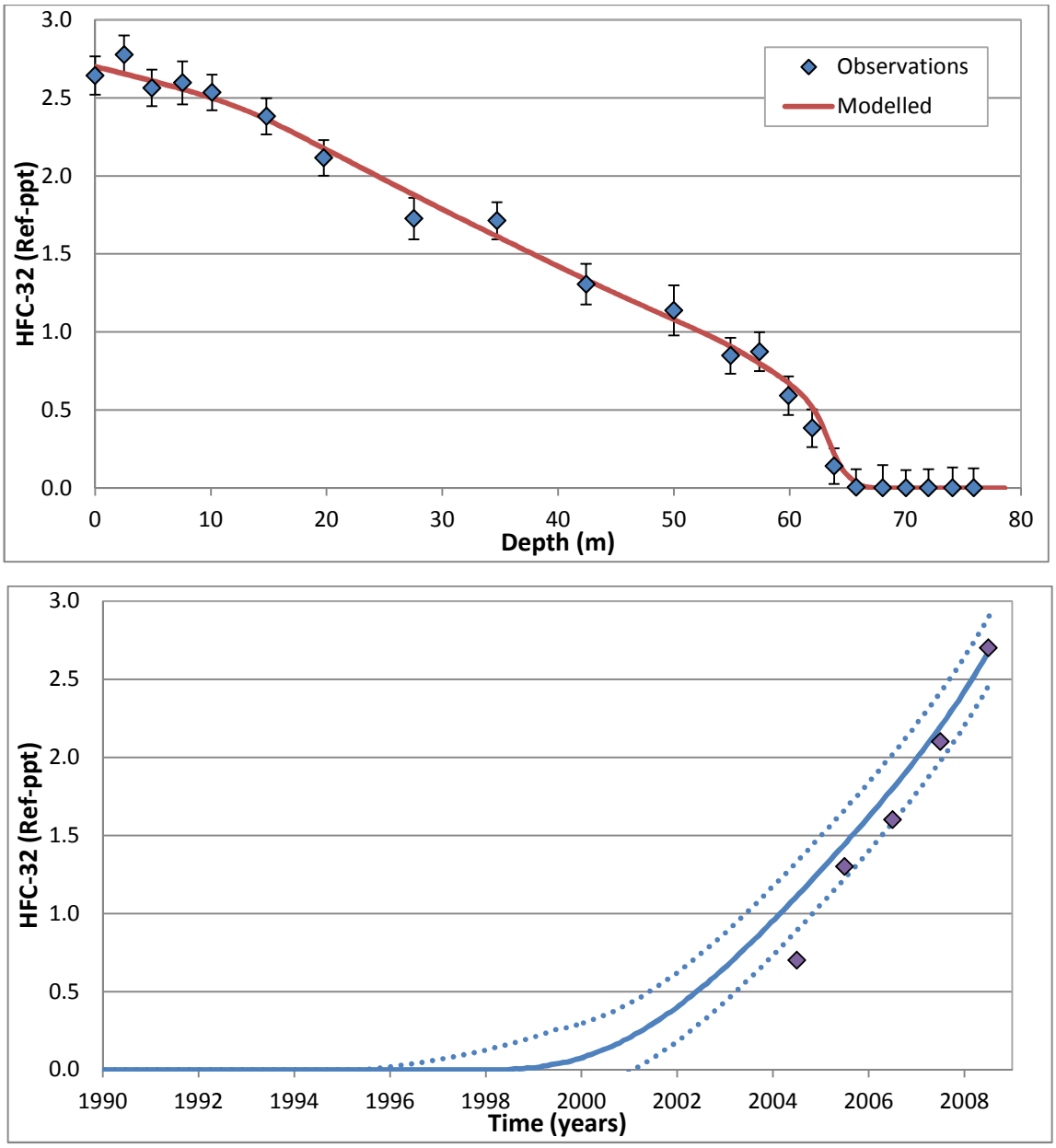

Figure 5.9: Top panel, depth profile of HFC-32 firn air measurements (points), compared with model simulations based on the atmospheric time series indicated in the bottom panel. The error bars represent the 1 σ of the measurements (See Chapter 2 for more details). The reference scale is used to scale the NEEM data to the AGAGE network. This was achieved by scaling the NEEM data so that the 2008 surface value equals 2.7 ppt (*Montzka et al.*, 2010). Bottom panel, atmospheric time series based on the NEEM firn air measurements using the *Trudinger* (2002) method. The dashed lines represent the errors in the time series as described in Figure 5.1. The purple diamonds are the AGAGE measurements of HFC-32 from Mace Head (Ireland) (*Montzka et al.*, 2010).

The atmospheric mixing ratio time series derived in the current study and shown in Figure 5.9 indicate that significant emissions of HFC-32 (emissions that produce an observable atmospheric mixing ratio) started in 1998. This indicates that HFC-32 is of entirely anthropogenic origins. This is in agreement with the EDGAR database for HFC-32 emissions in Figure 5.10 (*Olivier et al.*, 2010). Since 1998 the time series shows a period of sustained growth in the atmospheric mixing ratio of HFC-32 until mid-2008 when the firn air was collected. There is also agreement between the derived time series and the atmospheric observations made at Mace Head (Ireland) by the AGAGE network (purple diamonds, Figure 5.9), with exception of the 2004 measurement. *Greally et al.* (2005) noted there was an increase in the baseline growth rate during 2004. This result was explained as either indication of an instrumental problem or a true reflection of global atmosphere emissions. Nonetheless *Greally et al.* (2005) notes' that a rapid change in the baseline growth rate is unexpected as HFC-32 typically has a slow long-term release period.

The firn air derived average growth rate accelerated continuously from 0.16 ppt yr^{-1} in 2000 to 0.32 ppt yr^{-1} in 2005 to 0.45 ppt yr^{-1} in 2007. This reflects the increased use of HFC-32 in recent years as a commercial replacement for CFCs and HCFCs. These growth rates are similar to those stated by the AGAGE network. However the firn derived growth rate between 2007 and 2008 is less than the AGAGE rate of 0.6 ppt yr^{-1} (*Montzka et al.*, 2010). This increase in the growth rate is in agreement with the emission record from the EDGAR database HFC-32 emissions (Figure 5.10) which shows a year on year increase in emissions (*Olivier et al.*, 2010). It should also be note that these growth rates represent only the best estimates and do contain considerable uncertainties within the envelopes shown in Figure 5.9.

As HFCs have become increasingly more important to the chemical balance of the atmosphere, it is important to study the relative effect of HFC-32. A comparison of HFC-32 atmospheric mixing ratio to other observed HFCs is presented in Table 5.4.

Table 5.4: HFCs global atmospheric mixing ratios

HFCs	Mixing ratio (ppt)	% of total HFCs mixing ratio	Growth rate (ppt yr^{-1})	% of total growth rate	Date	Reference
HFC-32 (CH_2F_2)[†]	2.7	3%	0.5[#]	6%	2008	This study (Calibration based on AGAGE)
HFC-134a (CH_2FCF_3)	38.8-38.9	45%	4.4-4.9	52%	2008	(*Montzka et al.*, 2010)
HFC-23 (CHF_3)	21.8	25%	0.8	9%	2008	(*Montzka et al.*, 2010)
HFC-143a (CH_3CF_3)	8.5	10%	1.0	11%	2008	(*Montzka et al.*, 2010)
HFC-125 (CHF_2CF_3)	6.1	7%	0.9	10%	2008	(*Montzka et al.*, 2010)
HFC-152a (CH_3CHF_2)	5.9	7%	0.6	7%	2008	(*Montzka et al.*, 2010)
HFC-245fa ($CF_3CH_2CHF_2$)	1.0	1%	0.4	4%	2008	(*Montzka et al.*, 2010)
HFC-227ea (CF_3CHFCF_3)	0.59	1%	0.06	1%	2007	(*Laube et al.*, 2010)
HFC-365mfc ($CF_3CH_2CF_2CH_3$)	0.4	0.5%	0.1	1%	2008	(*Montzka et al.*, 2010)
Total	85.8		9.0			

†Northern hemispheric mixing ratios, # 2007 growth rate

Estimates from the current study show that HFC-32 has the sixth largest atmospheric mixing ratio of the HFCs and contributes around 3 % to the total atmospheric abundances of the HFCs (Table 5.4). Current analysis also shows that HFC-32 has the sixth largest growth rate and contributes around 6 % to the combined growth rates of the HFCs. These results indicates that even though HFC-32 is currently small in abundance in the atmosphere, it is becoming relatively more common and important to the total HFCs atmospheric mixing ratios.

5.4.3 Emission of HFC-32

The annual emissions of HFC-32 were derived using the atmospheric time series in Figure 5.9 and with the use of a 1 - box model, this method has been described in more detail earlier and in the methods chapter.

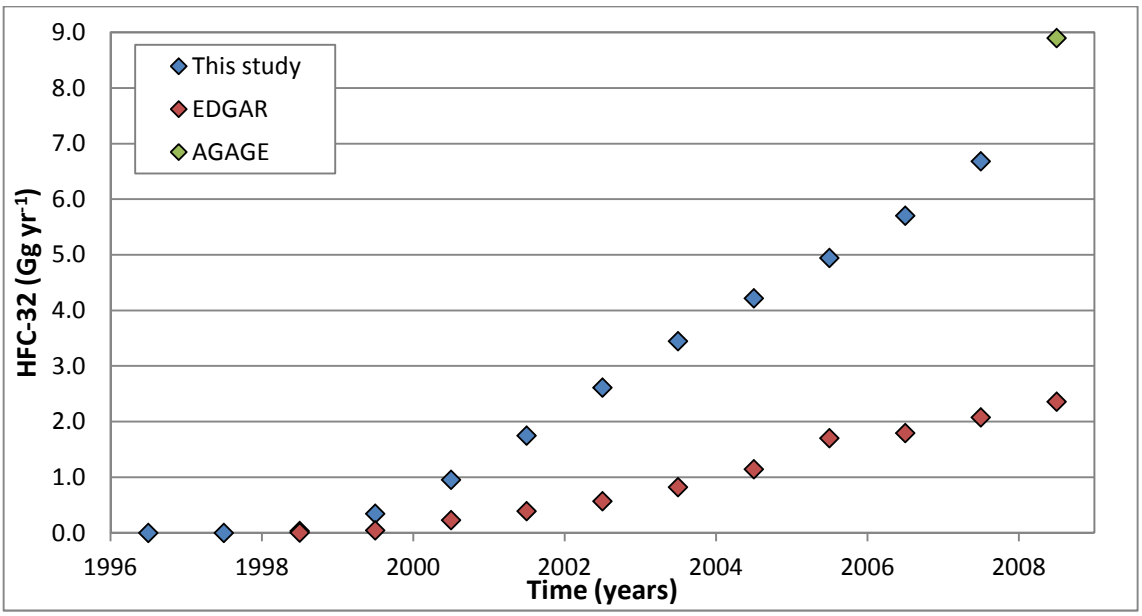

Figure 5.10: Annual emissions of HFC-32 based on the atmospheric time series in Figure 5.9 (blue points). The annual emissions from EDGAR (red points) (*Olivier et al.*, 2010) and AGAGE (green point) (*Montzka et al.*, 2010) are given as a comparison.

Figure 5.10 shows that current estimates of emissions of HFC-32 rose year-on-year from ~0 Gg yr^{-1} in 1998 to ~7 Gg yr^{-1} in 2007. These emissions estimates agree with those reported by EDGAR (*Olivier et al.*, 2010), in so far as the onset of emission in 1998 and the monotonically increase in emissions rates. However, the absolute strength of the emissions is larger in this study compared with EDGAR by a factor 3.5. Due to the limited number of reporting countries in the EDGAR emission estimates (*Olivier et al.*, 2010), the differences between the emissions database and the current study could well originate from applications in countries that have not reported emissions. An extrapolation of the emission estimates in this study would be consistent with the emission estimate of 8.9 Gg yr^{-1} in 2008 derived by the AGAGE network (*Montzka et al.*, 2010).

5.5 Equivalent CO_2 emissions of the fluorinated greenhouse gases

The compounds discussed in this chapter strongly absorb in the infrared and are all considered to be greenhouse gases. The dominant factor in the changes to radiative forcing of climate in the industrial era has been the increasing concentration of various greenhouse gases in the atmosphere (*Forster et al.*, 2007). It is therefore important to assess the effect that individual greenhouse gases have on the atmospheric energy budget.

The contribution of an individual greenhouse gas to the radiative forcing of the atmosphere over a particular period of time is determined by the change in its mixing ratios in the

atmosphere over that period and the effectiveness of the greenhouse gas in perturbing the radiative balance (*Forster et al.*, 2007).

Equivalent CO_2 emission is a quantity that describes, for a given compound and amount emitted of that compound, the amount of CO_2 that would have the same global warming potential (GWP), when measured over a 100 year time horizon as the observed amount of the target compounds. Equivalent CO_2 emission thus reflects the time-integrated radiative forcing of a quantity of emissions. Equivalent CO_2 emission is calculated by multiplying the emissions of an individual compound by their respective direct GWPs (100-year time horizon; CO_2 = 1) (Equation 1).

$$MMTCO_2Eq_i = (E_i) \times (GWP_i) \qquad \text{- Equation 1}$$

$MMTCO_2Eq_i$, is million metric tonnes of carbon dioxide equivalent of compound *i*, E_i is the emissions of compound *i* in million metric tons and GWP_i is the global warming potential of compound *i*. The GWPs reported in *Forster et al.* (2007) were applied to derive the CO_2 equivalent for 2007 emissions given in Table 5.5. As no GWP is reported for n-C_7F_{16} in neither *Bravo et al.* (2010) nor *Forster et al.* (2007) I assumed the same GWP to that of n-C_6F_{14}.

Table 5.5: GWP and $MMTCO_2Eq\ yr^{-1}$, for the fluorinated greenhouse gases presented in this chapter.

Compound	GWP[1]	Emission 2007 (Gg yr^{-1})	$MMTCO_2Eq\ yr^{-1}$ 2007
SF_6	22800	~6	130
SF_5CF_3	17700	~0.01	0.2
HFC-32	675	~7	5
n-C_4F_{10}	8860	~0.1	0.6
n-C_5F_{12}	9160	~0.1	1
n-C_6F_{14}	9300	~0.3	3
n-C_7F_{16}	9300[2]	~0.3	2
Total		~13	140

1: GWP on a 100 year time horizon (*Forster et al.*, 2007)

2: Using the GWP for n-C_6F_{14} from *Forster et al.* (2007)

Table 5.5 indicates that the total equivalent CO_2 emissions of the fluorinated gases considered here, was 140 MMT yr^{-1} in 2007. This is around 10 % of the total $MMTCO_2Eq\ yr^{-1}$ from ODSs which is estimated as being 1400 in 2010 (*Montzka et al.*, 2010) and around 0.5 % of the 32000 MMT of total CO_2 emitted in 2010 (*Montzka et al.*, 2010). It should be noted that these percentages are a comparison between 2007 and 2010 emissions. The largest contribution is from SF_6 with 130 $MMTCO_2Eq\ yr^{-1}$ and the total $MMTCO_2Eq\ yr^{-1}$ from the PFCs (n-C_4F_{10} – n-

C_7F_{16}) is estimated to have been ca. 7 in 2007, with n-C_6F_{14} making the largest contributor amongst the PFCs in this chapter. HFC-32 emissions were 5 $MMTCO_2Eq\ yr^{-1}$ in 2007 which is around 1 % of the total HFC emissions in 2010 of ~400 $MMTCO_2Eq\ yr^{-1}$ (*Montzka et al.*, 2010).

The Kyoto Protocol (see introduction chapter for more details), aims for an overall reduction of around 2000 $MMTCO_2Eq\ yr^{-1}$ emissions in Annex 1 countries by 2013 (*deBoer*, 2007). This is a 5.2 % reduction from the 1990 emission rate in Annex 1 countries. The Annex I countries are defined as industrialized countries or countries whom economy is in transition (*deBoer*, 2007).

Apart from HFC-32, all of the fluorinated greenhouse gases have atmospheric lifetimes on the order of thousands of years (*Montzka et al.*, 2010). As such, they accumulate almost quantitatively once released into the atmosphere. The cumulative carbon dioxide equivalency for the fluorinated greenhouse gases discussed in this chapter have been calculated and are shown in Figure 5.11.

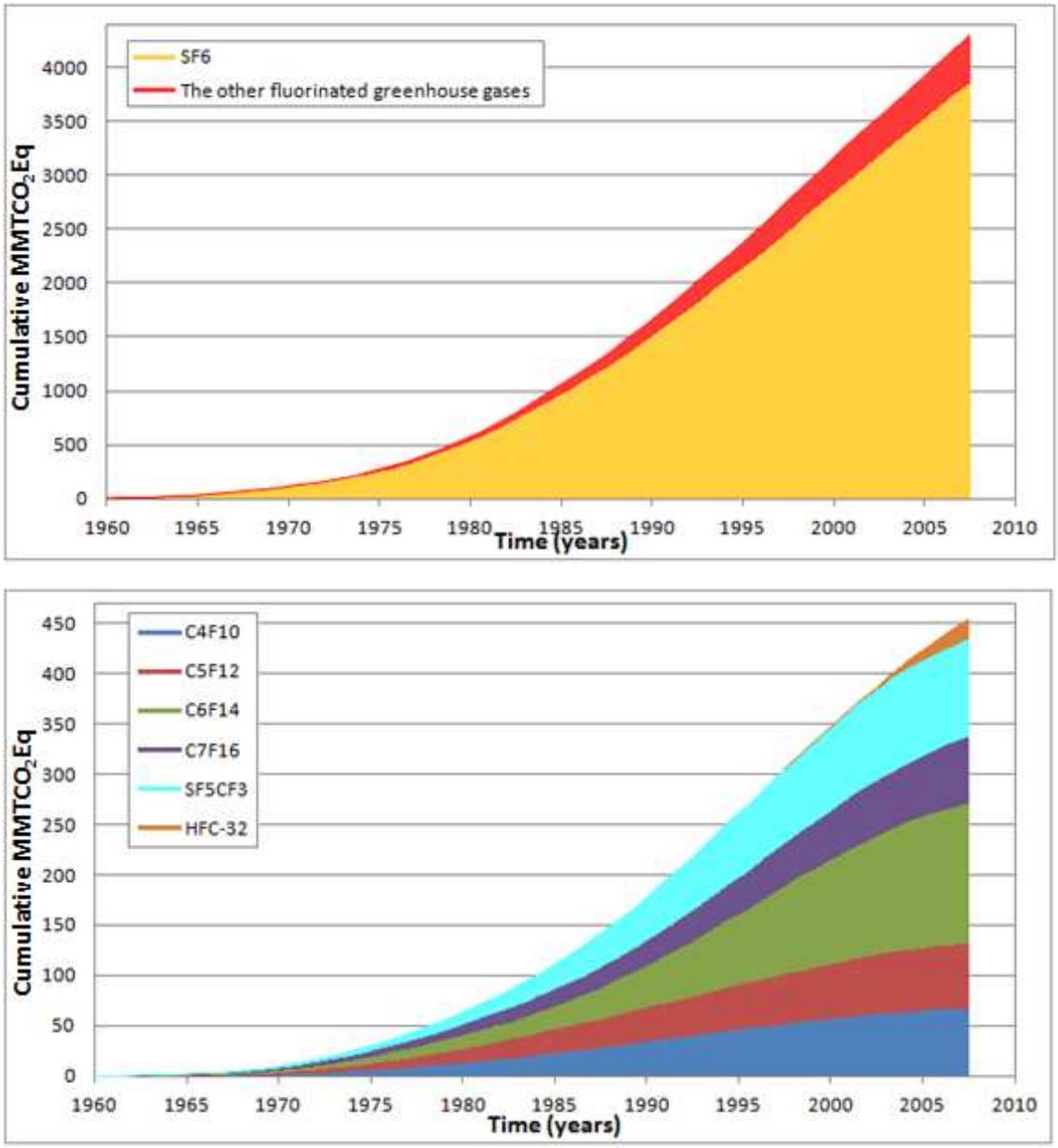

Figure 5.11: Top panel, cumulative $MMTCO_2Eq$ emitted since 1960 of SF_6 (yellow area) and the combined cumulative $MMTCO_2Eq$ emitted from the other fluorinated greenhouse gases since 1960 (red area). Bottom panel, the cumulative $MMTCO_2Eq$ of the other fluorinated greenhouse gases since 1960 (red area, top panel) showing the contribution from the individual compounds; n-C_4F_{10} (dark blue area), n-C_5F_{12} (red area), n-C_6F_{14} (green area), n-C_7F_{16} (purple area), SF_5CF_3 (light blue area) and HFC-32 (orange area).

Figure 5.11 indicates that SF_6 cumulative emissions reached 3800 $MMTCO_2Eq$ in 2007, whereas the sum of the cumulative emissions of the other fluorinated greenhouse gases only reached 450 $MMTCO_2Eq$ in 2007, giving a total of 4250 $MMTCO_2Eq$ in this year, representing around 0.1 % of the global abundance of 3.05 x 10^5 MMT of atmospheric CO_2 in 2007 (*Forster et al.*, 2007) and around 13 % of the emissions of CO_2 in the year 2010 (*Forster et al.*, 2007). It also shows that the sum of the cumulative emissions of the PFCs reached ~340 $MMTCO_2Eq$ in 2007,

with n-C_6F_{14} having the largest contribution, with a total of ~140 $MMTCO_2Eq$. The other PFCs contribute just ~60 $MMTCO_2Eq$ each. This is in general agreement with the emissions estimated by *Laube et al.* (2012) of 325 $MMTCO_2Eq$ for these PFCs at the end of 2009. HFC-32 has had the smallest cumulative emissions of CO_2 equivalent at ~20 $MMTCO_2Eq$ (orange area, Figure 5.11). However, it has the second largest current growth rate of the fluorinated greenhouse gases of ~5 $MMTCO_2Eq\ yr^{-1}$ in 2007 (Table 5.5)and therefore, is likely to become relatively more important to the atmospheric energy budget in future compared to the other compounds observed in this study.

5.6 Summary

In this chapter, I have reported observations of the fluorinated greenhouse gases from northern hemispheric firn air, with resulting derived atmospheric time series from the mid-20th century up until mid-2008 when the firn air was collected. Table 5.6 summarises the atmospheric time series, growth rates, emissions and CO_2-equivalence for the individual gases.

I have shown that all of these compounds have first appeared in detectable abundance in the atmosphere since 1950. Since their introduction into the atmosphere, all of these gases have shown significant growth, and apart from SF_5CF_3, all are showing continuing growth.

This study not only updated atmospheric time series for these gases from the mid-20th century to 2008 but also for the first time highlights the long term atmospheric time series for *n*-C_4F_{10}, *n*-C_5F_{12}, *n*-C_6F_{14} and *n*-C_7F_{16} and HFC-32 from firn air reconstructions that tracks their atmospheric mixing ratios back to zero and thus derive their first complete atmospheric time series.

Previous analysis of study of SF_6 has been used in the methods chapter to validate the NEEM measurements and subsequent analytical processes used in this chapter, through the comparison with well documented time series and emissions rates.

Even though the fluorinated greenhouse gases currently have small atmospheric mixing ratios they do have strong GWPs, hundreds to several thousand times higher than that of carbon dioxide. Apart from HFC-32, these fluorinated greenhouse gases have long atmospheric lifetimes of several hundred to thousands of years. This means that they are likely to represent an essentially irreversible change to the composition of the Earth's atmosphere and to the radiative forcing of the climate. The results also indicate that it would be desirable to minimise future emissions as these compounds contributed the equivalent of 4250 $MMTCO_2Eq$ by the end of 2007 and are still likely to be increasing.

Table 5.6: Summary of the fluorinated greenhouse gases.

Compound	Estimated date of first detectable mixing ratio	Mid–2008 mixing ratio (ppt)	2007 Growth rate (ppq yr^{-1})	Maximum annual emission (Gg yr^{-1})	Date of maximum annual emission	Total CO_2-equivalent ($MMTCO_2Eq$)	Key Finding
SF_6	1956	6.6	200	6	1998	3800	Largest effect on the atmospheric radiative forcing of the fluorinated greenhouse gases
SF_5CF_3	1960	0.15	0.4	0.3	1994	100	The atmospheric mixing ratios as now stabilise
n-C_4F_{10}	1969	0.17	1	0.3	1993	60	Growth rates and emissions rates are currently declining
n-C_5F_{12}	1966	0.14	3	0.2	1992	60	Growth rates and emissions rates are currently declining
n-C_6F_{14}	1961	0.25	5	0.7	1997	140	Growth rates and emissions rates are currently declining
n-C_7F_{16}	1962	0.11	0.4	0.3	2001	60	Shows no sign of significant decrease in growth rates or emissions rates
HFC-32	1998	2.7	500	7	2007	20	Is currently increasing rapidly in the atmosphere

Chapter 6: Conclusions, future scenarios and recommendations

6.1 Chlorocarbons and bromocarbons

6.2 Fluorinated greenhouse gases

6.3 Recommendations

6.1 Chlorocarbons and bromocarbons

One of the aims of this project was to measure chlorocarbon and bromocarbon concentrations from the NEEM firn air samples. I compared these measurements with those from other firn air samples to derive both northern and southern hemispheric atmospheric time series. The reconstruction of these time series was produced using a firn diffusion model (*Buizert et al.*, 2011 and *Witrant et al.*, 2011) and a multi-site inversion modelling technique developed at LGGE as well as with iterative dating techniques. Table 6.1 shows the summary of my key findings.

Table 6.1: Key finding from chlorocarbon and bromocarbon analysis.

Compound	**NH time series from firn air**	**SH time series from firn air**	**1950 mixing ratio (ppt)**	**Mid–2008 mixing ratio (ppt)**	**Date of maximum annual emission**
Chlorocarbons					
CH_3Cl[1]	First report[3]	Updated	517.8	516.7	1986
$CHCl_3$[1]	Updated[4]	Updated	6.5	8.3	1983
CH_2Cl_2[1]	First report	First report	2.0	24.1	1985
CCl_2CCl_2[1]	First report	First report	1.8	2.9	1978
CH_2ClCH_2Cl[2]	First report	-	1.5	5.5	1983
C_2H_5Cl[2]	First report	-	7.0	2.0	1973
$CHClCCl_2$[2]	First report	-	0.07	0.24[5]	1982
Bromocarbons			**1930 mixing ratio (ppt)**		
CH_2Br_2[1]	Updated	Updated	1.1	1.0	1979
CH_2BrCH_2Br[1]	First report	First report	0.2	0.07	1970
C_2H_5Br[2]	First report	-	1.6	1.0	1976
CH_2BrCl[2]	First report	-	0.17	0.10	1970
$CHBrCl_2$[2]	First report	-	0.15	0.15	1992
$CHBr_2Cl$[2]	First report	-	0.24	0.25	1992
$CF_3CHBrCl$[1]	First report	First report	0.0	0.005	1984

1: 'Global'. 2: Northern Hemisphere. 3: First report – The time series produced in this study is the first reported atmospheric time series from firn air of this compound. 4: Updated - The time series produced in this study has updated previously observed time series from other studies. 5: mid-2001 mixing ratio

Table 1 indicates that all of the compounds investigated in the current study apart from $CF_3CHBrCl$ have significant 1930 or 1950 atmospheric mixing ratios. All of the reported compounds also show significant growth during the 20th century before a period of decline. However, the rate of this decline has slowed significantly since 2000 for the majority of compounds whilst for, CH_2Cl_2 and CH_2ClCH_2Cl, atmospheric mixing ratios are currently increasing.

The atmospheric time series for CH_3Cl indicates a 10 % increase in mixing ratio up to 1990 before showing significant decline. However, it is still unclear if the atmospheric time series is largely effected by natural emissions sources or by anthropogenic emissions (e.g. human influenced biomass burning). $CHCl_3$ emissions estimates produced in this study support the fact that emissions from the paper and pulp industry have had a large effect on the atmospheric mixing ratio, and now that emissions from this source have stopped, the atmospheric mixing ratio has become stable. The most interesting result for this study is that CH_2Cl_2 is currently increasing in the atmosphere, which is most likely due to an increase in emissions from South East Asia. In contrast, atmospheric mixing ratios of CCl_2CCl_2 are currently decreasing, and I have shown that emissions are dominated by northern hemispheric anthropogenic sources. The mixing ratio of CH_2ClCH_2Cl is also currently increasing in the atmosphere, however, it is unclear which emissions source(s) has increased to also produce this trend. $CHClCCl_2$ shows a similar atmospheric time series to CH_2ClCH_2Cl which suggests a similar or related emission source(s). The emissions rate of C_2H_5Cl has decreased since the 1970s, which strongly reflect its use in leaded petrol.

The atmospheric mixing ratios of the bromocarbons generally peaked before the chlorocarbons. CH_2BrCH_2Br peaked the earliest in 1970 as a result of its use as an additive in leaded petrol. The atmospheric mixing ratio of CH_2BrCH_2Br correlates well with emissions from this source. In this study, a small but significant decline in northern hemispheric emissions of CH_2Br_2 since 1980 was observed, suggesting a possible anthropogenic source. The emissions patterns affecting the atmospheric mixing ratio of C_2H_5Br are currently unclear as mixing ratios remaining stable since 2000. The bromo-chloro methanes $CHBrCl_2$ and $CHBr_2Cl$ have similar time series, which indicates a possible similar source(s) driving their atmospheric mixing ratios. This could result from emissions from the chlorination of seawater used as cooling water in coastal power stations. The atmospheric time series for CH_2BrCl, reflects it use in fire extinguishers. Also $CF_3CHBrCl$ emissions rates strongly reflect its use in the medical profession.

Even though the chlorocarbons and the bromocarbons have small atmospheric mixing ratios, I have shown that they do significantly add to the abundance of halogenated compounds in the stratosphere. This was achieved by calculating the EESC of the chlorocarbons and the bromocarbons (see Chapter 3 and 4 for more details). The combined EESC of the VSL chlorocarbons, VSL bromocarbons and CH_3Cl are shown in Figure 6.1 as well as the EESC of chlorine and bromine containing ODSs based on the baseline scenario (*Montzka et al.*, 2010).

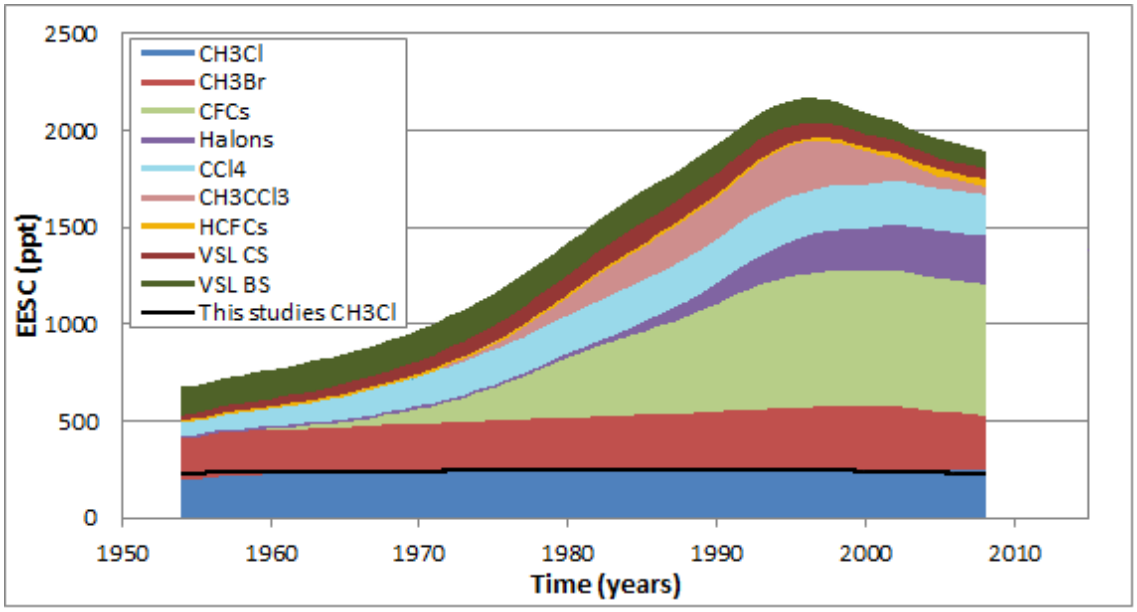

Figure 6.1: Equivalent effective stratospheric chlorine mixing ratios since 1954 from CH_3Cl (dark blue area), CH_3Br (light red area), CFCs (light green area), halons (purple area), CCl_4 (light blue area), CH_3CCl_3 (pink area) and HCFCs (yellow area) based on *Montzka et al.* (2010). As well as the contribution from the VSL chlorocarbons (brown area), VSL bromocarbons (dark green area) and CH_3Cl (black line) measured in the current study.

The mixing ratios from *Montzka et al.* (2010) shown in Figure 6.1 are taken as an average of the global mean observations from the NOAA and AGAGE networks. In terms of EESC contribution, the largest contribution comes from the CFCs and natural CH_3Cl and CH_3Br emissions. Figure 6.1 shows that the VSL chlorocarbons and the VSL bromocarbons contributed significantly to the total EESC mixing ratio between 1954 and 2008. In 2008, the VSL chlorocarbons contributed 61 ppt of EESC and the VSL bromocarbons contributed 94 ppt of EESC with a total from both groups of compounds at 155 ppt of EESC. This is ~ 9 % of the total EESC from the chlorine and bromine containing ODSs from *Montzka et al.* (2010). The peak in EESC from the VLS chlorocarbons occurred in 1984 and the VLS bromocarbons in 1974 which is before the peak in total EESC which occurred in 1997 (*Montzka et al.* 2010). This is due to the

fact that the anthropogenic sources of the chlorocarbons and bromocarbons were controlled much earlier than other halogenated compounds (*Kleiman and Prinn*, 2000 and *Santodonato et al.*, 1985). Figure 6.1 also shows that there is good agreement between the EESC from CH_3Cl measured in the current study and that calculated by *Montzka et al.* (2010).

As I have shown, (Figure 6.1) a significant EESC mixing ratio originates from VSL chlorocarbons and VSL bromocarbons. Therefore, it is important to assess the possible future emissions of these compounds. Possible future emissions sources were assessed by producing 3 different scenarios. Scenario 1 takes all of the compounds back to their natural background level by the year 2030 and then holding at this abundance up until 2050. The natural background was taken as the lowest mixing ratio that was observed in the current study. This scenario is known as the 'natural background' scenario. Scenario 2 continues on the current trend of these compounds year-on-year up until 2050. This scenario is known as the 'current trend' scenario. Scenario 3 was developed as a 'business as usual' scenario in which the compounds with anthropogenic sources were increased by 4 % year-on-year up until 2050. I used 4 % as the increase factor as this is similar to the upper limit of the increase in the hydrofluorocarbons predicted by *Forster et al.* (2007). The hydrofluorocarbons are compounds that are 100 % anthropogenic in origin and their production is predicted to increase in the future. Therefore, I have used them as a guide to a possible increase in the production rate of the VSL chlorocarbons and VSL bromocarbons. This scenario is known as the '4 %' scenario. These scenarios along with the time series of EESC based on observations up until 2008 are shown in Figure 6.2.

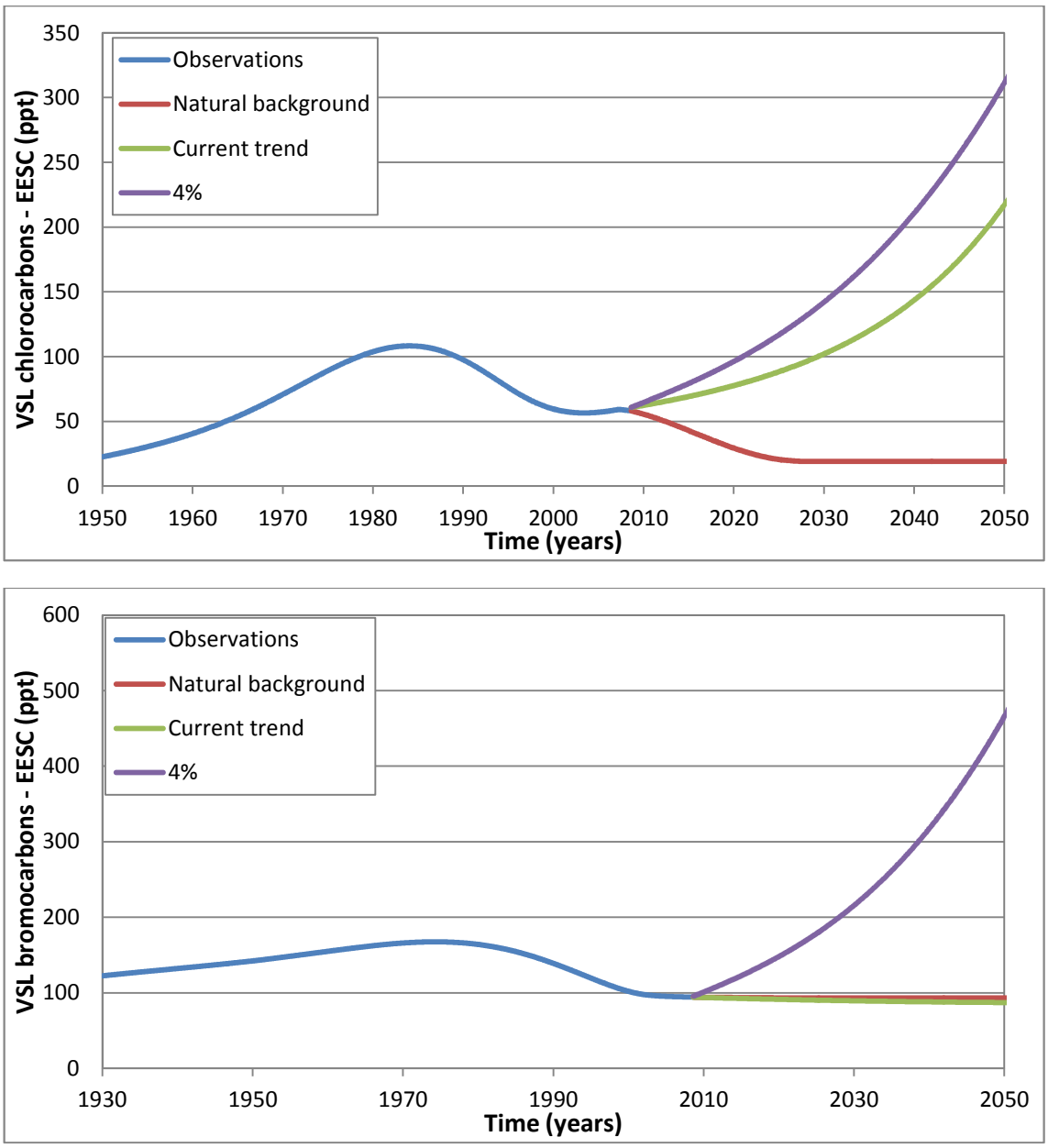

Figure 6.2: Historical and projected EESC mixing ratios for the VSL chlorocarbons (top panel) and the VSL bromocarbons (bottom panel). The EESC mixing ratios from observed data are shown by the blue line. The projected scenarios: Natural background – red lines, Current trend – green lines, 4 % increase – purple line.

Figure 2 indicates that the mixing ratio of VSL chlorocarbons are still above the natural background as the 'natural background' scenario shows a significant decline between 2008 and 2030. However, the VSL bromocarbons are currently at or around natural background level with the 'current trend' and the 'natural background' scenarios very similar between 2008 and 2050. The 'current trend' for the VSL chlorocarbons indicates that it is likely that EESC from these compounds will increase in the future. To find the relative contribution these compounds might have in the future, Figure 3 compares these scenarios to the baseline scenario of the chlorine and bromine containing ODSs up to 2050 (*Montzka et al.*, 2010).

Future emissions of chlorine and bromine containing ODSs are determined by using a fixed annual bank release fraction, calculated as the average ratio over the past 10 years between the annual emissions and estimated bank plus production. Future production figures are determined from the Protocol limitations and the most recent annual estimates (*Montzka et al.*, 2010).

Two future scenarios were produced for CH_3Cl. Scenario 1 assumes that the atmospheric time series of CH_3Cl during the 20th century was driven by anthropogenic sources and have now reached the natural background. This scenario continues at the current mixing ratio until 2050 and is known as the 'natural background' scenario. Scenario 2 assumes that the atmospheric time series of CH_3Cl during the 20th century was driven by natural flux in the atmosphere. This scenario consists of a sinusoid trend with an amplitude of 10 % of the mean and a period of 110 years as described in *Aydin et al.* (2004) and is known as the 'sinusoid' scenario. These scenarios are also shown in Figure 6.3.

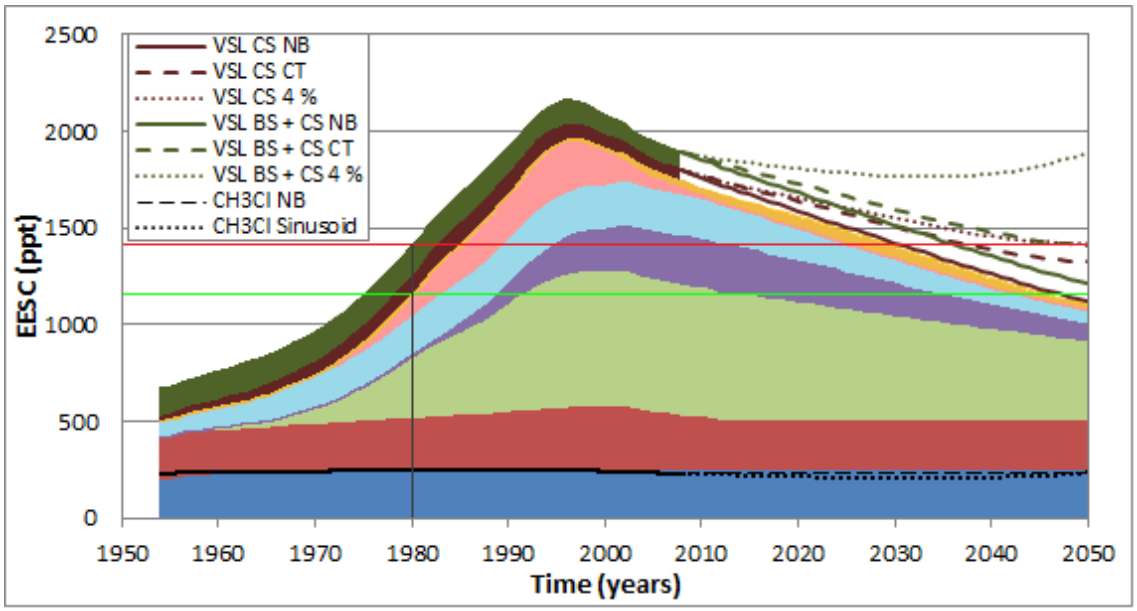

Figure 6.3: Historical and projected EESC mixing ratios between 1954 and 2050 from CH_3Cl (dark blue area), CH_3Br (light red area), CFCs (light green area), halons (purple area), CCl_4 (light blue area), CH_3CCl_3 (pink area) and HCFCs (yellow area) based on *Montzka et al.* (2010). As well as the contribution from the VSL chlorocarbons (brown area), VSL bromocarbons (dark green area) and CH_3Cl (black line) measured in this study. The future scenarios for the VSL chlorocarbons are shown by the brown lines. The future scenarios for the VSL bromocarbons are shown by the dark green lines, these lines have been added to the corresponding chlorocarbon scenario. The lines for the different scenarios are shown as 'natural background' (solid line), 'current trend' (dashed line) and '4 %' (dotted line). The future scenarios for CH_3Cl are shown by the black lines, 'natural background' (dashed line) and 'sinusoid' (dotted line). The 1980 bench-mark given by *Montzka et al.* (2010) is shown by the green line and the 1980 bench-mark predicted by this study is shown by the red line.

Figure 6.3 shows that even if the VSL chlorocarbons and the VSL bromocarbons return to their natural background by 2030, they will still increase relative to the other chlorine and bromine ODSs by 2050. In 2050 the 'natural background' scenario indicates that the contribution from the VSL chlorocarbons and the VSL bromocarbons will have increased from ~ 9 % to ~ 10 % of the total EESC from the chlorine and bromine containing ODSs whereas the 'current trend' scenario shows an increase to ~ 28 %. Figure 3 also shows that EESC from CH_3Cl will change very little over the next 50 years, as there is not much difference between the two scenarios.

If stratospheric ozone levels were affected by only by halocarbons, the ozone layer would be expected to recover from human activities as anthropogenic ODSs are removed from the atmosphere. The year 1980 is commonly taken as a as a benchmark year, representing a time before major stratospheric ozone losses occurred due to halocarbons. Therefore, analyses are often based on the time it will take for EESC mixing ratios to return to 1980 levels. However, some ozone losses caused by human activities had most likely already occurred before this date; for example by the VSL bromocarbons which peaked in the atmosphere before 1980. Nevertheless, the year EESC returns to 1980 levels has been used as a measure for the degree of ozone layer recovery and to compare scenarios.

In the baseline scenario of *Montzka et al.* (2010), only the Montreal Protocol-controlled ODSs was included and EESC returns to 1980 levels by 2046 for mid-latitude conditions (green line Figure 6.3). However, if you include the EESC from the VSL chlorocarbons and VSL bromocarbons, the total EESC will not recover to this value by 2050, even if all of the compounds return to their natural background. The 1980 benchmark level including the VSL chlorocarbons and VSL bromocarbons is shown in Figure 6.3 as the red line. The 'natural background' scenario returns to this benchmark level by 2037, whereas the 'current trend' scenario returns by 2050. However, it should be noted that this new benchmark does include significant anthropogenic emissions from the VSLs occurring before 1980. Therefore, the benchmark year for representing a time before the major stratospheric ozone losses might be improved if it is taken as 1975 (green line Figure 6.3). This is the year in the current study that has the same EESC mixing ratios as the '1980 benchmark'. It should also be noted that the impact of these declining EESC mixing ratios depends on the region of the stratosphere considered, with the greatest effect in regions where less halogen radicals have been liberated from long-lived source gases, but where chemical ozone loss is still important. Yet, currently it is unclear how VSLS emission reductions in specific locations and during different times of the year would quantitatively effect the abundance of stratospheric chlorine. The current results indicate that it would be desirable to minimise future anthropogenic emissions and that

further studies, which should include observations from global ground-based networks, are needed to improve our understanding of the emission processes, patterns and the global distribution of the chlorocarbons and bromocarbons.

6.2 Fluorinated greenhouse gases

Another aim of this project was to derive a northern hemispheric atmospheric time series for the fluorinated greenhouse gases from the NEEM firn air samples. The reconstruction of these time series were produced using a firn diffusion model (*Buizert et al.*, 2011 and *Witrant et al.*, 2011) and with iterative dating techniques. Table 6.2 shows a summary of the key findings.

Table 6.2: Key finding of the fluorinated greenhouse gases

Compound	**Publications – using this study's firn measurements**	**Date of first detectable mixing ratio**	**Mid–2008 mixing ratio (ppt)**
SF_6	*Buizert et al.* (2011) and *Witrant et al.* (2011)	1956	6.6
SF_5CF_3	*Sturges et al.* (2012)	1960	0.15
n-C_4F_{10}	*Laube et al.* (2012)	1969	0.17
n-C_5F_{12}	*Laube et al.* (2012)	1966	0.14
n-C_6F_{14}	*Laube et al.* (2012)	1961	0.25
n-C_7F_{16}	*Laube et al.* (2012)	1962	0.11
HFC-32	-	1998	2.7

Table 6.2 indicates that all of the compounds, investigated are detectable in the atmosphere after 1950. Since their introduction into the atmosphere, all of these gases have shown significant growth, and apart from SF_5CF_3 all are showing continuing growth.

Currently, SF_6 has the largest effect on the atmospheric energy budget of the fluorinated greenhouse gases with a mid-2008 mixing ratio of 6.6 ppt and a total CO_2-equivalent of 3800 $MMTCO_2Eq$. The key finding for SF_5CF_3 is that its emissions are not related to those of SF_6, in contradiction to earlier assertions (*Sturges et al.*, 2000), with the atmospheric mixing ratio of SF_5CF_3 becoming stable around 2000. The perfluorocarbons measured in this study have all increased in the atmosphere, during the 20th and early 21st centuries. However currently the growth rate and the emissions rates of n-C_4F_{10}, n-C_5F_{12} and n-C_6F_{14} are declining, whilst n-C_7F_{16} shows no major decline. Although significant HFC-32 emissions only began in 1998, they are currently increasing rapidly.

As with the VSL chlorocarbons and VSL bromocarbons, it is important to assess the possible future emissions of the fluorinated greenhouse gases. Possible future emissions trends were assessed by producing 3 different scenarios. Scenario 1 continues on the current trend of these compounds year-on-year up until 2050. This scenario is known as the 'current trend' scenario. Scenarios 2 and 3 are based on the emissions scenarios produced by IPCC reports (*Forster et al.*, 2007 and *Houghton et al.*, 2001).

The IPCC developed a set of scenarios to represent the range of driving forces and emissions as well as reflecting underlying uncertainties in future emissions. These scenarios are based on the driving forces and emissions in scenario literature, alternative modelling approaches, and an "open process" that solicited wide participation and feedback (*Forster et al.*, 2007). Four different scenario bases (A1, A2, B1 and B2) were developed, with each one representing different demographic and technological changes as well as social, economic and environmental developments. In the current study, scenarios A1 and B1 are used to estimate future emissions of fluorinated greenhouse gases.

A1 describes a scenario with very rapid economic growth, a global population that peaks in the mid-21st century and declines thereafter, and includes the rapid introduction of new and more efficient technologies (*Forster et al.*, 2007). The emphasis of scenario A1, is on convergence between regions, capacity building, and increased cultural and social interactions, with a substantial reduction in the regional differences in per capita income (*Forster et al.*, 2007). B1 describes a scenario with a convergent world with the same population trend as A1, but with rapid changes in economic structures toward a service and information economy, with reductions in material intensity, and the introduction of clean and resource-efficient technologies (*Forster et al.*, 2007). The emphasis of scenario B1 is on global solutions to economic, social and environmental sustainability, including improved equity, but without additional climate initiatives. The IPCC produced A1 and B1 scenarios for SF_6 and HFC-32 (*Forster et al.*, 2007 and *Houghton et al.*, 2001). I scaled these scenarios to emissions rates determined in the current study and then produced future emissions rates shown in Table 6.3. Future emission estimates for other fluorinated greenhouse gases produced by scaling the scenarios of each compound to that of SF_6. The scenario of SF_6 was selected to represent the most likely increase in anthropogenic source gases.

To examine the relative contribution each of these fluorinated greenhouse gases might have in the future, Table 6.4 compares these scenarios to the A1, B1 and '80 %' scenarios of future CO_2 emissions based on *Forster et al.* (2007). The '80 %' scenario is based on *Montzka et al.* (2011),

with a proposed cut of 80 % in 2007 emissions levels by 2050 and a linear phase out between 2009 and 2050. This is used because an 80 % reduction in anthropogenic emissions of CO_2 is required just to stabilize its direct radiative forcing (*Solomon et al.*, 2011).

Table 6.3: Future predicted emissions of the fluorinated greenhouse gases observed in this study in million metric tonnes of CO_2 equivalents per year

Compound	SF_6			SF_5CF_3			n-C_4F_{10}			n-C_5F_{12}			n-C_6F_{14}			n-C_7F_{16}			HFC-32		
Scenario	**CT**	**A1**	**B1**	**CT**	**A1**	**B1**	**CT**	**A1**	**B1**	**CT**	**A1**	**B1**	**CT**	**A1**	**B1**	**CT**	**A1**	**B1**	**CT**	**A1**	**B1**
2007	129	129	129	0.2	0.2	0.2	0.5	0.5	0.5	1.2	1.2	1.2	3.0	3.0	3.0	2.2	2.2	2.2	4.5	4.5	4.5
2020	201	140	131	0.2	0.3	0.2	0.6	0.6	0.6	1.6	1.3	1.2	4.0	3.3	3.1	3.5	2.4	2.3	6.5	9	9
2030	283	196	166	0.2	0.4	0.3	0.7	0.8	0.7	1.9	1.9	1.6	5.0	4.6	3.9	5.0	3.4	2.9	16.9	16	12
2050	561	352	194	0.3	0.6	0.4	0.8	1.5	0.8	2.8	3.3	1.8	7.8	8.3	4.5	9.9	6.1	3.4	113.5	27	17

CT - Current trend, A1 – A1 scenario from IPCC (*Forster et al.*, 2007 and *Houghton et al.*, 2001), B1 – B1 scenario from IPCC (*Forster et al.*, 2007 and *Houghton et al.*, 2001), units - $MMTCO_2$

Table 6.4: Comparison between the total fluorinated greenhouse gases observed in this study and CO_2 emissions

Compound	Total - Fluorinated GHGs from Table 3 ($MMTCO_2$)			Total CO_2 emissions* (MMT)			% of CO_2 A1 emissions scenario			% of CO_2 B1 emissions scenario			% of CO_2 '80 %' emissions scenario		
Scenario	**CT**	**A1**	**B1**	**A1**	**B1**	**80 %**	**CT**	**A1**	**B1**	**CT**	**A1**	**B1**	**CT**	**A1**	**B1**
2007	141	141	141	12000	12000	12000	1.2%	1.2%	1.2%	1.2%	1.2%	1.2%	1.2%	1.2%	1.2%
2020	218	157	148	12800	12600	9100	1.7%	1.2%	1.2%	1.7%	1.2%	1.2%	2.4%	1.7%	1.6%
2030	313	223	187	14300	13500	6900	2.2%	1.6%	1.3%	2.3%	1.7%	1.4%	4.6%	3.3%	2.7%
2050	696	399	222	16200	14500	2400	4.3%	2.5%	1.4%	4.8%	2.8%	1.5%	29.0%	16.6%	9.2%

* *Forster et al.* (2007)

Tables 6.3 and 6.4 show that all of the scenarios of the fluorinated greenhouse gases measured in this study indicate an increase relative to total CO_2 emissions by 2050. Also, if there is a reduction in total CO_2 emissions as in the '80 %' scenario then the relative emissions of the compounds observed in this study will increase dramatically. These results indicate that even though the fluorinated greenhouse gases currently have small atmospheric mixing ratios they do have strong Global Warming Potentials (hundreds to several thousand times higher than carbon dioxide). Apart from HFC-32, these fluorinated greenhouse gases have long atmospheric lifetimes of several hundred to thousands of years. This means that they could represent an essentially irreversible change to the composition of the Earth's atmosphere and to the radiative forcing of the climate in the future. These results also indicate that it is highly desirable to maximise any reduction in the emissions of these compounds in the future.

6.3 Recommendations

During this study, I have made a number of recommendations and suggest further studies that I would like to put into practice in the future. The first recommendation I would make on this project is that currently, CH_2ClCH_2Cl, C_2H_5Cl and HFC-32 are on a reference calibration scale, with CH_2BrCH_2Br and C_2H_5Br being on older 'UEA scales'. Therefore, these results need to be verified in the future with the rigorous calibration techniques as described in Chapter 2. There are also some calibration differences between this study and other previous VSL halocarbons studies. This is likely due to the lack of inter-calibration measurements of the VSL halocarbons between individually published datasets. The absence of a common calibration scale makes it difficult to distinguish true environmental variations from artefacts arising from differences between calibration methodologies. Therefore, global flux estimates would be improved if a database of collated global halocarbon observations was produced.

Future monitoring is very important for all the species observed in this study. These compounds are potent ozone depleting substances or greenhouse gases, and all have a significant impact on the chemical composition of the atmosphere. Subsequently, it will be very important to monitor the changing atmospheric mixing ratios of these compounds to support any future mitigation options should these be needed to control anthropogenic emissions. There is evidence that CH_2Cl_2, CH_2ClCH_2Cl (Chapter 3) and HFC-32 (Chapter 5) currently have rapidly increasing emissions and growth rates and thus require monitoring to confirm these findings.

It is also important to validate all firn air derived atmospheric time series. The best way of doing this is by taking new firn air measurements from Arctic and Antarctic firn sampling sites and then using these measurements along with the multi-site modelling method to produce new time series. These could be compared against results from the current study for consistency. This is especially true for the southern hemispheric firn air derived times series for which the last measurement was in 1999. A new Antarctic firn sampling project would be able to validate the current time series and bring it up-to-date by at least 13 years a period of time over which much change is likely to have occurred. This Antarctic firn could also be used to produce southern hemispheric time series for CH_2ClCH_2Cl, C_2H_5Cl, $CHClCCl_2$, C_2H_5Br, CH_2BrCl, $CHBrCl_2$ and $CHBr_2Cl$ which I was not able to produce in this study.

I would also recommend in future investigations, the use of either a 2-D or 3-D atmospheric chemistry-transport model to improve emissions and EESC estimates of the compounds. These models will improve the emissions estimates by removing a number of the assumptions made in the current study such as the instantaneous mixing in the atmosphere and the homogeneous OH field. These models will also refine EESC by improving estimate of source gas injection into the stratosphere. It would also significantly improve EESC estimates if the product gas injection from the VSL compounds were modelled using an atmospheric chemistry model.

I would recommend that in the future there are more stratospheric measurements of halogenated trace gases. These will help to reduce the uncertainties in the abundance of halogen-containing ODSs reaching the stratosphere, and the resulting ozone depletion. These measurements will also help with the understanding of the climate feedbacks that occur between the emissions and transport of ODSs, particularly in the tropics where short-lived ODSs can enter the stratosphere in powerful deep convective systems.

In the current study there have been several gross disagreements between top-down and bottom-up emissions estimates. Therefore, I recommend that there needs to be improvements in the emissions inventon's, by the increasing the countries that report emissions. As well as improving the identification and emission rates of sources. This is especially true for the compound like CH_2Cl_2 that are current increasing in the atmosphere.

References

3M (2012), http://solutions.3m.com/wps/portal/3M/en_US/PFOS/PFOA/Information/phase-out-technologies/, edited.

Andreae, M. O., and Merlet, P. (2001), Emission of trace gases and aerosols from biomass burning, *Global Biogeochemical Cycles*, *15*(4), 955-966.

Appenzeller, C., Stocker, T. F., and Anklin, M. (1998), North Atlantic Oscillation dynamics recorded in Greenland ice cores, *Science, 282, 446–449*.

Aschmann, J., Sinnhuber, B., Atlas, E., and Schauffler, S. (2009), Modeling the transport of very short-lived substances into the tropical upper troposphere and lower stratosphere, *Atmos. Chem. Phys*, *9*(23), 9237-9247.

Atlas, E., and Ridley, B. (1996), The Mauna Loa Observatory Photochemistry Experiment: Introduction, *Journal of Geophysical Research*, *101*(D9), 14531-14541.

Atlas, E., Pollock, W., Greenberg, J., Heidt, L., and Thompson, A. M. (1993), Alkyl Nitrates, Nonmethane Hydrocarbons, and Halocarbon Gases over the Equatorial Pacific-Ocean during Saga-3, *Journal of Geophysical Research-Atmospheres*, *98*(D9), 16933-16947.

Aucott, M., McCulloch, A., Graedel, T., Kleiman, G., Midgley, P., and Li, Y. F. (1999), Anthropogenic emissions of trichloromethane (chloroform, CHCl3) and chlorodifluoromethane (HCFC-22): Reactive Chlorine Emissions Inventory, *Journal of Geophysical Research*, *104*(D7), 8405-8415.

Aydin, M., Saltzman, E. S., De Bruyn, W. J., Montzka, S. A., Butler, J. H., and Battle, M. (2004), Atmospheric variability of methyl chloride during the last 300 years from an Antarctic ice core and firn air, *Geophysical Research Letters*, *31*(2), -.

Baker, J., Sturges, W., Sugier, J., Sunnenberg, G., Lovett, A., Reeves, C., Nightingale, P., and Penkett, S. (2001), Emissions of CH_3Br, organochlorines, and organoiodines from temperate macroalgae, *Chemosphere-Global Change Science*, *3*(1), 93-106.

Bales, R. C., and Wolff, E. W. (1995), Interpreting natural climate signals in ice cores, *EOS Transactions*, *76*, 477-483.

Ballschmiter, K. (1992), Transport and fate of organic compounds in the global environment, *Angewandte Chemie International Edition in English*, *31*(5), 487-515.

Barrie, L., Bottenheim, J., Schnell, R., Crutzen, P., and Rasmussen, R. (1988), Ozone destruction and photochemical reactions at polar sunrise in the lower Arctic atmosphere, *Nature*, *334*, 138-141.

Barth, M., Skamarock, W., and Stuart, A. (2001), Numerical simulations of the July 10, 1996, Stratospheric-Tropospheric Experiment: Radiation, Aerosols, and Ozone(STERAO)-Deep Convection experiment storm- Redistribution of soluble tracers, *Journal of Geophysical Research*, *106*, 12.

Battle, M., M Bender, T Sowers, PP Tans, and Butler, J. (1996), Histories of atmospheric gases from the firn at South Pole, *Nature 383, 231-235*.

Bauer, E. (1979), A catalog of perturbing influences on stratospheric ozone, 1955–1975, *Journal of Geophysical Research*, *84*(C11), 6929-6940.

Berg, W. W., Heidt, L. E., Pollock, W., Sperry, P. D., Cicerone, R. J., and Gladney, E. S. (1984), Brominated organic species in the Arctic atmosphere, *Geophysical Research Letters*, *11*(5), 429-432.

Bernard, S., Röckmann, T., Kaiser, J., Barnola, J., Fischer, H., Blunier, T., and Chappellaz, J. (2006), Constraints on N2O budget changes since pre-industrial time from new firn air and ice core isotope measurements, *Atmospheric Chemistry and Physics*, *6*(2), 493-503.

Beukes, J. A., and Nicolaisen, F. (2000), Infrared absorption cross-sections and integrated absorption intensities for difluoromethane (HFC-32) and 1, 1, 1, 2-tetrafluoroethane (HFC-134a) in the 650–50 cm region, *Journal of Quantitative Spectroscopy and Radiative Transfer*, *66*(2), 185-198.

Bilde, M., Wallington, T., Ferronato, C., Orlando, J., Tyndall, G., Estupinan, E., and Haberkorn, S. (1998), Atmospheric chemistry of CH_2BrCl, $CHBrCl_2$, $CHBr_2Cl$, $CF_3CHBrCl$, and CBr_2Cl_2, *The Journal of Physical Chemistry A*, *102*(11), 1976-1986.

Blake, N. J., Blake, D. R., Chen, T. Y., Collins, J. E., Sachse, G. W., Anderson, B. E., and Rowland, F. S. (1997), Distribution and seasonality of selected hydrocarbons and halocarbons over the western Pacific basin during PEM-West A and PEM-West B, *Journal of Geophysical Research-Atmospheres*, *102*(D23), 28315-28331.

Blake, N. J., Blake, D. R., Simpson, I. J., Meinardi, S., Swanson, A. L., Lopez, J. P., Katzenstein, A. S., Barletta, B., Shirai, T., and Atlas, E. (2003), NMHCs and halocarbons in Asian continental outflow during the Transport and Chemical Evolution over the Pacific (TRACE-P) Field Campaign: Comparison with PEM-West B, *J. Geophys. Res*, *108*, 8806.

Blei, E., Hardacre, C. J., Mills, G. P., Heal, K. V., and Heal, M. R. (2010), Identification and quantification of methyl halide sources in a lowland tropical rainforest, *Atmospheric Environment*, *44*(8), 1005-1010.

Blowers, P., and Hollingshead, K. (2009), Estimations of Global Warming Potentials from Computational Chemistry Calculations for CH_2F_2 and Other Fluorinated Methyl Species Verified by Comparison to Experiment, *The Journal of Physical Chemistry A*, *113*(20), 5942-5950.

Bosenberg, M. (2011), Anaesthetic gases: environmental impact and alternatives, *Southern African Journal of Anaesthesia and Analgesia*, *17*(5), 345-348.

Bovill, J. (2008), Inhalation anaesthesia: from diethyl ether to xenon, *Modern Anesthetics*, *182*, 121-142.

Bravo, I., Aranda, A., Hurley, M. D., Marston, G., Nutt, D. R., Shine, K. P., Smith, K., and Wallington, T. J. (2010), Infrared absorption spectra, radiative efficiencies, and global warming potentials of perfluorocarbons: Comparison between experiment and theory, *Journal of Geophysical Research*, *115*(D24).

Briffa, K. R., Osborn, T. J., Schweingruber, F. H., Harris, I. C., Jones, P. D., Shiyatov, S. G., and Vaganov, E. A. (2001), Low-frequency temperature variations from a northern tree ring density network, *J. Geophys. Res., 106(D3), 2929–2941*.

Brodzinsky, R., Cupitt, L. T., Singh, H., Center, S. I. A. S., Research, U. S. E. P. A. O. o., Development, Laboratory, E. S. R., and Service, U. S. N. T. I. (1997), *Volatile organic chemicals in the atmosphere: an assessment of available data*, Environmental Sciences Research Laboratory, Office of Research and Development, US Environmental Protection Agency.

Brown, A., Canosa-Mas, C., Parr, A., Pierce, J., and Wayne, R. (1989), Tropospheric lifetimes of halogenated anaesthetics, *Nature*, *341*(6243), 635-637.

Buizert, C., Martinerie, P., Petrenko, V. V., Severinghaus, J. P., Trudinger, C. M., E.Witrant, Rosen, J. L., Orsi, A., Rubino, M., Etheridge, D. M., Steele, L. P., Hogan, C., Laube, J. C., Sturges, W. T., Levchenko, V. A., Smith, A. M., Levin, I., Conway, T. J., Dlugokencky, E. J., Lang, P. M., Kawamura, K., Jenk, T. M., Sowers, T., Schwander, J., and Blunier, T. (2011), Gas transport in firn: multiple-tracer characterisation and model intercomparison for NEEM, Northern Greenland, *Atmos. Chem. Phys., 12, 4259–4277*, 15975-16021.

Bunker, J. P., and Forrest, W. H. (1969), *The national halothane study*, National Inst. of Health, National Inst. of General Medical Sciences.

Busenberg, E., and Plummer, L. N. (2000), Dating young groundwater with sulfur hexafluoride: Natural and anthropogenic sources of sulfur hexafluoride, *Water Resources Research*, *36*(10), 3011-3030.

Busenberg, E., and Plummer, L. N. (2008), Dating groundwater with trifluoromethyl sulfurpentafluoride (SF_5CF_3), sulfur hexafluoride (SF_6), CF_3Cl (CFC-13), and CF_2Cl_2 (CFC-12), *Water Resour. Res*, *44*, W02431.

Butler, J. H., Hofmann, D. J., Peterson, J. T., and Rosson, R. M. (1998a), in Summary Report 1996 -1997 (eds Hofmann, D. J., Peterson, J. T. & Rosson, R. M.), *91-121 Rep. No. 24, Climate Monitoring and Diagnostics Lab., US Dept of Commerce, Boulder,*.

Butler, J. H., Montzka, S. A., Clarke, A. D., and Lobertl, J. M. (1998b), Growth and distribution of halons in the atmosphere, *Journal of Geophysical Research*, *103*(D1), 1503-1511.

Butler, J. H., Battle, M., Bender, M. L., Montzka, S. A., Clarke, A. D., Saltzman, E. S., Sucher, C. M., Severinghaus, J. P., and Elkins, J. W. (1999), A record of atmospheric halocarbons during the twentieth century from polar firn air, *Nature*, *399*(6738), 749-755.

Butler, J. H., King, D. B., Lobert, J. M., Montzka, S. A., Yvon-Lewis, S. A., Hall, B. D., Warwick, N. J., Mondeel, D. J., Aydin, M., and Elkins, J. W. (2007), Oceanic distributions and emissions of short-lived halocarbons, *Global Biogeochem. Cycles*, *21*.

Carpenter, L., Malin, G., Liss, P., and Kupper, F. (2000), Novel biogenic iodine-containing trihalomethanes and other short-lived halocarbons in the coastal East Atlantic, *Global Biogeochemical Cycles*, *14*(4), 1191-1204.

Carpenter, L., Sturges, W., Penkett, S., Liss, P., Alicke, B., Hebestreit, K., and Platt, U. (1999), Short-lived alkyl iodides and bromides at Mace Head, Ireland: Links to biogenic sources and halogen oxide production, *Journal of Geophysical Research*, *104*(D1), 1679-1689.

Carpenter, L. J., Liss, P. S., and Penkett, S. A. (2003), Marine organohalogens in the atmosphere over the Atlantic and Southern Oceans, *Journal of Geophysical Research-Atmospheres*, *108*(D9).

Chamie, J., Chappell, L., Cortina, J., and Delgado-Wise, R. (1999), The world at six billion, *ESA/P/WP.154, Popul. Div., New York*.

Chen, N. H., and Othmer, D. F. (1962), New Generalized Equation for Gas Diffusion Coefficient, *Journal of Chemical and Engineering Data*, *7*(1), 37-41.

Class, T., and Ballschmiter, K. (1987), Global baseline pollution studies, *Fresenius' Journal of Analytical Chemistry*, *327*(2), 198-204.

Class, T., and Ballschmiter, K. (1988), Chemistry of organic traces in air, *Journal of Atmospheric Chemistry*, *6*(1), 35-46.

Clerbaux and Cunnold, D., Anderson, J., Engel, A., Fraser, P. J., Mahieu, E., Manning, A., Miller, J., Montzka, S. A., Nassar, R., Prinn, R., Reimann, S., Rinsland, C. P., Simmonds, P., Verdonik, D., Weiss, R., Wuebbles, D., and Yokouchi, Y. (2006), Scientific Assessment of Ozone Depletion: 2006, *Global Ozone Research and Montitoring Project, Geneva, Switzerland*.

Colbeck, S. (1989), Air movement in snow due to windpumping, *J. Glaciol*, *35*(120), 209-213.

Cox, M. L., Fraser, P. J., Sturrock, G. A., Siems, S. T., and Porter, L. W. (2004), Terrestrial sources and sinks of halomethanes near Cape Grim, Tasmania, *Atmospheric Environment*, *38*(23), 3839-3852.

Cox, M. L., Sturrock, G. A., Fraser, P. J., Siems, S. T., Krummel, P. B., and O'Doherty, S. (2003), Regional sources of methyl chloride, chloroform and dichloromethane identified from AGAGE observations at Cape Grim, Tasmania, 1998–2000, *J. Atmos. Chem., 45, 79–99*.

Craig, H., Horibe, Y., and Sowers, T. (1988), Gravitational separation of gases and isotopes in polar ice caps, *Science*, *242*(4886), 1675.

Crutzen, P. J., and Lawrence, M. G. (2000), The impact of precipitation scavenging on the transport of trace gases: A 3-dimensional model sensitivity study, *Journal of Atmospheric Chemistry*, *37*(1), 81-112.

Daniel, J., Fleming, E., Portmann, R., Velders, G., Jackman, C., and Ravishankara, A. (2010), Options to accelerate ozone recovery: ozone and climate benefits, *Atmospheric Chemistry and Physics*, *10*(16), 7697-7707.

deBoer, Y. (2007), Kyoto Protocol Reference Manual, On accounting of emissions and assigned amount, *United Nations framework convention on climate change, Kyoto Protocol, Kyoto*.

Dimmer, C., McCulloch, A., Simmonds, P., Nickless, G., Bassford, M., and Smythe-Wright, D. (2001a), Tropospheric concentrations of the chlorinated solvents, tetrachloroethene and

trichloroethene, measured in the remote northern hemisphere, *Atmospheric Environment*, *35*(7), 1171-1182.

Dimmer, C. H., Simmonds, P. G., Nickless, G., and Bassford, M. R. (2001b), Biogenic fluxes of halomethanes from Irish peatland ecosystems, *Atmospheric Environment*, *35*(2), 321-330.

Donner, L. J., Horowitz, L. W., Fiore, A. M., Seman, C. J., Blake, D. R., and Blake, N. J. (2007), Transport of radon-222 and methyl iodide by deep convection in the GFDL Global Atmospheric Model AM2, *J. Geophys. Res*, *112*, D17303.

Dorf, M., Butler, J., Butz, A., Camy-Peyret, C., Chipperfield, M., Kritten, L., Montzka, S., Simmes, B., Weidner, F., and Pfeilsticker, K. (2006), Long-term observations of stratospheric bromine reveal slow down in growth, *Geophys. Res. Lett*, *33*, L24803.

Duncan, B. N., Martin, R. V., Staudt, A. C., Yevich, R., and Logan, J. A. (2003), Interannual and seasonal variability of biomass burning emissions constrained by satellite observations, *J. Geophys. Res., 108(D2), 4100, doi:10.1029/2002JD002378*.

Ekdahl, A., Pedersén, M., and Abrahamsson, K. (1998), A study of the diurnal variation of biogenic volatile halocarbons, *Marine Chemistry*, *63*(1-2), 1-8.

Elkins, J. W., J. H. Butler, D. F. Hurst, S. A. Montzka, F. L. Moore, and T. M. Thompson (2001), Nitrous Oxide and Halocompounds Group, *Global Monitoring Division of NOAA Earth System Research Laboratory, Boulder, Colo.*

Ensminger, A. (1988), *Cahiers de Notes Documentaires*, *131*, 299-301.

Etheridge, D., Steele, L. P., Francey, R., and Langenfelds, R. (1998), Atmospheric methane between 1000 AD and present: Evidence of anthropogenic emissions and climatic variability, *Journal of Geophysical Research*, *103*(D13), 15979-15915,15993.

Eyring, V., Waugh, D., Bodeker, G., Cordero, E., Akiyoshi, H., Austin, J., Beagley, S., Boville, B., Braesicke, P., and Brühl, C. (2007), Multimodel projections of stratospheric ozone in the 21st century, *J. Geophys. Res*, *112*(D16303).

Feng, W., Chipperfield, M., Dorf, M., Pfeilsticker, K., and Ricaud, P. (2007), Mid-latitude ozone changes: studies with a 3-D CTM forced by ERA-40 analyses, *Atmospheric Chemistry and Physics*, *7*(9), 2369.

Fenton, P. (2000), Volatile anaesthetic agents, *Update in anaesthesia*(11).

Fishbein, L. (1980), Production, uses, and environmental fate of ethylene dichloride and ethylene dibromide, B. Ames, P. Infante, R. Reitz, Editors Banbury Report 5, edited, Cold Spring Harbor Laboratory, Coldr Spring Harbor.

Folkins, I., and Martin, R. V. (2005), The vertical structure of tropical convection and its impact on the budgets of water vapor and ozone, *Journal of the atmospheric sciences*, *62*(5), 1560-1573.

Forster, P., Ramaswamy, V., Artaxo, P., Berntsen, T., Betts, R., Fahey, D. W., Haywood, J., Lean, J., Lowe, D. C., Myhre, G., Nganga, J., Prinn, R., Raga, G., Schulz, M., and Dorland, R. V. (2007), *Climate change 2007: the physical science basis: contribution of Working Group I to the Fourth Assessment Report of the Intergovernmental Panel on Climate Change*, Cambridge Univ Pr.

Fox, J., Fox, E. J., and Villanueva, R. (1975), Letter: Stratospheric ozone destruction and halogenated anaesthetics, *Lancet*, *1*(7911), 864.

Fraser, P., Oram, D., Reeves, C., Penkett, S., and McCulloch, A. (1999), Southern Hemispheric halon trends (1978–1998) and global halon emissions, *Journal of Geophysical Research*, *104*(D13), 15985.

Fraser, P. J., L.W. Porter, S.B. Baly, P.B. Krummel, B.L. Dunse, L.P. Steele, N. Derek, R.L. Langenfelds, I. Levin, D.E. Oram, J.W. Elkins, M.K. Vollmer, and R.F. Weiss (2004), Sulfur hexafluoride at Cape Grim: long term trends and regional emissions, in Baseline Atmospheric Program (Australia) 2001-2002, *edited by J.M. Cainey, N. Derek, and P.B. Krummel, 18-23, Bureau of Meteorology and CSIRO Division of Atmospheric Research, Melbourne, Australia.*

Fueglistaler, S., Bonazzola, M., Haynes, P., and Peter, T. (2005), Stratospheric water vapor predicted from the Lagrangian temperature history of air entering the stratosphere in the tropics, *J. Geophys. Res*, *110*, D08107.

Fueglistaler, S., Dessler, A., Dunkerton, T., Folkins, I., Fu, Q., and Mote, P. W. (2009), Tropical tropopause layer, *Reviews of Geophysics*, *47*(1).

Garcia, J., Beyne-Masclet, S., Mouvier, G., and Masclet, P. (1992), Emissions of volatile organic compounds by coal-fired power stations, *Atmospheric Environment. Part A. General Topics*, *26*(9), 1589-1597.

Gebhardt, S., Colomb, A., Hofmann, R., Williams, J., and Lelieveld, J. (2008), Halogenated organic species over the tropical South American rainforest, *Atmospheric Chemistry and Physics*, *8*(12), 3185-3197.

Geller, L., Elkins, J., Lobert, J., Clarke, A., Hurst, D., Butler, J., and Myers, R. (1997), Tropospheric SF_6 Observed latitudinal distribution and trends, derived emissions and interhemispheric exchange time, *Geophysical Research Letters*, *24*(6), 675-678.

Gettelman, A., and Forster, P. M. F. (2002), A climatology of the tropical tropopause layer, *80*(4B), 911-924.

Gettelman, A., Lauritzen, P., Park, M., and Kay, J. (2009), Processes regulating short-lived species in the tropical tropopause layer, *J. Geophys. Res*, *114*, D13303.

Gleissberg, W. (1966), Ascent and descent in the eighty-year cycles of solar activity, *J. British Astron. Soc., 76, 265–270*.

González, M., Horwitz, P., Bankobeza, G., Seki, M., Batten, R., Mutisya, G., Mylona, S., and Saldanha, M. (2006), Handbook for the Montreal Protocol on Substances that Deplete the Ozone Layer, *Ozone Secr.,*.

Graedel, T., and Keene, W. (1996), The budget and cycle of Earth's natural chlorine, *Pure and Applied Chemistry*, *68*(9), 1689-1698.

Greally, B., Simmonds, P., O'Doherty, S., McCulloch, A., Miller, B., Salameh, P., Mühle, J., Tanhua, T., Harth, C., and Weiss, R. (2005), Improved continuous in situ measurements of C1–C3 PFCs, HFCs, HCFCs, CFCs and SF_6 in Europe and Australia, *Environmental Sciences*, *2*(2-3), 253-261.

Hall, D. B. D., Dutton, G. S., and Elkins, D. J. W. (2012), National Oceanic and Atmospheric Administration (NOAA), edited.

Hardacre, C. J., Blei, E., and Heal, M. R. (2009), Growing season methyl bromide and methyl chloride fluxes at a sub-arctic wetland in Sweden, *Geophysical Research Letters*, *36*.

Heard, D. E. (2006), *Analytical techniques for atmospheric measurement*, Wiley Online Library.

Highwood, E., and Shine, K. (2000), Radiative forcing and global warming potentials of 11 halogenated compounds, *Journal of Quantitative Spectroscopy and Radiative Transfer*, *66*(2), 169-183.

Hoekstra, E. J., De Leer, E. W. B., and Brinkman, U. A. T. (1998a), Natural formation of chloroform and brominated trihalomethanes in soil, *Environ. Sci. Technol*, *32*(23), 3724-3729.

Hoekstra, E. J., Verhagen, F. J. M., Field, J. A., Leer, E. W. B. D., and Brinkman, U. A. T. (1998b), Natural production of chloroform by fungi, *Phytochemistry*, *49*(1), 91-97.

Holton, J. R., Haynes, P. H., Mcintyre, M. E., Douglass, A. R., Rood, R. B., and Pfister, L. (1995), Stratosphere-troposphere exchange, *Rev. Geophys*, *33*(4), 403-439.

Homan, C. D., Volk, C. M., Kuhn, A., Werner, A., Baehr, J., Viciani, S., Ulanovski, A., and Ravegnani, F. (2010), Tracer measurements in the tropical tropopause layer during the AMMA/SCOUTO3 aircraft campaign, *Atmos. Chem. Phys*, *10*(8), 3615-3627.

Hopkins, K., Albanese, R., Joyner, B., Rodgers, R., and Ross, J. (1989), Anaesthetic Agents and the Ozone Layer, *The Lancet*, *333*(8648), 1209-1210.

Hossaini, R., Chipperfield, M., Monge-Sanz, B., D Richards, N., Atlas, E., and Blake, D. (2010a), Bromoform and dibromomethane in the tropics: a 3-D model study of chemistry and transport, *Atmospheric Chemistry and Physics*, *10*(2), 719-735.

Hossaini, R., Chipperfield, M., Monge-Sanz, B., Richards, N., Atlas, E., and Blake, D. (2010b), Bromoform and dibromomethane in the tropics: a 3-D model study of chemistry and transport, *Atmos. Chem. Phys*, *10*(2), 719-735.

Hossaini, R., Chipperfield, M., Feng, W., Breider, T., Atlas, E., Montzka, S., Miller, B., Moore, F., and Elkins, J. (2012), The contribution of natural and anthropogenic very short-lived species to stratospheric bromine, *Atmos. Chem. Phys*, *12*, 371-380.

Hough, A. M. (1989), The development of a two-dimensional global tropospheric model—1. The model transport, *Atmospheric Environment (1967)*, *23*(6), 1235-1261.

Houghton, J. T., Ding, Y., Griggs, D. J., Noguer, M., Linden, P. J. v. d., Dai, X., Maskell, K., and Johnson, C. A. (2001), *Climate change 2001: the scientific basis*, Cambridge University Press Cambridge.

Hu, L., Yvon-Lewis, S. A., Liu, Y., Salisbury, J. E., and O'Hern, J. E. (2010), Coastal emissions of methyl bromide and methyl chloride along the eastern Gulf of Mexico and the east coast of the United States, *Global Biogeochemical Cycles*, *24*.

Huang, L., Zhu, L. L., Pan, X. X., Zhang, J. L., Bin, O. Y., and Hou, H. Q. (2005), One potential source of the potent greenhouse gas SF_5CF_3: the reaction of SF_6 with fluorocarbon under discharge, *Atmospheric Environment*, *39*(9), 1641-1653.

Huber, C., Leuenberger, M., Spahni, R., Flückiger, J., Schwander, J., Stocker, T. F., Johnsen, S., Landais, A., and Jouzel, J. (2006), Isotope calibrated Greenland temperature record over Marine Isotope Stage 3 and its relation to CH_4, *Earth and Planetary Science Letters*, *243*(3), 504-519.

IPCC (2007), Contribution of Working Group I to the Fourth Assessment Report of the Intergovernmental Panel on Climate Change*Rep.*

IPCC/TEAP, Hayman, G., Kuijpers, L., Campbell, N., Shende, R., Bennett, M., Blinova, O., Derwent, R., McCulloch, A., Yamabe, M., Shevlin, J., Vink, T., Ashford, P., Midgley, P., and McFarland, M. (2005), HFCs and PFCs: current and future supply, demand and emissions, plus emissions of CFCs, HCFCs and halons, in: IPCC/TEAP Special Report on Safeguarding the Ozone Layer and the Global Climate System, *Cambridge University Press, Cambridge*.

Ishizawa, Y. (2011), General anesthetic gases and the global environment, *Anesthesia & Analgesia*, *112*(1), 213.

Ivy, D., Arnold, T., Harth, C., Steele, L., Muhle, J., Rigby, M., Salameh, P., Leist, M., Krummel, P., and Fraser, P. (2012), Atmospheric histories and growth trends of C_4F_{10}, C_5F_{12}, C_6F_{14}, C_7F_{16} and C_8F_{18}, *Atmos. Chem. Phys. Discuss.,* , *12, 4165–4184*.

Jacob, D. (1999), *Introduction to atmospheric chemistry*, Princeton University Press.

James, R., Bonazzola, M., Legras, B., Surbled, K., and Fueglistaler, S. (2008), Water vapor transport and dehydration above convective outflow during Asian monsoon, *Geophys. Res. Lett*, *35*(20).

Jensen, E., Pfister, L., and Toon, O. (2011), Impact of radiative heating, wind shear, temperature variability, and microphysical processes on the structure and evolution of thin cirrus in the tropical tropopause layer, *Journal of Geophysical Research*, *116*(D12).

Juuti, S., Vartiainen, T., Joutsenoja, P., and Ruuskanena, J. (1996), Volatile organochlorine compounds formed in the bleaching of pulp with ClO_2, *Chemosphere*, *33*(3), 437-448.

Kaspers, K. A. (2004), Chemical and physical analyses of firn and firn air: from Dronning Maud Land, Antarctica, Universiteit Utrecht, Utrecht.

Kaspers, K. A., van de Wal, R., de Gouw, J., Hofstede, C., van den Broeke, M., Reijmer, C., van der Veen, C., Neubert, R., Meijer, H., and Brenninkmeijer, C. (2004a), Seasonal cycles of nonmethane hydrocarbons and methyl chloride, as derived from firn air from Dronning Maud Land, Antarctica, *J. Geophys. Res*, *109*(D2), 245-250.

Kaspers, K. A., van de Wal, R. S. W., de Gouw, J. A., Hofstede, C. M., van den Broeke, M. R., van der Veen, C., Neubert, R. E. M., Meijer, H. A. J., Brenninkmeijer, C. A. M., Karlof, L., and Winther, J. G. (2004b), Analyses of firn gas samples from Dronning Maud Land, Antarctica:

Study of nonmethane hydrocarbons and methyl chloride, *Journal of Geophysical Research-Atmospheres*, *109*(D2),317-325.

Kawamura, K., Severinghaus, J. P., Ishidoya, S., Sugawara, S., Hashida, G., Motoyama, H., Fujii, Y., Aoki, S., and Nakazawa, T. (2006), Convective mixing of air in firn at four polar sites, *Earth and Planetary Science Letters*, *244*(3), 672-682.

Keeling, C. D. (1994), Global historical CO_2 emissions, Trends '93: A Compendium of Data on Global Change, edited by T. A. Boden, D. P. Kaiser, R. J. Sepanski, and F. W. Stoss, *501–504, U.S. Dept. of Energy, Oak Ridge*.

Keene, W. C., Khalil, M. A. K., Erickson, D. J., McCulloch, A., Graedel, T. E., Lobert, J. M., Aucott, M. L., Gong, S. L., Harper, D. B., Kleiman, G., Midgley, P., Moore, R. M., Seuzaret, C., Sturges, W. T., Benkovitz, C. M., Koropalov, V., Barrie, L. A., and Li, Y. F. (1999), Composite global emissions of reactive chlorine from anthropogenic and natural sources: Reactive Chlorine Emissions Inventory, *Journal of Geophysical Research-Atmospheres*, *104*(D7), 8429-8440.

Kerkweg, A., Jöckel, P., Warwick, N., Gebhardt, S., Brenninkmeijer, C., and Lelieveld, J. (2008), Consistent simulation of bromine chemistry from the marine boundary layer to the stratosphere–Part 2: Bromocarbons, *Atmos. Chem. Phys*, *8*(19), 5919-5939.

Khalil, M., and Rasmussen, R. (1985), The trend of CBrClF2 and other Br-containing gases at the South Pole, *Antarct. J. US*, *19*, 206-207.

Khalil, M., and Rasmussen, R. (1999a), Atmospheric chloroform, *Atmospheric Environment*, *33*(7), 1151-1158.

Khalil, M., Rasmussen, R., Shearer, M., Chen, Z. L., Yao, H., and Yang, J. (1998), Emissions of methane, nitrous oxide, and other trace gases from rice fields in China, *Journal of Geophysical Research*, *103*(D19), 25241.

Khalil, M., Moore, R. M., Harper, D. B., Lobert, J. M., Erickson, D. J., Koropalov, V., Sturges, W. T., and Keene, W. C. (1999), Reactive chlorine compounds in the atmosphere, *Reactive Halogen Compounds in the Atmosphere*, 45-79.

Khalil, M. A. K., and Rasmussen, R. A. (1999b), Atmospheric methyl chloride, *Atmospheric Environment*, *33*(8), 1305-1321.

Kiehl, J., and Trenberth, K. E. (1997), Earth's annual global mean energy budget, *Bulletin of the American Meteorological Society*, *78*(2), 197-208.

Kindler, T., Chameides, W., Wine, P., Cunnold, D., Alyea, F., and Franklin, J. (1995), The fate of atmospheric phosgene and the stratospheric chlorine loadings of its parent compounds: CCl_4, C_2Cl_4, C_2HCl_3, CH_3CCl_3, and $CHCl_3$, *Journal of Geophysical Research*, *100*(D1), 1235-1251.

Kleiman, G., and Prinn, R. (2000), Measurement and deduction of emissions of trichloroethene, tetrachloroethene, and trichloromethane (chloroform) in the northeastern United States and southeastern Canada, *Journal of Geophysical Research*, *105*(D23), 28875-28828,28893.

Kloster, S., Six, K., Feichter, J., Maier-Reimer, E., Roeckner, E., Wetzel, P., Stier, P., and Esch, M. (2007), Response of dimethylsulfide (DMS) in the ocean and atmosphere to global warming, *Journal of Geophysical Research*, *112*(G3), G03005.

Ko, M. K. W., and Poulet, G. (2003), Very short-lived halogens and sulfur substances, in Scientific Assessment of Ozone Depletion: 2002, Global Ozone Res. and Monit. Proj, *47, chap. 2, pp. 2.1 – 2.57, World Meteorol. Organ., Geneva, Switzerland*.

Ko, M. K. W., Sze, N. D., Wang, W. C., Shia, G., Goldman, A., Murcray, F. J., Murcray, D. G., and Rinsland, C. P. (1993), Atmospheric Sulfur-Hexafluoride - Sources, Sinks and Greenhouse Warming, *Journal of Geophysical Research-Atmospheres*, *98*(D6), 10499-10507.

Kricker, A., Armstrong, B. K., and McMichael, A. J. (1994), Skin cancer and ultraviolet, *Nature*, *368*(6472), 594.

Krüger, K., Tegtmeier, S., and Rex, M. (2009), Variability of residence time in the Tropical Tropopause Layer during Northern Hemisphere winter, *Atmospheric Chemistry and Physics*, *9*, 6717-6725.

Kurylo, M. J., and Rodriguez, J. M. (1999), Short-lived ozone related compounds, in Scientific Assessment of Ozone Depletion: 1998, *Global Ozone Res. and Monit. Proj., Rep. 44, chap. 2, World Meteorol. Organ., Geneva, Switzerland.*

Landais, A., Barnola, J. M., Kawamura, K., Caillon, N., Delmotte, M., Van Ommen, T., Dreyfus, G., Jouzel, J., Masson-Delmotte, V., and Minster, B. (2006), Firn-air $\delta^{15}N$ in modern polar sites and glacial-interglacial ice: a model-data mismatch during glacial periods in Antarctica?, *Quaternary science reviews*, *25*(1-2), 49-62.

Langbein, T., Sonntag, H., Trapp, D., Hoffmann, A., Malms, W., Röth, E., Mörs, V., and Zellner, R. (1999), Volatile anaesthetics and the atmosphere: atmospheric lifetimes and atmospheric effects of halothane, enflurane, isoflurane, desflurane and sevoflurane, *British journal of anaesthesia*, *82*(1), 66-73.

Larson, R. A., and Weber, E. J. (1994), *Reaction mechanisms in environmental organic chemistry*, Lewis Boca Raton, FL, USA.

Laturnus, F., Wiencke, C., and Klöser, H. (1996), Antarctic macroalgae-Sources of volatile halogenated organic compounds, *Marine Environmental Research*, *41*(2), 169-181.

Laube, J., Hogan, C., Newland, M., Mani, F., Fraser, P., Brenninkmeijer, C., Martinerie, P., Oram, D., Röckmann, T., and Schwander, J. (2012), Distributions, long term trends and emissions of four perfluorocarbons in remote parts of the atmosphere and firn air, *Atmos. Chem. Phys.*, *12*, 4081–4090.

Laube, J. C., Engel, A., Bönisch, H., Möbius, T., Worton, D. R., Sturges, W. T., Grunow, K., and Schmidt, U. (2008), Contribution of very short-lived organic substances to stratospheric chlorine and bromine in the tropics? a case study, *Atmospheric Chemistry and Physics Discussions*, *8*(3), 8491-8515.

Laube, J. C., Martinerie, P., E.Witrant, Blunier, T., Schwander, J., Brenninkmeijer, C. A. M., Schuck, T. J., Bolder, M., Rockmann, T., Veen, C. v. d., Bonisch, H., Engel, A., Mills, G. P., Newland, M. J., Oram, D. E., Reeves, C. E., and Sturges, W. T. (2010), Accelerating growth of HFC-227ea (1,1,1,2,3,3,3-heptafluoropropane) in the atmosphere, *Atmos. Chem. Phys., 10, 5903–5910, 2010*.

Law, R. M., Peters, W., Rodenbeck, C., Aulagnier, C., Baker, I., Bergmann, D. J., Bousquet, P., Brandt, J., Bruhwiler, L., Cameron-Smith, P. J., Christensen, J. H., Delage, F., Denning, A. S., Fan, S., Geels, C., Houweling, S., Imasu, R., Karstens, U., Kawa, S. R., Kleist, J., Krol, M. C., Lin, S. J., Lokupitiya, R., Maki, T., Maksyutov, S., Niwa, Y., Onishi, R., Parazoo, N., Patra, P. K., Pieterse, G., Rivier, L., Satoh, M., Serrar, S., Taguchi, S., Takigawa, M., Vautard, R., Vermeulen, A. T., and Zhu, Z. (2008), TransCom model simulations of hourly atmospheric CO_2: Experimental overview and diurnal cycle results for 2002, *Global Biogeochemical Cycles*, *22*(3), 1029-1035.

Lee-Taylor, J., and Redeker, K. R. (2005), Reevaluation of global emissions from rice paddies of methyl iodide and other species, *Geophysical Research Letters*, *32*(15), 158-166.

Lepine, L., and Archambault, J. F. (1992), Parts-per-trillion determination of trihalomethanes in water by purge-and-trap gas chromatography with electron capture detection, *Analytical Chemistry*, *64*(7), 810-814.

Levin, I., and Hesshaimer, V. (1996), Refining of atmospheric transport model entries by the globally observed passive tracer distributions of 85krypton and sulfur hexafluoride (SF_6), *Journal of Geophysical Research*, *101*, 16.

Levin, I., Naegler, T., Heinz, R., Osusko, D., Cuevas, E., Engel, A., Ilmberger, J., Langenfelds, R. L., Neininger, B., and Rohden, C. (2009), Atmospheric observation-based global SF_6 emissions–comparison of top-down and bottom-up estimates, *Atmos. Chem. Phys. Discuss*, *9*, 26653-26672.

Levin, L., Naegler, T., Heinz, R., Osusko, D., Cuevas, E., Engel, A., Ilmberger, J., Langenfelds, R. L., Neininger, B., and Steele, L. (2010), The global SF_6 source inferred from long-term high precision atmospheric measurements and its comparison with emission inventories, *Atmospheric Chemistry and Physics*, *10*, 2655-2662.

Liang, Q., Stolarski, R., Kawa, S., Nielsen, J., Douglass, A., Rodriguez, J., Blake, D., Atlas, E., and Ott, L. (2010), Finding the missing stratospheric Bry: a global modeling study of $CHBr_3$ and CH_2Br_2, *Atmos. Chem. Phys*, *10*(5), 2269-2286.

Liu, C., and Zipser, E. J. (2005), Global distribution of convection penetrating the tropical tropopause, *J. Geophys. Res*, *110*(D23), D23104.

Lobert, J. M., Keene, W. C., Logan, J. A., and Yevich, R. (1999), Global chlorine emissions from biomass burning: Reactive Chlorine Emissions Inventory, *Journal of Geophysical Research-Atmospheres*, *104*(D7), 8373-8389.

Low, J. C., Wang, N. Y., Williams, J., and Cicerone, R. J. (2003), Measurements of ambient atmospheric C_2H_5Cl and other ethyl and methyl halides at coastal California sites and over the Pacific Ocean, *J. Geophys. Res*, *108*(19), 4608.

Lu, X. L., Yang, G. P., Song, G. S., and Zhang, L. (2010), Distributions and fluxes of methyl chloride and methyl bromide in the East China Sea and the Southern Yellow Sea in autumn, *Marine Chemistry*, *118*(1-2), 75-84.

Maiss, M., and Levin, I. (1994), Global Increase of SF_6 Observed in the Atmosphere, *Geophysical Research Letters*, *21*(7), 569-572.

Maiss, M., and Brenninkmeijer, C. A. M. (1998), Atmospheric SF_6: Trends, sources, and prospects, *Environmental Science & Technology*, *32*(20), 3077-3086.

Manley, S. L., Goodwin, K., and North, W. J. (1992), Laboratory Production of Bromoform, Methylene Bromide, and Methyl-Iodide by Macroalgae and Distribution in Nearshore Southern California Waters, *Limnology and Oceanography*, *37*(8), 1652-1659.

Mann, M. E., Bradley, R. S., and Hughes, M. K. (1998), Global-scale temperature patterns and climate forcing over the past six centuries, *Nature, 392, 779– 787*.

Mari, C., Jacob, D. J., and Bechtold, P. (2000), Transport and scavenging of soluble gases in a deep, *Journal of Geophysical Research*, *105*(D17), 22,255-222,267.

Marland, G., Boden, T. A., and Andres, R. J. (2003), Global, regional, and national CO_2 emissions, in Trends: A Compendium of Data on Global Change, Carbon Dioxide Inf. Anal. Cent., Oak Ridge Natl. Lab, *U.S. Dep. of Energy, Oak Ridge, Tenn.*

Martinerie, P., Nourtier-Mazauric, E., Barnola, J. M., Sturges, W., R Worton, D., Atlas, E., Gohar, L., Shine, K., and P Brasseur, G. (2009), Long-lived halocarbon trends and budgets from atmospheric chemistry modelling constrained with measurements in polar firn, *Atmospheric Chemistry and Physics*, *9*(12), 3911-3934.

Mazurin, I. M., Stolyarevsky, A. Y., Doronin, A. S., and Shevtsov, A. V. (1995), Ozone-friendly working mixture for refrigeration equipment, edited, WO Patent WO/1995/009,214.

McCulloch, A. (1992), Global production and emissions of bromochlorodifluoromethane and bromotrifluoromethane (halons 1211 and 1301), *Atmospheric Environment. Part A. General Topics*, *26*(7), 1325-1329.

McCulloch, A. (2000), Volatile anaesthetics and the atmosphere: atmospheric lifetimes and atmospheric effects of halothane, enflurane, isoflurane, desflurane and sevoflurane, *British journal of anaesthesia*, *84*(4), 534.

McCulloch, A. (2002), Trichloroacetic acid in the environment, *Chemosphere*, *47*(7), 667-686.

McCulloch, A. (2003a), Fluorocarbons in the global environment: a review of the important interactions with atmospheric chemistry and physics, *J. Fluorine Chem. 123 21-29*.

McCulloch, A. (2003b), Chloroform in the environment: occurrence, sources, sinks and effects, *Chemosphere*, *50*(10), 1291-1308.

McCulloch, A., Aucott, M. L., Graedel, T. E., Kleiman, G., Midgley, P. M., and Li, Y. F. (1999), Industrial emissions of trichloroethene, tetrachloroethene, and dichloromethane:

Reactive Chlorine Emissions Inventory, *Journal of Geophysical Research*, *104*(D7), 8417-8427.

Meeker, L. D., and Mayewski, P. A. (2002), A 1400-year high resolution record of atmospheric circulation over the North Atlantic and Asia, *The Holocene, 12, 257– 266*.

Montzka, S., Dlugokencky, E., and Butler, J. (2011), Non-CO_2 greenhouse gases and climate change, *Nature*, *476*(7358), 43-50.

Montzka, S. A., and Elkins, J. W. (2006), Halocarbons and Other Atmosphere Trace Species Group (HATS)/NOAA/ESRL Global Monitoring Division, edited.

Montzka, S. A., Butler, J. H., Hall, B. D., Mondeel, D. J., and Elkins, J. W. (2003), A decline in tropospheric organic bromine, *Geophysical Research Letters*, *30*(15).

Montzka, S. A., Reimann, S., Engel, A., Krüger, K., O'Doherty, S., Sturges, W. T., Blake, D., Dorf, M., Fraser, P., Froidevaux, L., Jucks, K., Kreher, K., Kurylo, M. J., Mellouki, A., Miller, J., Nielsen, O.-J., Orkin, V. L., Prinn, R. G., Rhew, R., Santee, M. L., Stohl, A., and Verdonik, D. (2010), Ozone-Depleting Substances (ODSs) and Related Chemicals: Chapter 1, Scientific Assessment of Ozone Depletion: 2010, *Global Ozone Research and Montitoring Project, Geneva, Switzerland*.

Moore, R. (2004), Dichloromethane in North Atlantic waters, *J. Geophys. Res*, *109*, C09004.

Moore, R. M. (2000), The solubility of a suite of low molecular weight organochlorine compounds in seawater and implications for estimating the marine source of methyl chloride to the atmosphere, *Chemosphere: Global Change Sci., 2 (1), 95-99*.

Moore, R. M. (2008), A photochemical source of methyl chloride in saline waters, *Environmental Science & Technology*, *42*(6), 1933-1937.

Moore, R. M., and Tokarczyk, R. (1993), Volatile Biogenic Halocarbons in the Northwest Atlantic, *Global Biogeochemical Cycles*, *7*(1), 195-210.

Murray, A., and Riley, J. (1973), Occurrence of some chlorinated aliphatic hydrocarbons in the environment, *Nature*, *242*, 37-38.

Newman, P., Daniel, J., Waugh, D., and Nash, E. (2007), A new formulation of equivalent effective stratospheric chlorine (EESC), *Atmospheric Chemistry and Physics*, *7*(17), 4537-4552.

Norreslet, J., Friberg, S., Nielsen, T., and Romer, U. (1989), Halothane Anaesthetic and the Ozone Layer, *The Lancet*, *333*(8640), 719-719.

O'Brien, L., Harris, P., Robinson, A., Gostlow, B., Warwick, N., Yang, X., and Pyle, J. (2009), Bromocarbons in the tropical marine boundary layer at the Cape Verde Observatory-measurements and modelling, *Atmospheric Chemistry and Physics*, *9*(22), 9083-9099.

O'Doherty, S., Simmonds, P., Cunnold, D., Wang, H., Sturrock, G., Fraser, P., Ryall, D., Derwent, R., Weiss, R., and Salameh, P. (2001), In situ chloroform measurements at Advanced Global Atmospheric Gases Experiment atmospheric research stations from 1994 to 1998, *Journal of Geophysical Research*, *106*(D17), 20429.

O'Doherty, S., Cunnold, D. M., Manning, A., Miller, B. R., Wang, R. H. J., Krummel, P. B., Fraser, P. J., Simmonds, P. G., McCulloch, A., Weiss, R. F., Salameh, P., Porter, L. W., Prinn, R. G., Huang, J., Sturrock, G., Ryall, D., Derwent, R. G., and Montzka, S. A. (2004), Rapid growth of hydrofluorocarbon 134a and hydrochlorofluorocarbons 141b, 142b, and 22 from Advanced Global Atmospheric Gases Experiment (AGAGE) observations at Cape Grim, Tasmania, and Mace Head, Ireland, *Journal of Geophysical Research-Atmospheres*, *109*(D6), 427-438.

Olivier, J., Orlandini, L., Maenhout, G., Monni, S., Peters, J., Petrescu, R., Sanmartin, F., and VanAardenne, J. (2010), European Commission, Joint Research Centre (JRC)/PBL Netherlands Environmental Assessment Agency. Emission Database for Global Atmospheric Research (EDGAR), release version 4.2.

Olivier, J. G. J., Van Aardenne, J. A., Dentener, F., Ganzeveld, L., and Peters, J. A. H. W (2005), Recent trends in global greenhouse gas emissions: regional trends and spatial distribution

of key sources, in: Non-CO_2 Greenhouse Gases (NCGG-4), in *edited by: v. Amstel, A., Millpress, Rotterdam, 325-330*, edited.

Oram, D., Mani, F., Laube, J., Newland, M., Reeves, C., Sturges, W., Penkett, S., Brenninkmeijer, C., Röckmann, T., and Fraser, P. (2011), Long-term tropospheric trend of octafluorocyclobutane (c-C_4F_8 or PFC-318), *Atmos. Chem. Phys. Discuss*, *11*(7), 19,089-019,111.

Otto, K., and Montreuil, C. (1976), Influence of tetraethyllead and lead scavengers on oxidation of carbon monoxide and hydrocarbons over platinum and palladium, *Environmental Science & Technology*, *10*(2), 154-158.

Overpeck, J., Hughen, K., Hardy, D., and Bradley, R. (1997), Arctic environmental change of the last four centuries, *Science, 278, 1251– 1256*.

Palmer, C. J., and Reason, C. J. (2009), Relationships of surface bromoform concentrations with mixed layer depth and salinity in the tropical oceans, *Global Biogeochemical Cycles*, *23*(2), GB2014.

Patra, P. K., Takigawa, M., Dutton, G. S., Uhse, K., Ishijima, K., Lintner, B. R., Miyazaki, K., and Elkins, J. W. (2009), Transport mechanisms for synoptic, seasonal and interannual SF_6 variations and "age" of air in troposphere, *Atmospheric Chemistry and Physics*, *9*(4), 1209-1225.

Pellizzari, E., Bunch, J., Berkley, R., and McRae, J. (1976), Determination of trace hazardous organic vapor pollutants in ambient atmospheres by gas chromatography/mass spectrometry/computer, *Analytical Chemistry*, *48*(6), 803-807.

Penkett, S. A., Jones, B. M. R., Rycroft, M. J., and Simmons, D. A. (1985), An Interhemispheric Comparison of the Concentrations of Bromine Compounds in the Atmosphere, *Nature*, *318*(6046), 550-553.

Penkett, S. A., J.H. Butler, C.E. Reeves, H. Singh, D . Toohey, and R. Weiss (1995), Chapter 10 - Methyl bromide, in Scientific Assessment of Ozone Depletion: 1994, *World Meteorological Organisation Global Ozone and Monitoring Project Report No. 37, Geneva*.

Pfeilsticker, K., Sturges, W. T., Bösch, H., Camy-Peyret, C., Chipperfield, M., Engel, A., Fitzenbergerl, R., Miillers, M., and Payan, S. (2000), budget for the arctic winter 1998/99, *Geophysical Research Letters*, *27*(20), 3305-3308.

Phillips, S. J. (2006), Hazardous Substances Data Bank (HSDB), *United States, National Library of Medicine*.

Ploeger, F., Konopka, P., Günther, G., Grooß, J., and Müller, R. (2010), Impact of the vertical velocity scheme on modeling transport in the tropical tropopause layer, *J. Geophys. Res*, *115*, D03301.

Potts, D. L., and Craft, B. F. (1988), Occupational exposure of veterinarians to waste anesthetic gases, *Applied Industrial Hygiene*, *3*(4), 132-138.

Pratt, G. C., Palmer, K., Wu, C. Y., Oliaei, F., Hollerbach, C., and Fenske, M. J. (2000), An assessment of air toxics in Minnesota, *Environmental Health Perspectives*, 815-825.

Prinn, R. G., Huang, J., Weiss, R. F., Cunnold, D. M., Fraser, P. J., Simmonds, P. G., McCulloch, A., Harth, C., Reimann, S., Salameh, P., O'Doherty, S., Wang, R. H. J., Porter, L. W., Miller, B. R., and Krummel, P. B. (2005), Evidence for variability of atmospheric hydroxyl radicals over the past quarter century, *Geophysical Research Letters*, *32*(7).

Quack, B., Atlas, E., Petrick, G., and Wallace, D. W. R. (2007), Bromoform and dibromomethane above the Mauritanian upwelling: Atmospheric distributions and oceanic emissions, *Journal of Geophysical Research-Atmospheres*, *112*.

Ramaswamy, V., Boucher, O., Haigh, J., Hauglustaine, D., Haywood, J., Myhre, G., Nakajima, T., Shi, G., Solomon, S., and Betts, R. E. (2001), Radiative forcing of climate change, *Rep.*, Pacific Northwest National Laboratory (PNNL), Richland, WA (US).

Randel, W. J., Park, M., Emmons, L., Kinnison, D., Bernath, P., Walker, K. A., Boone, C., and Pumphrey, H. (2010), Asian monsoon transport of pollution to the stratosphere, *Science*, *328*(5978), 611-613.

Randi, M. (1952), The determination of ethylene dibromide in antiknock mixtures, *Chimica e Industria*, *34, 143-144*.

Rasmussen, R. A., and Khalil, M. A. K. (1984), Gaseous Bromine in the Arctic and Arctic Haze, *Geophysical Research Letters*, *11*(5), 433-436.

Reeves, C. E. (2003), Atmospheric budget implications of the temporal and spatial trends in methyl bromide concentration, *Journal of Geophysical Research-Atmospheres*, *108*(D11).

Reeves, C. E., Sturges, W. T., Sturrock, G. A., Preston, K., Oram, D. E., Schwander, J., Mulvaney, R., Barnola, J. M., and Chappellaz, J. (2005), Trends of halon gases in polar firn air: implications for their emission distributions, *Atmospheric Chemistry and Physics*, *5*, 2055-2064.

Reimer, P. J., Baillie, M. G. L., Bard, E., Bayliss, A., Beck, J. W., Bertrand, C. J. H., Blackwell, P. G., Buck, C. E., Burr, G. S., and Cutler, K. B. (2007), IntCal04 terrestrial radiocarbon age calibration, 0-26 cal kyr BP, *Radiocarbon*, *46*(3), 1029-1058.

Renner, R. (2006), The long and the short of perfluorinated replacements, *Environmental Science & Technology*, *40*(1), 12-13.

Rhew, R. C., and Abel, T. (2007), Measuring simultaneous production and consumption fluxes of methyl chloride and methyl bromide in annual temperate grasslands, *Environmental Science & Technology*, *41*(22), 7837-7843.

Rhew, R. C., Miller, B. R., and Weiss, R. F. (2000), Natural methyl bromide and methyl chloride emissions from coastal salt marshes, *Nature*, *403*(6767), 292-295.

Rhew, R. C., Miller, B. R., Vollmer, M. K., and Weiss, R. F. (2001), Shrubland fluxes of methyl bromide and methyl chloride, *Journal of Geophysical Research-Atmospheres*, *106*(D18), 20875-20882.

Ricaud, P., Barret, B., Attié, J. L., Motte, E., Le Flochmoën, E., Teyssedre, H., Peuch, V. H., Livesey, N., Lambert, A., and Pommereau, J. P. (2007), Impact of land convection on troposphere-stratosphere exchange in the tropics, *Atmospheric Chemistry and Physics*, *7*(21), 5657.

Riviere, J. E., and Papich, M. G. (2009), *Veterinary pharmacology and therapeutics*, Blackwell Pub.

Robin, M. L., and Iikubo, Y. (1992), Fire extinguishing methods utilizing perfluorocarbons, edited, Google Patents.

Rommelaere, V., Arnaud, L., and M., B. J. (1997), Reconstructing recent atmospheric trace gas concentrations from polar firn and bubbly ice data by inverse methods, *edited, J. Geophys. Res., 102(D25), 30 069–30 083*.

Roper. W (1992), Toxicological profile for 1,2-Dibromoethane, *Agency for Toxic Substances and Disease Registry U.S. Public Health Service*.

Rosiek, J., Lasa, J., Sliwka, I., and Rozannski, K. (2007), Application of GC and modulated ECD for the determination of SF_5CF_3 mixing ratios in the atmosphere, *Chemia analityczna*, *52*(2), 235-242.

Rudolph, J., Koppmann, R., and Plass-Dülmer, C. (1996), The budgets of ethane and tetrachloroethene: Is there evidence for an impact of reactions with chlorine atoms in the troposphere?, *Atmospheric Environment*, *30*(10-11), 1887-1894.

Saito, T., and Yokouchi, Y. (2006), Diurnal variation in methyl halide emission rates from tropical ferns, *Atmospheric Environment*, *40*(16), 2806-2811.

Salas, L., Shigeishi, H., and Crawford, A. (1977), Urban-nonurban relationships of halocarbons, SF_6, N_2O, and other atmospheric trace constituents, *Atmospheric Environment (1967)*, *11*(9), 819-828.

Salawitch, R., Weisenstein, D., Kovalenko, L., Sioris, C., Wennberg, P., Chance, K., Ko, M., and McLinden, C. (2005), Sensitivity of ozone to bromine in the lower stratosphere, *Geophysical Research Letters*, *32*, L05811.

Sander, S. P., R.R. Friedl, D.M. Golden, M.J. Kurylo, R.E., Huie, V. L. O., G.K. Moortgat, A.R., Ravishankara, C. E. K., M.J. Molina, and B.J., and Finlayson-Pitts (2003), Chemical Kinetics

and Photochemical data for use in atmospheric studies: Evaluation No. 14, *JPL Publication 02-25, Jet Propulsion Laboratory, Pasadena, Calif.*

Santodonato, J., Bosch S, and Meylan W (1985), Monograph on human exposure to chemicals in the workplace: Ethylene dibromide (EDB), in *Center for Chemical Hazard Assessment. Syracuse,*, edited, New York: Syracuse Research Corporation.

Santoro, M. A. (2000), Clarifying the SF_5CF_3 record, *Science, 290, (5493), 935-935*.

Schauffler, S., Atlas, E., Blake, D., Flocke, F., Lueb, R., Lee-Taylor, J., Stroud, V., and Travnicek, W. (1999a), Distributions of brominated organic compounds in the troposphere and lower stratosphere, *Journal of Geophysical Research*, *104*(D17), 21513-21521,21535.

Schauffler, S., Atlas, E., Donnelly, S., Andrews, A., Montzka, S., Elkins, J., Hurst, D., Romashkin, P., Dutton, G., and Stroud, V. (2003), Chlorine budget and partitioning during the Stratospheric Aerosol and Gas Experiment (SAGE) III Ozone Loss and Validation Experiment (SOLVE), *J. Geophys. Res*, *108*(D5), 4173.

Schauffler, S. M., Atlas, E. L., Blake, D. R., Flocke, F., Lueb, R. A., Lee-Taylor, J. M., Stroud, V., and Travnicek, W. (1999b), Distributions of brominated organic compounds in the troposphere and lower stratosphere, *Journal of Geophysical Research-Atmospheres*, *104*(D17), 21513-21535.

Schmittner, A., Oschlies, A., Matthews, H. D., and Galbraith, E. D. (2008), Future changes in climate, ocean circulation, ecosystems, and biogeochemical cycling simulated for a business-as-usual CO_2 emission scenario until year 4000 AD, *Global Biogeochemical Cycles*, *22*(1).

Schulze, J., Weiser, M., Umweltbundesamt, B., and Bundesministerium des Innern, B. (1985), Residue abatement and utilization from the production of chloroorganic chemicals Report date: 30.11. 1983.

Schwander, J., and Stauffer, B. (1984), Age difference between polar ice and the air trapped in its bubbles, *Nature*, *311*(5981), 45-47.

Schwander, J., Stauffer, B., and Sigg, A. (1989), Air mixing in firn and the age of the air at pore close-off, *Annals of Glaciology, vol.10, pp.141-145*.

Schwander, J., Sowers, T., Blunier, T., and Petrenko, V. (2008), Firn Air Sampling - Field report, *NEEM*.

Schwander, J., Sowers, T., Barnola, J. M., Blunier, T., Fuchs, A., and Malaizé, B. (1997), Age scale of the air in the summit ice: Implication for glacial-interglacial temperature change, *Journal of Geophysical Research*, *102*(D16), 19483-19419,19493.

Schwander, J., Barnola, J. M., Andrie, C., Leuenberger, M., Ludin, A., Raynaud, D., and Stauffer, B. (1993), The Age of the Air in the Firn and the Ice at Summit, Greenland, *Journal of Geophysical Research-Atmospheres*, *98*(D2), 2831-2838.

Schwartz, M., Marshall, P., Berry, R., Ehlers, C., and Petersson, G. (1998), Computational study of the kinetics of hydrogen abstraction from fluoromethanes by the hydroxyl radical, *The Journal of Physical Chemistry A*, *102*(49), 10074-10081.

Seinfeld, J. H., Pandis, S. N., and Knovel (1998), *Atmospheric chemistry and physics: from air pollution to climate change*.

Shah, J. J., and Singh, H. B. (1988), Distribution of volatile organic chemicals in outdoor and indoor air, *Environ. Sci. Technol.;(United States)*, *22*(12).

Shiraishi, Y., and Ikeda, K. (1990), Uptake and biotransformation of sevof lurane in humans: A comparative study of sevof lurane with halothane, enflurane, and isoflurane, *Journal of clinical anesthesia*, *2*(6), 381-386.

Simmonds, P., Manning, A., Cunnold, D., McCulloch, A., O'Doherty, S., Derwent, R., Krummel, P., Fraser, P., Dunse, B., and Porter, L. (2006), Global trends, seasonal cycles, and European emissions of dichloromethane, trichloroethene, and tetrachloroethene from the AGAGE observations at Mace Head, Ireland, and Cape Grim, Tasmania, *Journal of Geophysical Research*, *111*(D18), D18304.

Simmonds, P. G., Derwent, R. G., Manning, A. J., Fraser, P. J., Krummel, P. B., O'Doherty, S., Prinn, R. G., Cunnold, D. M., Miller, B. R., Wang, H. J., Ryall, D. B., Porter, L. W., Weiss, R. F., and Salameh, P. K. (2004), AGAGE observations of methyl bromide and methyl chloride at Mace Head, Ireland, and Cape Grim, Tasmania, 1998-2001, *Journal of Atmospheric Chemistry*, *47*(3), 243-269.

Simpson, I. J., Meinardi, S., Blake, N. J., Rowland, F. S., and Blake, D. R. (2004), Long-term decrease in the global atmospheric burden of tetrachloroethene (C_2Cl_4), *Geophys. Res. Lett*, *31*.

Simpson, I. J., Wingenter, O. W., Westberg, D. J., Fuelberg, H. E., Kiley, C. M., Crawford, J. H., Meinardi, S., Blake, D. R., and Rowland, F. S. (2003), Airborne measurements of cirrus-activated C_2Cl_4 depletion in the upper troposphere with evidence against Cl reactions, *Geophys. Res. Lett*, *30*(20), 2025.

Singh, H. B., Salas, L. J., and Stiles, R. E. (1983), Selected man-made halogenated chemicals in the air and oceanic environment, *Journal of Geophysical Research*, *88*(C6), 3675-3683.

Sinnhuber, B., Sheode, N., Sinnhuber, M., Chipperfield, M., and Feng, W. (2009), The contribution of anthropogenic bromine emissions to past stratospheric ozone trends: A modelling study, *Atmospheric Chemistry and Physics*, *9*(8), 2863-2871.

Sinnhuber, B. M., and Folkins, I. (2005), Estimating the contribution of bromoform to stratospheric bromine and its relation to dehydration in the tropical tropopause layer, *Atmospheric Chemistry and Physics Discussions*, *5*(6), 12939-12956.

Sinnhuber, B. M., Sheode, N., Sinnhuber, M., Chipperfield, M., and Feng, W. (2006), The contribution of anthropogenic bromine emissions to past stratospheric ozone trends: A modelling study, *Atmospheric Chemistry and Physics Discussions*, *6*(4), 6497-6524.

Skoog, D. A. (2004), *Fundamentals of analytical chemistry*, Brooks/Cole Pub Co.

Smith, K., Newnham, D., Page, M., Ballard, J., and Duxbury, G. (1996), Infrared band strengths and absorption cross-sections of HFC-32 vapour, *Journal of Quantitative Spectroscopy and Radiative Transfer*, *56*(1), 73-82.

Solomon, S., D, B., Doney, S., Hayhoe, H., Held, I., Lettenmaier, D., Lobell, D., Matthews, D., Pierrehumbert, R., Raphael, M., Richels, R., Root, T., Steffen, K., Tebaldi, C., and Yohe, G. (2011), *Climate Stabilization Targets: Emissions, Concentrations, and Impacts over Decades to Millennia*, Natl Academy Pr.

Solovev, S., Palmentieri, A., Potekhina, N., and Madey, T. E. (2007), Mechanism for Electron-Induced SF_5CF_3 Formation in Condensed Molecular Films, *The Journal of Physical Chemistry C*, *111*(49), 18271-18278.

Sowers, T., Bender, M., and Raynaud, D. (1989), Elemental and isotopic composition of occluded O_2 and N_2 in polar ice, *Journal of Geophysical Research*, *94*(D4), 5137-5150.

Sowers, T., Bender, M., Raynaud, D., and Korotkevich, Y. (1992), $\delta^{15}N$ of N_2 in air trapped in polar ice: a tracer of gas transport in the firn and a possible constraint on ice age-gas age differences, *Journal of Geophysical Research*, *97*(D14), 15683-15615,15697.

Sowers, T., Bernard, S., Aballain, O., Chappellaz, J., Barnola, J.-M., and Marik, T. (2005), Records of the $\delta^{13}C$ of atmospheric CH_4 over the last 2 centuries as recorded in Antarctic snow and ice,, *Global Biogeochem. Cycles*.

Stiller, G., Von Clarmann, T., Höpfner, M., Glatthor, N., Grabowski, U., Kellmann, S., Kleinert, A., Linden, A., Milz, M., and Reddmann, T. (2008), Global distribution of mean age of stratospheric air from MIPAS SF_6 measurements, *Atmospheric Chemistry and Physics*, *8*(3), 677-695.

Stohl, A., Eckhardt, S., Forster, C., James, P., and Spichtinger, N. (2002), On the pathways and timescales of intercontinental air pollution transport, *J. Geophys. Res*, *107*, 1-17.

Stone, K. R., and Springer Jr, J. (1995), Review of solvent cleaning in aerospace operations and pollution prevention alternatives, *Environmental progress*, *14*(4), 261-265.

Sturges, W., Sullivan, C., Schnell, R., Heidt, L., and Pollock, W. (1993a), Bromoalkane production by Antarctic ice algae, *Tellus B*, *45*(2), 120-126.

Sturges, W., Oram, D., Laube, J., Reeves, C., Newland, M., Hogan, C., Martinerie, P., Witrant, E., Brenninkmeijer, C., and Schuck, T. (2012), Emissions halted of the potent greenhouse gas SF_5CF_3, *Atmos. Chem. Phys.*, *12, 3653-3658,*.

Sturges, W. T., Sullivan, C. W., Schnell, R. C., Heidt, L. E., and Pollock, W. H. (1993b), Bromoalkane Production by Antarctic Ice Algae, *Tellus Series B-Chemical and Physical Meteorology*, *45*(2), 120-126.

Sturges, W. T., Penkett, S. A., Barnola, J. M., Chappellaz, J., Atlas, E., and Stroud, V. (2001a), A long-term record of carbonyl sulfide (COS) in two hemispheres from firn air measurements, *Geophysical Research Letters*, *28*(21), 4095-4098.

Sturges, W. T., McIntyre, H. P., Penkett, S. A., Chappellaz, J., Barnola, J. M., Mulvaney, R., Atlas, E., and Stroud, V. (2001b), Methyl bromide, other brominated methanes, and methyl iodide in polar firn air, *Journal of Geophysical Research-Atmospheres*, *106*(D2), 1595-1606.

Sturges, W. T., Wallington, T. J., Hurley, M. D., Shine, K. P., Sihra, K., Engel, A., Oram, D. E., Penkett, S. A., Mulvaney, R., and Brenninkmeijer, C. A. M. (2000), A potent greenhouse gas identified in the atmosphere: SF_5CF_3, *Science*, *289*(5479), 611-613.

Sturrock, G., Etheridge, D., Trudinger, C., Fraser, P., and Smith, A. (2002), Atmospheric histories of halocarbons from analysis of Antarctic firn air: Major Montreal Protocol species, *J. Geophys. Res*, *107*(4765), 1029-1035.

Swanson, A. L., Blake, N. J., Dibb, J. E., Albert, M. R., Blake, D. R., and Rowland, F. S. (2002), Photochemically induced production of CH_3Br, CH_3I, C_2H_5I, ethene, and propene within surface snow at Summit, Greenland, *Atmospheric Environment*, *36*(15-16), 2671-2682.

Teh, Y. I. T. A. R. N., Rhew, R. C., Atwood, A., and Abel, T. (2008), Water, temperature, and vegetation regulation of methyl chloride and methyl bromide fluxes from a shortgrass steppe ecosystem, *Global Change Biology*, *14*(1), 77-91.

Thomas, V. M., Bedford, J. A., and Cicerone, R. J. (1997), Bromine emissions from leaded gasoline, *Geophysical Research Letters*, *24*(11), 1371-1374.

Thompson, T. M. E., J.H. Butler, B.C. Daube, G.S. Dutton, J.W. Elkins, B.D. Hall, D.F. Hurst, D.B. King, E.S. Kline, B.G. LaFleur, J. Lind, S. Lovitz, D.J. Mondeel, S.A. Montzka, F.L. Moore, J.D. Nance, J.L. Neu, P.A. Romashkin, A. Scheffer and W.J. Snible (2004), Halocarbons and other atmospheric trace species, Section 5 in Climate Monitoring and Diagnostics Laboratory: Summary Report No. 27, 2002-2003, *edited by R. Schnell, A.-M. Buggle, and R. Rosson, 115-135, NOAA/Climate Monitoring and Diagnostics Laboratory, Boulder, Colo.*

Thuburn, J., and Craig, G. C. (2002), On the temperature structure of the tropical substratosphere, *J. Geophys. Res*, *107*(10.1029).

Tokarczyk, R., and Moore, R. M. (1994), Production of Volatile Organohalogens by Phytoplankton Cultures, *Geophysical Research Letters*, *21*(4), 285-288.

Trudinger, C., Enting, I. G., Etheridge, D. M., Francey, R. J., Levchenko, V. A., Steele, L. P., Raynaud, D., and Arnaud, L. (1997), Modeling air movement and bubble trapping in firn, *J. Geophys. Res., 102, 6747–6763*.

Trudinger, C. M., Etheridge, D. M., Sturrock, G. A., Fraser, P. J., Krummel, P. B., and McCulloch, A. (2004), Atmospheric histories of halocarbons from analysis of Antarctic firn air: Methyl bromide, methyl chloride, chloroform, and dichloromethane, *Journal of Geophysical Research-Atmospheres*, *109*(D22).

Trudinger, C. M., D. M. Etheridge, P. J. Rayner, I. G. Enting, G. A. Sturrock, and R. L. Langenfelds (2002), Reconstructing atmospheric histories from measurements of air composition in firn, *J. Geophys. Res., 107(D24), 4780, doi:10.1029/2002JD002545*.

Tsai, W. T., Chen, H. P., and Hsien, W. Y. (2002), A review of uses, environmental hazards and recovery/recycle technologies of perfluorocarbons (PFCs) emissions from the semiconductor manufacturing processes, *Journal of Loss Prevention in the Process Industries*, *15*(2), 65-75.

Varner, R. K., Crill, P. M., and Talbot, R. W. (1999), Wetlands: a potentially significant source of atmospheric methyl bromide and methyl chloride, *Geophysical Research Letters*, *26*(16), 2433-2435.

Velders, G., Madronich, S., Clerbaux, C., Derwent, R., Grutter, M., Hauglustaine, D., Incecik, S., Ko, M., Libre, J. M., and Nielsen, O. J. (2005), Chemical and radiative effects of halocarbons and their replacement compounds*Rep. 0521682061*, Cambridge University Press UK.

von Glasow, R., von Kuhlmann, R., Lawrence, M., Platt, U., and Crutzen, P. (2004), Impact of reactive bromine chemistry in the troposphere, *Atmospheric Chemistry and Physics*, *4*(11/12), 2481-2497.

Wamsley, P., Elkins, J., Fahey, D., Dutton, G., Volk, C., Myers, R., Montzka, S., Butler, J., Clarke, A., and Fraser, P. (1998), Distribution of Halon-1211 in the upper troposphere and lower stratosphere and the 1994 total bromine budget, *Journal of Geophysical Research*, *103*(D1), 1513-1526.

Wang, C. J. L., Blake, D. R., and Rowland, F. S. (1995), Seasonal variations in the atmospheric distribution of a reactive chlorine compound, tetrachloroethene (CCl_2=CCl_2), *Geophysical Research Letters*, *22*(9), 1097-1100.

Wang, Z., Chappellaz, J., Martinerie, P., Park, K., Petrenko, V., Witrant, E., Emmons, L., Blunier, T., Brenninkmeijer, C., and Mak, J. (2012), The isotopic record of Northern Hemisphere atmospheric carbon monoxide since 1950: implications for the CO budget, *Atmos. Chem. Phys*, *12*, 4365-4377.

Warwick, N., Pyle, J., Carver, G., Yang, X., Savage, N., O'Connor, F., and Cox, R. (2006), Global modeling of biogenic bromocarbons, *Journal of Geophysical Research*, *111*(D24).

Waugh, C., Paltsev, S., Selin, N., Reilly, J., Morris, J., and Sarofim, M. (2011), Emission Inventory for Non-CO_2 Greenhouse Gases and Air Pollutants in EPPA 5, edited, MIT Joint Program on the Science and Policy of Global Change, Technical Note.

WHO (2011), WHO Model Lists of Essential Medicines(17th).

Williams, J., Wang, N. Y., Cicerone, R. J., Yagi, K., Kurihara, M., and Terada, F. (1999), Atmospheric methyl halides and dimethyl sulfide from cattle, *Glob. Biogeochem. Cycles*, *13*, 485-491.

Winther, J.-G., et al. (2002), European Project for Ice Coring in Antarctica (EPICA): Nordic traverse in 2000/01, in Norwegian Antarctic Research Expedition 2000/01, *edited by J.-G. Winther, Norsk Polarinst. Rep. Ser., 120, 18– 29.*

Witrant, E., Martinerie, P., Hogan, C., Laube, J., Kawamura, K., Capron, E., Montzka, S., Dlugokencky, E., Etheridge, D., and Blunier, T. (2011), A new multi-gas constrained model of trace gas non-homogeneous transport in firn: evaluation and behavior at eleven polar sites, *Atmopsheric Chemistry and Physics (11) 23029-23080*.

Worton, D. R., Sturges, W. T., Schwander, J., Mulvaney, R., Barnola, J. M., and Chappellaz, J. (2006), 20th century trends and budget implications of chloroform and related tri-and dihalomethanes inferred from firn air, *Atmospheric Chemistry and Physics*, *6*, 2847-2863.

Worton, D. R., Sturges, W. T., Gohar, L. K., Shine, K. P., Martinerie, P., Oram, D. E., Humphrey, S. P., Begley, P., Gunn, L., Barnola, J. M., Schwander, J., and Mulvaney, R. (2007), Atmospheric trends and radiative forcings of CF_4 and C_2F_6 inferred from firn air, *Environmental Science & Technology*, *41*(7), 2184-2189.

Xiao, X. (2008), Optimal Estimation of the Surface Fluxes of Chloromethanes Using a 3-D Global Atmospheric Chemical Transport Model, Massachusetts Institute of Technology, Boston.

Xiao, X., Prinn, R. G., Fraser, P. J., Simmonds, P. G., Weiss, R. F., O'Doherty, S., Miller, B. R., Salameh, P. K., Harth, C. M., Krummel, P. B., Porter, L. W., Muhle, J., Greally, B. R., Cunnold, D., Wang, R., Montzka, S. A., Elkins, J. W., Dutton, G. S., Thompson, T. M., Butler, J. H., Hall, B. D., Reimann, S., Vollmer, M. K., Stordal, F., Lunder, C., Maione, M., Arduini, J., and Yokouchi, Y. (2010), Optimal estimation of the surface fluxes of methyl chloride using

a 3-D global chemical transport model, *Atmospheric Chemistry and Physics*, *10*(12), 5515-5533.

Yang, X., Cox, R. A., Warwick, N. J., Pyle, J. A., Carver, G. D., O'Connor, F. M., and Savage, N. H. (2005), Tropospheric bromine chemistry and its impacts on ozone: A model study, *Journal of Geophysical Research*, *110*(D23).

Yokouchi, Y., Barrie, L., Toom, D., and Akimoto, H. (1996), The seasonal variation of selected natural and anthropogenic halocarbons in the Arctic troposphere, *Atmospheric Environment*, *30*(10-11), 1723-1727.

Yokouchi, Y., Ikeda, M., Inuzuka, Y., and Yukawa, T. (2002a), Strong emission of methyl chloride from tropical plants, *Nature*, *416*(6877), 163-165.

Yokouchi, Y., Saito, T., Ishigaki, C., and Aramoto, M. (2007), Identification of methyl chloride-emitting plants and atmospheric measurements on a subtropical island, *Chemosphere*, *69*(4), 549-553.

Yokouchi, Y., Toom-Sauntry, D., Yazawa, K., Inagaki, T., and Tamaru, T. (2002b), Recent decline of methyl bromide in the troposphere, *Atmospheric Environment*, *36*(32), 4985-4989.

Yokouchi, Y., Hasebe, F., Fujiwara, M., Takashima, H., Shiotani, M., Nishi, N., Kanaya, Y., Hashimoto, S., Fraser, P., Toom-Sauntry, D., Mukai, H., and Nojiri, Y. (2005), Correlations and emission ratios among bromoform, dibromochloromethane, and dibromomethane in the atmosphere, *Journal of Geophysical Research-Atmospheres*, *110*(D23).

Zander, R., Mahieu, E., Demoulin, P., Duchatelet, P., Roland, G., Servais, C., Mazière, M. D., Reimann, S., and Rinsland, C. P. (2008), Our changing atmosphere: Evidence based on long-term infrared solar observations at the Jungfraujoch since 1950, *Science of the Total Environment*, *391*(2-3), 184-195.

Zok, S., Boutonnet, J. C., De Rooij, C., Garny, V., Lecloux, A., Papp, R., Thompson, R. S., and van Wijk, D. (1998), Euro Chlorine risk assessment for the marine environment OSPARCOM Region: North Sea-Chloroform, *Environmental monitoring and assessment*, *53*(3), 401-424.